

Alma Mater Studiorum - Università di Bologna

DOTTORATO DI RICERCA IN  
CHIMICA

Ciclo 33

**Settore Concorsuale:** 03/C1 - CHIMICA ORGANICA

**Settore Scientifico Disciplinare:** CHIM/06 - CHIMICA ORGANICA

MULTIFARIOUS TUMOR-ORIENTED SMALL MOLECULES: DEVELOPMENT OF  
SYNTHETIC METHODOLOGIES AND APPLICATION FOR DIAGNOSTIC  
PLATFORMS

**Presentata da:** Dario Corbisiero

**Coordinatore Dottorato**

Domenica Tonelli

**Supervisore**

Alessandra Tolomelli

**Co-supervisore**

Pier Giorgio Cozzi

**Esame finale anno 2021**



---

## Abstract

---

**Cancer** represents one of the most relevant and widespread diseases in the modern age. One of the critical point of cancer-associated pathologies is the difficult identification of a single reason for their onset; for this reason its spread can be justified by several phenomena. In particular, **inflammation** is a physiological phenomenon strictly related to cancer growth and proliferation, and epidemiological studies have established that nearly 15% of the cancer cases in the world is associated with infection and resulting inflammation. On the other hand, evidences suggest that the inflammation response and immune system may inhibit the development of cancer processes.

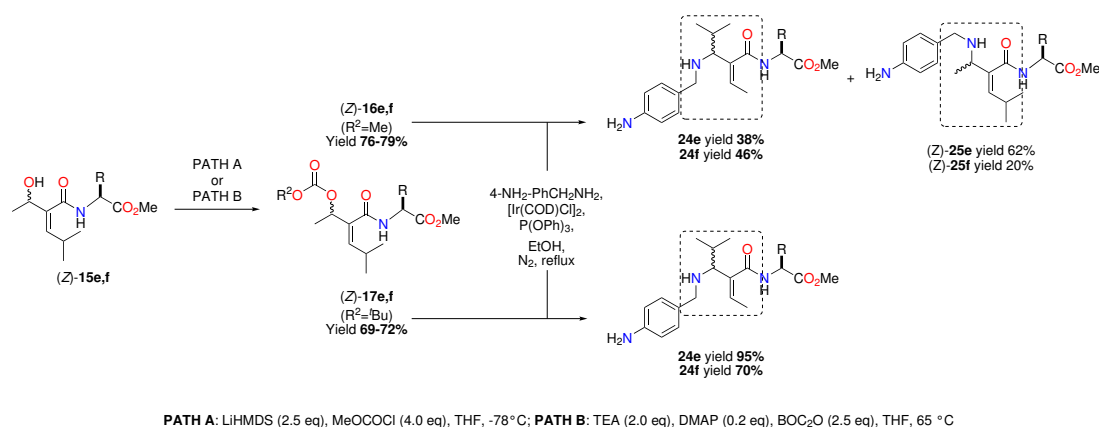
In this context, **integrin** receptors, a family of structurally related cell surface heterodimers, are important for the interactions of cells with extracellular matrix and for the development of both inflammation and carcinogenic phenomena. For this reason, researchers have identified these receptors as very promising biological targets, spending a lot of efforts on the development of efficacious drugs that use these receptors as target to contrast tumor expansion.

Integrins are cell surface receptors structurally comprised of non-covalent associations between  $\alpha$  and  $\beta$  subunits, which exhibit peculiar binding affinity with specific extracellular ligands. The greatest influence on ligand-binding specificity is provided by the  $\alpha$ -subunit and allows to classify the integrins in several ligand-dependent families, among which *Arg-Gly-Asp* (**RGD**) motifs-binding and intercellular adhesion molecules are the most interesting. Among the 24 possible integrin heterodimers, RGD-binding subtypes  $\alpha_V\beta_3$  and  $\alpha_5\beta_1$  represent two interesting holds for further studies.

The first important goal from the point of view of medicinal chemistry was the discovery of the minimal cell-binding motif in fibronectin, the tripeptide *Arg-Gly-Asp* (**RGD**). In fact, both  $\alpha_V\beta_3$  and  $\alpha_5\beta_1$  receptors were inhibited by the same RGD sequence and it has been well-established that multiple factors were relevant for the specificity of ligand-integrin interaction. Although there are significant examples regarding integrin specificity conferred by synergistic domains, the conformation and spatial arrangement of the RGD motif in the ECM ligands is one of the most important aspects of their interaction.

There are many tricks to improve the bioactivity and receptor selectivity of exogenous ligands; one of these is to integrate the amino acid sequence into a cyclic peptide to restrict its conformational space. Another approach is to develop small peptidomimetic molecules in order to enhance the molecular stability and open the way to versatile synthetic strategies. Starting from isoxazoline-based peptidomimetic molecules we recently reported, in this thesis we are going to present the synthesis of new integrin ligands obtained by modifying or introducing appendages on already reported structures.

Initially, we are going to introduce the synthesis of linear and cyclic  $\alpha$ -dehydro- $\beta$ -amino acids as scaffolds for the preparation of bioactive peptidomimetics (**Chapter 2**, subsection 2.4.1). In particular, we have focused our attention on the design, synthesis, and biological evaluation of  $\alpha_V\beta_3/\alpha_5\beta_1$  and  $\alpha_4\beta_1$  integrin ligands. The synthesis of  $\alpha/\beta$  dipeptides containing linear or cyclic  $\alpha$ -dehydro- $\beta$ -amino acids has been performed starting from alkylidene acetamides, which were obtained from  $\alpha$ -amino esters via Ir-catalyzed allylic amination. Differently hindered carbonates were synthesised via a protocol involving chemoselective Luche's reduction, acylation, and allylic amination. Depending on the nature of the selected  $\alpha$ -amino acid, we observed strong influence on the product regiochemistry due to the carbonate size and the amino acid side chain. In particular, complete regioselectivity was observed in the aminic allylation of carbonates deriving from amino acids possessing a methylene unit in  $\beta$ -position. On the contrary, methyl carbonates deriving from  $\beta$ -branched amino acid afforded different results depending on the hindrance of the carbonate. Moreover, spontaneous cyclization was observed for carbamate-containing intermediates, allowing to obtain peptidomimetic polyfunctionalized dihydropyrimidine-2,4-dione. Finally, by inverting the order of reduction/acylation steps on the starting alkylidene acetoacetamides, the formation of polyfunctionalized 1,3-oxazinane-2,4-dione was obtained, demonstrating the wide applications of these substrates for the preparation of bioactive peptidomimetics (Scheme 1).



**Scheme 1:** Synthesis of carbonates (Z)-16e,f and (Z)-17e,f and allylic substitution with 4-aminobenzylamine on (Z)-16e,f and (Z)-17e,f.

Subsequently, we are going to present the construction of small molecule ligands (SMLs) based delivery systems performed starting from a polyfunctionalised isoxazoline scaffold, whose potency towards  $\alpha_V\beta_3$  and  $\alpha_5\beta_1$  integrins has already been established by our research group (Chapter 2, subsection 2.4.2). The synthesis of this novel class of ligands was obtained by conjugation of linkers to the heterocyclic core via Huisgen-click reaction, with the aim to use them as "shuttles" for selective delivery of diagnostic agents to cancer cells, exploring the effects of the side chains in the interaction with the target. Compounds **42b** and **48** showed excellent potency towards  $\alpha_5\beta_1$  integrin acting as either selective antagonist or agonist, respectively. Further investigations confirmed their effects on target receptor through the analysis of fibronectin-induced ERK1/2 phosphorylation. In addition, confocal microscopy analysis allowed us to follow the fate of EGFP-conjugated  $\alpha_5\beta_1$  integrin and FITC conjugated analog of **42b** (compound **55**) inside the cells. Moreover, the stability in water solution at different values of pH and in bovine serum confirmed the possible exploitation of these peptidomimetic molecules for pharmaceutical applications (Figure 1).

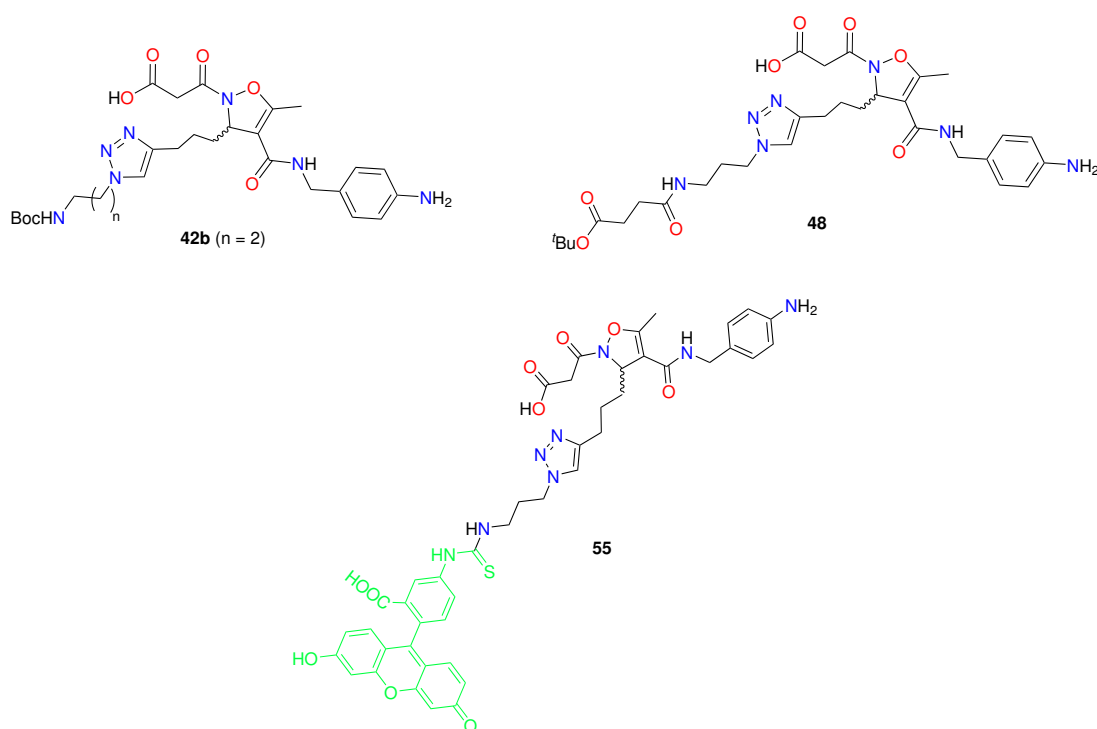
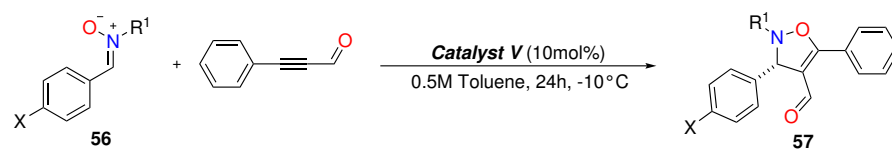


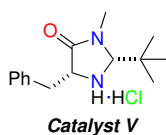
**Figure 1:** Compounds **42b**, **48** and **55** which exhibited the most interesting biological results.

In the light of these results and due to the necessity to understand the behaviour of a single enantiomer of the isoxazoline-based compounds reported above, the research group decided to synthesise the enantiopure heterocycle using a 1,3-dipolar cycloaddition approach (Chapter 2, subsection 2.4.3). This strategy involves the reaction between a nitron and a propargylic aldehyde in which the latter was activated through the formation of an iminium ion species using a chiral aminocatalyst. Therefore, a small library of nitrones have been

synthesised modifying the starting materials both on the protecting group of the hydroxylamine ( $R^1$ ) and on the chain of the aldehyde (X). Initially, five amino-catalysts have been selected (three belonging to the pyrrolidine's family and two belonging to imidazolidinone's one) to identify which one would have guaranteed the best yield/er ratio. N-*t*Bu protecting group and catalyst V were chosen since they provided better results during the preliminary studies. Based on this observation, a screening of solvents and starting materials have been deepened. Subsequently, the influence of the temperature on the enantiomeric ratio (er) of the process has been explored: surprisingly, catalyst V has provided very similar results both at RT and  $-10^\circ\text{C}$ , confirming its role as lead catalyst. Moreover, the  $R^1$  group has been modified to introduce a functionalised side chain or a removable protecting group, according to our goal to synthesise a bioactive compound for further functionalisations. Then, the attention has been focused on the para-substituent on the aryl moiety (Figure 2). The reactions have been carried out with halo-, nitro-, and cyano-derivatives to demonstrate a wide substrate feasibility and versatility to functionalisation. Also in this case, all the reactions provided very similar yields and er, confirming the versatility of this catalyst. Finally, the isoxazolines **57Cb** and **57Db** (entry 3 and 4, Figure 2) were synthesised to obtain a scaffold as similar as possible to the target peptidomimetic molecules, already known to be bioactive compounds towards  $\alpha_V\beta_3$  and  $\alpha_5\beta_1$  integrins. Once completed this screening, the attention was focused on the derivatisation of the aldehyde to carboxylic acid in position 4 by using Pinnick's reaction.



Entry	$R^1$	X	C (%)	er <sup>a</sup>	<b>57</b>
1	<i>t</i> Bu	H	>99	1:99 (3:97)	<b>Ab</b>
2	Bn	H	>99	9:91 (12:88)	<b>Bb</b>
3	(CH <sub>2</sub> ) <sub>2</sub> CO <sub>2</sub> Me	H	>99	13:87 (22:78)	<b>Cb</b>
4	(CH <sub>2</sub> ) <sub>2</sub> CO <sub>2</sub> <i>t</i> Bu	H	>99	8:92 (19:81)	<b>Db</b>
5	<i>t</i> Bu	Cl	>99	3:97 (4:96)	<b>Ac</b>
6	<i>t</i> Bu	Br	>99	4:96 (9:91)	<b>Ad</b>
7	<i>t</i> Bu	I	>99	3:97 (5:95)	<b>Ae</b>
8	<i>t</i> Bu	NO <sub>2</sub>	>99	3:97 (8:92)	<b>Af</b>
9	<i>t</i> Bu	CN	>99	6:94 (9:91)	<b>Ag</b>



<sup>a</sup> in brackets the er values obtained by carrying out the reaction at RT

**Figure 2:** Synthesis of a small library of isoxazolines **57** by changing  $R^1$  and X, alternately.

Subsequently, we are going to introduce the synthesis of a **Reporting Drug Delivery System** (Figure 3) composed by a carrier, a first spacer, a linker, a self-immolative system, a second spacer and a latent fluorophore (**Chapter 3**). The structure was divided into four fragments (A, B, C, D) to be coupled each other. Regarding the synthesis of the linker by

adopting consolidated peptide chemistry, Val-Ala dipeptide was synthesised since its simple sequence is recognized and cleaved by *Cathepsin B*, a peptidase over-expressed in proximity to cancer cells. Moreover, the synthesis of **Fragment B** was made up of three peptide couplings, optimising the first two reactions using DIC/Oxyma pure<sup>®</sup> and the last one (between the Ala and self immolative system) using EDC·HCl/HOBt as coupling reagents. On the other hand, the synthesis of the latent fluorophore was carried out starting from a *Perkin* reaction between 2,4-dihydroxybenzaldehyde, propionic anhydride and sodium propionate providing a coumarin derivative. Then, through a radical process, this coumarin derivative was oxidised to the corresponding aldehyde **10**, ready for the coupling with the diamine spacer (second spacer). Unfortunately, the coupling between **Fragment B** and **Fragment C** highlighted several drawbacks that will be addressed and overcome in future optimisation studies. Finally, in the last step intermediate **Fragment B+C** will be linked with a suitable alkyne isoxazoline derivative by means of click reaction (Figure 3).

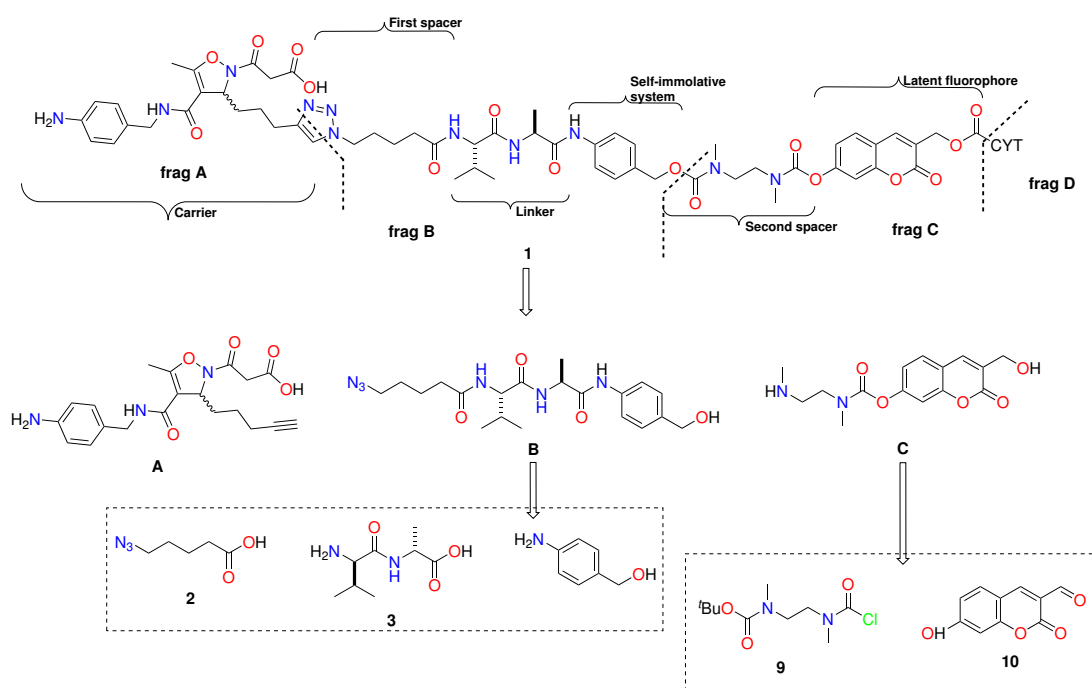


**Figure 3:** Retrosynthetic analysis of compound **1**.

The last part of this work will describe the results obtained during the internship abroad in Prof. Aggarwal's laboratory at the University of Bristol. The project was focused on the *Mycapolyol A* synthesis, a polyketide isolated from the marine sponge *Mycale izuensis* which exhibit cytotoxic properties (Figure 4, **Chapter 4**). In particular, the aim of the work was directed on the synthetic scale up of the building blocks necessary for the optimisation of the late steps of the synthesis.

The *Mycapolyol A* synthesis is based on the **lithiation-borylation** chemistry to build up the polyhydroxyl chain in an enantioselective way. Lithiation-borylation strategy was developed

by *Aggarwal* and coworkers starting from 2007 and is a versatile strategy for the synthesis of several moieties which require stereospecificity and periodicity of functional groups. Mycapolyol A was divided in three fragments and at the end of the synthesis of each fragment, they were coupled together to obtain the desired product (Figure 4).

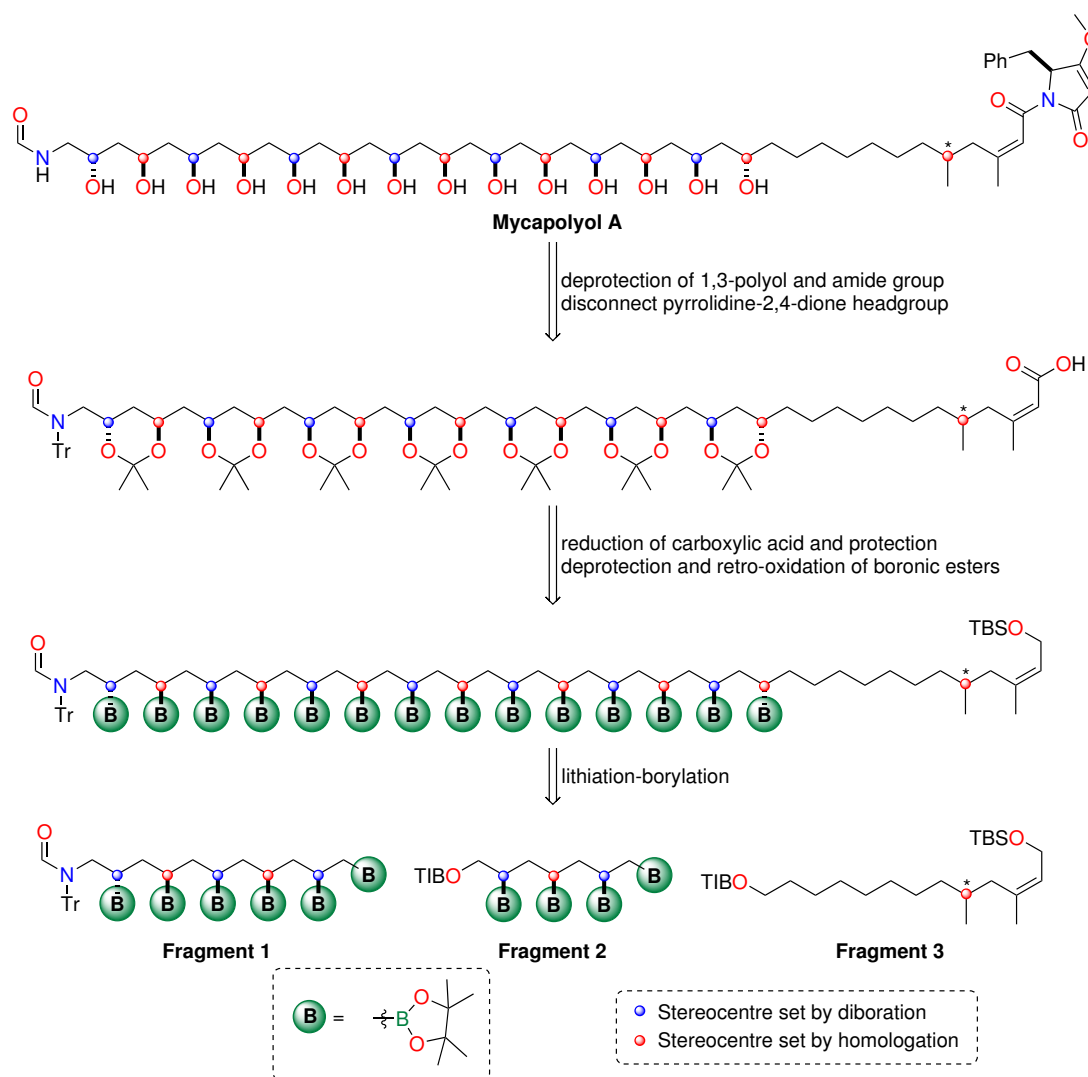


Figure 4: Mycapolyol A and retrosynthetic approach.



---

## Contents

---

<b>Abstract</b>	<b>i</b>
<b>1 Integrin: a Door for the Treatment of Cancer</b>	<b>1</b>
1.1 Mutual Connections Between Cancer and Inflammation . . . . .	2
1.2 Integrins . . . . .	6
1.2.1 Role of Integrins in Cancer Cells Communication . . . . .	9
1.3 Integrin Ligands: Structural Information . . . . .	14
1.4 Aim of the Thesis . . . . .	21
<b>2 Heterocyclic Chemistry and Biological Applications</b>	<b>25</b>
2.1 Introduction . . . . .	25
2.2 Heterocyclic Moieties in Medicinal Chemistry . . . . .	26
2.2.1 Heterocycles Serving Peptidomimetics . . . . .	30
2.2.2 Heterocycles-Based Bioactive Molecules . . . . .	32
2.2.3 Isoxazoline Ring: Overview on its Synthesis . . . . .	34
2.3 Organocatalysis and Organocatalysis in Medicinal Chemistry . . . . .	38
2.3.1 Via-Enamine Catalysis in the Synthesis of Antitumor Agents . . . . .	41
2.3.2 Via-Iminium Ion Catalysis in the Synthesis of Anticoagulant Agents . . . . .	43
2.4 Results and Discussions . . . . .	45
2.4.1 Linear and Cyclic $\alpha$ -Dehydro- $\beta$ -Amino Acids as Scaffolds for Bioactive Compounds . . . . .	45
2.4.2 Synthesis of New Isoxazoline-Based Integrin Ligands . . . . .	53
2.4.3 Enantioselective Synthesis of Isoxazoline Scaffolds . . . . .	67
2.5 Conclusions . . . . .	78
2.6 Experimental Procedures . . . . .	79
2.6.1 General Methods . . . . .	79
2.6.2 Synthesis and Characterisation . . . . .	80

---

<b>3</b>	<b>Reporting Drug Delivery System (RDDS)</b>	<b>115</b>
3.1	Introduction . . . . .	115
3.2	Enzyme-Activable Linkers . . . . .	119
3.3	Self-Immolative Spacer . . . . .	122
3.4	Latent Fluorophore . . . . .	126
3.5	Results and Discussion . . . . .	129
3.5.1	Synthesis of Fragment B . . . . .	131
3.5.2	Synthesis of Fragment C . . . . .	132
3.6	Conclusions . . . . .	137
3.7	Experimental Procedures . . . . .	138
3.7.1	General Methods . . . . .	138
3.7.2	Synthesis and Characterization . . . . .	138
<b>4</b>	<b>Total Synthesis of Mycapolyol A</b>	<b>143</b>
4.1	Introduction . . . . .	143
4.1.1	Lithiation-Borylation: from a Single Homologation to the Assembly-Line Synthesis . . . . .	144
4.1.2	Stereocontrolled Synthesis of 1,3-diols . . . . .	148
4.1.3	Development of New $\alpha$ -Sulfinyl Benzoates as Carbenoid Precursors . . . . .	150
4.2	Mycapolyol A . . . . .	154
4.3	Conclusions . . . . .	162
4.4	Experimental Procedures . . . . .	162
4.4.1	General Methods . . . . .	162
4.4.2	Synthesis and Characterization . . . . .	163
	<b>Appendix</b>	<b>171</b>
	<b>Bibliography</b>	<b>173</b>

## Chapter 1

---

### Integrin: a Door for the Treatment of Cancer

---

Cancer represents one of the most relevant and widespread diseases in the modern age. In 2018 the *World Health Organization* (WHO) has estimated the spread of this illness in 18 million of new cases, with 48.4% of patients only in Asia, 2.1 million (12%) of sufferers are under 45 and 9.5 million of people dead due to this disease in 2017. From a medical point of view, lung (11.6%), breast (11.6%) and colorectum (10.2%) are the most affected organs. These numbers tell us that cancer is an ubiquitous pathology and a plague of our time (Figure 1.1).<sup>1</sup>

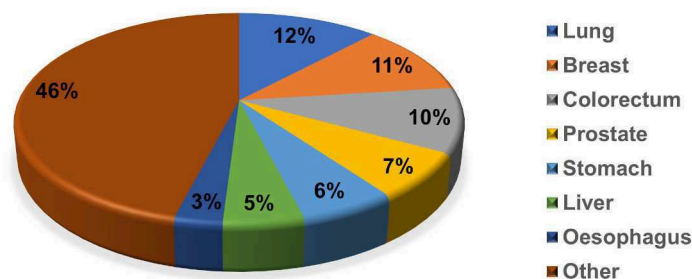


Figure 1.1: Estimated number of new cancer cases in 2018.

Cancer results from the outgrowth of a clonal population of cells from tissues and genetic changes are fundamental issues in the development of the illness. One critical point of cancer-associated pathologies is the difficult identification of a single etiology for their onset; for this reason, its spread can be caused by several concomitant phenomena.

One possibility to explain why cancer is so aggressive towards the organism is through its essential features. In fact, cancer development is based on seven fundamental properties: 1) self-sufficient proliferation; 2) no response to anti-proliferative signals; 3) maintenance of an inflammatory microenvironment; 4) tissue invasion and metastasis; 5) unlimited replicative potential; 6) maintenance of vascularization, and 7) lack of apoptosis process (Figure 1.2).<sup>2,3</sup>

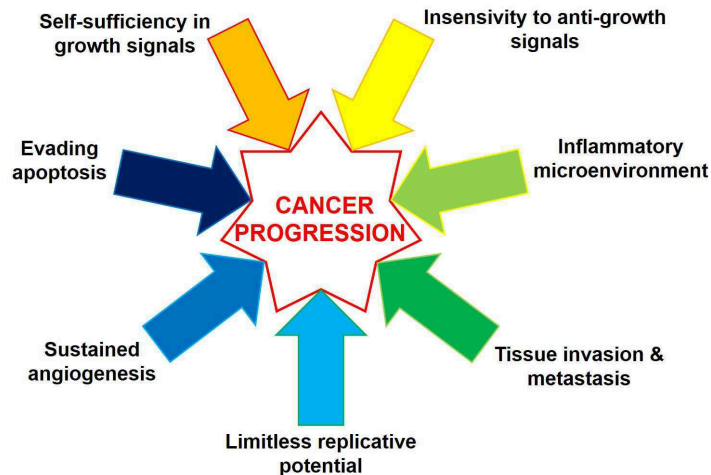


Figure 1.2: Cancer progression in seven hallmarks (modified from Colotta F. et al.<sup>11</sup>)

*Peyton Rous*<sup>4</sup> recognized that cancer increases from "subthreshold neoplastic states" and he used another way to describe the cancer development dividing this process in three general phases: *initiation*, *promotion*, and *progression*. Initiation is characterized by DNA alterations and can persist until another type of stimulation occurs; promotion is the result of exposure of "initiated cells" to chemical irritants (e.g. factors released at wounding's site, resection, hormones or chronic inflammation) and it is a process of survival and expansion of these "cells-primer". Finally, progression induces several processes necessary for malignant tissues growth as cell proliferation, recruitment of inflammatory cells, increase in production of reactive oxygen species inducing oxidative DNA damage and reducing DNA repair. Modification in cell death/repair cycle programmes occurs in chronically inflamed tissues, thus resulting in an upregulated growth of unhealthy cells (growth in tumor size and formation-related metastasis). In all these phases, the generation and retention of genetic lesions are fundamental and normal inflammation processes are self-limiting with a fine tuned production of pro-inflammatory/anti-inflammatory cytokines.<sup>5</sup>

However, the mentioned cancer properties are necessary but not sufficient to describe the overall picture, since tumor development involves healthy cells as well (e.g., vascular endothelial cells).<sup>6</sup>

### 1.1 Mutual Connections Between Cancer and Inflammation

**Inflammation** is the physiological phenomenon more related to cancer growth and proliferation, and epidemiological studies have established that nearly 15% of cancer cases in the world is associated with infection and resulting inflammation.<sup>7</sup> Furthermore, even in 1863 *Virchow* hypothesized that cancer was originated by chronic irritation triggered by microbial infections, autoimmune diseases, inflammatory conditions without certain origin and the presence of inflammatory cells and mediators (e.g. chemokines, cytokines and prostaglandins)

in tumour tissues, hallmarks of linkage between cancer and inflammation.<sup>8</sup>

In response to injured tissue, a chemical signaling network initiates and maintains the host response involving activation and directed migration of leukocytes (e.g. neutrophils) from the venous system to sites of damage. It is known that neutrophils use a four-step mechanism to recruit the inflammatory cells to injury sites and to the provisional extracellular matrix (ECM).<sup>9</sup> These steps are: 1) activation of selectins (adhesion molecules); 2) activation and upregulation of leukocyte integrins mediated by cytokines and leukocytes themselves; 3) immobilization of neutrophils on the surface of the vascular endothelium by means of tight adhesion through  $\alpha_4\beta_1$  and  $\alpha_4\beta_7$  integrins, and 4) transmigration through the endothelium to sites of injury (probably by extracellular proteases such as matrix metalloproteinases - MMPs).<sup>10</sup>

The linkage between inflammation and cancer is composed by two different pathways: *extrinsic pathway* (inflammatory conditions related with an increased cancer risk) and *intrinsic pathway* (genetic alterations responsible for the onset of inflammation and neoplasia) (Figure 1.3).<sup>8</sup> The second route is the most interesting because associated with an impressive number of endogenous responses that lead to tumor development.

Early 2000's studies suggest that the induction of genetic instability by inflammatory mediators is an additional mechanism involved in cancer-related inflammation (CRI). As a consequence, the infiltration of white blood cells has been observed (tumor-associated macrophages - TAMs) along with reactive oxygen species, proteases, Matrix MetalloProteinases (MMPs), membrane perforating agents, cytokines (e.g. tumor necrosis factor - TNF), interleukin (e.g. IL-1), chemokines, tissue remodeling and angiogenesis.<sup>11</sup>

Among the mentioned features, it is noteworthy the dual role of TAMs that kill neoplastic cells following activation by IL-2 and produce angiogenic and lymphangiogenic growth factors. Moreover, TAMs and tumour cells produce IL-10, which inhibits the anti-tumour response by cytotoxic T-cells. Finally, TAMs are capable to express several Vascular Endothelial Growth Factor (VEGF) subtypes and associated receptors which are implicated in the formation of lymphatic vessels and lymphatic metastases.<sup>12</sup>

CRI employs several endogenous promoters including transcription factors (e.g. nuclear factor-kappaB - NF- $\kappa$ B) and inflammatory cytokines (e.g. IL-1 $\beta$  and TNF- $\alpha$ ). NF- $\kappa$ B controls inflammatory cell populations fostering cytokines TNF- $\alpha$  and IL-1 $\beta$  (both in inflammatory and cancer cells, and its aberrant regulation has been observed in many tumors). NF- $\kappa$ B is also involved in the expression of inflammatory cytokines, adhesion molecules and enzymes which are fundamental in the prostaglandin synthase pathway, nitric oxide (NO) synthesis and angiogenic factors. Furthermore, it promotes tumor cells survival and the initiation/progression of CRI.<sup>13</sup>

Along with NF- $\kappa$ B, STAT3 (a gene encoding Signal transducer and activator of transcription 3 - Stat3) is a key point of several oncogenic signaling pathways. In 2009, Lee et al. showed that STAT3 is required to keep NF- $\kappa$ B active<sup>14</sup> and it is one of the most important check-

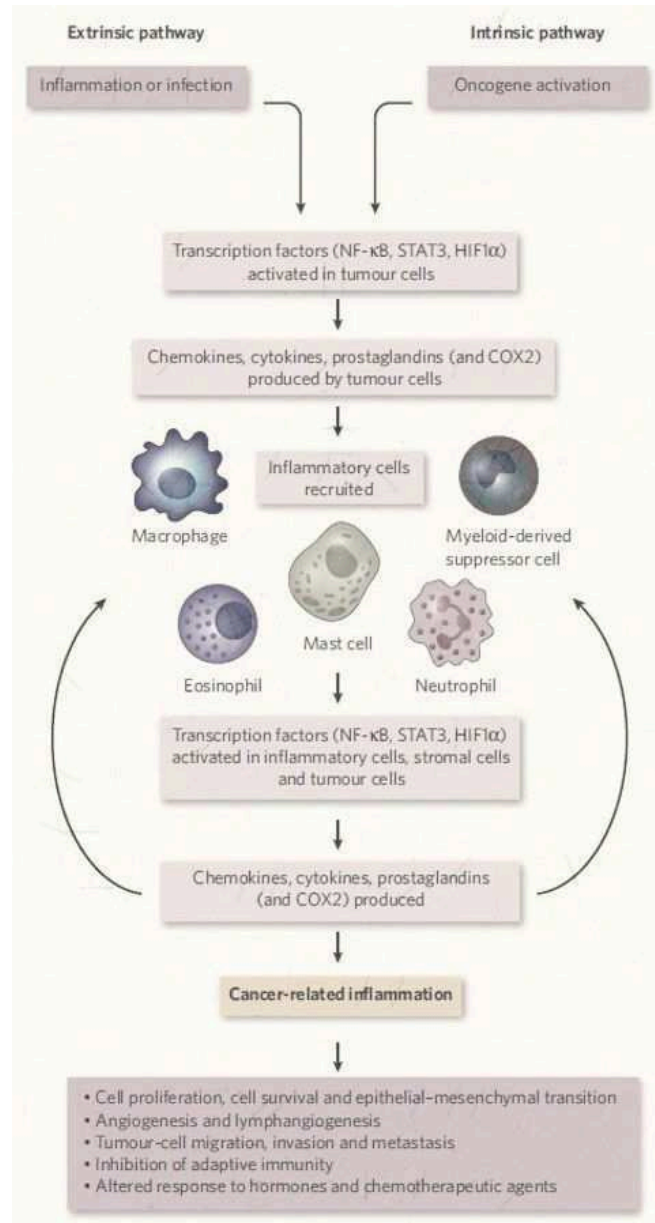


Figure 1.3: Connection between inflammation and cancer (adapted from Mantovani A. et al.<sup>8</sup>)

points of cell proliferation and survival. IL-6, a multi-functional cytokine promoting the growth and antiapoptotic activity in unhealthy tissues, is the major effector in the activation of NF- $\kappa$ B and is also related to STAT3, generating the NF- $\kappa$ B-IL-6-STAT3 cascade. IL-6 protects both normal and premalignant intestinal epithelial cells from apoptosis, promotes the proliferation of tumor cell primer, promotes liver inflammation, injury and carcinogenesis.<sup>15</sup>

Among pro-inflammatory cytokines, the Tumor Necrosis Factor (TNF) is the most important one and it has been revealed a protumoral molecule involved in the tumor growth and invasion, leukocyte recruitment, and angiogenesis; it also facilitates epithelial to mesenchymal transition.<sup>16</sup>

IL-1, another cytokine subtype, has long been known to improve the metastasis formation acting on CRI cascade, together with TNF and IL-6. Two different IL-1 subsets (IL-1b and IL-1ra) act in opposite ways to each other: IL-1b contributes to increase the tumor adhesiveness, invasion, angiogenesis and immune suppression, whereas IL-1ra, on the contrary, operates a negative control of the processes.<sup>17</sup>

Finally, Myc is an oncogene encoding a transcription factor over-expressed in many human tumours and, in addition to promoting cell proliferation, it controls the remodelling of the extracellular microenvironment in which inflammatory cells and mediators are fundamental for the process. Thus, the activated transcriptional program elicits the production of several chemokines that recruit mast cells which drive angiogenesis and sustain new blood-vessel formation for the tumour growth (Figure 1.4).<sup>18</sup>

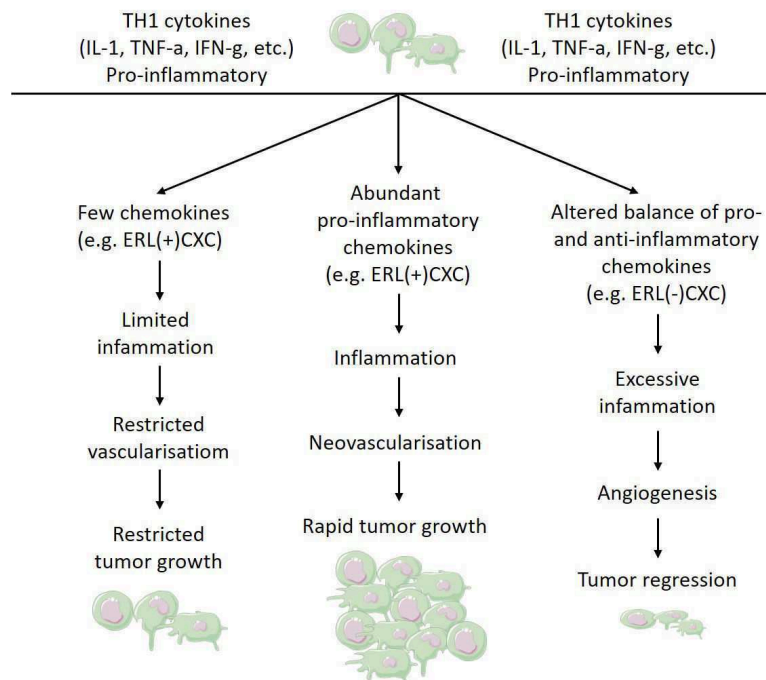


**Figure 1.4:** Dual role of cytokines and chemokines in inflammatory processes (modified from *Coussens L. M. et al.*<sup>10</sup>)

On the other hand, inflammatory conditions increase cancer development and the triggers of this growth are infections, autoimmune diseases and inflammator conditions of unknoun origin.<sup>11</sup> The presence of all these factors show that an early genetic event is necessary and sufficient for building-up an inflammatory microenvironment related to a tumor development. On the contrary, evidences suggest that the inflammation response and immune systems may inhibit the development of cancer processes. This is supported by two cancer-associated recognition events: 1) the presence in the host of mechanisms to detect and eliminate the transformed cells; 2) the recognition by the immune system of antigens associated with cancer cells.<sup>19</sup>

The fundamental aspect to take into account regarding the linkage between inflammation and cancer is that normal inflammation is self-limiting; however, dysregulation of any gears of the process can increase pathogenesis, such as neoplastic progression.

In this context, a family of structurally related cell surface heterodimers, namely **integrin** receptors<sup>20</sup>, is important for the interactions of cells with extracellular matrix and for the development of both inflammation and carcinogenic phenomena. These interplays are apical in determining the behavior during cell growth, differentiation and migration, playing important roles in cancer progression. For this reason, researchers have identified these receptors as very promising biological targets, spending a lot of efforts on the development of efficacious drugs that use these receptors as a targets to contrast tumor expansion.

## 1.2 Integrins

Human health and tissue integrity are mainly regulated by cell adhesion to the extracellular matrix. **Integrins** represent the most important family of cell adhesion receptors and their expression is frequently altered in tumours, where these receptors have roles in supporting oncogenic growth factor receptor (GFR) signalling, from primary tumour development to metastasis.<sup>21</sup>

Integrins are cell surface receptors structurally comprised of non-covalent associations between  $\alpha$  and  $\beta$  subunits. Both subunits are type I transmembrane glycoproteins made up of three distinct parts: a relatively large extracellular domain, a single transmembrane domain and a short cytoplasmic tail.<sup>22</sup> In mammals, each tissue contains different integrin heterodimers among 24 possible non-covalent associations of 18  $\alpha$  subunits and 8  $\beta$  subunits. Moreover, in addition to this tissue specificity, a peculiar binding affinity is exhibited between each integrin and a specific ligands (Figure 1.5).<sup>23</sup>

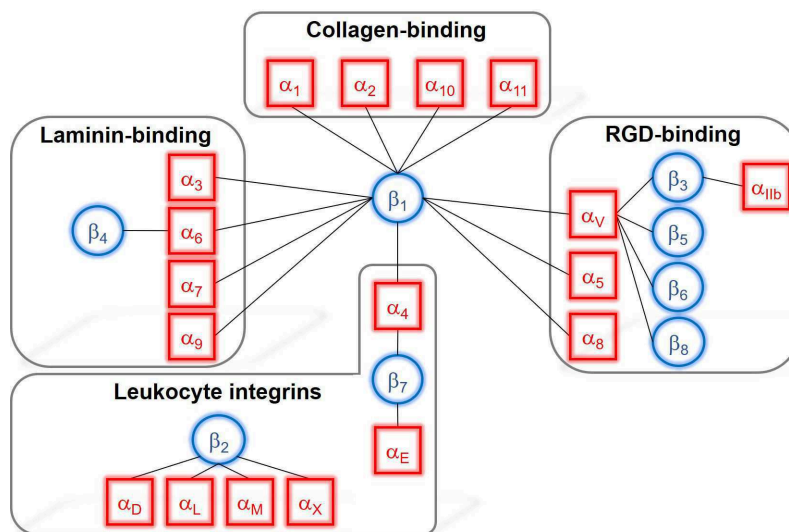


Figure 1.5: Ligand-based integrins classification (modified from Tolomelli A. et al.<sup>24</sup>)



The greatest influence on ligand-binding specificity is provided by the  $\alpha$ -subunit type and allows to classify the integrins in several ligand-dependent families: 1) *Arg-Gly-Asp* (RGD) motifs-binding  $\alpha_{IIB}$ ,  $\alpha_V$ ,  $\alpha_5$  and  $\alpha_8$ ; 2) intercellular adhesion molecules and inflammatory ligands  $\alpha_4$ ,  $\alpha_D$ ,  $\alpha_E$ ,  $\alpha_L$ ,  $\alpha_M$  and  $\alpha_X$ ; 3) collagens-binding  $\alpha_1$ ,  $\alpha_2$ ,  $\alpha_{10}$  and  $\alpha_{11}$ , and 4) laminins-binding  $\alpha_3$ ,  $\alpha_6$ ,  $\alpha_7$  and  $\alpha_9$ .<sup>24</sup> While some integrins bind only specific ECM ligands (e.g., fibronectin for  $\alpha_5\beta_1$  integrin), others exhibit a broader ligand binding (e.g.,  $\alpha_V\beta_3$  integrin to fibronectin, vitronectin, fibrinogen and thrombospondin).<sup>23</sup> As a consequence, distinct cells signaling can be triggered by the engage with the same ligand by different integrin heterodimers and thus the cell behaviour is finely tuned by the integrin expression on the cell surface.<sup>22,25</sup>

The adhesiveness in cell-cell and cell-matrix interactions is not the unique role of integrins; in fact, they can transmit information regarding their ligands into cells, regulating migration, survival and growth of the cells. Moreover, cell shape, motility, proliferation and cell-type-specific gene expression are some of features controlled by intracellular signaling pathways. These receptors arise in the endoplasmic reticulum from the dimerisation of  $\alpha$  and  $\beta$  subunits and, upon post-translational modifications in the Golgi, are trafficked to the cell surface in an inactive conformation that will become active during the ligand binding.<sup>26</sup>

Indeed, integrins are usually in an *inactive* form with low affinity for their endogenous ligands, but upon various stimuli they rapidly convert into an *active* form. The active state, with different ligand binding affinities, is achieved by intracellular signaling (*inside-out* signaling) and, as bidirectional receptors, integrins can also transmit signals back into cells (*outside-in* signaling). The transmission of an *outside-in* signaling upon ligand binding in the extracellular domain activates all the processes mentioned above.<sup>24</sup>

The structural conformations of the two  $\alpha$  and  $\beta$  subunits are fundamental for the ability of integrins to bind to various components of the extracellular matrix (ECM) or soluble ligands and to regulate also both inside-out and outside-in cell signaling; for example, during ligand binding, the abrogation of a salt bridge (which stabilises the resting state of the receptor) formed by  $\alpha$  and  $\beta$  subunit tails strengthens the binding between integrin and ECM ligand.<sup>27,28</sup>

Conversely, conformational changes in integrin structure are induced by the binding of ECM ligands, producing dissociation of the transmembrane helices and contributing to clustering into oligomers, thereby leading to outside-in signaling.<sup>29</sup>

From a structural point of view, the  $\alpha$ -subunits can be divided in  $\alpha$ -subunits with an inserted domain ( $\alpha I$  domain), in which the  $\alpha I$  domain is the binding site for ligands) and in  $\alpha$ -subunits without the inserted domain, in which the ligand-binding site is formed at the interface between the  $\alpha$  and the  $\beta$ -subunit in its  $\beta I$  domain.<sup>27</sup> Thus, in the second type of integrins, the  $\beta$ -subunit contributes to modulate the ligand specificity. The  $\alpha I$  and  $\beta I$  domains are structurally homologous and can bind *Asp*, *Glu* or carboxylic acid residues in ligands by means of a metal ion-dependent adhesion site (MIDAS).

In RGD-binding integrins (without  $\alpha 1$ ), the Arg moiety binds the  $\alpha$ -subunit while the Asp coordinates to a  $Mg^{2+}$  ion in the  $\beta I$  domain MIDAS.<sup>24</sup> Regarding active/inactive forms, structural studies (crystallography, NMR and EM studies) have revealed three overall conformational states: *bent* (low affinity conformer), *extended-closed* (activated) and *extended-open* (activated together with ligand-occupied integrin conformers) conformations.<sup>30</sup> It is well accepted that the extended-open integrin conformation corresponds to the conformation with highest affinity for the ligand.

During the binding of extracellular ligands, the stabilisation of this conformation produces enhanced separation of the integrin intracellular tails that, in turn, transmit signals to the cytoplasm (outside-in signaling). For this reason, for many integrins (if not all), such conformational changes are required to "switch-on" their adhesive function and signal transduction (Figure 1.6).<sup>31</sup>

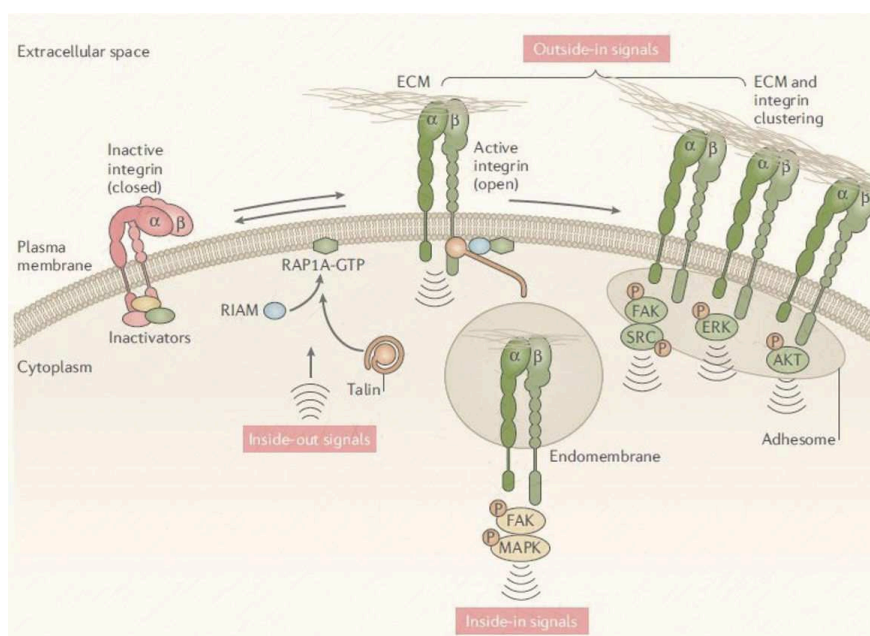


Figure 1.6: Mode of action of the integrin receptors (adapted from Hamidi H. et al.<sup>21</sup>)

Regarding this integrin feature, recently it was reported that N-glycosylation affects the conformational equilibria of integrins and their activation. More specifically, it has been verified that minor N-glycosylation on  $\alpha_5\beta_1$  integrins corresponds to more stable bent-closed/extended-closed conformations, with lower affinity to ligand binding.<sup>32</sup>

From a biological point of view, it was demonstrated that the integrins and adhesion constituents have a strategical role in the cross-talk interactions between outside and inside of the cells, playing as an essential gear in the regulating aspects of cell fate such as cell proliferation, invasive protrusions, influence on tumour-stroma crosstalk and resistance to apoptosis, contributing, as a consequence, to arise aggressive diseases.

As mentioned before, outside-in signaling is activated by ligands binding to integrins which

triggers the recruitment of the adhesome, an array of signalling, scaffolding and cytoskeletal proteins engaging directly or indirectly with integrin cytoplasmic tails.<sup>33</sup> Therefore, for normal physiological function, a tight regulation of signaling via integrins is paramount and a misregulated activity is associated with the pathogenesis of many human diseases, including bleeding disorders, cardiovascular disease and cancer.<sup>34</sup>

### 1.2.1 Role of Integrins in Cancer Cells Communication

Integrins also play a fundamental role in other cancer processes including metastases, drug resistance, white blood cell trafficking and activation, chronic inflammation, immune mimicry and angiogenesis.<sup>21</sup>

However, the mere expression of integrin receptors is a multi-level phenomenon and these receptors are constantly endocytosed and recycled back. The kinetics of these processes are frequently altered in cancer cells, resulting in an abnormal number of receptors on the cell surface that alter the adhesion functions and increase integrin signaling.<sup>34</sup> Looking at the number of integrin-dependent processes, it is evident that these receptors have been implicated in almost every step of cancer progression and at the moment it is not completely understood how integrin ligands activate or inhibit this cross-talk.<sup>35</sup>

In particular, they play a critical role in local invasion and intravasation into vasculature, the survival of circulating tumour cells (CTCs), extravasation into the secondary site and metastatic colonization of the new tissue. For most solid tumours, the integrins contribute to metastatic cascade upregulating the expression of matrix metalloproteinase gene responsible of the extravasation process. In these events, invasive carcinomas penetrate the stroma and migrate into the surrounding tissues as individual cells or as cell clusters by multiple and different integrin-dependent mechanisms (Figure 1.7).<sup>36</sup>

As a consequence of the continuous entry of cancer cells into the bloodstream, CTCs are readily detected in unhealthy patients. However, while normal epithelial cells undergo *anoikis* (a specialized form of programmed apoptosis),<sup>37</sup> altered integrin signaling generates anoikis resistance in CTCs.<sup>38</sup> For a successful metastatic process, CTCs must attach distant organs and extravasate into the perivascular tissue where integrins, binding ECM ligands, dictate whether the seeded cancer cells continue to proliferate or become dormant.<sup>39</sup>

From another point of view, integrins are able to activate transforming growth factor- $\beta$  (TGF $\beta$ ) that is a tumour suppressor<sup>40</sup> until the cancer becomes resistant to the anti-proliferative effects of TGF $\beta$ ; after this behaviour change, the same integrins can drive tumour progression.

Under a more specific aspect, genetic depletion of  $\beta_1$  integrin induces a compensatory up-regulation of  $\beta_3$  integrin that may promote activation of TGF $\beta$  in breast cancer cells.<sup>41</sup> However, the pro-metastatic response cannot be explained by  $\beta_3$  integrin overexpression, suggesting that other factors are involved in the regulation of TGF $\beta$  signalling.

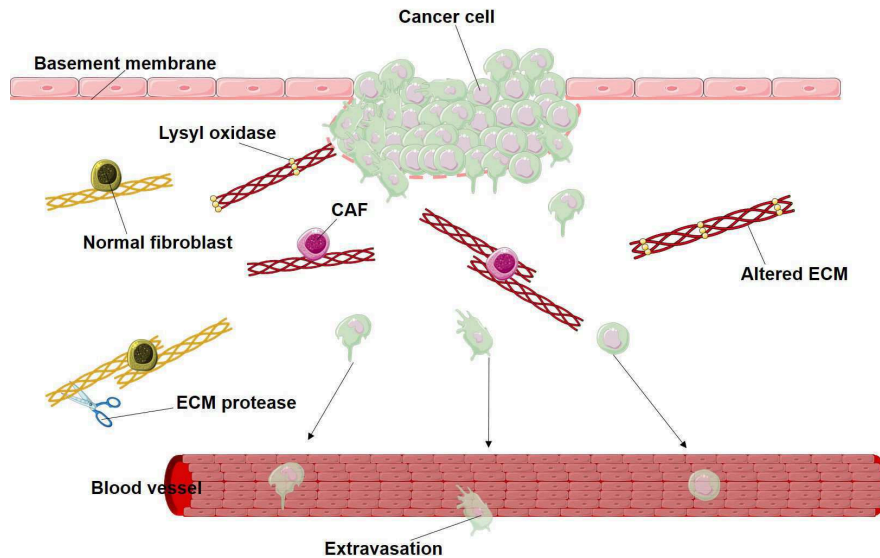


Figure 1.7: Integrin-based extravasation process of cancer cells (modified from Hamidi H. et al.<sup>21</sup>)

Being the principal receptors for endogenous ECM ligands in normal physiological processes, integrins are pivotal in regulating cell motility (e.g., wound development, wound healing and cancer dissemination). "Non-motile tumours" undergo rapidly growth inhibition due to steric hindrance and crowding, whereas higher growth rates are reached by local cell dispersal.<sup>42</sup> Moreover, a general aspect that is emerged by biological studies is that the crosstalk between integrins (or other cell adhesion receptors) and actin cytoskeleton is a fundamental feature for cancer cell migration.<sup>21</sup>

On the other hand, the cancer-associated ECM is a rich source of pro-migratory and pro-invasive cues that provide a suitable microenvironment to cancer progression. In this respect, microscopy analysis in mouse breast tumor models have suggested that a relevant parameter for predicting breast cancer dissemination is collagen reorganization at the tumor-stromal interface.<sup>43</sup> In addition, intravasation and metastasis of mammary tumour are enhanced by elevated collagen deposition in the ECM. In fact, the mediation carried out by integrin collagen-binding may alter collagen deposition and this evidence can be a general hallmark of poor prognosis in cancer.

Classically, integrin functions in cancer regulation have been considered to be restricted to the plasma membrane and to the adhesion process. However, in the last years researchers have identified unconventional integrin-mediated mechanisms promoting cancer cells survival and metastasis. Several hypothesis have been formulated to explain the endocytosis trigger of active integrins and the most interesting one is that, upon matrix degradation, the uptake of active integrins is enabled by loss of ECM tension. In accordance with this hypothesis, researchers have detected integrins and corresponding ligands (e.g. fibronectin) in endosomes of cancer cells.<sup>44</sup>

While the biology and cancer relevance of integrin endosomal signalling require deep stu-

dies, the role of integrins in anoikis resistance via other mechanisms is well established. For example, the "outside-in" integrin signaling entails ligand binding and receptor clustering, but in non-anchored cells the integrins clustering by binding with ECM ligands is lost.

On the other hand, in healthy cells such events are sufficient to trigger anoikis; however, anoikis resistance is conferred by upregulation of specific integrins.  $\alpha_V\beta_3$  integrins are the only one that are able to maintain receptor clustering in non-adherent cells and this feature lends anoikis resistance to cancer cells by recruiting SRC (a family of nonreceptor tyrosine kinases) to the  $\beta_3$  subunit tail and leading to SRC activation and cell survival.<sup>45</sup> In addition, several studies suggest that integrin-binding to non-structural ECM component can provide anoikis resistance.

Another contribution to cell-cell communication occurs by means of exosomes, small membrane-bound vesicles released by healthy and unhealthy cells. On the surface of these vesicles, integrins are the most expressed receptors and it was demonstrated that they can drive these vesicles to specific sites to act as "primers" of the metastatic niche.<sup>46</sup>

For the circulating tumour cells (CTCs) survival, extravasation is the next critical step related to the integrin expression both on cancer cells and endothelial cells which use these receptors to interact with the underlying basement membrane.<sup>21</sup> Regarding these processes, it is noteworthy that the blood vessel integrity is regulated by the cell-ECM contacts combined with protein tyrosine kinase-induced signalling.<sup>47</sup> In cancer, for example, a fine tuning of angiopoietin 2 (ANG2) signalling and levels of angiopoietin receptor (TIE2, also known as TEK) increases vascular permeability and ANG2 blocking antibodies can inhibit metastasis. On the contrary, when the cancer takes control of these mechanisms, the absence of TIE2 leads to the interaction between ANG2 and  $\alpha_5\beta_1$  integrin, which results in compromised vascular integrity.<sup>48</sup>

Interaction between endothelial  $\alpha_5$  integrin and neuropilin 2 (NRP2) contributes to extravasation of cancer cells. Evidence in zebrafish and mouse cancer models highlight that the vascular extravasation and cancer cell binding to endothelium are facilitated by the NRP2- $\alpha_5$  trans-interaction.<sup>49</sup> Thus, the clinical correlation between elevated NRP2 levels and metastasis in breast cancer is strongly associated to endothelial  $\alpha_5$  integrin expression.

In addition to the active role of  $\alpha_5$  subunits in extravasation of cancer cells, even the inhibition of  $\beta_1$  integrin plays a relevant role both in formation and reduction of metastatic foci of several cancer types. However, it is not completely clear how  $\beta_1$  integrin regulates specific metastatic steps and to overcome this issue the researchers have used an in vitro model of microvasculature. It has been elucidated that the initial contact between cancer cell and the subendothelial matrix is stabilised by  $\beta_1$ -mediated adhesion and activation. Then, after the elimination of the endothelial barrier,  $\beta_1$  integrins are necessary to the cancer cell to invade the vessels through the basement membrane. These insights are in agreement with the findings that an increased metastatic colonisation in the mouse liver is activated by the expression of activated mutants  $\beta_1$  integrins.<sup>50</sup> In conclusion, biological studies suggested

that the extravasation is coupled to an increased integrin activity in cancer or endothelial cells, promoting an intense development of drugs selective towards these transmembrane receptors.<sup>21</sup>

The above reported information suggest a complex role of  $\alpha_V\beta_3$  and  $\alpha_5\beta_1$  in cancer physiology. For this reason, among the 24 possible integrin heterodimers, RGD-binding subtypes  $\alpha_V\beta_3$  and  $\alpha_5\beta_1$  represent two interesting holds for further studies.

*Ruoslahti* and coworkers<sup>51</sup> identified these two integrin subtypes in 1985 and named them according to their endogenous ECM ligands as *vitronectin* (VN) and *fibronectin* (FN) receptors, for  $\alpha_V\beta_3$  and  $\alpha_5\beta_1$  respectively. As described by *Ruoslahti* in 1984, the RGD sequence is recognized by both subtypes as minimal adhesive binding motif and to date, one third of the 24 integrin subtypes are reported to bind this sequence.<sup>52</sup> In particular,  $\alpha_V\beta_3$  binds several ECM proteins including FN, VN and osteopontin, whereas  $\alpha_5\beta_1$  integrin, due to the presence of the sequence PHSRN in the ligand-binding site of the protein, can primarily recognize FN. Nevertheless, other ECM endogenous proteins have been described to bind both integrins with various degrees of affinity.<sup>52</sup>

Integrins are able to form and develop focal contacts and in 2000, *Geiger* verified that the nascent focal complexes were rich in  $\alpha_V\beta_3$ , while in mature fibrillar (FAs) were present  $\alpha_5\beta_1$ .<sup>53</sup> Moreover, different organizations of the actin cytoskeleton and, therefore, of cell shape were associated with each integrin subtype. Furthermore, in 2013 *Rahmouni* and coworkers<sup>54</sup> verified that  $\alpha_5\beta_1$  integrins exert higher forces than  $\alpha_V\beta_3$  in cell binding to endogenous substrate. In another study, *Fässler's* group has shown that force generation is accomplished by  $\alpha_5\beta_1$  integrins, whereas adaption to forces on FN-based microenvironment is structurally mediated by  $\alpha_V$  subtypes. All these studies have highlighted different functions of both integrin subtypes, which cooperate to regulate rigidity sensing of cells and cell contractility.

On the other hand, it was shown that cell proliferation and differentiation were influenced by the engagement of a specific integrin subtype; however, the role of the  $\alpha_V\beta_3$  and  $\alpha_5\beta_1$  subclasses in these processes is still unclear. Several studies have demonstrated that the  $\alpha_5\beta_1$  receptor is able to support cell adhesion and proliferation.<sup>55</sup> *Martino* and coworkers<sup>56</sup> have reported the different affinities of FN fragments for  $\alpha_5\beta_1$  pointing out that this receptor was blocked in its proliferation function by high affinity substrates (containing both RGD and PHSRN sequences), while cell growth was still fostered by full-length FN motif due to numerous unspecific signals mediated by other receptors. On the other hand, only few studies were focused on  $\alpha_V\beta_3$  behaviour in these processes and they were contradictory as well.

To explain these discrepancies, different reasons can be taken into account. Each integrin subtype is usually associated to specific ECM ligand, but the determination of their binding affinity for other subtypes is often neglected. Thus, one specific integrin receptor may be

associated to a particular biological effect, even though the role of other integrins could be underestimated. Moreover, cell type, culturing conditions and substrate could strongly condition the pattern of integrin expression on each cell, thus not allowing a direct comparison between different studies. On top of that, integrins have overlapping roles, thus a different integrin subtype can substitute a blocked one in the suppressed biological function.<sup>57</sup>

A very hot topic, developed in the last ten years, is the role of  $\alpha_V\beta_3$  and  $\alpha_5\beta_1$  on the differentiation of Mesenchymal Stem Cells (MSCs), with rising interest in stem cell therapies and in the development of cell instructive biomaterials. In this regard, it is not yet fully established the role of integrins in the progression of the undifferentiated cell towards a specific lineage. For example,  $\alpha_5\beta_1$  subtype has demonstrated a positive role in the induction of osteogenesis and it has shown to upregulate the expression of osteogenic markers in vitro<sup>58</sup> and to induce osseointegration of implants in vivo.<sup>59</sup>

On the other hand, the role of  $\alpha_V\beta_3$  subtype remains controversial; in several studies a suppression of osteoblastic differentiation caused by this receptor was claimed;<sup>60</sup> while an increased matrix mineralization due to the binding of  $\alpha_V\beta_3$  was highlighted in others.<sup>61</sup> On this regard, ten years ago *Kilian* and *Mrksich* demonstrated that MSCs were directed toward the osteoblastic lineage by means of the binding of a high affinity cyclic RGD peptide with  $\alpha_V\beta_3$  receptor.<sup>62</sup> They observed a greater cell spreading on surfaces coated with the cyclic peptide and an increased expression of several osteogenic markers. Surprisingly, a myogenic differentiation was instead induced by linear RGD peptide with a lower affinity for  $\alpha_V\beta_3$ . However,  $\alpha_V\beta_3$  was object of few studies focused on their osteogenic potential, since bone resorption was the main investigated role of this receptor. In fact,  $\alpha_V\beta_3$  receptors are greatly expressed on the surface of osteoclasts, making these cells the primary ones for expression of this receptor. Several studies have demonstrated that this integrin subtype mediates the binding of osteoclasts to the ECM and bone resorption is inhibited by interference with this receptor<sup>63</sup> attributing this effect to the  $\alpha_V\beta_3$ -dependent migration of osteoclasts. It is noteworthy that the  $\alpha_V\beta_3$ -dependent cell migration has been observed in many other cell types (e.g. endothelial cells and different tumor cell lines).<sup>64</sup>

In fact, physiological and pathological angiogenesis, which are crucial steps in tumor development and metastasis formation, are finely regulated by  $\alpha_V\beta_3$  integrin. At the beginning of tumor growing, "angiogenic switch" can be induced in dormant tumors through hypoxia, thus inducing secretion of growth factors, such as VEGF, leading to upregulation of integrins themselves.<sup>65</sup> Thus,  $\alpha_V\beta_3$  integrin binds its endogenous ECM ligands activating endothelial cells migration in the formation of new blood vessels which provide oxygen and nutrients to cancer cells.<sup>66</sup> Since the first studies, pathological angiogenesis was associated to the involvement of  $\alpha_V\beta_3$  receptor<sup>67</sup> showing upregulation of this subtype on tumor cells. However, animal models have shown that this receptor was important, but non essential since mice lacking  $\alpha_V$  shown widespread angiogenesis and mice lacking  $\beta_3$  and  $\beta_5$  subunits shown pathological angiogenesis.<sup>68</sup>

On the other hand, the biological role of  $\alpha_5\beta_1$  in angiogenesis is controversial since its up-regulation during angiogenesis and on blood vessels as well as its collaboration with EGFR suggests a tumor-promoting role.<sup>69</sup> However, other studies pointed to a tumor-dependent behaviour, with a promoting role in certain tumors and an inhibitory role in others. In 2010, *Hynes* and coworkers<sup>70</sup> have shown that in vascular remodelling,  $\alpha_V$  and  $\alpha_5$  integrins could work together and even replace each other.

### 1.3 Integrin Ligands: Structural Information

The first important discovery from the point of view of medicinal chemistry was found by *Pierschbacher* and *Ruoslahti* in 1984, who claimed that the minimal cell-binding motif in FN was the tetrapeptide *Arg-Gly-Asp-Ser* (RGDS).<sup>71</sup> Further investigations revealed that only the first three amino acids were essential for the binding, while the fourth could have been substituted without loss of the biological activity. Interestingly, the **RGD** motif was also found in fibrinogen and type I collagen, and other proteins containing this short peptide sequence also supported cell attachment.<sup>71</sup> These studies suggested that the RGD sequence in ECM ligands bound receptors of several cellular lineage and more detailed studies identified the tripeptide sequence in many ECM proteins, including VN, osteopontin and laminin.<sup>72,73</sup> Even if several studies have demonstrated that integrins recognise ECM proteins by means of the RGD sequence, the reasons behind this interaction were not trivial. For example, the subtypes  $\alpha_V\beta_3$  and  $\alpha_5\beta_1$  have shown mutually exclusive interactions with the endogenous proteins. In detail, liposomes containing  $\alpha_5\beta_1$  bound FN-coated surfaces but not VN-coated ones and the opposite behavior was observed for  $\alpha_V\beta_3$  receptors.<sup>74</sup> Nevertheless, both receptors were inhibited by the same RGD sequence and it has been well-established that multiple factors were relevant for the specificity of ligand-integrin interaction. Although there are significant examples regarding integrin specificity conferred by synergistic domains (e.g. PHSRN sequence in  $\alpha_5\beta_1$ -FN interaction),<sup>75</sup> the conformation and spatial arrangement of the RGD motif in the ECM ligands is one of the most important aspects of their interaction.<sup>76</sup>

There are many tricks to improve the bioactivity and receptor selectivity of exogenous ligands; one of this is to integrate the amino acid sequence into a cyclic peptide in such a way to restrict its conformational space.<sup>77</sup> Early studies have shown that an improved inhibition of VN-mediated adhesion of fibroblasts was obtained using a disulfide-bridged RGD cyclopeptide, but no effects regarding cell adhesion FN-mediated ones (compared to the unselective linear peptide).<sup>78</sup> In a parallel study, suppression of the inhibitory activity is observed after the reduction of disulfide bridge in an RGD-containing cyclic peptide, likely due to a reduced affinity for the receptor by means of the loss of the bioactive conformation.<sup>79</sup>

In this context, in 90's *Kessler* and coworkers<sup>80</sup> have carried out a series of studies to elucidate the effect of peptide conformation on the selectivity towards integrin subtypes. A *spatial*



screening, a process in which the researchers observe the effect of a single D-amino acid substitution in a cyclic peptide, resulted in the development of the pentapeptide **c(RGDfV)** which showed a 100-fold increased inhibition of the adhesion compared to the linear control peptide, as well as an improved selectivity against  $\alpha_{IIb}\beta_3$  subtype (Figure 1.8). Using this peptide, the researchers have observed a disruption of tumor-induced angiogenesis in a chick model and it has led to the development of many  $\alpha_V\beta_3$  selective derivatives.<sup>80</sup> As such, *Kessler's* group have adopted a series of tools to improve the very remarkable results obtained with **c(RGDfV)**, such as the incorporation of turn mimetics, the synthesis of retro-inverso analogues, the reduction of peptide bond and the use of sugar amino acids.<sup>81</sup> For this purpose, they<sup>82</sup> developed a drug candidate called **Cilengitide** resulting from the N-methylation of **c(RGDfV)** peptide, which provides an antagonistic activity against  $\alpha_V\beta_3$  in the subnanomolar range ( $IC_{50} = 0.58$  nM) and a nanomolar range activity against  $\alpha_V\beta_5$  and  $\alpha_5\beta_1$  ( $IC_{50} = 11.7$  nM and  $IC_{50} = 13.2$  nM, respectively)(Figure 1.8). Moreover, *Sewald's* group has investigated the role of  $\beta$ -amino acids in the secondary structure of several cyclic RGD peptides. From this study, they have obtained the cyclic pentapeptide containing a constrained *cis*- $\beta$ -aminocyclopropanecarboxylic acid motif ( $\beta$ -Acc). **c(RGD-(+)- $\beta$ -Acc-V)** exhibited a good activity against  $\alpha_V\beta_3$  integrin ( $IC_{50} = 20$  nM), but the more interesting poin was the good selectivity over  $\alpha_5\beta_1$  one ( $IC_{50} = 1.5$  mM) in a cellular adhesion assay to FN (Figure 1.8).<sup>83</sup>

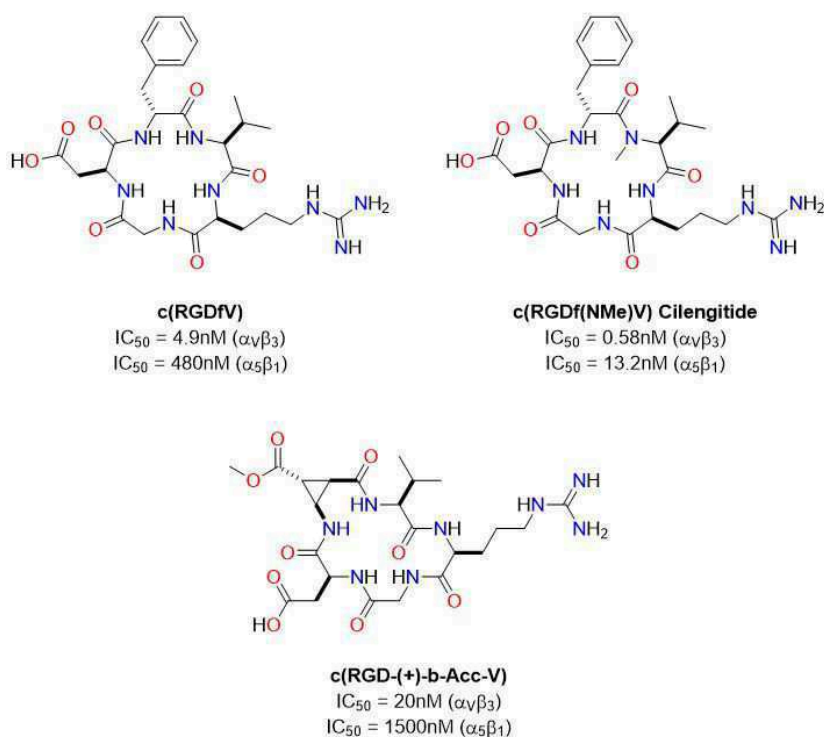


Figure 1.8: **c(RGDfV)**, Cilengitide and **c(RGD-(+)- $\beta$ -Acc-V)** structures and biological activity.

Cilengitide features (being cyclic and N-methylated) allowed to overcome the critical per-

spectives connected to the very poor enzymatic stability of peptidic compounds, making it quite stable to the metabolic conditions.<sup>84</sup> As a consequence of its high activity against proangiogenic  $\alpha_V\beta_3$  integrins and its selectivity against  $\alpha_{IIb}\beta_3$  subtype, Cilengitide had been selected as a drug candidate for the treatment of several tumor types; unfortunately, it failed in phase III clinical trial (in combination with chemoradiotherapy) to improve survival of patients with glioblastoma.<sup>85</sup>

To explain this, a deeper study has revealed that a cross-talk between  $\alpha_5\beta_1$  integrin (not described for  $\alpha_V\beta_3$  subtype) and the tumor suppressor protein p53 exists to overcome the induction of apoptosis in glioma cells. Thus, the lack of efficacy of Cilengitide in the treatment of glioblastoma could be explained by the reduced affinity of the peptide towards  $\alpha_5\beta_1$ .<sup>86</sup> Nevertheless, at the moment Cilengitide is one of the most powerful and promising drug candidate that are studied to reach a lead compound for the cancer treatment, even if none integrin ligand targeting  $\alpha_V\beta_3$  or  $\alpha_5\beta_1$  is still approved by FDA as drug for the tumor treatment.<sup>87</sup>

For more than 20 years, several research groups have focused their attention to identify a compound targeting the  $\alpha_5\beta_1$  integrins. In this regard, *Kessler* and *Ruoslahti's* groups have developed cyclic and linear peptides with good activity towards  $\alpha_5\beta_1$  subtype, but with no remarkable selectivity over  $\alpha_V\beta_3$  one. On this topic, several efforts have been carried out and all these studies show a relevant problem for the development of peptide with higher activity towards  $\alpha_5\beta_1$  and higher selectivity over  $\alpha_V\beta_3$ . In this regard, cyclic peptide containing a reverse RGD sequence in which the peptide bond between the second and third amino acid is performed on the side chain of Asp residue, called *isoDGR* motif, represents one of the few examples able to overcome these setbacks. This sequence was identified in 2006 by the *Corti's* research group as an unexpected integrin binding motif and one year later the *Kessler's* research group designed a head-to-tail cyclic peptides containing the *isoDGR* motif (Figure 1.9).<sup>88</sup> In these peptides, *Kessler* and coworkers<sup>89</sup> have inserted a Gly residue to flank the *isoDGR* sequence and an aromatic amino acid (in either the L- or D-configuration) since they have observed its crucial role in  $\alpha_V\beta_3$  binding. Interestingly, the relative affinity towards  $\alpha_V\beta_3$  or  $\alpha_5\beta_1$  is strictly dependent by the relative position of the flanking residues (*c(phg-isoDGR-G)*,  $IC_{50} = 19$  nM for  $\alpha_5\beta_1$  and inactive against  $\alpha_V\beta_3$ ; *c(G-isoDGR-phg)* exhibits the opposite biological behavior) (Figure 1.9).<sup>90</sup>

After the discovery of the  $\alpha_5\beta_1$ -selective peptide *c(phg-isoDGR-G)*, deeper studies were carried out substituting the flanked Gly with other L- and D-amino acids. From the resulting library, the best compound obtained was the *c(phg-isoDGR-k)* which showed a very high active level for  $\alpha_5\beta_1$  ( $IC_{50} = 8.7$  nM) and an increased activity for  $\alpha_V\beta_6$  ( $IC_{50} = 19$  nM) remaining quite selective over  $\alpha_V\beta_3$  (Figure 1.9).<sup>88</sup>

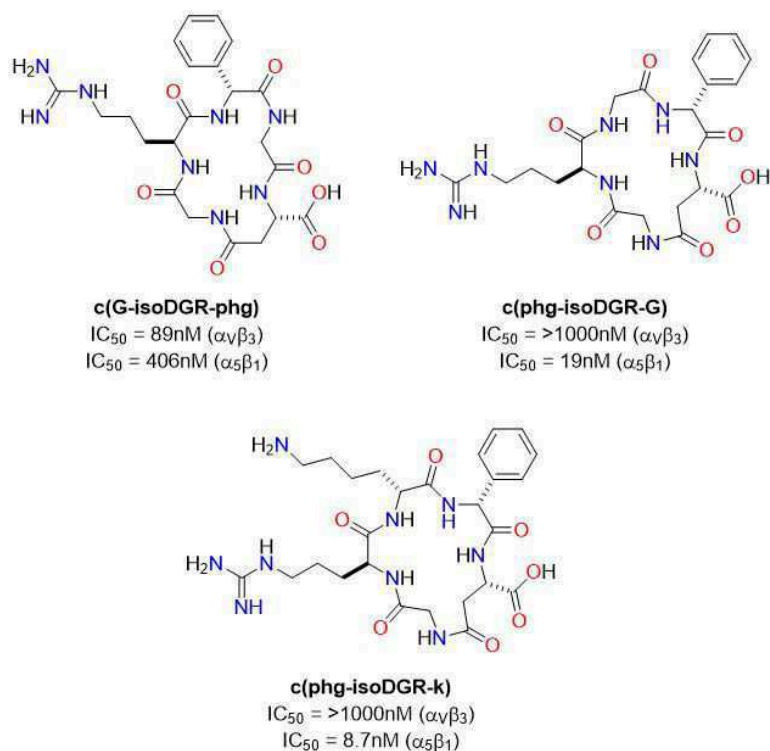


Figure 1.9: c(G-isoDGR-phg), c(phg-isoDGR-G) and c(phg-isoDGR-k) structures and biological activity.

The push provided by the results obtained with cyclic RGD peptide ligands has stimulated the researchers to design and to synthesise totally non-peptidic antagonists with the aim to improve the activity and selectivity obtained with the peptidic ones.<sup>80</sup> In 2002, one year later the first crystal structure of the extracellular domain of the  $\alpha_V\beta_3$  integrin, *Xiong* and coworkers<sup>91</sup> published the crystal structure of the same extracellular domain complexed with Cilengitide. After the noteworthy insight, a spread of docking studies arose to identify new drug candidate molecules; for example, in 2005 *Kessler* and coworkers<sup>92</sup> published a 3D model for the ligand- $\alpha_5\beta_1$  interaction (the crystal structure of its extracellular domain was still unknown) based on homology modeling of the experimental three-dimensional structure of  $\alpha_V\beta_3$  ( $\alpha_V:\alpha_5$  53% identity,  $\beta_3:\beta_1$  55% identity in integrins head group). Few years later,<sup>93</sup> they elucidated the composition of the two binding pockets ( $\alpha_V\beta_3$  vs  $\alpha_5\beta_1$ ) in order to improve the knowledge regarding the interactions between the receptors and the ligands, *J. M. Smallheer* and coworkers<sup>94</sup> synthesised a small nonpeptidic molecule, spirooxazoline based, which exhibited for the first time a very high activity towards  $\alpha_5\beta_1$  receptor ( $IC_{50} = 0.18\text{ nM}$ ) and a selectivity of at least 200-fold over  $\alpha_V\beta_3$  (Figure 1.10). In particular, they focused their attention on two specific regions that seemed to be considerable to explain the selectivity between  $\alpha_V\beta_3$  and  $\alpha_5\beta_1$ : in the  $\beta$ -subunit, ( $\beta_3$ )-Arg214 and ( $\beta_3$ )-Arg216 are replaced by ( $\beta_1$ )-Gly217 and ( $\beta_1$ )-Leu219, respectively. These substitutions increase the available space in the  $\alpha_5\beta_1$  allowing the introduction of bulky functionalisations

in the ligands structures. Moreover, the replacement of ( $\alpha_V$ )-Thr212 by ( $\alpha_5$ )-Gln221 entails a different geometry of this binding region and offers the opportunity to gain selectivity by modification of the basic moiety of the ligand. Furthermore, the  $\alpha_5$  subunit results to be less acidic than  $\alpha_V$  one, due to the mutation of ( $\alpha_V$ )-Asp150 to ( $\alpha_5$ )-Ala159.<sup>93</sup>

Then, *Jerini AG* developed a small library of highly active compounds leading to proline derivatives that showed high activity towards  $\alpha_5\beta_1$  receptor ( $IC_{50} = 0.54$  nM) and good selectivity over  $\alpha_V\beta_3$  ( $\alpha_V\beta_3:\alpha_5\beta_1 = >6000$ ) (Figure 1.10).

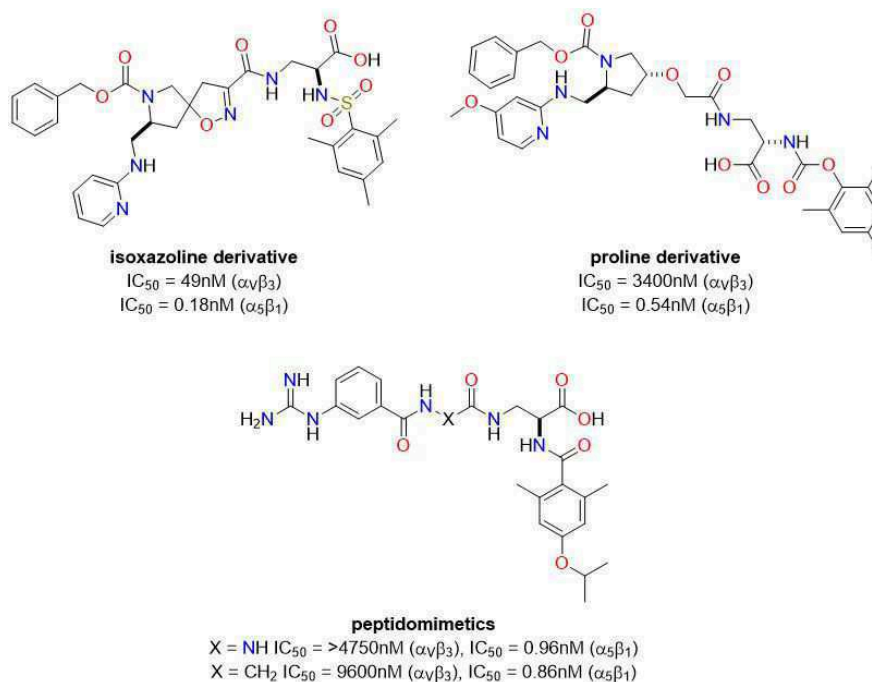


Figure 1.10: Isoxazoline, proline and peptidomimetic derivatives structures and biological activity.

On the other hand, the preservation of biological activity and selectivity towards  $\alpha_V\beta_3$  receptor obtained replacing the glycine residue with azaglycine in a RGD-containing linear peptides, led to apply the same approach to develop  $\alpha_5\beta_1$  ligands. Using this strategy, *Kessler* and coworkers<sup>93</sup> developed several peptidomimetics with very high affinity for  $\alpha_5\beta_1$  ( $IC_{50} = 0.96$  nM and  $IC_{50} = 0.86$  nM) and remarkable selectivity over  $\alpha_V\beta_3$  compared to the tyrosine scaffold due to the less flexibility of the diacylhydrazone scaffold compared to the tyrosine one (Figure 1.10).

To understand the specific role of  $\alpha_5\beta_1$  and  $\alpha_V\beta_3$  receptors, a high number of  $\alpha_V\beta_3$ -specific ligands was reported even if the molecular leads did not shown a satisfactory selectivity over  $\alpha_5\beta_1$ . In 2000, *GlaxoSmithKline* researchers synthesised two  $\alpha_V\beta_3$ -inhibitors belonging to benzodiazepine-family and showing excellent pharmacokinetic profiles in rats ( $IC_{50} = 1.2$  nM and  $IC_{50} = 0.9$  nM against  $\alpha_V\beta_3$  receptors vs  $IC_{50} = 110$  nM and  $IC_{50} = 1000$  nM against  $\alpha_5\beta_1$ ).<sup>95</sup>

Finally, in 2014, *Galletti et al.* developed  $\alpha_V\beta_3$ -active peptidomimetics library built around a  $\beta$ -lactam scaffold in which the most active and selective compound exhibited  $EC_{50} = 11$  nM with a reasonable selectivity over  $\alpha_5\beta_1$  receptor ( $EC_{50} = 763$  nM) (Figure 1.11).<sup>96</sup>

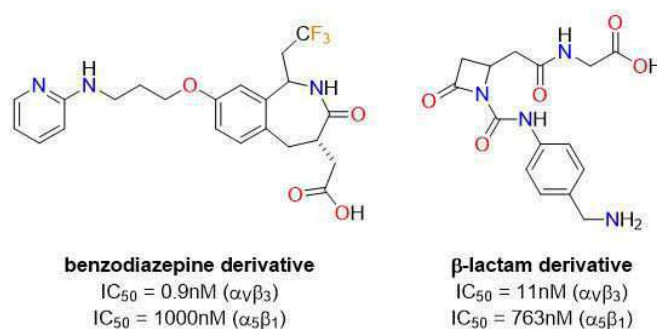


Figure 1.11: Benzodiazepine and  $\beta$ -lactam derivatives structure and biological activity.

In parallel, it emerged the necessity to identify new synthetic ligands of  $\alpha_V\beta_3$  and  $\alpha_5\beta_1$  receptors able to boost the design of imaging biomarkers for early detection of cancer, as well as in the engineering of cell-targeted anticancer agents. Even if in some cases it is better to envisage selective compounds for a specific enzyme or receptor, in others as in angiogenesis, targeting multiple pathogenic pathways could enhance efficacy of the therapy minimizing pharmacokinetic problems. For this reason, the suppression of the angiogenesis could be reached by means of the design of antagonists to both  $\alpha_V\beta_3$  and  $\alpha_5\beta_1$  integrins.

After the synthesis of Cilengitide and its X-ray crystallographic analysis in a complex with  $\alpha_V\beta_3$ , the design of non-peptidic integrin inhibitors was directed towards the idea to mimic the Arg-Gly-Asp (RGD) motif to bind the receptor mainly by means of electrostatic interactions. Noteworthy, the synthesis of selective ligands for  $\alpha_5\beta_1$  receptor has been performed working by homology due to not still available high-resolution information regarding the complex integrin-Cilengitide.

Typically, a rigid heterocycle scaffold is incorporated as the central core, having suitable pharmacophoric groups with optimal distance and orientation. In this context, **isoxazolines** have been extensively explored as conformational constraint elements in several transcriptional activator and nucleoside analogues.<sup>97</sup> In 2011, *Tolomelli et al.*<sup>98</sup> described the synthesis of isoxazoline scaffolds as central cores of RGD peptidomimetics and tested the obtained small library towards  $\alpha_V\beta_3$  and  $\alpha_5\beta_1$  receptors (Figure 1.12). The introduction of the heterocyclic core provided the desired rigidity, but of fundamental relevance was the selection of proper appendages for a good activity. The basicity and length of the Arg-mimicking moiety was found to play a central role in the ligand-receptor interaction, while the carboxylate function that mimics Asp was necessary to create an electrostatic interaction with the metal cation located in the binding pocket. This study suggested that the 4-aminobenzylamine and malonic acid, as basic and acidic termini, provided access to  $\alpha_V\beta_3$  and  $\alpha_5\beta_1$  receptors (the

synthetic pathway will be discussed in depth in Chapter 2).

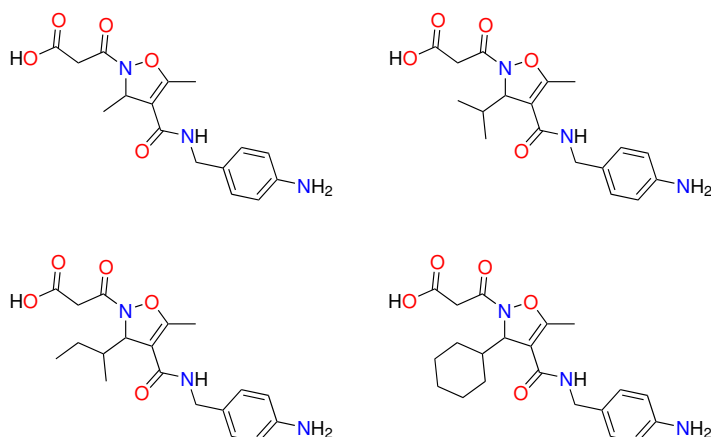


Figure 1.12: Isoxazoline-based peptidomimetics.

After the synthesis, *Tolomelli et al.* evaluated the ability of these compounds to inhibit the adhesion of SK-MEL-24 (human malignant melanoma expressing  $\alpha_V\beta_3$  integrin) or K562 (human erythroleukemia expressing  $\alpha_5\beta_1$  integrin) cells to immobilised fibronectin compared with that of the standard compounds (Ac-Asp-Arg-Leu-Asp-Ser-OH and H-Gly-Arg-Gly-Asp-Asn-Pro-OH).<sup>99</sup>

Entry	C3-substituent	$IC_{50}[\text{nM}]^a$	
		$\alpha_V\beta_3$	$\alpha_5\beta_1$
1	Met	$32 \pm 3$	$12 \pm 4$
2	<sup>i</sup> Pr	$8.8 \pm 0.6$	$1.05 \pm 0.3$
3	<sup>s</sup> Bu	$360 \pm 70$	$1320 \pm 80$
4	<sup>c</sup> Hex	$20 \pm 6$	$1030 \pm 50$
5 <sup>a</sup>	Ac-Asp-Arg-Leu-Asp-Ser-OH	$25 \pm 3$	$>100000$
6 <sup>a</sup>	H-Gly-Arg-Gly-Asp-Asn-Pro-OH	$234 \pm 32$	$>100000$

<sup>a</sup>Values represent the mean  $\pm$ SD of three experiments.

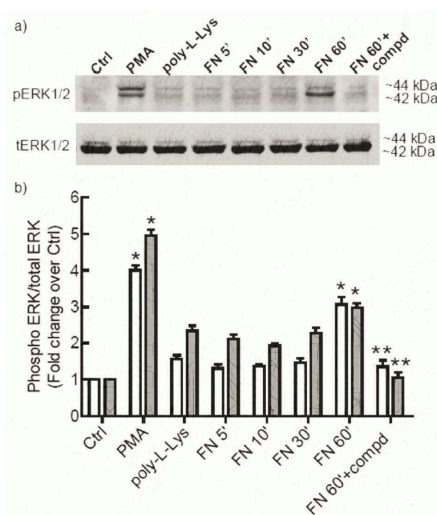
<sup>b</sup> Reference compounds.

Table 1.1: Inhibition of  $\alpha_V\beta_3$  and  $\alpha_5\beta_1$  integrin-mediated cell adhesion to fibronectin (FN) in the presence of isoxazoline-based peptidomimetics or reference standards.

Among the tested compounds, the one bearing isopropyl side chain in position 3 of the isoxazoline scaffold exhibited the highest potency as inhibitor of cell adhesion mediated by  $\alpha_V\beta_3$  and  $\alpha_5\beta_1$  integrins (Figure 1.12). As shown in Table 1.1, the isoxazoline ring is an effective scaffold for inducing the proper orientation for the pharmacophore groups and the

modification of other side chains allows to tune the integrin-mediated adhesion towards inhibition, making these small molecules a perfect example of dual inhibitors.

Finally, *Tolomelli et al.* tested the ability of isoxazoline-based molecules to block the adhesion of SK-MEL-24 cells to vitronectin showing to be 100 times more potent compared to the standard peptide Ac-Asp-Arg-Leu-Asp-Ser-OH ( $IC_{50} = 3.14 \text{ nM}$  vs  $IC_{50} = 0.33 \mu\text{M}$ ).



**Figure 1.13:** ERK phosphorylation behaviour in presence of fibronectin or fibronectin and pre-incubated isoxazoline ligand bearing  $^1\text{Pr}$  at C3.

Since the adhesion of fibronectin to integrins activate extracellular signal-regulated kinase (ERK), *Tolomelli et al.* evaluated the most active compound (bearing  $^1\text{Pr}$  at C3) in a phosphorylation test compared to the endogenous peptide figuring out that, with pre-incubation of the new compound, a significant decrease in the amount of fibronectin-induced ERK phosphorylation in K562 cells was observed compared to the exposure to fibronectin without the pre-incubation (Figure 1.13).

#### 1.4 Aim of the Thesis

As declared in the previous section, the identification of new synthetic ligands of  $\alpha_V\beta_3$  and  $\alpha_5\beta_1$  receptors is increasingly necessary. The interesting results obtained with already available compounds have risen the efforts of researchers for the synthesis of more active and selective ligands. Moreover, the chance of making these molecules as imaging biomarkers for early detection of cancer is one of the most attractive features for researchers. For the latter reason, the research towards new isoxazoline-based ligands of  $\alpha_V\beta_3$  and  $\alpha_5\beta_1$  receptors conjugated with fluorophore moiety has been one of the basis of this work (Figure 1.14).

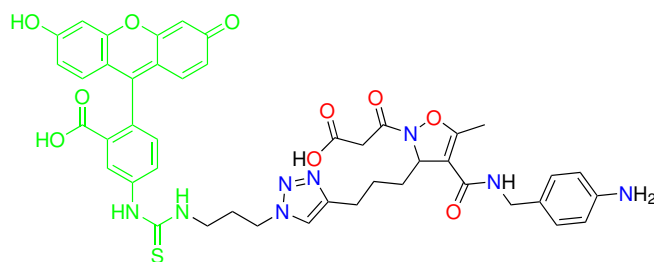


Figure 1.14: Isoxazoline-based ligand conjugated with a fluorophore (FITC).

In particular, inspired by the synthesis of previously reported isoxazoline-based ligands,<sup>98</sup> the attention was paid to the optimisation of the synthesis of C3-alkyne substituted heterocycle, opening the way to the "click chemistry" widely used in the design of bioactive compounds (the synthetic pathway will be discussed in the section "Results and Discussions" of Chapter 2). This strategy allowed us to create a library of molecules by changing the side chain attached to the triazole ring and to evaluate their biological efficacy. Finally, the most active isoxazoline ligand was conjugated with fluorescein isochiocyanate (FITC) to lend diagnostic feature to the leading compound.

As demonstrated in several reported papers,<sup>82,96,98</sup> small molecules are versatile compounds that can act either as simple bioactive compounds towards many diseases or as drug-carrier for more complex applications, such as imaging biomarkers.<sup>100</sup> In this context, the **drug delivery system** (DDS) is the most attractive application of small molecules due to the possibility to carry a payload directly close to the target, minimising eventual side effects. In other cases, the addition of a **latent fluorophore** (LF) can provide instantaneous detection on the release of the active drug coupled in a non-invasive manner, allowing the development of theranostic platform. This particular type of DDS is called **reporting drug delivery dystem** (RDDS) and it is essentially composed by four parts: a *carrier*; a *self-immolative linker*, consisting of a short sequence peptide-based; a *latent fluorophore* (in our case a *coumarin* derivative), and a *drug* (Figure 1.15).

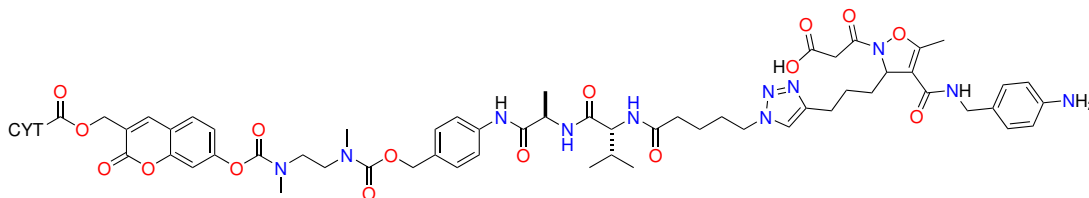


Figure 1.15: RDDS planned for a selective interaction with  $\alpha_V\beta_3$  and  $\alpha_5\beta_1$  integrin receptors (CYT: cytotoxic drug).

As depicted in Figure 1.15, our idea is to use our isoxazoline moiety as carrier head to deliver the system in proximity of cancer cells which overexpress the integrins targets. At this point,



the self-immolative system should be cleaved by *Cathepsin B* (a peptidase overexpressed by cancer cells) releasing the linker, the fluorophore and the cytotoxic agent by means of a chemical cascade (the synthetic pathway will be discussed in the section "Results and Discussions" of Chapter 3).

On the other hand, the stereochemistry control is a well known trick to improve the activity and to make a bioactive compound safer. In the last 20 years, several synthetic and characterisation techniques were developed to help chemists in the enantioselective synthesis of bioactive molecules.<sup>101</sup> Molecular docking on the most active isoxazoline ligand has revealed that the C3-stereochemistry could influence the activity of the heterocycle in connection with the interactions with the receptor binding pocket. Therefore, we developed a synthetic strategy for the enantioselective synthesis of a small library of  $\Delta^4$ -isoxazoline derivatives suitable for our scope (Figure 1.16).

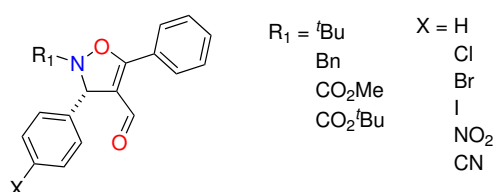


Figure 1.16: Library of Enantioselective isoxazoline scaffold.

In our previous reports,<sup>98</sup> we described several efforts to synthesise the heterocyclic moiety via enantioselective metal-catalysis without profitable results. Generally, the use of metals is not a good choice for the synthesis of bioactive compounds, therefore we decided to address our attention towards **organocatalysis**. Inspired by some examples reported in the literature, we developed an organocatalytic 1,3-dipolar cycloaddition reaction (*Huisgen reaction*) between a nitron and an aldehyde in order to synthesise the desired isoxazoline scaffold (the synthetic pathway will be discussed in the section "Results and Discussions" of the Chapter 2). Unfortunately, the attempts for synthesising 3-alkylic isoxazoline didn't provide satisfactory results and for this reason we have changed our plans by modifying the structure in a p-substituted-3-aryl isoxazoline suitable for functionalisation reactions, such as *Sonogashira* type coupling.

In addition to small molecules that mimic endogenous compounds, natural products have great relevance in the bioactive molecules scenario and for this reason several efforts are spent in the synthesis of the species extracted from natural sources. Bioactive molecules can be extracted from plant, animals or sponges and their structures can be used as models to improve their biological features.<sup>102</sup>

The last part of this work describes the results obtained during the internship abroad in Prof. *Aggarwal's* laboratory at the University of Bristol. The project was focused on the *Mycapolyol A* synthesis, a polyketide isolated from the marine sponge *Mycale izuensis* which

exhibit cytotoxic properties (Figure 1.17).<sup>103</sup> In particular, the aim of the work was directed on the synthetic scale up of the building blocks necessary for the optimisation of the late steps of the synthesis.

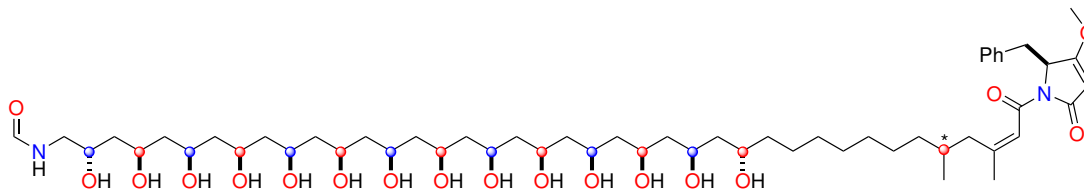


Figure 1.17: Mycapolyol A.

The Mycapolyol A synthesis is based on the **lithiation-borylation** chemistry<sup>104</sup> to build up the polyhydroxyl chain in enantioselective way (the synthetic pathway will be discussed in the section "Results and Discussions" of the Chapter 4). Lithiation-borylation strategy was developed by *Aggarwal* and coworkers<sup>105</sup> starting from 2007 and is a versatile strategy for the synthesis of several moieties which require stereospecificity and periodicity of functional groups. Mycapolyol A was divided in three fragments and at the end of the synthesis of each fragment, they were coupled together to obtain the desired product. Noteworthy, the boronic esters intermediate already mask the hydroxyl functionality, therefore no protecting groups are required and the stereochemistry is fine tuned by the right choice of the lithiation-borylation reagents.

## Chapter 2

---

# Heterocyclic Chemistry and Biological Applications

---

### 2.1 Introduction

Since the beginning of the modern organic synthesis, the chemistry of heterocycles has represented a fundamental branch of organic chemistry. As defined by *IUPAC*, the heterocyclic compounds are "cyclic compounds having as ring members atoms of at least two different elements (e.g., quinoline, 1,2-thiazole, etc)".<sup>106</sup> According with this definition, it is possible to classify ring systems on the basis of the type and the number of heteroatoms and on the basis of the dimension of the resulting heterocyclic structure; after that, heterocycles in each ring-size-group are further subdivided according to the type of heteroatoms, starting from one heteroatom, two heteroatoms, etc.<sup>107</sup>

The monocyclic systems are subdivided in four heterocyclic groups: 1) saturated heterocycles, in which the compounds react largely like their aliphatic analogues; 2) partially unsaturated systems, in which if the multiple bonds are between two C-atoms of the ring, the compounds react essentially like alkenes or alkynes; 3) systems with the greatest possible number of noncumulated double bonds; and 4) heteroaromatic systems.<sup>107</sup>

The most important heterocyclic compounds are the five- and six-membered rings and the nitrogen is the most common heteroatom in this kind of molecules, followed by oxygen and sulfur.

These features can explain the different physicochemical properties of the heterocycles and, more generally, of the compounds that contain them. For this reason, it is crucial understanding their reactions, syntheses and their synthetic applications.<sup>107</sup>

Thanks to their peculiarities, heterocyclic cores are employed in several fields of chemistry, with particular attention in medicinal chemistry to the synthesis of compounds with anti-bacterial, anti-inflammatory, anti-cancer and anti-fungal properties. Intrinsic features of heterocycles lend the possibility to modulate the properties of a drug by means of their introduction in the molecular structure.

One of the most relevant strategies opted for overcoming the multifactorial optimization

(pharmacokinetic, pharmacodynamic and toxicological properties) of a drug is the development and application of bioisosterically equivalent motifs or functional groups.<sup>108</sup>

In 1919, *Langmuir*<sup>109</sup> suggested a bioisosteric rationale for the modification of lead compounds basing his idea on the similarities of various physicochemical properties of atoms, groups, radicals and molecules. In his studies, *Langmuir* compared the physical properties of several molecules such as N<sub>2</sub> and CO, founding them similar. On the basis of these similarities, he observed 21 groups of *isosteres* and he defined the isosteres as "those compounds or groups of atoms that have the same number and arrangement of electrons".

From 1925 to 1932, *Grimm*<sup>110</sup> and *Erlenmeyer*<sup>111</sup> extended the concept of isosteres with the introduction of Grimm's Hydride Displacement Law and its expansion, redefining isosteres as "atoms, ions, and molecules in which the peripheral layers of electrons can be considered identical". The application of this concept to modify biological activity has given rise to the term *bioisosteres*, defined by *Friedman*<sup>112</sup> as "all atoms and molecules which fit the broadest definition for isosteres and have a similar type of biological activity" and then by *Burger*<sup>113</sup> as "Compounds or groups that possess near-equal molecular shapes and volumes, approximately the same distribution of electrons, and which exhibit similar physical properties".

According to these definitions, the biological activity is unconnected with the similarity between molecules or chemical structures, as demonstrated for example by the replacement of a carboxylic acid with a tetrazole ring.<sup>114</sup>

In 1970, *Burger* coined the common classification for bioisosteres, dividing them in classical or nonclassical. Classical bioisosteres are usually divided into several categories, when they possess: 1) monovalent atoms or groups; 2) divalent atoms and groups; 3) trivalent atoms and groups; 4) tetrasubstituted atoms, and 5) ring equivalents. On the other hand, nonclassical bioisosteres do not follow the steric and electronic definition of classical ones; moreover, they do not have the same number of atoms compared to the moiety they replace. Nonclassical bioisosteres can be divided in two categories: 1) rings vs noncyclic structures, and 2) exchangeable groups. Despite these classifications, it is difficult to define clearly the belonging of a specific heterocyclic structure to only a single subsection, since more a one characteristic can be present at the same time.

## 2.2 Heterocyclic Moieties in Medicinal Chemistry

**Heterocycles** are widely distributed in nature; from neurotransmitters to DNA building blocks, from biological metabolites to bioactive compounds, all these classes of molecules contain heterocyclic moieties (Figure 2.1).

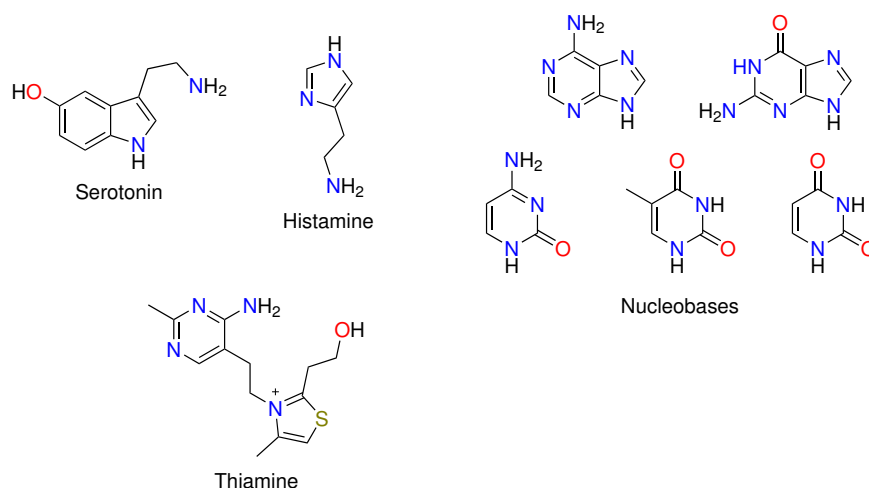


Figure 2.1: Heterocycles in biochemistry.

The history of heterocyclic chemistry began in the 19th century and has progressed hand in hand with the developments in organic chemistry. Some crucial steps are: (1818) *Luigi Valentino Brugnatelli* isolates alloxan from uric acid; (1832) *Johann Wolfgang Döbereiner* produces furfural by treating starch with sulfuric acid; (1834) *Friedlieb Ferdinand Runge* obtains pyrrole by dry distillation of bones; (1906) *Paul Friedländer* synthesises indigo dye; (1936) *Alfred Treibs* isolates chlorophyll derivatives from crude oil, and (1951) *Erwin Chargaff* describes with his rules the role of heterocyclic compounds in the genetic code.<sup>115</sup>

The relevance of heterocycles is due to their role in modulating several physicochemical properties such as potency and selectivity, lipophilicity, polarity and aqueous solubility of the containing compounds; furthermore they can incorporate functional groups either as substituents or as part of the ring itself, making them useful as bioisosteres.<sup>116</sup> Lipophilicity is an important parameter that can influence the efficacy of a drug. In general, at least for orally available drugs, it is important to follow the Lipinski's rule in which it is indicated that the ClogP (octanol-water partition coefficient) should not exceed 5 to guarantee a right lipophilicity profile and hence a good metabolic stability.<sup>117</sup> Moreover, lipophilicity influences several properties of drugs. Up today, the average for the descriptor ClogP for marketed drugs is circa 2.7 and the heterocycles keep this value lower than the compared all carbon counterparts (e.g pyridine ClogP = 0.65 vs benzene ClogP = 2.12). On the other hand, reduced lipophilicity not always produces optimised compounds in particular when a drug needs to pass through the cell membrane (e.g by replacing the carboxylic acid group with the ten times more lipophilic tatrazole ring, it is possible to obtain a better lipophilicity profile without losing bioactivity).

Polarity is described with Polar Surface Area (PSA) and Topological Polar Surface Area (TPSA) and the introduction of heterocycles can either increase or decrease the PSA/TPSA value. Aqueous solubility is another relevant drug property strictly related to the bioavail-

ability and the possible formulations of a drug.

Finally, the pharmacological benefits conferred by heterocycles can be explained (in many cases) by their tendency to establish hydrogen bonds with target protein, as well. These moieties can behave either as H-acceptor (heteroaromatic rings) or H-donor (saturated *N*-heterocycles) modifying drastically the compounds bioactivity.<sup>118</sup>

It is noteworthy that the hydrogen bonding is a fundamental non-covalent interaction between the drug and the biological target and for this reason it is one of the first parameters commonly evaluated in medicinal chemistry. For convenience, medicinal chemists use the *Brønsted proton basicity scale* as indicative parameter for hydrogen bonding capacity of heterocycles and other functional groups. However, this assumption is generally incorrect and it should be better to use the  $pK_{BH\bar{X}}$  scale of hydrogen bond basicity to measuring the hydrogen bond strength (Figure 2.2).<sup>119</sup>

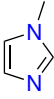
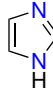
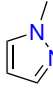
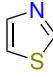
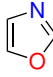
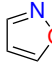
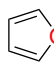
							
$pK_{BH\bar{X}}$	2.72	2.42	1.84	1.37	1.30	0.81	-0.40
$pK_{BH^+}$	7.12	6.95	2.06	2.52	0.80	1.30	

Figure 2.2: Hydrogen bonding ( $pK_{BH\bar{X}}$ ) and Brønsted basicities ( $pK_{BH^+}$ ) for five-membered heterocycles (adapted from *Dudkin V. Y.*<sup>118</sup>).

At the same time, other relevant parameters are the energies and the effects of C-H hydrogen bonds. These non-covalent bonds are weaker than other interactions; however, depending on the relative position between these bonds and the heteroatom, C-H can form hydrogen bonds with enough energy to influence both binding and conformational behaviour of drugs (Figure 2.3).<sup>118</sup>

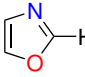
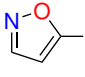
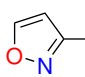
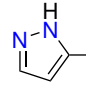
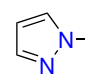
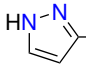
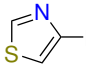
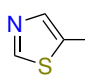
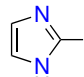
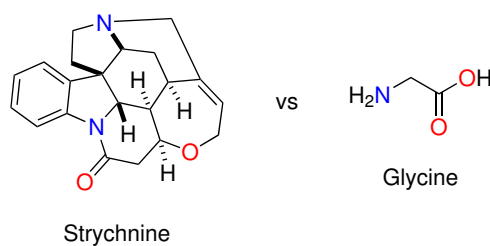
					
H-bond energy (Kcal/mol)	-3.06	-3.48	-3.04	-2.91	-6.31
					
H-bond energy (Kcal/mol)	-2.08	-2.41	-2.71	-3.21	

Figure 2.3: Calculated energies for C-H hydrogen interactions with water for five-membered heterocycles (adapted from *Dudkin V. Y.*<sup>118</sup>).

To contextualise the effect of heterocycles in the development of drugs or, more in general, of bioactive molecules, it is important to look at the way a drug works. In fact, drugs exert

their effects by means of several mechanisms including: 1) mimicking or opposing the effects of endogenous molecules being defined as *agonist* or *antagonist*, respectively; 2) interacting with enzymes by means of binding at the active site of the biopolymer, usually through inhibition of its activity, and 3) modifying natural macromolecules such as DNA or RNA either by direct interaction or by the incorporation into the polymer. The mechanism related to the interaction with a target enzyme is particularly interesting and allows to highlight some functional peculiarities like the possibility to bind the receptor in competitive (an equilibrium between the drug and the endogenous molecule) or non-competitive (firmly bound) manner and the presence in the organism of several subtypes for the same receptor. This aspect is fundamental to devise drugs with selective interaction for just one subtype. Furthermore, it is well known that a bioactive molecule can interact with the active site of an enzyme but also with the allosteric site. This binding can modify the shape of the enzyme itself and, as consequence, influence the reactivity of the receptor. However, the binding to the active or allosteric site proceeds by physical (e.g. H-bond) or covalent (e.g. *N*-alkylation) interactions in any case.

Traditionally, drug design involves the synthesis of molecules strictly correlated to natural agents by modifying substituents, electronic properties or dimension of cyclic moieties. Each one of these alterations can be achieved by means of the introduction of heterocycles. Despite this is the most common approach in drug design, a surprising number of bioactive substances containing heterocycles are barely similar to the related natural molecules. An amazing example is the competitive behavior between strychnine -an indole alkaloid- and glycine (Figure 2.4).



**Figure 2.4:** Strychnine vs Glycine: competition for Central Nervous System (CNS).

At the same time, heterocycles are common moieties in the structure of the majority of marketed drugs. In the top 200 pharmaceuticals by retail sales in 2019, 59% is composed by *small molecules* and over 85% thereof contain at least one heterocycle. Moreover, among the ten most sold pharmaceuticals four are small molecules and in all are present heterocyclic moieties (Figure 2.5).<sup>120</sup>

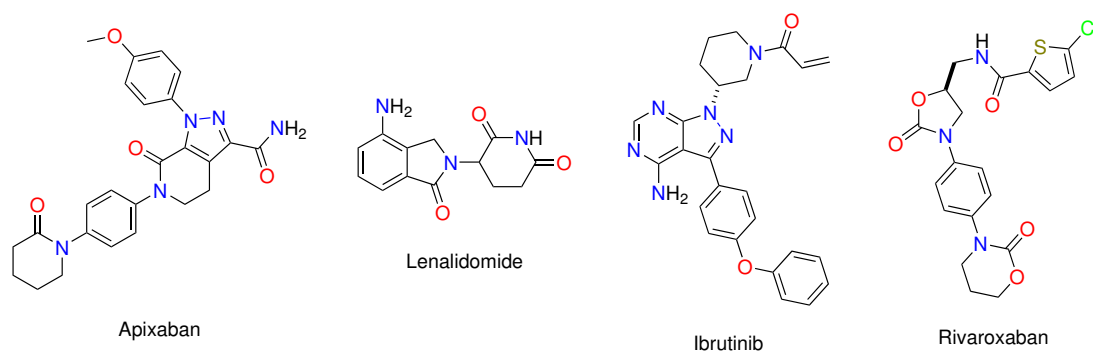


Figure 2.5: Top 4 small molecules by retail sales in 2019.

Even if the linkage between medicinal chemistry and heterocycles is incredibly wide, it is possible to simplify the approach focusing the attention on two possible correlations: the role of heterocycles in the molecular structure as modulator of the bioactivity (e.g. peptidomimetics) and the structural requirements of a heterocyclic-based compound to become a bioactive molecule (e.g. isoxazoline ring).

### 2.2.1 Heterocycles Serving Peptidomimetics

Since almost all the physiological processes involve peptides and proteins, these biopolymers appear particularly attractive as starting point for drug discovery programs. Unfortunately, their potential as therapeutics is limited by intrinsic instability towards peptidase and protease, insufficient oral bioavailability and inability to cross the blood-brain barrier.<sup>121</sup> Therefore, the general approach to overcome these limitations is the introduction of modifications in the peptides and proteins structures to keep unchanged or to improve the biochemical properties associated to an efficient drug action. These results can be obtained changing the backbone structure of the peptide or incorporating peptide bond isosteres. In general, **peptidomimetics** are molecules in which the pharmacophore is represented by a structure that mimics a peptide or a protein in their 3D disposition and biological behaviour. Finally, the pre-organisation of peptide shape is evaluated. It's possible to distinguish four different types of peptidomimetics:

- 1) type I, backbone mimetics are peptides backbone mimetics (strictly defined peptidomimetics);
- 2) type II, small molecules that act as functional mimetics;
- 3) type III, structures which possess functional groups acting as topographical mimetics, and
- 4) type IV, GRAB-peptidomimetics (Group Replacement Assisted-Binding) which possess type I-properties and bind receptor forms not accessible to the first one.<sup>122</sup>

The use of peptide bond surrogate allows to overcome some problems associated to peptidic compounds, such as poor stability towards proteolysis, lack of oral absorption, low bioavailability, and in some cases peptidomimetics are used to improve receptor affinity



and selectivity allowing to understand the protease enzyme activity when the structure of the isoster mimics the transition state of the hydrolytic degradation.<sup>123,124</sup>

Generally, non-peptidic elements are introduced in the backbone structure and in pharmacophore position in order to improve the lipophilicity and, as a consequence, the bioavailability of the molecules. Then, an isoster of amide bond is required to enhance the resistance to peptidases and the pharmacokinetic (Figure 2.6).

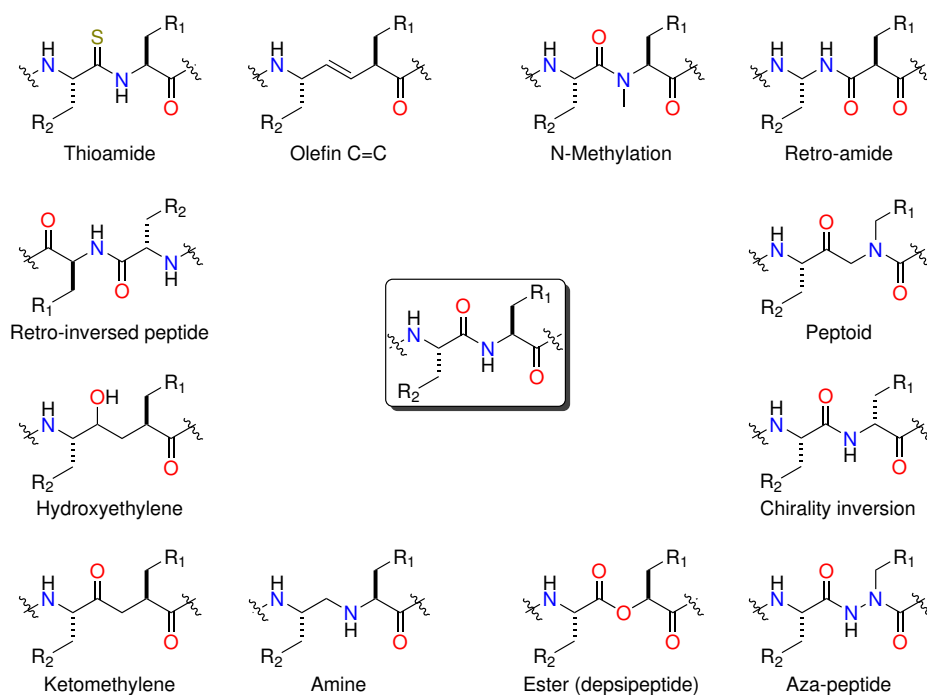


Figure 2.6: Peptidomimetic moieties.

Among the different approaches, it is noteworthy the introduction of heterocycles in the structure of a drug-candidate in order to match with the properties previously mentioned and to provide additional ones. For example, heterocyclic-based constrained peptidomimetics and mimetics of peptide secondary structures can be employed to study a known biologically active conformation (e.g., particularly true regarding *cis*-proline mimetics) (Figure 2.7).<sup>121</sup>

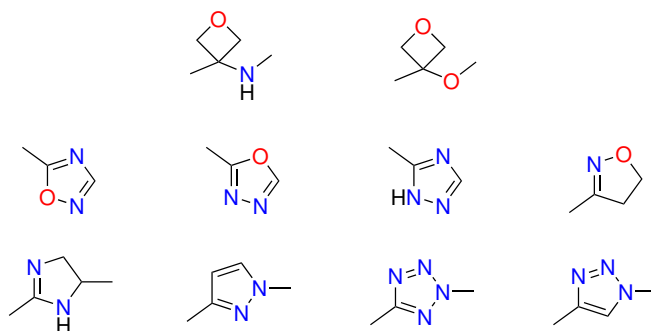


Figure 2.7: Heterocycles employed as peptidomimetic moiety.

*Hruby* and coworkers have studied the effect of the introduction of conformationally restricted  $\beta$ -substituted amino acids in peptidic sequences to synthesise analogues peptidomimetics. Among several  $\beta$ -substitution, they focused the attention on external  $\beta$ -turn dipeptide mimetics (Figure 2.8).<sup>125</sup>

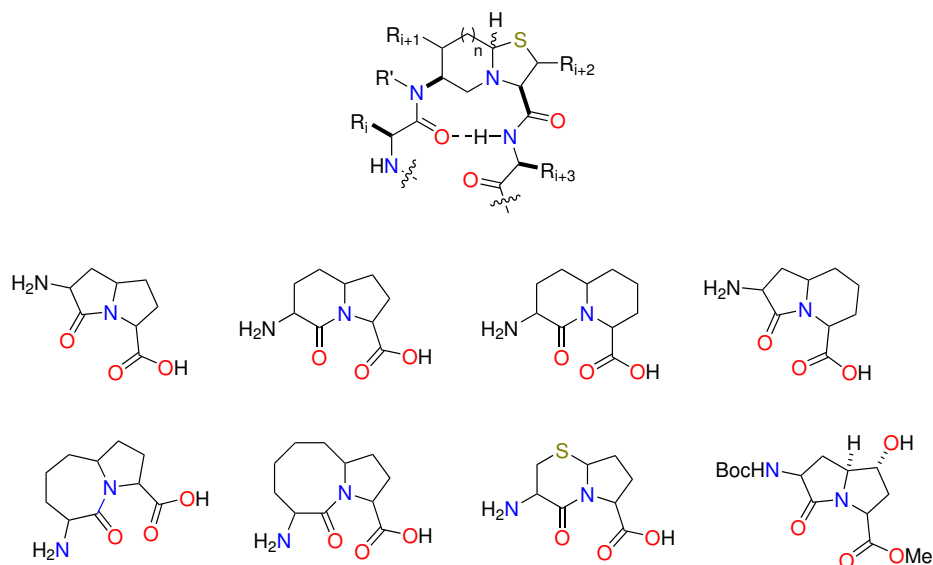


Figure 2.8: Azabicycloalkanone amino acid scaffolds.

This bicyclic template restricts conformations through a combination of structural constraints and steric interactions probably due to the presence of substituents, the size of the moiety and the stereochemistry of the scaffold. Moreover, taking advantage of its peculiarities, it is possible to incorporate various side chain groups to evaluate the correlation between topography and molecular recognition. Moreover, the use of azabicycloalkanone amino acid scaffolds as dipeptide surrogates to mimic the  $\beta$ -turns is well documented. Belonging to this class, several variations in size systems (including 5.5-, 6.5-, 5.6- and 6.6-) and sites for substitution have been published providing the opportunity to extend the drug discovery scope. Of particular interest, the enantioselective introduction of hydroxyl functionality in the 5.5-derivative has paved the way to a fine-tuned diversification of the peptidomimetic product (Figure 2.8).<sup>126</sup>

A practical example of the use of bicyclic heterocycles in this field is furnished by the synthesis of the HIV-1 protease inhibitors. HIV protease is a  $C_2$ -symmetric homodimeric protein and it selectively cleaves the amide bond Phe-Pro (or Tyr-Pro); therefore, a rational design of peptidomimetics as inhibitors is possible, along with a decrease of the multidrug-resistant variants. In this perspective, *Bonini* and coworkers have explored the effects of the introduction of a thienyl ring in the middle of several commercial anti HIV protease drugs belonging to the *Saquinavir* family. The choice of this heterocycle was made knowing the ability of this ring to mimic the phenyl group of aromatic aminoacids (Figure 2.9).<sup>127</sup>

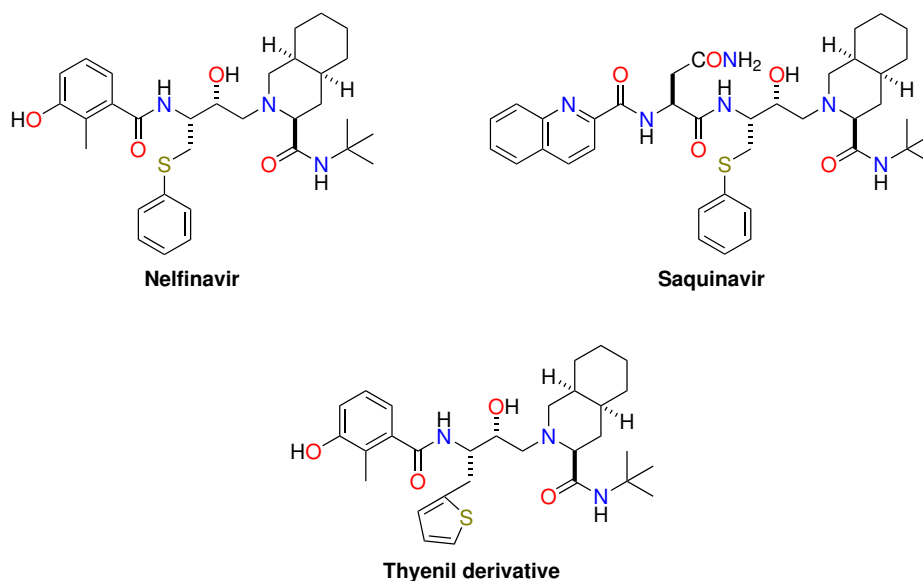


Figure 2.9: Structures of Nelfinavir and Saquinavir and their thienyl derivative.

### 2.2.2 Heterocycles-Based Bioactive Molecules

As mentioned in the introduction of Chapter 2, heterocycles are strictly defined according to the type, the dimension and the elements which build up the ring. Despite there is no upper limit and almost all types of heterocycles are presented in natural or synthetic molecules, the most important rings are the five- and six-membered heterocycles. In the organic heterocyclic scenario, the *N*-atom is the most common heteroatom followed by *O*- and *S*-atoms, whereas heterocycles with *Se*-, *Te*-, *P*-, *As*-, *Sb*-, *Bi*-, *Si*-, *Ge*-, *Sn*-, *Pb*- or *B*-atoms are much less common.<sup>107</sup>

Since the aim of this thesis is to synthesise an **isoxazoline** ring and evaluate its features as bioactive compound and as carrier in a Drug Delivery System, this subsection will debate on the synthesis and the medical applications of this heterocycle.

In general, biologically active compounds are frequently composed by heterocycles containing *N*- and/or *O*-atoms. Among such classes of compounds, five-membered heterocycles as isoxazole, isoxazoline and isoxazolidine are considered key scaffolds for their biological applications (Figure 2.10).



Figure 2.10: Isoxazole, Isoxazoline and Isoxazolidine structures.

Isoxazole, isoxazolines and isoxazolidine are important classes of nitrogen and oxygen heterocycles that belong to the azole family; in particular, isoxazolines exist in three different isomers depending on the location of the double bond ( $\Delta^2$ -,  $\Delta^3$ - and  $\Delta^4$ -isoxazoline).

These compounds hold a privileged position in pharmacology since they are present in many natural products with biological activity, such as antimicrobial, antiviral, anticancer, anti-inflammatory, immunomodulatory, anticonvulsant or anti-diabetic. In fact, isoxazole is the main scaffold of *Ibotenic acid* and *Muscimol*, psychoactive compounds which occur naturally in *Amanita muscaria* and related species of mushrooms.<sup>128</sup> On the other hand,  $\Delta^2$ -isoxazoline-based natural products can be extracted with organic solvents from several types of marine sponges and used as anticancer agents in chemotherapy, although the most employed bioactive isoxazoline-based molecules are *Fluralaner* and *Afoxolaner*, two drugs for the prevention of the flea infestations.<sup>129</sup> Finally, isoxazolidines are often found in several types of alkaloids extracted from marine sponges, fungal metabolites and, the only animal source example, frogs (Figure 2.11).<sup>130</sup>

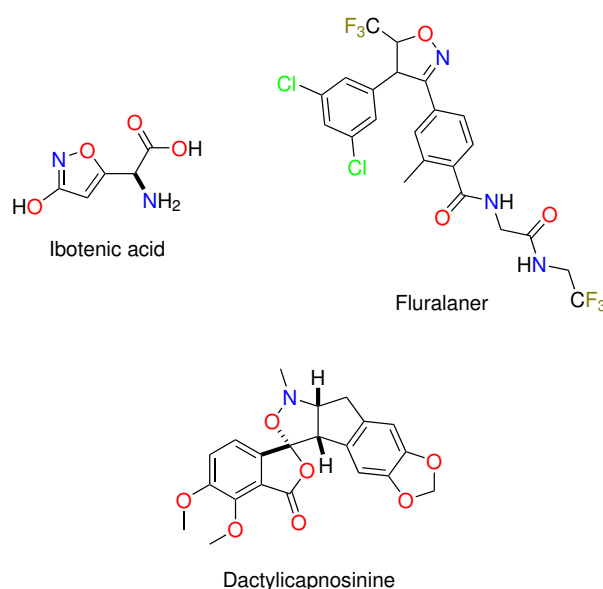


Figure 2.11: Natural compounds containing Isoxazole, Isoxazoline and Isoxazolidine moieties.

### 2.2.3 Isoxazoline Ring: Overview on its Synthesis

As consequence of the diffusion of isoxazoline scaffolds in natural bioactive products, researchers have made a great effort in the optimisation of their synthesis.

Generally, both in biological environments and in laboratory, these heterocycles can be obtained by means of the **1,3-dipolar cycloaddition** (1,3-DC) reaction, providing access to a vast array of substituted moieties. Historically, the first strict study of 1,3-DC reaction was conferred to *Buchner* in 1888, who carried out the reaction of diazoacetic ester with  $\alpha,\beta$ -unsaturated esters.<sup>131</sup> In 1898, *Beckmann*, *Werner* and *Buss* discovered nitrones and nitrile oxides, two of the most important 1,3-dipole systems used for the synthesis of this class of compounds. During the following 100 years, the researchers studied the 1,3-DC reaction, with no remarkable improvements; only in 1960's, *Huisgen*<sup>132</sup> was able to furnish

a rigorous description of the reaction making it of general application in organic synthesis. At the same time, *Woodward* and *Hoffmann*<sup>133</sup> developed a new concept of conservation of orbital symmetry to explain the general reactivity of the species and on the basis of this concept, *Houk* and coworkers<sup>134</sup> provided other contributions to understanding the 1,3-DC reaction's mechanism.

The last step of the development process was achieved in 2000's, when researchers introduced the control of the reaction stereochemistry, which is obtained through the selection of appropriated substrates or reaction catalysts; in particular, the enantioselectivity can be controlled by either choosing a chiral 1,3-dipole, a chiral alkene, or a chiral catalyst.

From the mechanistic point of view, 1,3-DC occurs between a 1,3-dipole and an alkene/alkyne counterpart. It is possible to divide 1,3-dipoles in two types: 1) allyl anion type, with bent arrangement, and 2) propargyl/allenyl anion, with linear arrangement (Figure 2.12). It is fundamental to highlight that in the allyl anion the central atom can be nitrogen, oxygen or sulfur, whereas in propargyl/allenyl anion the central atom must be only the nitrogen, limiting the product structures.<sup>135</sup>

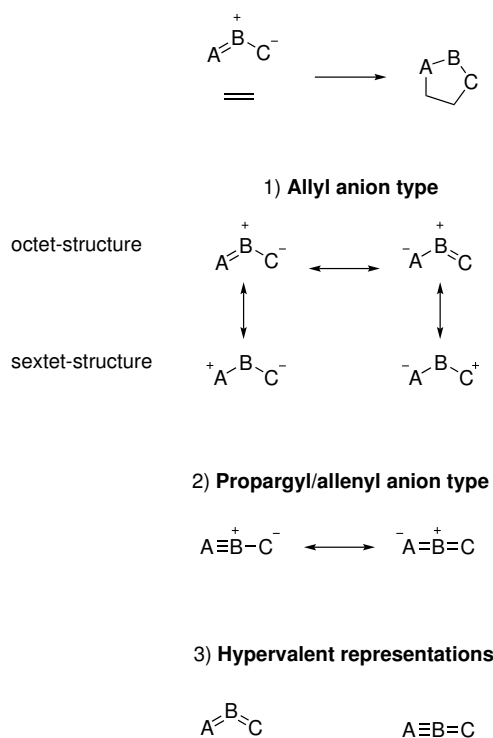


**Figure 2.12:** The basic resonance structure of 1,3-dipoles (adapted from *Gothelf K.V.*, et al.<sup>135</sup>)

Generally, the reaction between 1,3-dipoles and alkenes/alkynes involves  $4\pi$ -electrons from the dipole and  $2\pi$ -electrons from dipolarophile, but a debate regarding the mechanism whereby this reaction proceeds went on for a long time. *Huisgen* and coworkers developed a detailed study in favour of a concerted mechanism, whereas *Firestone* affirmed that the reaction proceeded via a singlet diradical intermediate. Nowadays, it is known that

the mechanism postulated by *Huisgen* was correct and supported by the stereospecificity observed during the reaction between benzonitrile oxide and trans-dideuterated ethylene. However, *Huisgen* and coworkers have later demonstrated that the 1,3-DC reactions can occur by a stepwise mechanism involving an intermediate, losing the stereospecific information.<sup>136</sup>

At that point, these results made possible to postulate that 1,3-DC was controlled by the frontier molecular orbitals (FMO) of the substrates. Starting from these observations, *Sustman* classified 1,3-DC reactions into three categories according to the dominant FMO interaction: 1)  $\text{HOMO}_{\text{dipole}}\text{-LUMO}_{\text{alkene}}$ ; 2)  $\text{LUMO}_{\text{dipole}}\text{-HOMO}_{\text{alkene}}$ , and 3) none significant difference in FMO energy of substrates, thus both interactions are relevant. However, the introduction of electron-donating group (EDG), electron-withdrawing group (EWG), or metals (such as Lewis acid) can modify the FMO energy profile of the substrates and therefore the reaction's class.<sup>137</sup>

The perturbation caused by using metal Lewis acids is probably the most interesting one and the altered reactivity can be accounted for by using a mathematical simplification of the second-order perturbation theory, assuming that the reactivity control is only governed by the HOMO-LUMO interaction (eq 2.1).

$$\Delta E \propto \frac{C_H C_L}{E_H - E_L} \quad (2.1)$$

$C_H$  and  $C_L$ : orbital coefficients at the reacting atoms in the HOMO and LUMO, respectively.  
 $E_H - E_L$ : energy difference between the HOMO and LUMO.

The coordination of a Lewis acid to the alkene (e.g. via a conjugated group) lowers its FMOs' energy, produces a decrease in the energy difference between  $E_{\text{HOMO}}$  and  $E_{\text{LUMO}}$  and increases the  $\Delta E$  value of the eq 1 resulting in a faster reaction.<sup>135</sup>

On the other hand, isoxazolidine rings can be obtained through the reactivity of the alkylidene and arylidene malonates, acetoacetates, malonamides and acetoacetamides. One of the most widely employed reactivity of these systems is their versatility in conjugated addition reactions. This kind of reactions has a not so long story since the first example was reported in 1883 by *Komnenos*, who studied the reaction between sodium diethyl malonate and diethyl ethylidenemalonate. In 1887, *Michael* presented further developments on this topic in the base-catalysed reaction between sodium malonates and  $\beta$ -ketoesters to ethylcinnamate. Starting from the first examples in which the main nucleophiles were stabilized carbanions, several improvements were made in order to expand the spectrum of nucleophiles able to be employed for this purpose. In fact, talking about conjugated addition or 1,4-addition, it is commonly referred to addition of any kind of nucleophile to an unsaturated system usually

conjugated with an activating group, in particular an electron-withdrawing group. However, since there is possibility to choose several nucleophiles, carbon- or heteroatom-based, a distinction can be made: "Michael addition" is referred to addition of stabilized carbanion species on  $\alpha,\beta$ -unsaturated substrates, in the conjugation with an activating group like a carbonyl group; "heteroconjugate addition" is referred to addition of heteroatom-based nucleophiles to the same unsaturated systems.<sup>138</sup> Considering the existence of more than one electrophilic functionalities on  $\alpha,\beta$ -unsaturated systems, it is important to clarify why the 4-position is so reactive towards carbanion and some heteroatom-based nucleophiles: the explanation is based on the theory of frontier molecular orbital (FMO) which shows that the coefficient of LUMO orbital is larger in the  $\beta$ -position, so soft nucleophiles should attack in this position.<sup>139</sup>

In particular for hetero-nucleophiles, the great reactivity in 1,4-addition is also due to thermodynamic and kinetic factors related to the gain in terms of energy in the product of the reaction compared to the energies of the two starting materials. Particularly intriguing for our purpose, alkylidene malonate and acetoacetate have been largely employed in the synthesis of isoxazolidin-5-ones, isoxazolidines and isoxazolines (Figure 2.13).

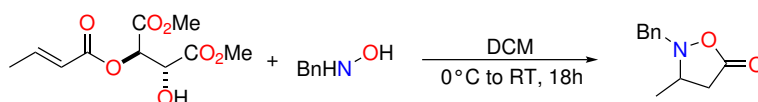


Figure 2.13: Synthesis of isoxazolidin-5-one starting from homochiral esters proposed by Saito.<sup>140</sup>

One of the most used synthetic route is based on the heteroconjugated addition of *N*-hydroxylamine on  $\alpha,\beta$ -unsaturated esters or ketones with consequent cyclization of the *N*-hydroxyl group on ester for the synthesis of isoxazolidin-5-one and on ketone for the synthesis of isoxazolidine and its derivative isoxazoline. For example, in 1995 Saito et al.<sup>140</sup> reported the addition of *N*-methyl benzylhydroxylamine to homochiral esters for the synthesis of isoxazolidin-5-one.

Among the several applications of these heterocycles, probably the most interesting one is their use as anticancer agents. Almost 50% of all anticancer drugs approved are natural products or their mimics and in this panorama,  $\Delta^2$ -isoxazoline derivatives have emerged as compounds with promising antineoplastic properties (Figure 2.14).

Noteworthy is the *Subereamolline A*, a bioactive dibrominated metabolite extracted from *Suberea mollis* sponge which can inhibit the migration and invasion of metastatic human breast cancer cells (Figure 2.15).

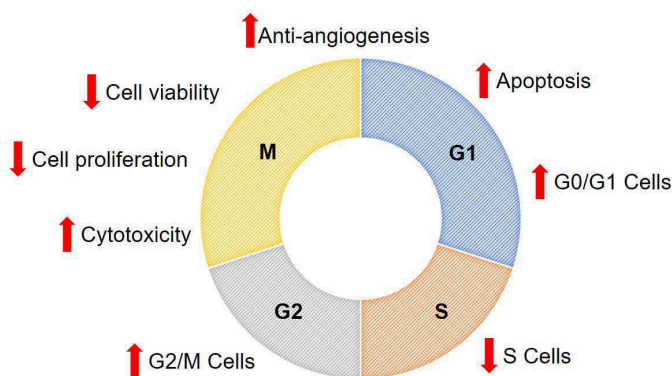


Figure 2.14: Proposed anticancer properties of isoxazoline compounds (modified from *Kaur K. et al.*<sup>129</sup>)

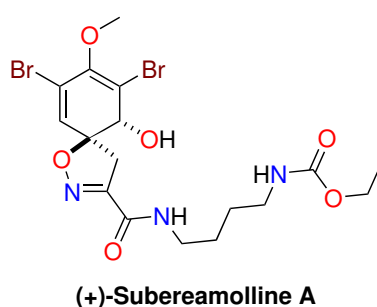


Figure 2.15: Structure of (+)-Subereamolline A.

From *Shaala et al.* studies, the presence of ethyl carbamate moiety and the (S)-configuration at the spirocentre were emerged as two fundamental factors to justify the high potency against cancer cells displayed by Subereamolline A ( $IC_{50} = 1.7 \mu M$ ), making compound (+)-Subereamolline A an interesting scaffold for the design of more efficient anticancer agents.<sup>129,141</sup>

### 2.3 Organocatalysis and Organocatalysis in Medicinal Chemistry

Since the 19<sup>th</sup> century, chemists believed that everything was the result of a fine equilibrium between symmetry and asymmetry. In fact, although the macrostructures (e.g. biopolymers) have high symmetry, their building blocks are frequently asymmetric. The concept of **chirality** (from greek *kheir* - which means hand) was born in 1848 when *Louis Pasteur* started his works on the crystallinity of tartaric and para-tartaric acid; nowadays, chirality is considered the most attractive point of view regarding the stereochemistry.<sup>142</sup>

Pioneering *Pasteur's* studies were only the first of a series of steps in an unexplored field of organic chemistry: (1848) *Louis Pasteur*<sup>143</sup> coins the term *racemic mixture*; (1857) *Louis Pasteur*<sup>144</sup> discovers the first example of enantioselective bio-transformation; (1886) *Arnaldo Piutti*<sup>145</sup> states that the biological receptors themselves are enantioselective.

After these key moments in the stereochemistry knowledge, several synthetic compounds



were marketed in both enantiomeric forms allowing further pharmacokinetic and pharmacodynamic studies. For example, in the 60's the toxic feature of the D-enantiomer of 3,4-dihydroxyphenylalanine was clarified until then administered as racemic mixture in the treatment of Parkinson's disease.<sup>146</sup>

Even if at the end of 20<sup>th</sup> century much more information about chirality was available, a simultaneous development and market of new enantiopure synthetic drugs was not observed, probably also due to an unclear assessment of the benefits generated by the use of enantiopure compounds. Finally, in 1992 the Food and Drug Administration *FDA* reported the first guideline for the enantioselective development of new drugs due to two fundamental aspects: the development of the *enantioselective synthesis*, and the introduction of powerful enantioselective analytic tool (e.g. Chiral HPLC) in chemical characterisation.<sup>147</sup>

Inspired by enzymatic processes, chemists mainly developed metal-catalyst-based systems, but in 2000 *David W. C. MacMillan* coined and defined the term **organocatalysis** as the use of organic molecules with low molecular weight as catalysts in organic reactions, changing the paradigm of the enantioselective synthesis.<sup>148</sup> However, several publications concerning the use of organocatalysts had already been published but unfortunately without recognition of the value of the discovery: (1912) *Bredig* and *Fiske* describe a cinchona alkaloid catalysed addition of HCN to aldehyde; (1960) *Pracejus* describes the addition of methanol to ketenes; (1970's) pharmaceutical companies Hoffman-La Roche and Shering AG develops the first intramolecular aldol reaction catalysed by proline (*Hajos-Perrish-Eder-Sauer-Wiechert* reaction).<sup>149,150</sup>

In general, organocatalysts are non-toxic and robust compounds, and air stable. The reactions are usually carried out under mild conditions and in high concentration, reducing solvent wasting. Moreover, organocatalysts are tolerant towards many functional groups and a large number of them is commercially available, providing different alternatives for the same reaction. One of the key points of organocatalysis is the possibility to identify only five general activation pathways, while organocatalysts generally operate in two different ways; either they can activate the nucleophile or the electrophile (or both), or they can create an asymmetric environment responsible of the transmission of the chiral information. In the first catalysts' category it is possible to arrange aminocatalysts and carbenes able to catalyse via enamine, iminium ion and SOMO pathways,<sup>148,151,152</sup> on the other hand, thioureas and cinchona alkaloids can activate a reaction via hydrogen bond or ionic interactions (Figure 2.16).<sup>153,154</sup>

Since 2000, the field of organocatalysis has grown exponentially and many researchers from both academia and chemical industry were involved in this topic; however, looking at the publications and citations data of the last years, it is possible to highlight a decrease in the chemical community attention (Figure 2.17) and this fact could be explained, for example, by means of the limitation in the use of this methodology for scale-up processes for bulky industrial purposes.<sup>155</sup>

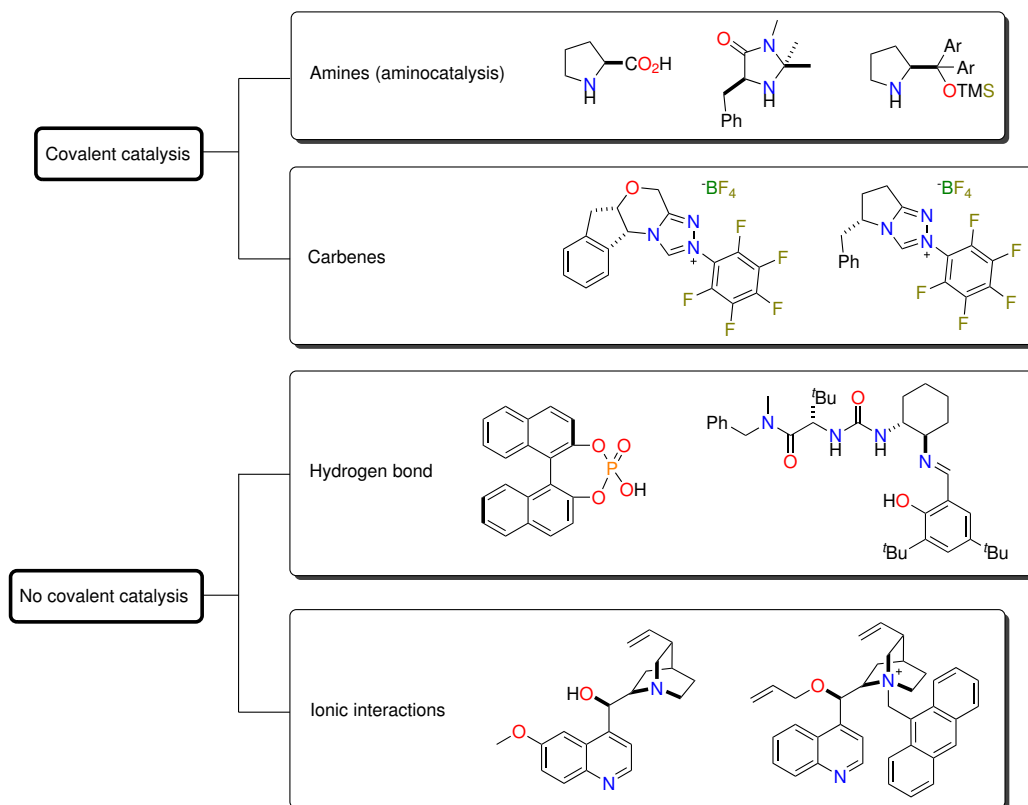


Figure 2.16: General classification of the activation mode in organocatalysis (modified from Aléman J., et al.<sup>101</sup>)

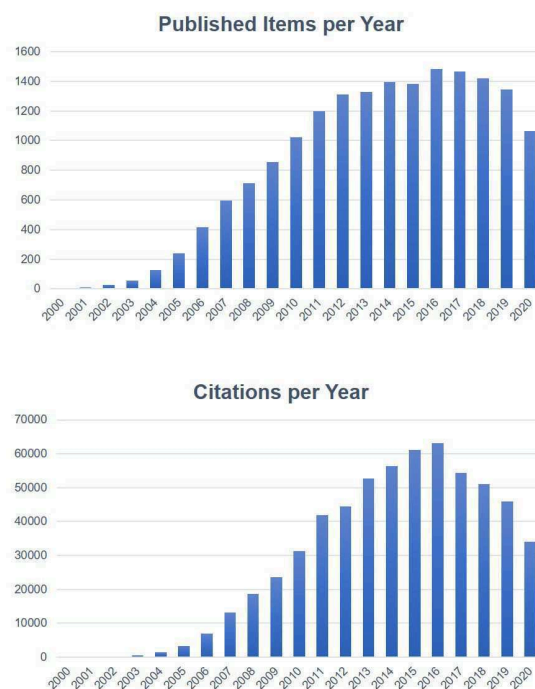


Figure 2.17: Publications with the term "organocat\*" searched in the Web of Knowledge<sup>SM</sup> (20/11/2020).

On the contrary, organocatalytic methods are especially attractive for the preparation of compounds that do not tolerate metal contamination or other toxic conditions, such as active pharmaceutical compounds, demonstrating that organocatalysis is still a fundamental tool for relevant synthetic applications.

In particular, enamine and iminium catalysis have been the most employed in the last twenty years in the synthesis of several pharmaceutical targets with different biological applications such as antiviral, antitumor, antipyretic or neuroprotector agents.

### 2.3.1 Via-Enamine Catalysis in the Synthesis of Antitumor Agents

Thirty years after the discovery of the *Hajos-Perrish-Eder-Sauer-Wiechert* reaction, in 2000 *Barbas III*, *Lerner* and *List* employed the **catalysis via enamine** for the functionalisation of carbonilic compounds in  $\alpha$ -position making this activation tool a widely used.<sup>152</sup> Until early 2000's, **(L)-Proline** was the most successful catalyst and even though the proteinogenic form (L) was the usually most employed, both enantiomers were equally used representing a relevant advantage compared to an enzymatic approach. In addition, proline is an amphoteric compound (as all the aminoacids) and this feature confers to the catalyst specific properties. In fact, proline can react as nucleophile with carbonilic compounds or Michael acceptors, due to its high  $pK_a$  value and relative nucleophilicity, while the acid functionality acts as Brønsted acid making this molecule a perfect example of *bifunctional catalyst*.<sup>156</sup> However, in the last twenty years several researchers have synthesised new catalysts deriving from proline scaffold with the aim to improve their activity and selectivity features. In the extended panorama of proline-like catalysts, the most relevant are *Jørgensen* and *Hayashi* silyl-prolinol derivatives (Figure 2.18).<sup>157,158</sup>

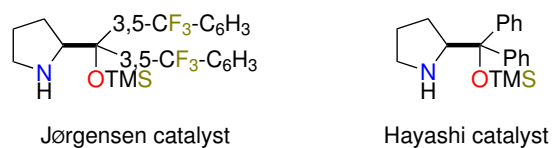
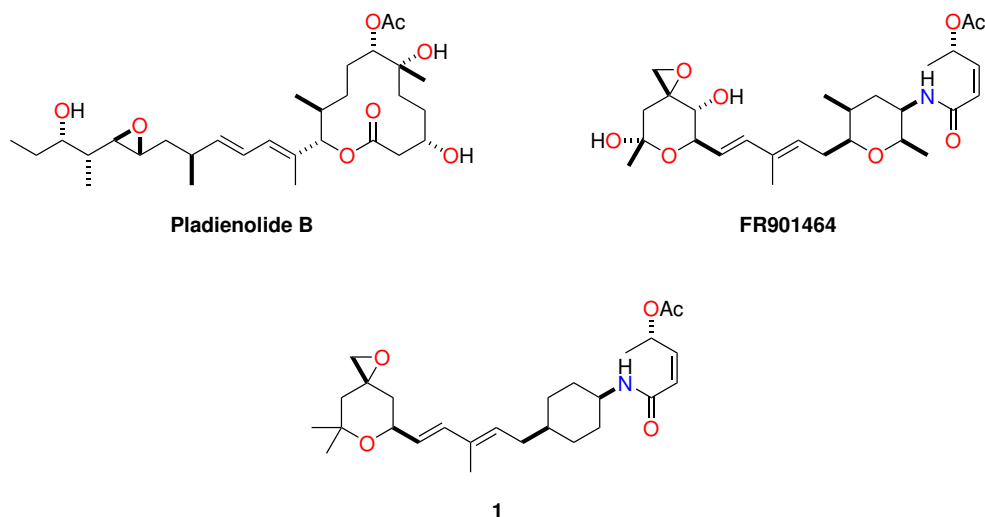


Figure 2.18: *Jørgensen* and *Hayashi* catalysts.

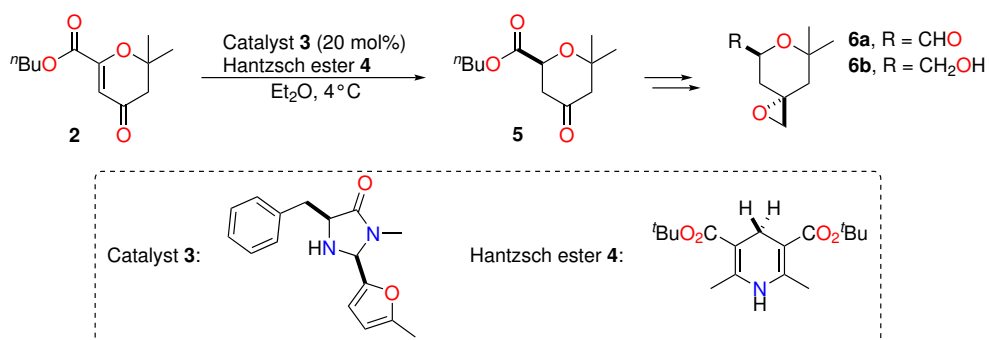
This family of catalysts has been widely employed in medicinal chemistry providing a key tool for the synthesis of several bioactive compounds; among these, **pladienolide B** and **FR901464** derivatives are very interesting compounds employed as anticancer agents (Figure 2.19).<sup>159</sup>

In 2008, *Webb* and coworkers reported one of the first applications of organocatalysis in medicinal chemistry, designing several compounds on the basis of the pharmacophore model of the low energy conformation of the reference bioactive compounds. In this model, it was possible to identify three key features: an epoxy group, a carbonyloxy group and a constrained linker connecting the other two moieties, all incorporated in the design of the



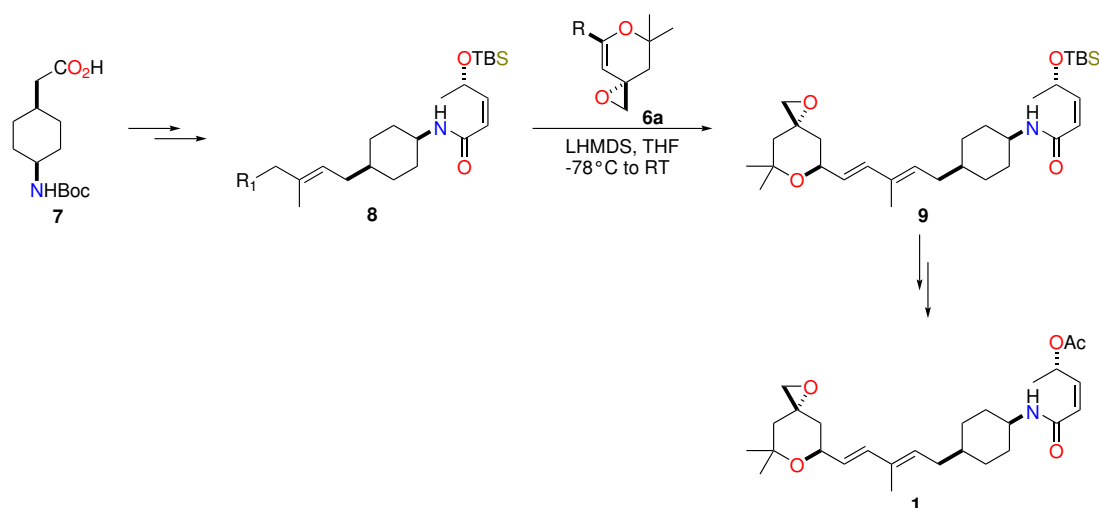
**Figure 2.19:** Structures of the target compound **1** and pladienolide **B** and FR901464 (adapted from *Aléman J. et al.*<sup>101</sup>)

synthetic derivative **1**. In particular, the spirobicyclic fragment of **1** was synthesised by an enantioselective organocatalytic reduction using a particular MacMillan catalyst (Scheme 2.1).<sup>160</sup> Hence, enone **2** was reduced using *t*Bu-derived Hantzsch ester **4** and catalysed by 20 mol% of catalyst **3**, affording the desired ketoester **5** in good yield and 91% ee. It is noteworthy that the reduction of **2** under enantioselective transition metal catalysis conditions was unsuccessful, giving even more value to this result.



**Scheme 2.1:** Organocatalytic reduction of **2** for the synthesis of intermediates **6a,b** (adapted from *Aléman J. et al.*<sup>101</sup>)

After that, in two more steps it was possible to transform the ketoester **5** into epoxides **6a** and **6b** which are key intermediates for the synthesis of the desired products. Focusing the attention on the synthesis of compound **1**, *Webb* attached the spirocyclic intermediate **6a** to the remaining part of the molecule via nucleophilic attack of the carbanion **8** and the intermediate **9** was obtained after a dehydration step. Finally, deprotection of hydroxyl group of **9** and further acylation afforded the desired product **1** in 2.7% yield starting from **2** (Scheme 2.2).

Scheme 2.2: Synthetic route to **1** (adapted from Aléman. J et al.<sup>101</sup>)

### 2.3.2 Via-Iminium Ion Catalysis in the Synthesis of Anticoagulant Agents

The **catalysis via iminium ion** was designed in 1999 by *MacMillan* and coworkers and introduced as a general synthetic tool in asymmetric organic chemistry. This strategy was based on chiral amines that acted as enantioselective catalysts able to activate the starting material by lowering the LUMO energy to allow several transformations traditionally carried out using Lewis acids. *MacMillan* hypothesised that the reversible transformation of iminium ion from the reaction between  $\alpha,\beta$ -unsaturated aldehyde and asymmetric amines could mimic the dynamic equilibrium and the electronic state of  $\pi$  orbitals obtained in a reaction catalysed by Lewis acids. To this purpose, *MacMillan* and coworkers have developed several imidazolidinone-based catalysts currently employed in dozens procedures with high enantioselective control.<sup>148</sup>

The first experimental evidences and computational studies have demonstrated the relevance of four perspectives in the design of broad spectrum catalysts: 1) chiral amines have to effectively and selectively form the iminium ion; 2) iminium ion must have high geometric control; 3) selective discrimination of the olefin's  $\pi$  faces is necessary to control the enantioselectivity of the reaction, and 4) catalyst has to be easily synthesised and functionalised. (5*S*)-2,2,3-Trimethyl-5-phenyl-4-imidazolidinone was the first catalyst developed by *MacMillan* and it formed selectively the (*E*)-iminium isomer in order to minimise the steric interactions between the olefin and the dimethyl substituent of the catalyst. From a computational point of view, it was observed that the facial enantioselectivity was provided by the benzylic group in position 5 which blocked the Si iminium ion face leaving the Re one free to form enantioselective new bonds. Two years later, *MacMillan* and coworkers<sup>161</sup> developed a "second generation" of imidazolidinone-based catalysts with the aim to improve the reactivity and versatility features exhibited by the first one. Thus, they synthesised several new secondary amine scaffold in which the pivotal compound was (2*S*,5*S*)-(-)-2-*tert*-butyl-3-

methyl-5-benzyl-4-imidazolidinone (Figure 2.20).

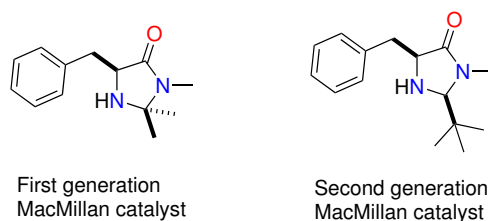
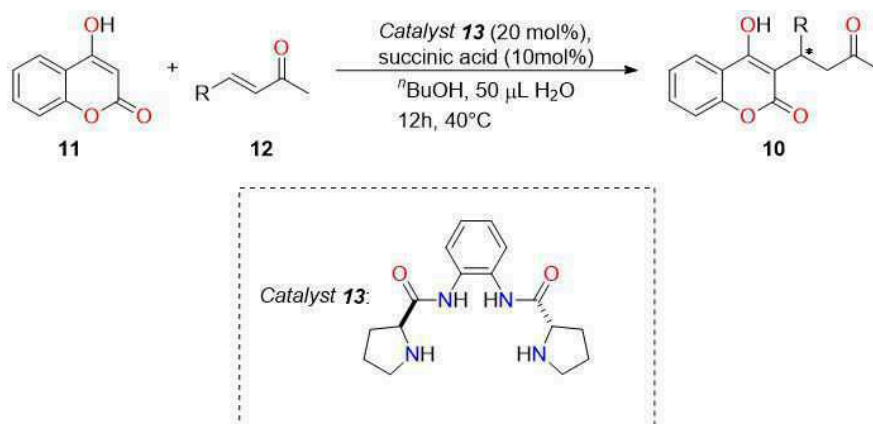


Figure 2.20: First and second generation of *MacMillan* catalysts.

The iminium ion catalysis is one of the most employed tools in medicinal chemistry for the synthesis of several simple and considerable bioactive compounds; among these molecules, one of the most remarkable examples is **Warfarin**. Warfarin is a vitamin K analogue able to inhibit the vitamin K epoxide reductase and is commercialised as sodic salt with the commercial name of <sup>®</sup>Coumadin and <sup>®</sup>Marevan. Warfarin is one of the most prescribed anticoagulant and for more than 50 years it was distributed as racemic mixture, however its enantiomers exhibited different pharmacodynamic and pharmacokinetic profiles: (S)-Warfarin is more active than the (R) enantiomer, but the higher bioavailability of the (R)-Warfarin makes it overall more active than the (S) enantiomer.

In 2009, *Feng* and coworkers synthesised a library of Warfarin derivatives **10** via organocatalytic reaction. This synthesis involved the reaction between 4-hydroxycoumarin **11** and various benzylidene- or alkylideneacetones **12**, catalysed by 20 mol% of (L)-proline derivative **13** at 40°C in n-butanol. Moreover, they improved the enantioselectivity of the process adding 10% of succinic acid and a small amount of water as additive (Scheme 2.3).



Scheme 2.3: Synthesis of **10** proposed by *Feng* et al.<sup>162</sup>

Thus, 16 different Warfarin derivatives were prepared in high yields (up to 99%) and good selectivity (up to 89%ee) with the best results obtained using aromatic  $\alpha,\beta$ -unsaturated ketones with electron-donating substituents. In addition, they demonstrated the feasibility of gram scale reaction obtaining good results and by means of a single recrystallisation they

isolated optically pure product in 54% yield.<sup>162</sup>

The mechanism proposed by *Feng* and coworkers involves the formation of the iminium ion intermediate obtained from the reaction between  $\alpha,\beta$ -unsaturated ketone **12** and (L)-proline derivative **13**. Then, 4-hydroxycoumarin **11** was introduced by H-bond activation and the desired (R)-Warfarin **10** was obtained through attack to the Re face of iminium ion (Figure 2.21).

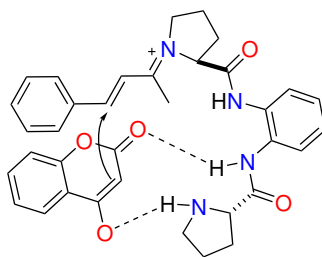


Figure 2.21: Proposed transition state by *Dong Z.* et al.<sup>162</sup>

## 2.4 Results and Discussions

### 2.4.1 Linear and Cyclic $\alpha$ -Dehydro- $\beta$ -Amino Acids as Scaffolds for Bioactive Compounds

The design of small molecule-based peptidomimetics<sup>163</sup> has received increasing attention in medicinal chemistry<sup>164</sup> with the aim to obtain new chemical entities with enhanced activity towards biological targets. These compounds often reduce peptide disadvantages as low solubility, high flexibility and low stability. Among the different approaches, introduction of  $\beta$ -amino acids in a peptide sequence has been widely explored.<sup>165</sup> Homologues of  $\alpha$ -amino acids, obtained via simple incorporation of an additional methylene between the carboxylate and amine moieties, allow to increase stability to protease degradation. Moreover, the staggered conformation around  $sp^3$  carbons induces the formation of ordered secondary structures in  $\beta$ -peptides.<sup>166–168</sup> Heterogenous  $\alpha,\beta$ -peptides, including both constrained  $\beta$ -amino acids and  $\alpha$ -amino acids, have been explored instead with the aim to design fragments assuming a defined bioactive conformation.<sup>169,170</sup> In particular, introducing  $\alpha$ -substituents is a common way to reduce conformational freedom of  $\beta$ -amino acids and  $\alpha$ -dehydro- $\beta$ -amino acids have been reported to play a role similar to L-proline in inducing  $\beta$ -turns, due to the presence of the double bond as torsional restriction.<sup>171,172</sup>

In the last few years, we have been interested in the synthesis of linear and cyclic  $\alpha$ -dehydro- $\beta$ -amino acids as scaffolds for the preparation of bioactive peptidomimetics. In particular, we have focused our attention on the design, synthesis and biological evaluation of  $\alpha_V\beta_3$  /  $\alpha_5\beta_1$  and  $\alpha_4\beta_1$  integrin ligands. These transmembrane receptors are overexpressed on the surface of cancers cells and have a paramount role in cell adhesion and survival. Modulation of their activity has received much attention as a tool for treatment of cancer and

inflammatory diseases treatment by several research groups all over the world. Low molecular weight ligands of  $\alpha_V\beta_3$  and  $\alpha_5\beta_1$  integrins, possessing a linear  $\alpha$ -dehydro- $\beta$ -amino acid linked to pharmacophoric moieties mimicking the RGD recognition sequence, showed affinity in the micromolar range toward target receptors.<sup>173</sup> Structural models for  $\alpha_V\beta_3$  integrin-ligand binding confirmed that the  $\alpha$ -dehydro- $\beta$ -amino acid core induces the formation of stabilizing conformations. In addition, isoxazoline<sup>98</sup> and dehydroproline rings<sup>173</sup> are representative examples of cyclic  $\alpha$ -dehydro- $\beta$ -amino acids, and were exploited as rigid scaffolds for the synthesis of  $\alpha_V\beta_3/\alpha_5\beta_1$  integrin and  $\alpha_4\beta_1$  integrin ligands, respectively. In both cases, compounds displaying nanomolar affinity in cell adhesion assays were obtained (Figure 2.22).

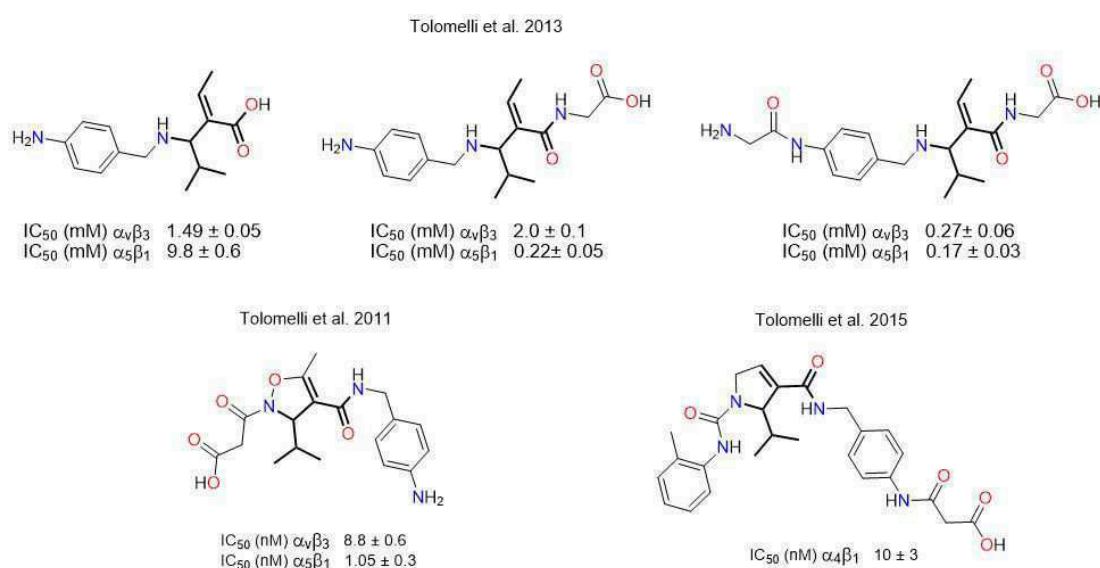


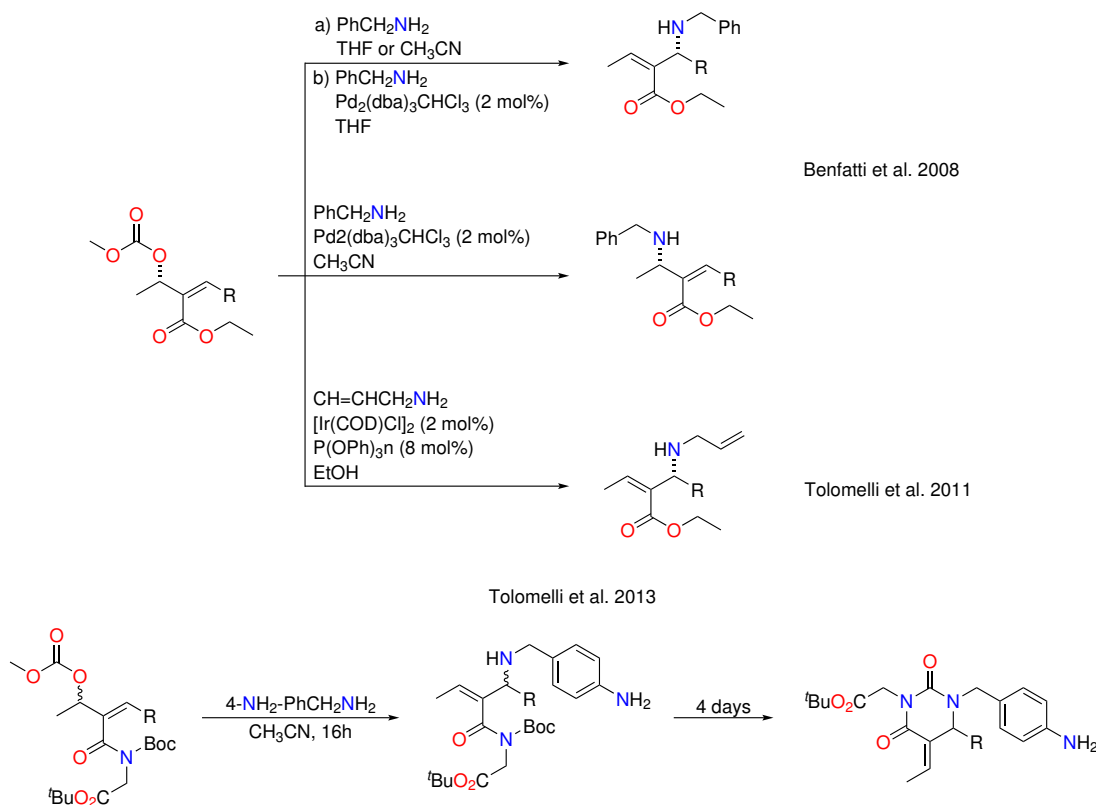
**Figure 2.22:** Representative examples of integrin ligands containing  $\alpha$ -dehydro- $\beta$ -amino acids.

The key reaction for the synthesis of  $\alpha$ -dehydro- $\beta$ -amino acids, independently from the nature and length of the side chains, is the  $SN2'$  allylic amination on carbonate esters or amides deriving from alkylidene malonates or acetoacetates. The reaction conditions explored in previous studies are summarized in Scheme 2.4.<sup>174,175</sup>

Transition metal-catalyzed allylic amination is a reliable method for the formation of C-N bonds.<sup>176</sup> The regiochemistry and stereochemistry of the reaction, starting from linear allylic systems bearing a good leaving group as carbonate,<sup>177</sup> has been deeply investigated in the past decades. In particular, asymmetric Pd-catalysed reactions allowed to synthesise a great number of structurally complex molecules with broad application.<sup>178</sup> On the other hand, the Pd-catalyzed reaction generally leads to the functionalization of the allylic terminus, and for this reason Ir-catalysed allylic amination has been exploited as an excellent alternative when branched derivatives were required.<sup>179,179</sup>

The observed unusual reactivity of alkylidene acetoacetamide deriving from glycine<sup>180</sup>, prompted us in extending the study to other amino acid-deriving substrates, in order to



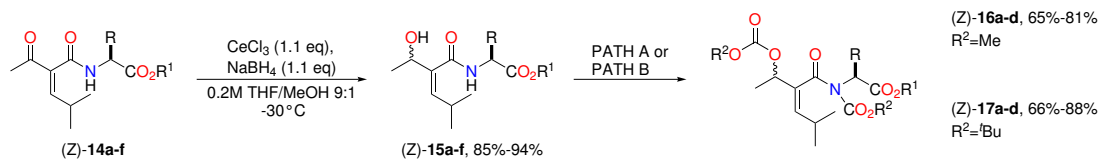


Scheme 2.4: Allylic amination reported in previous papers.

synthesize a novel class of  $\alpha/\beta$  dipeptides containing linear or cyclic  $\alpha$ -dehydro- $\beta$ -amino acids. Moreover, we wanted to investigate the effect of steric hindrance on the regioselectivity of the Ir-catalyzed substitution on the cyclization step in order to propose a rationalization of the reaction outcome.

Our group recently reported a telescopic microwave-induced, one pot-two steps synthesis of alkylidene acetoacetamides deriving from amino acids.<sup>181</sup> The protocol always afforded  $\geq 9/1$  mixtures of *Z/E* isomers that were separated by flash chromatography. Due to the small amount of the minor (*E*) isomer, further studies were carried out on the pure (*Z*) isomer. Starting from these substrates, in this thesis work we exploited our expertise in the synthesis and transformations of allylic alcohols deriving from alkylidene acetoacetates to obtain allylic carbonates. Selective reduction of the keto group in (*Z*)-**14a-f** was successfully performed under Luche's conditions,<sup>182</sup> with a careful temperature control ( $-30^\circ\text{C}$ ) to obtain the corresponding allylic alcohols (*Z*)-**15a-f** in excellent yields (Scheme 2.5).

The results obtained on different amino acid derivatives are reported in Table 2.1. As expected, the amino acid side chain did not induce any preference on the formation of the new stereocenter. Despite the separation of the diastereomeric mixture obtained in the reduction step was attempted, no significant improvements in  $\text{SN}2'/\text{SN}2$  reactions on the single diastereomer were observed.



**PATH A:** LiHMDS (2.5 eq), MeOCOCl (4.0 eq), THF,  $-78^\circ\text{C}$ ; **PATH B:** TEA (2.0 eq), DMAP (0.2 eq),  $\text{BOC}_2\text{O}$  (2.5 eq), THF,  $65^\circ\text{C}$

**Scheme 2.5:** Luche's reduction on alkylidene acetacetamides (Z)-14a-f and synthesis of carbonates (Z)-16a-d and (Z)-17a-d starting from (Z)-15a-d.

Entry	Substrate	Amino acid	$\text{R}^1$	Yield(%) <sup>a</sup>
1	14a	Gly	<sup>t</sup> Bu	92
2	14b	Leu	Me	85
3	14c	Phe	Me	94
4	14d	Asp(OMe)	Me	75
5	14e	Val	Me	72
6	14f	Thr(O <sup>t</sup> Bu)	Me	83

<sup>a</sup>Yields of products 15a-f purified by flash chromatography on silica gel

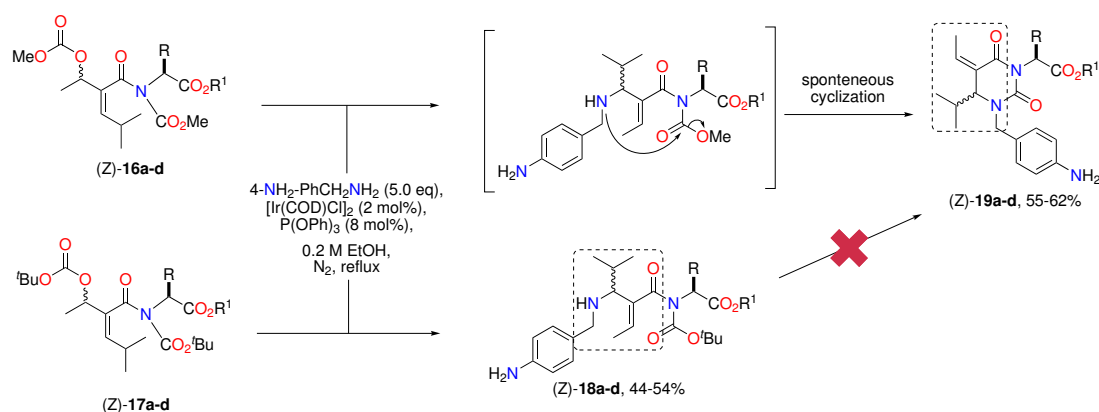
**Table 2.1:** Luche's reduction on amino-acid-deriving acetacetamides 14a-f.

Transformation of the hydroxyl group into a carbonate was performed with LiHMDS and methyl chloroformate (Path A) or di-*tert*-butyldicarbonate ( $\text{BOC}_2\text{O}$ ) in the presence of DMAP (Path B), to obtain carbonates with a good leaving group and different steric hindrance. Concerning pathway A, any attempt to introduce the carbamate with a milder base (TEA, NaH,  $\text{Na}_2\text{CO}_3$ ) failed, as already observed for similar derivatives.<sup>174</sup> The influence of amino acid side chain was also investigated, since compounds possessing a methylene group in the  $\beta$ -position of the amino acid side chain, as (Z)-15a-d, didn't behave as  $\beta$ -branched ones, as valine or threonine derivatives (Z)-15e-f, both in the carbonate formation and in the following transformations.

Treatment of (Z)-15a-d with an equimolar amount of the acylating reagents to obtain allylic carbonates, afforded a complex mixture of O-acylated, N-acylated and diacylated derivatives, both using methyl chloroformate or di-*tert*-butyldicarbonate ( $\text{BOC}_2\text{O}$ ) at room temperature. To overcome this drawback, an excess of the acylating reagent was used in both cases to completely convert the alcohols into the diacylated derivatives (Scheme 2.5). For the protection with BOC group, the reaction was performed in refluxing THF to increase speed and reduce side products. The reactions afforded the expected diacylated compounds (Z)-16a-d and (Z)-17a-d in yields ranging from 65% to 88% (see experimental section). Acylation of the alcohol moiety was necessary to obtain a good leaving group, but a further advantage is represented by the introduction of the electron withdrawing carbamate group on the amide

nitrogen, that could favour the allylic substitution by avoiding mesomeric delocalization of nitrogen lone pair.

Since the synthesis of  $\alpha$ -dehydro- $\beta$ -amino acids was our goal, we explored the SN2' substitution with amines on allylic carbonates. The reaction was first performed in refluxing solvent without any catalyst but a very slow conversion was observed, as previously reported for similar substrates.<sup>174</sup> For this reason an iridium-catalysed protocol was planned and the uncatalysed process was not considered to occur as a possible back reaction. To this purpose, (Z)-16a-d and (Z)-17a-d were treated with 4-aminobenzylamine under the catalysis of the complex, generated in situ, between [Ir(COD)Cl]<sub>2</sub> and P(OPh)<sub>3</sub> (Scheme 2.6). The choice of 4-aminobenzylamine as nucleophile was due to the possible exploitation of the reaction products as scaffolds for  $\alpha_V\beta_3$  and  $\alpha_5\beta_1$  integrin ligands preparation. Generally, aromatic amines are not sufficiently reactive to act as nucleophile in allylic substitution<sup>183</sup> without activation with a base. Thus the aniline moiety doesn't afford any side reaction, being the benzylic amine moiety the only reacting nucleophile under the selected conditions.



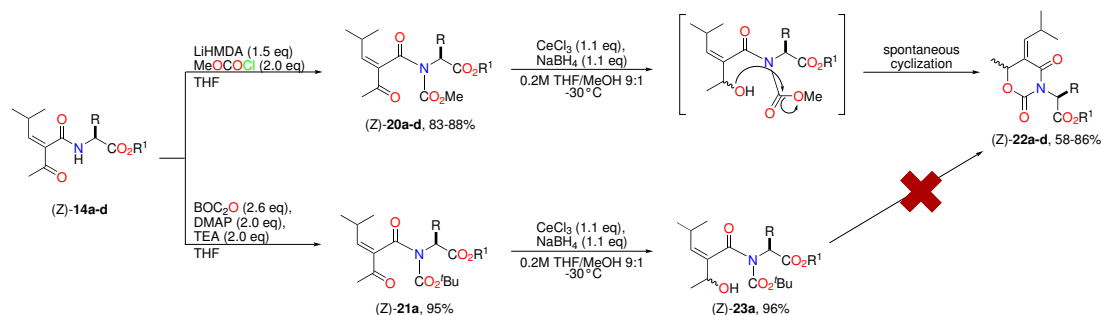
Scheme 2.6: Allylic substitution with 4-aminobenzylamine on (Z)-16a-d, and (Z)-17a-d.

As reported in Scheme 2.4, the issue of regioselectivity in the allylic substitution had been already studied by our group on similar substrates. To perform the reaction on (Z)-16a-d and (Z)-17a-d we selected suitable conditions to drive the reaction toward the substitution at the allylic position. The results of amination on these substrates further confirmed our hypothesis. The products deriving from amination in the allylic position were indeed favoured and the products deriving from direct SN2 substitution were detected only in traces in the NMR spectra of the crude reactions. The reaction performed on (Z)-16a-d followed the SN2' pathway and afforded exclusively the functionalised dihydropyrimidine-2,4-dione (Z)-19a-d, via the spontaneous cyclization of the secondary amine on the methyl carbamate moiety in the intermediate adduct (Scheme 2.6). The Z isomer of the newly formed double bond was always observed as the unique product. According to previously reported results, the cyclic compounds 19a-d can be easily identified by LC-MS from the molecular weight that lacks the methoxy group, and from the <sup>1</sup>H NMR, that shows distinguished signals for

the two geminal benzylic hydrogens.

Under the same conditions, (*Z*)-**17a-d** afforded the linear  $\alpha$ -dehydro- $\beta$ -amino acid-containing dipeptide (*Z*)-**18a-d**. The different reactivity has been ascribed to the steric hindrance of the *tert*-butyl carbamate moiety that doesn't allow the intramolecular cyclization, thus affording exclusively the linear derivative (*Z*)-**18a-d**. The regiochemistry and the (*Z*) stereochemistry of double bond in the final products has been established by comparison with similar products, being the signal of the vinyl proton a quartet around 6.60–6.75 ppm. The reaction on (*Z*)-**17d** was sluggish and afforded a complex mixture of compound (*Z*)-**18d** (20%) together with transesterification products (32%) and decarboxylated derivative (48%).

To complete our study, we also explored the reactivity of alkylidene acetacetamides by changing the order of the reaction steps. For this reason, we performed the protection of amides (*Z*)-**14a-d** before reducing the keto moiety (Scheme 2.7). Protection as methyl carbamates, obtained following the conditions above reported, afforded compounds (*Z*)-**20a-d** in excellent yields (83%–88%). In agreement with the results reported above, when the Luche's reduction was performed on (*Z*)-**20a-d**, the spontaneous cyclization of intermediate alkoxyde to the functionalized 1,3-oxazinane-2,4-dione (*Z*)-**22a-d** occurred. The 1,3-oxazinane-2,4-dione scaffold, being isoster of benzoxazine-2,4-dione, may be exploited as central constrained core in the synthesis of potential drug candidates as psychotics,<sup>184</sup> anticancers,<sup>185</sup> and inhibitors of hepatitis C virus.<sup>186</sup>

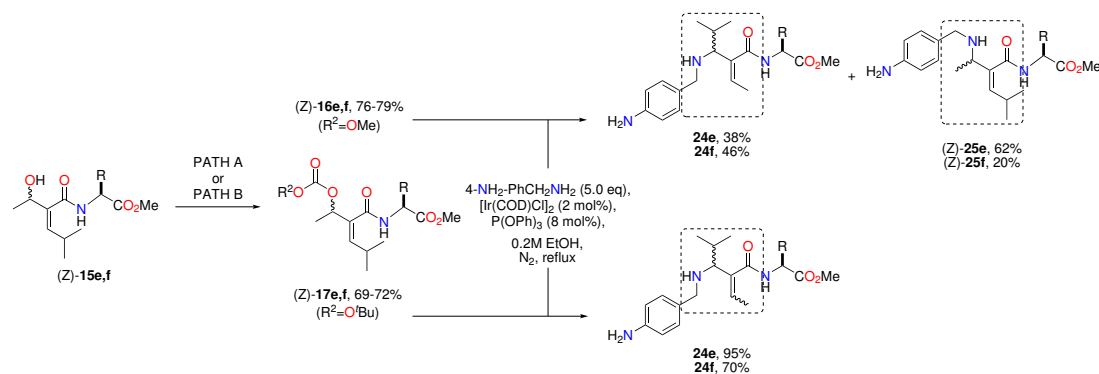


Scheme 2.7: Protection and reduction of acetacetamides (*Z*)-**14a-d**.

On the other hand, as expected, by performing the reaction on *tert*-butyl carbamate (*Z*)-**21a**, formation of the cyclic compound was inhibited by the *tert*-butyl carbamate hindrance and the allyl alcohol (*Z*)-**23a** was stable enough to be isolated and consequently functionalized as *tert*-butyl carbonate (*Z*)-**17a** (95%).

Preparation of allylic carbonates from alcohols (*Z*)-**15e,f**, deriving from  $\beta$ -branched amino acids as valine and threonine respectively, allowed to observe a different behaviour. Acylation of compounds (*Z*)-**15e,f**, indeed afforded exclusively the *O*-acylated derivatives (*Z*)-**16e,f** and (*Z*)-**17e,f** even by adding a large excess of acylating reagents or increasing temperature (Scheme 2.8). This result can only be due to the presence of a substituent in the  $\beta$ -position

of the amino acid side chain, whose hindrance prevents the acylation of the amide.



PATH A: LiHMDS (2.5 eq), MeOCOCI (4.0 eq), THF, -78 °C; PATH B: TEA (2.0 eq), DMAP (0.5 eq), Boc<sub>2</sub>O (6.0 eq), THF 65 °C

**Scheme 2.8:** Synthesis of carbonates (Z)-16e,f and (Z)-17e,f and allylic substitution with 4-aminobenzylamine on (Z)-16e,f and (Z)-17e,f.

No difference in reactivity was observed between valine and threonine derivatives, confirming that the hindrance of the ramification is detrimental for the nitrogen acylation, independently from the nature of the substituent.

Lacking the carbamate protection at the amide nitrogen, the allylic amination performed on carbonates (Z)-16e,f and (Z)-17e,f could afford exclusively linear compounds. The reactivity of these derivatives showed again a strong dependence on the alkyl carbonate chain (Scheme 2.8).

The allylic amination on compounds (Z)-16e,f, bearing the methylcarbonate leaving group, afforded a mixture of products deriving both from the S<sub>N</sub>2 and S<sub>N</sub>2' substitution. When the reaction was performed on the valine derivative (Z)-16e, the product (Z)-25e deriving from the direct substitution was obtained as the major product (62%) together with a 1/1 mixture of 24e, deriving from the substitution in the allylic position. The reaction on the threonine derivative (Z)-16f afforded on the contrary compound 24f as the main product (46%), even if 25f was isolated in significant amount (20%). The regiochemistry and the configuration of the double bond in the final products 24e,f and 25e,f were recognised on the basis of the multiplicity and position of the vinyl proton signal, that appeared as a doublet for 24e,f, being in this case coupled with the isopropyl group. The position around 6.95 ppm for the major isomer allowed to assign the (Z) configuration, the minor (E) isomer generating a doublet around 5.75÷5.85 ppm. On the other hand, treatment of (Z)-17e,f with 4-aminobenzylamine afforded the expected S<sub>N</sub>2' products 24e,f, as 1/1 E/Z mixture. Finally, the reduced reactivity of the amide nitrogen in valine and threonine derivatives was confirmed by the failure of any effort to introduce the carbamate moiety in alkylidene acetoacetamides (Z)-14e,f, thus confirming the disadvantageous hindrance of the amino acids' side chain

ramification. For this reason, the Luche's reduction could not afford any cyclization of intermediate alkoxydes to the functionalized 1,3-oxazinane-2,4-diones, giving exclusively the allylic alcohols (*Z*)-**15e,f**.

Iridium-catalysed allylic amination has been applied in the last few years to a number of complex substrates. Anyway, while linear allylic electrophiles have been well studied, more complex substrates have been rarely reported,<sup>187,188</sup> mainly for the difficulty to control and rationalise the reaction outcome. The mechanism of the reaction has been deeply investigated in order to obtain the control of the regio- and stereochemistry. The allylic substitution proceeds through the oxidative addition of the substrate to iridium complex with the loss of the carbonate, followed by the nucleophilic attack of the amine.  $\pi$ - $\sigma$ - $\pi$  isomerization of the allyl-iridium complex may occur, depending on the relative speed of the isomerization vs the nucleophilic attack. To understand the origin of the regioselectivity, Helmchem and coworkers<sup>189</sup> performed DFT calculation based studies, but a simple rule couldn't be deduced. Hartwig and coworkers<sup>190</sup> suggested that the length of the Ir-C bond in the complex had a strong effect, but still the explanation was not exhaustive to justify regiocontrol. On the other hand, even if the nature of the leaving group is not usually taken into consideration in the catalytic cycle after the oxidative addition step, differences in the reactivity of methyl and *tert*-butyl carbonates have been reported, mostly limited to by-product generation due to different reaction speeds.<sup>191,192</sup>

In our case, being the conditions applied for the reaction on **16a-d/17a-d** the same used for the amination of **16e,f/17e,f**, steric and electronic effects should play a fundamental concomitant role in driving the regioselectivity of the nucleophilic attack (Figure 2.23).

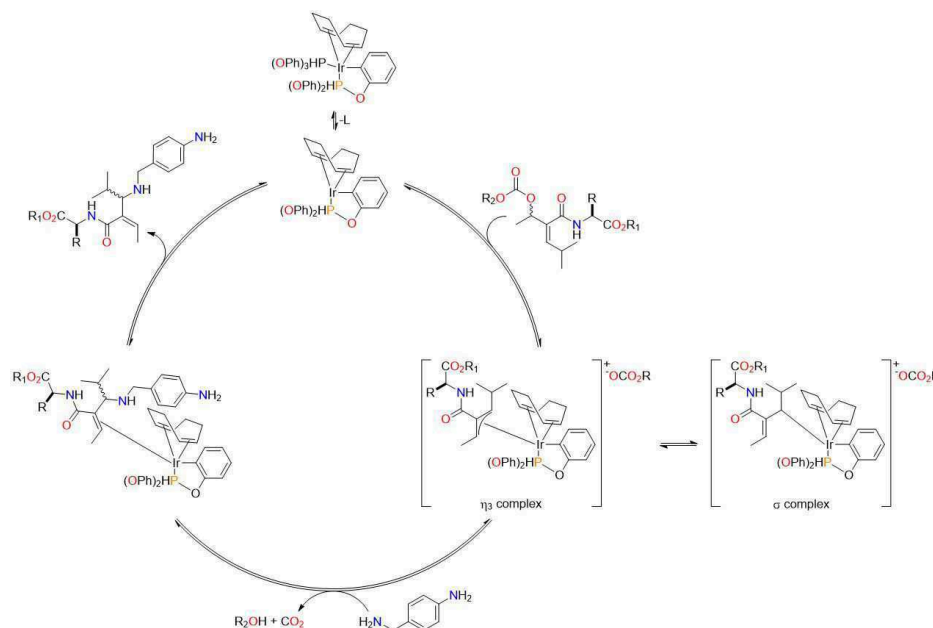


Figure 2.23: Example of Ir-catalysed allylic amination on **17e,f**.

All the studied carbonates have the same isopropyl substituent on the allylic terminus. The effect of the hindrance in this position had been previously explored<sup>180</sup> and an effect on the spontaneous intramolecular cyclization step was exclusively observed, due to the different conformational arrangement induced by the bulky side chain.

For compounds **16a-d/17a-d**, the presence of *N*-carbamate moiety, although increasing the steric hindrance, imparts further activation to the allylic terminus since the electron withdrawing effect inhibits the nitrogen doublet back donation. The Ir-catalysed allylic amination on these substrates afforded, as expected, the preferential nucleophilic attack in the  $\beta$ -position leading to SN2' prevailing mechanism (Figure 2.23).

For compounds **16e,f/17e,f**, having branched amino acids linked to the amide bond, different results were observed on methyl and *tert*-butyl carbonates. Since small differences in reactivity were observed between valine and threonine derivatives, the nature of the amino acids side chain didn't strongly influence the process. The experimental evidence showed that *tert*-butyl carbonates **17e,f** afforded preferentially products deriving from the attack on the allylic terminus via a SN2' mechanism, as observed for above reported carbonates **16a-d/17a-d**. Since **17e,f** lack of the carbamate protection on the amide, no further cyclization to dihydropyrimidine-2,4-dione could occur (Figure 2.23).

On the contrary, the reactions performed on methyl carbonates **16e,f** afforded mixture of products, demonstrating a low control of the regiochemistry. In general, regioselectivity is due to thermodynamic preference in the oxidative addition step, but in the case of sterically hindered substrates, a weaker and longer bond to iridium could turn into a less defined situation. Moreover, compounds **16e,f/17e,f** still display the NH amide group since the steric hindrance of the branched side chain of the amino acid inhibited the amide acylation. It is possible that the formation of hydrogen bonds with the nucleophile could give rise to structurally different intermediates and have a role in the regiochemical preference, as already observed for Pd-catalyzed enantioselective allylic substitutions.<sup>193</sup>

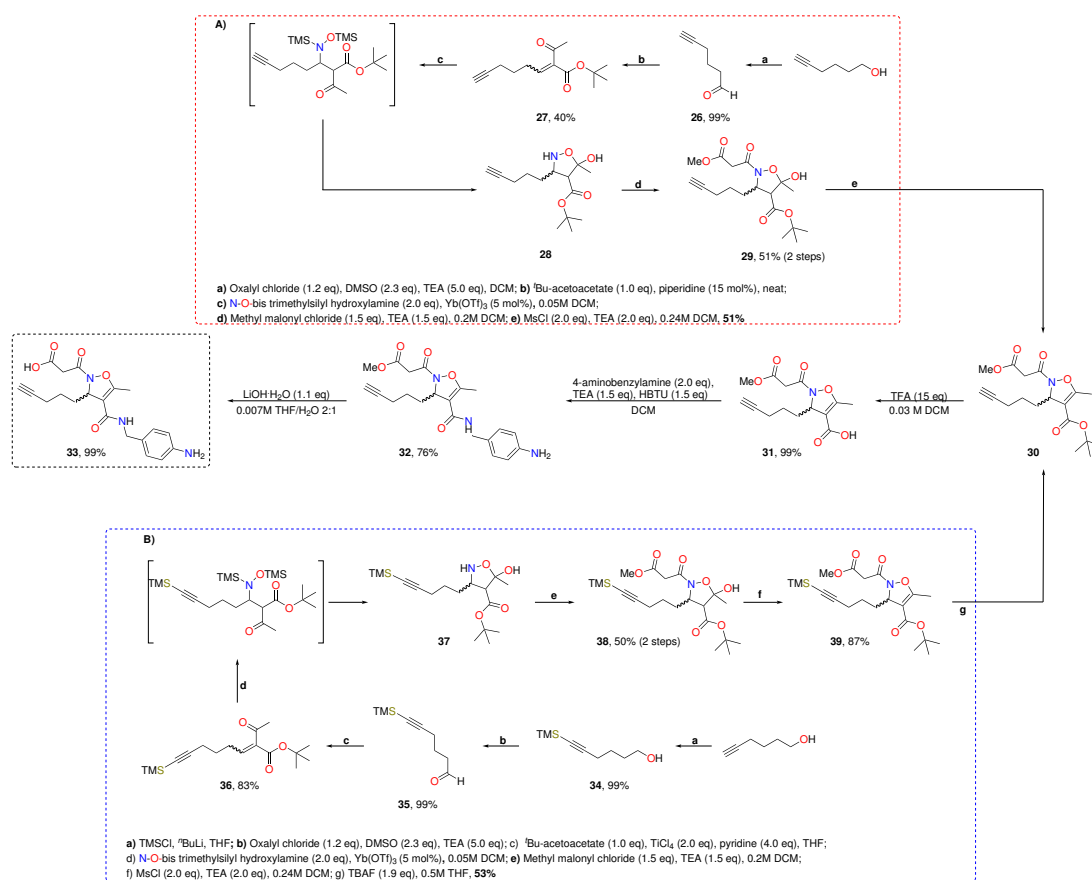
#### 2.4.2 Synthesis of New Isoxazoline-Based Integrin Ligands

In the last decades, peptides and peptidomimetics designed to mimic the recognition sequence RGD (Arg-Gly-Asp),<sup>194</sup> present in the extracellular endogenous ligands of these receptors, have received great attention as targeting motifs.<sup>195</sup> Their exploitation as therapeutic tools, per se, is still an option but some recent unsatisfactory results<sup>196</sup> prompted the researchers to turn their attention towards the possible use of these ligands as shuttles for selective delivery of therapeutic payloads and diagnostics.<sup>197</sup> In 2011, our research group has reported the synthesis and biological evaluation of a small library of isoxazoline-based RGD mimetics where the pharmacophores were mimicked by malonic acid and aniline moieties.<sup>98</sup> Despite the known tox-risk associated to the presence of aniline, the molecules already reported showed very good efficacy in binding the target receptors, probably as

consequence of the basicity and length of this arginine-mimicking group. All the members of the library, differing only for the substituent in position 3 of the heterocycle, displayed excellent potency to modulate cell adhesion mediated by  $\alpha_V\beta_3$  integrins (Figure 1.12).

On the basis of this consideration, we selected the functionalisation in position 3 as a useful anchorage of the heterocyclic scaffold for covalent ligation of diverse linkers, with the aim to not compromise the integrin binding capabilities. The purpose of this investigation was the synthesis of a variety of rather well sized ligand-linker systems to demonstrate the broad utility of the isoxazoline ligands for diverse and efficient bioconjugation strategies in drug and diagnostic tumor homing.

To introduce a functionalisable chain in position 3 of the isoxazoline scaffold, we thought that a terminal alkyne could be a versatile moiety to be exploited in 1,3-dipolar Huisgen cycloaddition with different azide-linkers. To follow our previously reported synthetic protocol, 5-hexynal **26** had to be synthesized from the corresponding commercially available alcohol, via Swern oxidation with oxalyl chloride and TEA in DMSO (99% yield, Scheme 2.9).



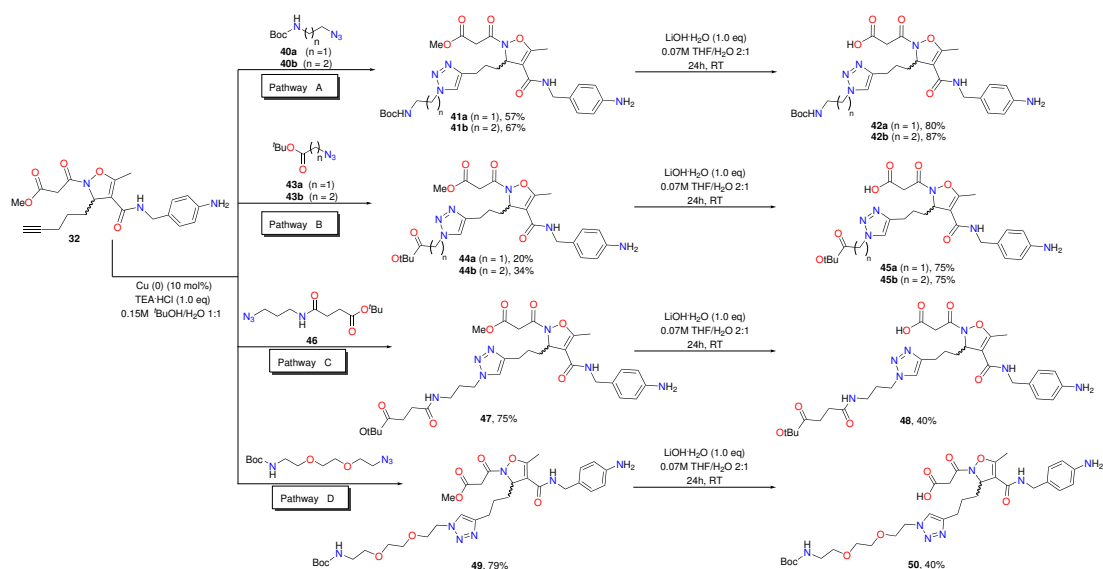
**Scheme 2.9:** Synthetic pathways for the synthesis of methyl ester **32** and the corresponding acid **33**, using the route A) or B) to evaluate the effects of alkyne-side chain on the yield of some critical steps of reaction.



The Knövenagel reaction between **26** and *t*-butyl-acetoacetate afforded the alkylidene acetoacetate **27** in 40% yield as a 1/4 mixture of *Z/E* isomers (Scheme 2.9, path A). The unsatisfactory yield, never observed previously for simpler aldehydes, even using a microwave assisted protocol,<sup>174</sup> was attributed to alkyne side reactions. For this reason, we protected the alkyne moiety with TMS group as reported by *Cruciani* and coworkers.<sup>198</sup> As a consequence, the Knövenagel reaction was performed using TiCl<sub>4</sub>/pyridine affording the alkyne-protected alkylidene acetoacetate **36** in 83% yield as 1/4 mixture of *Z/E* isomers as well and confirming the previous hypothesis of alkyne side reactivity (Scheme 2.9, path B). As already reported, isoxazoline may be obtained via 1,4-addition. Reaction conditions for the addition of bis-(*N,O*)-trimethylsilylhydroxylamine to **27** and **36** were optimized on the basis of our previous experience,<sup>199,200</sup> in order to avoid the formation of oxime by-product as a result of the undesired 1,2-addition process.<sup>201</sup> According to these considerations, the reaction was performed in DCM in the presence of a catalytic amount (5%) of ytterbium triflate as Lewis acid. It should be noticed that the TMS protecting group of the hydroxylamine was removed during the usual work up procedure, inducing the fast conversion of the intermediate adduct to *trans* 5-hydroxyisoxazolidine-4-carboxylate **28** or **37**, as a single *trans* epimer, via intramolecular hemiketalisation. Introduction of the malonic pharmacophore was performed at this stage by acylation at the nitrogen with methyl malonyl chloride, in the presence of TEA. The isoxazolidines **29** or **38** were isolated in 51% and 50% overall yields after two steps, respectively. Dehydration to the unsaturated racemic isoxazolines **30** or **39** was accomplished by mesylation of the hydroxyl group followed by base-induced elimination. The removal of TMS protecting group on alkyne moiety of **39** by tetrabutylammonium fluoride afforded the product **30** in 53% yield. Selective removal of the *t*-butyl ester was then accomplished by treatment of **30** with an excess of trifluoroacetic acid in dichloromethane. The arginine mimetic chain was introduced by reaction of the acid **31** with 4-aminobenzylamine, following standard coupling conditions (HBTU/TEA in DCM) to give **32** in 76% yield. Hydrolysis of the methyl ester required a particular effort, since the undesired removal of the malonic side chain easily occurred, favored by the following spontaneous aromatization of the heterocycle as confirmed by LC-MS analysis. After several trials under different conditions, excellent results were obtained with a  $7 \cdot 10^{-3}$  M solution of LiOH·H<sub>2</sub>O in a 2:1 mixture of THF/water, following the reaction evolution by TLC, and stopping it at the disappearance of the starting ester. The acid **33** was obtained in quantitative yield.

In the design of the ligand-linker library, molecules terminating with an amine were prepared in order to obtain carriers for molecules with carboxylates or thiocarboxylates as active functionalisation, as for instance the cytotoxic agent fumagillin or the fluorescein isothiocyanate diagnostic derivatives. To this purpose, *N*-Boc-2-azido-ethylamine **40a** and *N*-Boc-3-azido-propylamine **40b** were prepared from the corresponding 2-bromo-ethylamine and 3-bromo-propylamine by protection of the amino moiety followed by substitution of

the bromide with  $\text{NaN}_3$ . The two azides were then reacted with methyl ester **32** in the presence of 10% copper<sup>(0)</sup> powder and TEA·HCl salt at room temperature in a 1:1 mixture of *t*BuOH and water.<sup>202</sup> The click reaction led to the exclusive formation of the desired 1,4-disubstituted [1,2,3]-triazoles **41a** and **41b**<sup>203</sup> in 57% and 67% yields, respectively. Removal of the methyl ester under the above reported conditions afforded compounds **42a** (80%) and **42b** (87%) (Scheme 2.10, pathway A). Initially, the *N*-Boc protection at the linker amine moiety was retained in order to avoid the possible interference of a second amine group in the ligand-receptor binding and to mimic the ester connection with a payload.



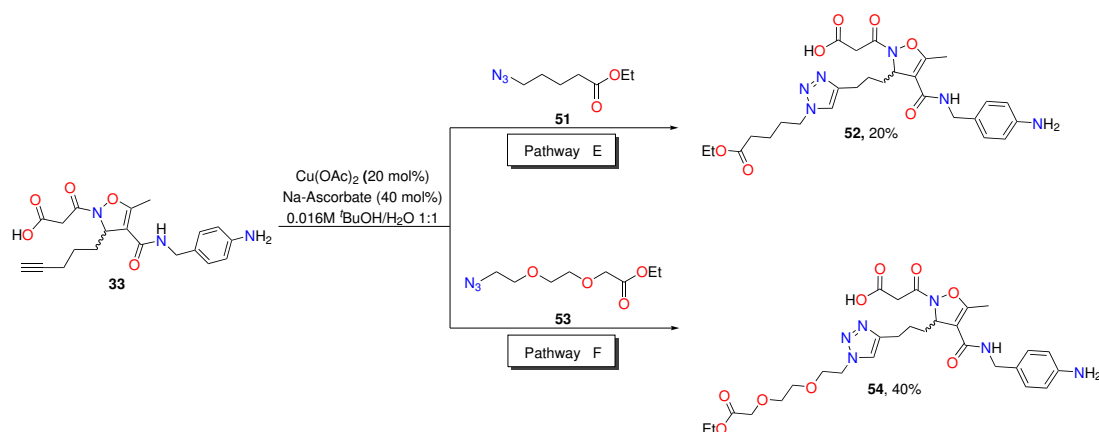
**Scheme 2.10:** Synthesis of ligands **42a,b**, **45a,b**, **48** and **50** functionalized by Huisgen 1,3-dipolar cycloaddition with copper(0) powder, TEA·HCl in *t*BuOH/H<sub>2</sub>O, starting from intermediate **32**.

For the preparation of molecules terminating with a carboxylate, able to conjugate drugs or diagnostics possessing functionalisable amines or hydroxyl groups, as for instance paclitaxel, compound **32** was submitted to Huisgen reaction in the presence of *t*-butyl 2-azidoacetate **43a** and *t*-butyl 3-azidopropionate **43b**, easily prepared from the corresponding bromides. The cycloaddition afforded compounds **44a** and **44b** in low yields (20% and 34%, respectively).

Complete regiocontrol was observed also in this case, affording exclusively the 1,4-disubstituted triazoles. Selective removal of the methyl ester was accomplished as reported above, to afford acids **45a** and **45b** (Scheme 2.10, pathway B). Even in this case, the *t*-butyl group was retained to avoid interferences in the binding and to mimic the ester connection with a payload. In order to verify if elongation of the linker could turn into a lower interference in integrin-endogenous ligand binding, we planned to synthesise more complex systems. The assembly of these composite molecules could be faced through several protocols, differing for the order of formation of the strategic bonds. Therefore, the synthetic protocol was optimised for each specific substrate. To obtain compound **48**, having the succinic moiety as

a typical and stable spacer between the carrier and the payload,<sup>204</sup> 3-bromo-propylamine was coupled with mono *t*-butyl succinic acid and the bromide was substituted with NaN<sub>3</sub>, to afford compound **46** in good yield (90%). Then, the click reaction with methyl ester **32** was performed under the usual conditions (75% yield). Removal of the methyl ester moiety, afforded the acid **48** in 40% yield (Scheme 2.10, pathway C). The synthesis of the simpler compound **52** was accomplished in one step by performing the Huisgen reaction on the acid **33** with ethyl 5-azido-pentanoate. Due to the nature of substrate **33**, the conditions of the reaction were modified and Cu(OAc)<sub>2</sub> was used in the presence of sodium ascorbate.<sup>205</sup> The click reaction afforded **52** in 20% yield, as consequence of the difficulties in the purification of the product from the copper salts (Scheme 2.11, pathway E). Many examples in the literature report the use of PEG as linker for drug-ligand connection for its ability to increase the solubility and to decrease the immunogenicity of the products.<sup>206</sup> Moreover, PEG-drug conjugates often exhibit a favourable *in vivo* behaviour and are less prone to enzymatic digestion. These data prompted us to design further carriers, containing the PEG fragment. To this purpose, compound **32** was reacted with commercially available *N*-Boc-1-amino-3,6-dioxo-8-octaneazide (Boc-NH-PEG(2)-N<sub>3</sub>) as reported in Scheme 2.10 (pathway D). Compound **49**, isolated in 79% yield, was then transformed into the corresponding acid **50** under the usual hydrolytic conditions (Scheme 2.10).

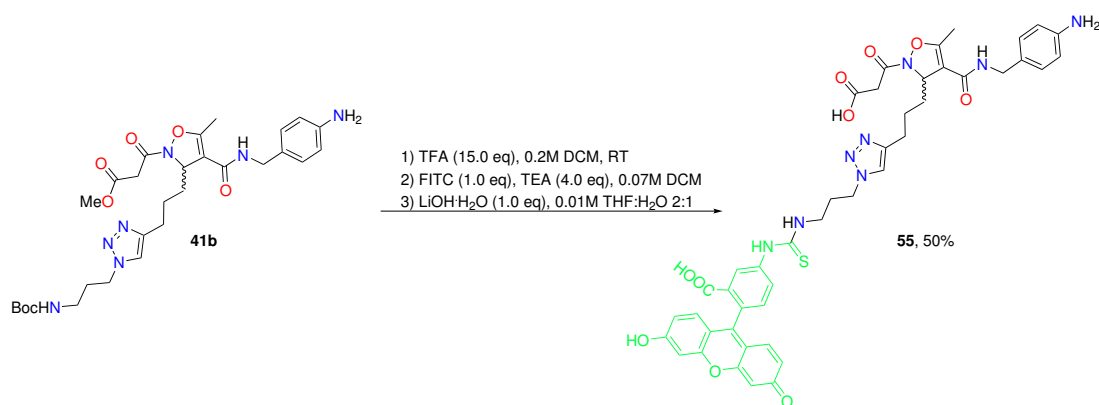
Finally, the acid **33** was treated with the PEG-azide **53**, easily prepared from the corresponding commercially available acid. As previously observed, the nature of the starting isoxazoline suggested the use of Cu(OAc)<sub>2</sub> and sodium ascorbate as catalysts (Scheme 2.11, pathway F). Under these conditions, compound **54** was isolated in 40% yield given the difficult purification step.



**Scheme 2.11:** Synthesis of ligands **52** and **54** functionalized by Huisgen 1,3-dipolar cycloaddition with Cu(OAc)<sub>2</sub>, Na-Ascorbate in H<sub>2</sub>O, starting from intermediate **33**.

Fluorescent labelled molecules are useful for localisation of proteins, visualisation of intracellular processes and study of interactions between ligand and receptors. In particular, imaging by fluorescence provides many advantages in terms of selectivity and sensitivity of

the detection. For this purpose, compound **42b**, showing good selectivity and potency toward  $\alpha_5\beta_1$  integrins (Table 2.2), was subjected to further functionalisation with a diagnostic dye. To this purpose, its precursor (**41b**) was deprotected at the *N*-terminal position of the side chain by using TFA in DCM, and conjugated with FITC (fluorescein isothiocyanate) in presence of an excess of TEA in DCM. The FITC-labelled intermediate was subjected, without further purification, to the basic hydrolysis of the methyl ester, following the procedure previously reported, to afford the final compound **55** in 50% yield over three steps (Scheme 2.12).



Scheme 2.12: Synthesis of targeting delivery system **55** by conjugation of intermediate **41b** with FITC.

In our previous experience, isoxazoline-based integrin ligands showed a strong potency towards  $\alpha_V\beta_3$  and  $\alpha_5\beta_1$  integrins, not affected by changing the alkyl group linked to position 3.<sup>98</sup> In designing this novel small library of peptidomimetics, alkyl chains were substituted by polyfunctionalised linkers including the triazole ring and amide, carbamate or ester moieties, that may create further interactions within the binding pocket. The ability of the synthesised racemic ligands to inhibit the adhesion of K562 cells (human erythroleukemic cells, expressing  $\alpha_5\beta_1$  integrin) or SK-MEL-24 cells (human malignant melanoma cells, expressing  $\alpha_V\beta_3$  integrin) to immobilised fibronectin was evaluated in collaboration with Prof. *Spampinato* and coworkers (Department of Pharmacy and Biotechnology, FABIT, University of Bologna).<sup>207</sup> These cell models are widely used to investigate potential antagonists/agonists of  $\alpha_5\beta_1$  or  $\alpha_V\beta_3$  integrin-mediated cell adhesion.<sup>96,180,208–211</sup>

In these experiments, the cells were seeded onto plates coated with fibronectin and allowed to adhere before quantitation of the number of adherent cells, in presence of increasing concentrations of the compounds. As a negative control, under these conditions, no significant cell adhesion was observed for BSA-coated plates or nonspecific substrate-coated plates (e.g., collagen I for SK-MEL-24 expressing  $\alpha_V\beta_3$  and poly-L-lysine for K562 expressing  $\alpha_5\beta_1$  integrin, data not shown). The ability of the new compounds to inhibit the adhesion of SK-MEL-24 and K562 cells to fibronectin was compared with that of the standard antagonist compounds, Ac-Asp-Arg-Leu-Asp-Ser-OH (Ac-DRLDS) and H-Gly-Arg-Gly-Asp-

Thr-Pro-OH (GRGDTP), known to be potent inhibitors of cell adhesion mediated by  $\alpha_V\beta_3$  and  $\alpha_5\beta_1$  integrins, respectively<sup>212</sup> and standard agonist Ref E (entry 15, Table 2.2), a potent and selective  $\alpha_5\beta_1$  ligand.<sup>208</sup>

Entry	Compound	$\alpha_V\beta_3$ IC <sub>50</sub> /EC <sub>50</sub> (nM) <sup>a</sup>	$\alpha_5\beta_1$ IC <sub>50</sub> /EC <sub>50</sub> (nM) <sup>a</sup>
1	33	830±50 (A)	>1000
2	42a	880±70 (AA)	0.28±0.03 (AA)
3	42b	>1·10 <sup>6</sup>	2.7±0.4 (AA)
4	45a	230±80 (A)	>1·10 <sup>6</sup>
5	45b	68±11 (A)	>1·10 <sup>6</sup>
6	48	>1·10 <sup>6</sup>	6590±160 (A)
7	52	610±80 (A)	>1·10 <sup>6</sup>
8	50	8840±140 (AA)	>1·10 <sup>6</sup>
9	54	>1·10 <sup>6</sup>	>1·10 <sup>6</sup>
10	55	n.d.	130±10 (AA)
11 <sup>b</sup>	RefA	32±3 (AA)	12±4 (AA)
12 <sup>b</sup>	RefB	8.8±0.6 (AA)	0.105±0.3 (AA)
13 <sup>b</sup>	RefC	360±70 (AA)	1320±80 (AA)
14 <sup>b</sup>	RefD	20±6 (AA)	1030±50 (AA)
15 <sup>c</sup>	RefE	>1·10 <sup>6</sup>	12.9±0.6 (A)
16 <sup>d, e, f</sup>	Ac-DRLDS	25±3 (AA)	>1·10 <sup>6</sup>
17 <sup>d, f</sup>	GRGDTP	926±6 (AA)	0.62±0.09 (AA)
18 <sup>g</sup>	c(RGDfV)	146±43 (AA)	n.d
19 <sup>h</sup>	Cilengitide	0.58±0.01 (AA)	n.d

A=agonist, AA=antagonist; <sup>a</sup>Data are presented as EC<sub>50</sub> for agonists and as IC<sub>50</sub> for antagonists ( $\mu$ M). Values are the mean  $\pm$  SD of three independent experiments carried out in quadruplicate; <sup>b</sup>Compounds reported in Figure 1 and extracted from reference<sup>98</sup>;

<sup>c</sup>Ref E= 2-(2-(4-Oxo-(o-tolylcarbamoyl)azetidin-2-yl)acetamido)acetic acid. Extracted from reference<sup>208</sup>; <sup>d</sup>Reference compounds; <sup>e</sup>See reference<sup>213</sup>; <sup>f</sup>See reference<sup>214</sup>; <sup>g</sup>See reference<sup>208</sup>; <sup>h</sup>See reference Dechantsreiter et al. *J. Med. Chem.* 1999, 42, 3033-3040; n.d. = not determined

**Table 2.2:** Effects of isoxazoline ligands on  $\alpha_V\beta_3$  and  $\alpha_5\beta_1$  integrin-mediated cell adhesion to Fibronectin (FN).

The obtained results are summarised in Table 2.2. From the results, it may be observed that the potency towards integrin  $\alpha_V\beta_3$  is generally maintained, while few compounds show high potency towards  $\alpha_5\beta_1$ . Compounds terminating with a carbamate moiety (42a, 42b and 50) behave as antagonists to integrin receptors, displaying anyway different selectivity. In particular, 42a displayed similar potency towards both receptors (entry 2), while the longer 42b is an excellent selective ligand for  $\alpha_5\beta_1$  (entry 3), displaying IC<sub>50</sub> in the low nanomolar range. The opposite preference could be observed for compound 50 that

showed a good potency for  $\alpha_V\beta_3$  receptor (entry 8). On the other hand, compounds having a terminal ester group (**45a**, **45b**, **48**, **52**) in the side chain, behaved generally as agonists, inducing an increase in cell adhesion. All the molecules having a linear chain linked to the triazole ring (**45a**, **45b**, **52**) displayed high affinity for  $\alpha_V\beta_3$  integrin (entries 4, 5 and 7) in the sub-micromolar range. By introducing an amide moiety in the central part of an elongated linker, as in compound **48**, the opposite selectivity was observed, still maintaining an agonist effect (entry 6). The introduction of a short PEG fragment induced complete loss of the activity (compound **54**, entry 9). To complete the study, we also performed cell adhesion assay with the alkyne intermediate **33**, which showed a good potency and selectivity for  $\alpha_V\beta_3$ . These data seem to suggest a possible influence of the terminal moiety on the agonist/antagonist role. A structure-activity relationship rationalisation is still elusive, because agonist/antagonist behaviour<sup>214</sup> for integrin ligands is known to depend also on the concentration.<sup>215,216</sup> Anyway, the good to excellent potency of the members of this class of peptidomimetics confirms their possible use as shuttle for drugs or diagnostic selective delivery to cells overexpressing these two classes of integrins.

To gain further information about the agonist/antagonist role of our peptidomimetic integrin ligands and to verify the effect on intracellular signalling, we investigated the effect of most active compounds **42b** and **48** on fibronectin-induced phosphorylation of ERK1/2 in K562 cells, which express  $\alpha_5\beta_1$  integrin. The mechanism by which components of extracellular matrix generate intracellular signalling through integrins requires indeed an increased phosphorylation of cytoplasmatic second messengers. Phosphorylation of ERK1/2 plays a central role in fibronectin-mediated survival signalling through integrins: in fact, cell adhesion activates ERK1/2 by binding of  $\alpha_5\beta_1$  integrins at the cell surface to extracellular matrix proteins such as fibronectin. The experiment was performed by serum-starving K562 cells in RPMI-1640 containing 1% FBS for 16 h; thereafter, they were preincubated with compound **42b**, **48** ( $10^{-7}$ - $10^{-9}$  M) or the vehicle for 60 minutes and then plated for 60 minutes on fibronectin. When K562 cells were exposed to fibronectin for 60 minutes, a much stronger signal was observed for phosphorylated ERK1/2, in comparison to vehicle-treated cells (Figure 2.24). Preincubation with compound **42b** ( $10^{-7}$ - $10^{-9}$  M) caused a significant, concentration-dependent reduction in the amount of fibronectin-induced ERK1/2 phosphorylation levels in K562 cells (Figure 2.24), thus confirming a significant effect of the ligand binding on intracellular signalling cascade. On the contrary, when K562 cells, not preincubated with fibronectin, were exposed to compound **48**, a significant concentration dependent increase in ERK1/2-phosphorylation was recorded thus confirming its agonistic behaviour (Figure 2.24).

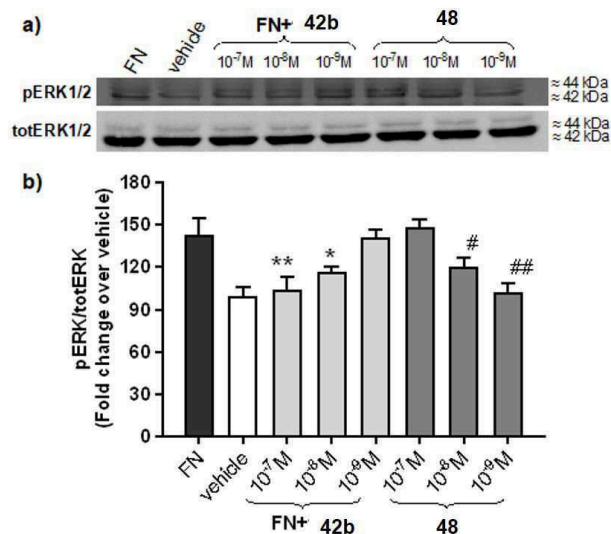


**Figure 2.24:** a) Cropped blots related to the effect of compounds **42b** and **48** on  $\alpha_5\beta_1$  integrin-mediated phosphorylation of ERK1/2 in K562 cells. Cells were serum-starved in RPMI-1640 containing 1% FBS for 16 h; then cells were preincubated with different concentrations of the antagonist **42b** ( $10^{-7}$ - $10^{-9}$  M) or its vehicle for 1 h in suspension and then were allowed to adhere for 1 h on fibronectin (FN). Cells treated with the agonist **48** ( $10^{-7}$ - $10^{-9}$  M) were not incubated with fibronectin. Thereafter cells were lysed and lysates were analysed in Western blot using an antibody directed against phosphorylated ERK1/2 (pERK1/2) or total ERK1/2 (totERK1/2). Western blot showed that cells plated on FN had a much stronger signal for phosphorylated ERK1/2 than vehicle-treated cells. Compound **42b** prevented FN-induced phosphorylation of ERK1/2 in a concentration-dependent manner, while agonist **48** significantly increased ERK1/2 phosphorylation. Full-length blots are presented in Supplementary Figure. b) Densitometric analysis of the bands (Mean $\pm$ SEM; n=4); the amount of pERK1/2 is normalized to that of totERK1/2. \*p<0.05, \*\*p<0.001 vs. FN; #p<0.05. ##p<0.01 vs. vehicle (Newman-Keuls test after ANOVA).

Integrin trafficking is an important mechanism employed by cells to regulate integrin-extracellular matrix interactions, and thus cellular signalling, during processes such as cell migration and invasion.<sup>217</sup>  $\alpha_5\beta_1$  integrin is internalised, trafficked to recycling endosomes and then recycled to the plasma membrane.<sup>218,219</sup> Membrane trafficking pathways influence  $\alpha_5\beta_1$  ability to promote invasion and metastasis.<sup>220,221</sup> In order to investigate the effects of peptidomimetics on integrin trafficking,  $\alpha_5\beta_1$  integrin internalisation was observed by confocal microscopy on HEK293 cells transfected with  $\alpha_5$ -enhanced green fluorescent protein (EGFP) plasmid (Figure 2.25), as these cells endogenously express  $\beta_1$  subunit.<sup>222,223</sup> HEK293+ $\alpha_5$ -EGFP cells were treated with fibronectin (10  $\mu$ g/mL) alone or in combination with the antagonist **42b** (1  $\mu$ M) or with the agonist **48** (1  $\mu$ M) alone.

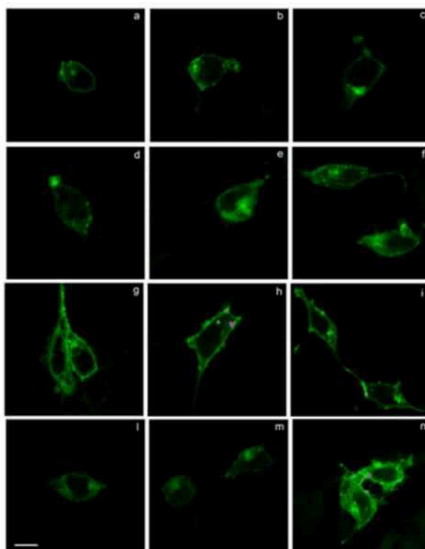


**Figure 2.25:** Confocal imaging on HEK293 cells transfected with  $\alpha_5$ -enhanced green fluorescent protein (EGFP) plasmid and treated with compounds **42b** or **48**. **Panels a-c)** Vehicle-treated cells: integrins are located on the plasma membrane. **Panels d-f)** FN-treated cells with 1 h incubation at 4°C:  $\alpha_5\beta_1$  integrin was mainly located in the cytoplasm. **Panels g-i)** FN-treated cells pre-incubated with the antagonist **42b** for 20 minutes at 4°C: compound **42b** prevents FN-induced  $\alpha_5\beta_1$  internalization, being located in the cytoplasm. **Panels l-n)** Cells treated with the agonist **48**: mimicking FN agonistic effect, compound **48** induced  $\alpha_5\beta_1$  integrin internalization. Scale bar: 10  $\mu\text{m}$ . The images have been elaborated using NIS-Elements C Software.

As shown in Figure 2.25, after 15 minutes of treatment with the endogenous agonist fibronectin,  $\alpha_5\beta_1$  integrin was mainly localised in the cytoplasm (Figure 2.25, panels d-f), if compared with vehicle-treated cells in which the integrin is quite completely located on the plasma membrane (Figure 2.25, panels a-c). Moreover, when HEK293+ $\alpha_5$ -EGFP cells were pre-treated with the antagonist **42b** before the addition of fibronectin, it prevented integrin internalisation, that remained mainly located on the membrane (Figure 2.25, panels g-i). On the contrary, compound **48**, mimicking the agonist behaviour of fibronectin, induced  $\alpha_5\beta_1$  internalisation (Figure 2.25, panels l-n): in fact, the integrin was mostly localised in the cytoplasm.

The ligand **42b**, which showed best results in the pharmacological evaluation, was subjected to stability assays at neutral (pH=7), basic (pH=10) and acidic (pH=3) conditions, as representative of the class of compounds. LC-MS injections were performed after 30 min from the preparation of the samples and then after each 1.5 hours, following the experiments for 14 h (Figure 2.26). During the last synthetic step, the methyl ester deprotection, the amidic bond between the heterocycle and malonyl group showed high sensitivity to the basic environment and, as expected, the hydrolysed **A** was detected in traces as the unique degradation product.



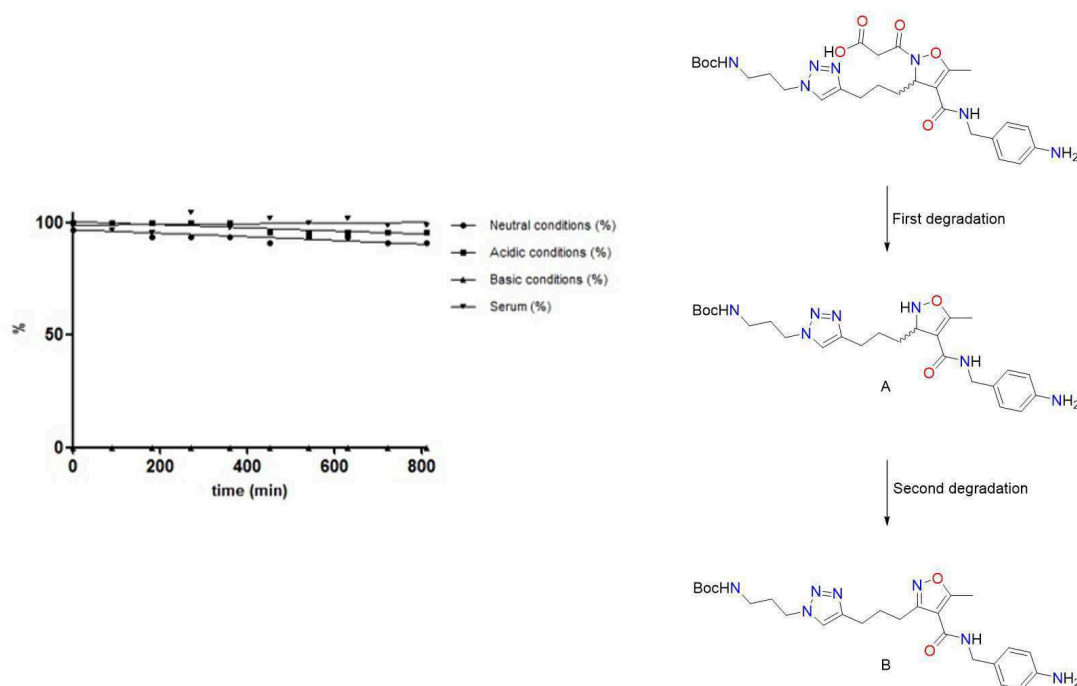


**Figure 2.26:** Stability of **42b** in neutral, basic, acidic and physiological conditions and its possible degradation pathway. Conditions: **42b** (0.1 mmol) in 300  $\mu$ L of solvent (water or bovine serum). 5 eq of LiOH $\cdot$ H<sub>2</sub>O or HCl 1M were added.

As a consequence of the spontaneous aromatisation of **A**, also an increasing amount of **B** was observed after a short period. The aromatised form **B** was tested to evaluate its effect on the activity of selected integrins but, as consequence of the absence of a crucial pharmacophore, it was not active. This behaviour doesn't represent a big issue, since strong basic conditions are quite unusual in physiological environment. In fact, under stress conditions with a large excess of base, the decomposition of **42b** to **A** occurred in few minutes. On the contrary, during the acidic treatment and under neutral conditions, **42b** resulted quite stable and after several hours only a 5% loss of product was detected, in favour of the formation of **A** and **B**. Finally, the stability of **42b** was also checked in bovine serum, confirming that no significant degradation occurs in this physiological medium.

In order to visualise the localisation of isoxazolines inside the cells and to explore the possibility to use them as shuttles for selective delivery of therapeutic payloads and diagnostics, compound **55** was synthesised conjugating **42b** with FITC, as described above. This FITC-conjugated isoxazoline maintained the ability to reduce K562 cells adhesion in a concentration-dependent manner, similar to compound **42b**, but with a lower potency ( $IC_{50} = 0.13 \pm 0.01 \mu$ M). To study intracellular localisation of compound **55**, HEK293 cells were transfected with a plasmid coding for  $\alpha_5$  integrin subunit (HEK293+ $\alpha_5$ ), as they do not express this subunit endogenously<sup>222,223</sup> but they express  $\beta_1$ . When HEK293+ $\alpha_5$  cells were treated with **55** (0.1-1  $\mu$ M), we observed that the compound was localised in the cell

cytoplasm, since it could be internalised (Figure 2.27). In addition, the internalisation of compound **55** was concentration-dependent: at a higher concentration (1  $\mu\text{M}$ ) it accumulated inside the cells to a greater extent. Moreover, we observed that the internalisation of compound **55** is  $\alpha_5$  integrin-mediated because it was not able to enter inside HEK293 cells that do not express  $\alpha_5$  integrin endogenously (Figure 2.27a). In order to establish the possibility for compound **55** to be internalised also in cancer cells, endogenously expressing  $\alpha_5\beta_1$ , K562 cells, derived from chronic myelogenous leukemia, were exposed to compound **55** (0.1-1  $\mu\text{M}$ ), as reported in methods section.

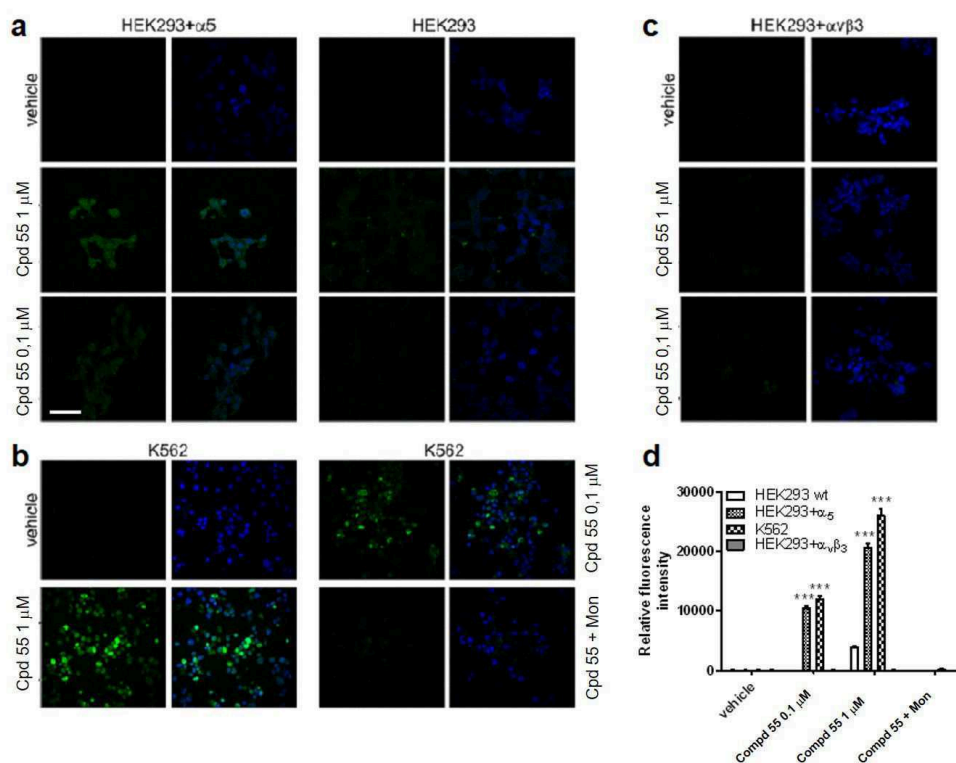


**Figure 2.27:** Confocal microscopy images of HEK293 or HEK293+ $\alpha_5$ ; (a), HEK293+ $\alpha_V\beta_3$  and K562 cells treated with compound **55** (Cpd **55**). Cells were exposed to compound **55** (0.1-1  $\mu\text{M}$ ) or its vehicle for 60 minutes at 4°C and thereafter cells were moved to 37°C for 15 minutes to promote integrin internalisation and fixed as described in Methods. a) Compound **55**, conjugated with FITC was able to enter the cells in  $\alpha_5$  integrin-dependent manner: it was internalized in HEK293+ $\alpha_5$  but not in HEK293 cells. Right Panels: HEK293 cells not expressing  $\alpha_5$  integrin subunit. Left Panels: HEK293+ $\alpha_5$ . b) Concentration-dependent internalization of compound **55** was observed also in K562 cancer cells, endogenously expressing  $\alpha_5\beta_1$  integrin. Treatment with monensin (an inhibitor of integrin trafficking, 2  $\mu\text{M}$  for 2 h) significantly inhibited compound **55** internalisation in K562 cells. c) Compound **55** was not able to enter in HEK293+ $\alpha_V\beta_3$  cells, not expressing  $\alpha_5\beta_1$ . In the left column of each panel green (FITC) fluorescence was shown, whereas in right one green and blue (DAPI) signals were merged. Nuclei were counterstained with DAPI. Scale bar: 30  $\mu\text{m}$ . d) Compound **55** internalisation was evaluated according to green fluorescence intensity in the cells and is reported in the graph. (Mean $\pm$ SEM; n=2). \*\*\* $p$ <0.001 vs vehicle treated cells (Newman-Keuls test after ANOVA). The images have been elaborated using NIS-Elements C Software.

As shown in Figure 2.27b, compound **55** was internalised in K562 cells in a concentration-dependent way. In addition, to confirm that compound **55** is internalised through an active mechanism of endocytosis, K562 cells were exposed for 2 h to monensin (2  $\mu\text{M}$ ), which blocks the trafficking of  $\alpha_5$  integrin from the Golgi stack to the trans Golgi network.<sup>224</sup> Inhibition of integrin trafficking prevented compound **55** internalisation in K562 cells (Figure 2.27b); these results demonstrate that compound **55** enters cells relying on internalisation rather than on passive permeability. Compound **55** derived from the conjugation of FITC to compound **42b** that was a specific  $\alpha_5\beta_1$  integrin ligand; to confirm that this selectivity was maintained for **55**, we treated HEK293 cells transfected with plasmids coding for  $\alpha_V$  and  $\beta_3$  subunits (HEK293+ $\alpha_V\beta_3$ ) with compound **55** (0.1-1  $\mu\text{M}$ ) (Figure 2.27c). In cells not expressing  $\alpha_5\beta_1$  integrin, compound **55** was not able to be internalised. These results confirm from one hand the  $\alpha_5\beta_1$ -dependent internalisation mechanism of compound **55**, and from the other hand displayed that the specificity towards  $\alpha_5\beta_1$  of compound **42b** was maintained in spite of conjugation with FITC molecule.

To rationalise the pharmacological activity observed for the new isoxazoline-RGD-mimetics, compounds **42b**, **45b** and **48** were selected to investigate the effects of the side chain in position 3 of the isoxazoline core on the interaction with the target receptors. In the family of the selective  $\alpha_5\beta_1$  ligands, we chose the most active compound **42b** which inhibits  $\alpha_5\beta_1$  integrin-mediated cell adhesion at low nM concentrations, and compound **48** acting as an agonist of  $\alpha_5\beta_1$  receptor at  $\mu\text{M}$  levels. On the other hand, compound **45b** was chosen as selective agonist ligand of  $\alpha_V\beta_3$  integrin. Automated docking calculations were carried out with the Glide software package (version 7.0) by using the crystal structure of the extracellular segment of integrin  $\alpha_5\beta_1$  in complex with a disulfide-bonded cyclic RGD peptide (PDB code 4WK4) and the crystal structure of the extracellular domain of integrin  $\alpha_V\beta_3$  in complex with the cyclic pentapeptide Cilengitide (PDB code 1L5G), according to the procedures reported in the experimental section. As the docking approaches were successful in reproducing the crystallographic binding mode of the cyclic peptides at the interface of the  $\alpha$  and  $\beta$  subunits by means of electrostatic and H-bond interactions, we applied the same docking protocols to both enantiomers of compounds **42b**, **45b** and **48** to generate computational models for the interaction of these ligands with  $\alpha_5\beta_1$  and  $\alpha_V\beta_3$  integrins and evaluate their ability to properly fit the receptor site. In all the calculations evaluated in collaboration with Prof. *Belvisi* and coworkers (Department of Chemistry, University of Milano), the experimentally observed binding modes of the cyclic peptides with  $\alpha_5\beta_1$  and  $\alpha_V\beta_3$  integrins were used as reference models for the analysis of the docking results in terms of protein-ligand interactions. Docking results pointed out that the (*R*) and (*S*) enantiomers of the new functionalised isoxazolines show different behavior, with better performances exhibited by the (*R*)-isomer, especially in the  $\alpha_5\beta_1$  integrin. Based on the number of docking poses reproducing the key interactions of the X-ray complex, (*R*)-**42b** was the best  $\alpha_5\beta_1$  ligand confirming

the pharmacological results. In the best pose of (*R*)-**42b** (as well as in ten other poses) into the  $\alpha_5\beta_1$  binding pocket, the carboxylate group of the ligand is coordinated to the metal cation in the MIDAS region of the  $\beta_1$  subunit, while the aniline moiety forms H-bond interactions with the negatively charged side chain of Asp227 in the  $\alpha_5$  subunit (Figure 2.28, left). Further stabilising interactions involve the formation of H-bonds between the ligand carboxylate group and the backbone amide hydrogen of Asn224 and Ser134 (and Tyr133 in some poses) in the  $\beta_1$  unit, and  $\pi$ -stacking interactions between the ligand aromatic group and the  $\alpha_5$ -Phe187 side chain. A H-bond between the Boc carbonyl moiety of ligand and the amino group of  $\beta_1$ -Lys182 side chain is also observed. The long-chain substituent (bearing the triazole ring) at the position 3 of the isoxazoline is well accommodated at the interface between the  $\alpha$  and  $\beta$  subunit; in particular, the triazole ring establishes stabilising contacts with the side chains of residues  $\alpha_5$ -Trp157,  $\beta_1$ -Tyr133,  $\beta_1$ -Ser177 and  $\beta_1$ -Lys182 (Figure 2.28, left).

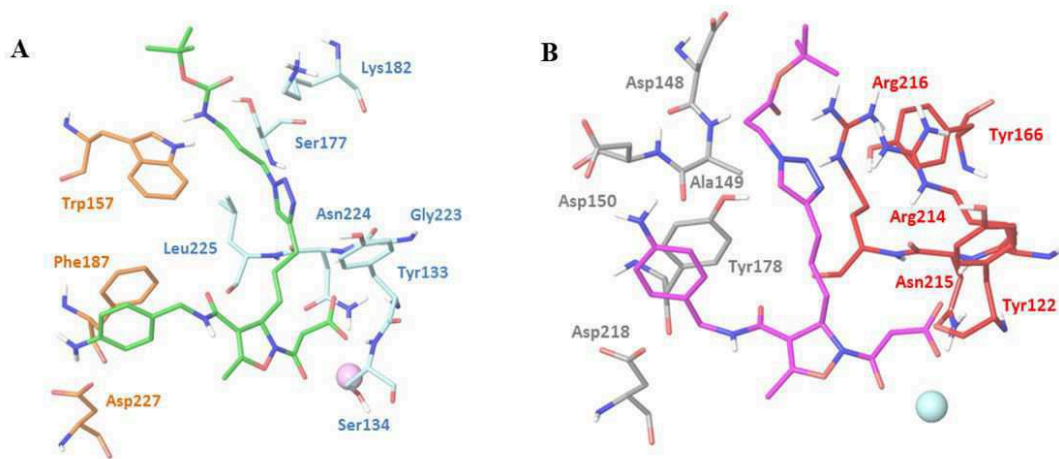


**Figure 2.28:** A) Docking best pose of (*R*)-**42b** (green) into the crystal structure of the extracellular domain of  $\alpha_5\beta_1$  integrin ( $\alpha_5$  orange,  $\beta_1$  blue). Only selected integrin residues involved in the interactions with the ligand are shown. The metal ion at MIDAS is displayed as a magenta CPK sphere. Non polar hydrogens are hidden for better visual representation. B) Docking best pose of (*R*)-**45b** (purple) into the crystal structure of the extracellular domain of  $\alpha_V\beta_3$  integrin ( $\alpha_V$  grey,  $\beta_3$  red). The metal ion at MIDAS is displayed as a cyan CPK sphere. The image has been generated using Maestro graphical interface [Maestro, version 10.5, Schrödinger, LLC, New York, NY, 2016].

On the contrary, docking results show that most poses of compound **42b** (both *R* and *S* enantiomers) into  $\alpha_V\beta_3$  lack the H-bond interaction between the ligand aniline moiety and the side chain of  $\alpha_V$ -Asp218, and display an unfavorable arrangement of the long-chain substituent at the position 3 of the isoxazoline at the  $\alpha/\beta$  integrin interface. Due to residue differences between the binding sites, the long chain bearing the triazole ring of compound **42b** can fit unhindered only into the pocket available at the  $\alpha_5\beta_1$  interface, thus confirming the pharmacological results in terms of selectivity. A comparison of  $\alpha_5\beta_1$  and  $\alpha_V\beta_3$  integrins highlights that the mutations of  $\alpha_5$ -Phe187 into  $\alpha_V$ -Tyr178 and of  $\alpha_5$ -Asp227 into

$\alpha_V$ -Asp218 might allow the aniline moiety of the ligand to maintain the same H-bond and  $\pi$ -stacking interactions in the two binding sites. Other mutations at the  $\alpha/\beta$  interface modify size and shape of the pocket accessible to the isoxazoline substituent, thus affecting the ligand binding mode (see supplementary Figure S41). Molecular dynamics simulations allowing partial receptor flexibility showed that (*R*)-**42b** maintains stable interactions with  $\alpha_5\beta_1$ , similar to those observed in the docking poses. In particular, the long-chain substituent is firmly placed at the  $\alpha/\beta$  integrin interface, with the triazole and the Boc carbonyl moiety engaged in interactions with residues  $\alpha_5$ -Trp157,  $\beta_1$ -Tyr133 and  $\beta_1$ -Lys182. Instead, the docking poses of compound **48** reveal some difficulties in establishing the key interactions with the  $\alpha_5\beta_1$  pocket, mainly due to the lack of a simultaneous favorable fitting of the long-chain substituent at the  $\alpha/\beta$  interface. Compared to **42b**, a reduced number of docking poses reproducing the X-ray interactions is achieved and MD simulations confirm high mobility of (*R*)-**48** in the binding pocket. The binding determinants of **45b** were finally investigated. The docking poses of (*R*)-**45b** into  $\alpha_V\beta_3$  integrin are characterised by the interaction of the carboxylate group with the metal cation in the MIDAS region and the Asn215 and Tyr122 residues in the  $\beta_3$  subunit, and by the interaction of the aniline moiety with the side chains of  $\alpha_V$ -Asp218 or  $\alpha_V$ -Asp150, and of  $\alpha_V$ -Tyr178. Moreover, the Boc carbonyl moiety of the substituent at the position 3 of the isoxazoline can create H-bonds with the backbone amide hydrogen of  $\alpha_V$ -Ala149 or the guanidinium group of  $\beta_3$ -Arg216, while the triazole ring can form H-bond or cation- $\pi$  interactions with the side chain of  $\beta_3$ -Arg214 (Figure 2.28, right). Molecular dynamics simulations allowing partial receptor flexibility showed that (*R*)-**45b** maintains stable interactions with  $\alpha_V\beta_3$ , especially those involving the acid pharmacophoric group and the triazole ring. In short, according to these results, only the subtle fitting of suitable features of the isoxazoline substituent with appropriate receptor traits at the  $\alpha/\beta$  integrin interface seems to allow the optimal interaction of both the pharmacophoric moieties and the functionalisable chain of the isoxazoline-RGD-mimetics with the integrin binding site.

#### 2.4.3 Enantioselective Synthesis of Isoxazoline Scaffolds

In the last thirty years, the discovery that different enantiomers of bioactive compounds can interact differently with their biological targets has accelerated the use of enantioselective methods for the synthesis of drugs previously administered in racemic mixture. In the literature, many examples of improved activity using a single drug enantiomer are reported,<sup>225</sup> even though some others demonstrate the efficacy of the racemic mixture already employed.<sup>226</sup> In the development of the enantioselective synthesis of bioactive compounds it is of pivotal relevance to avoid the use of metal contaminants and achieve high levels of enantiomeric excess.

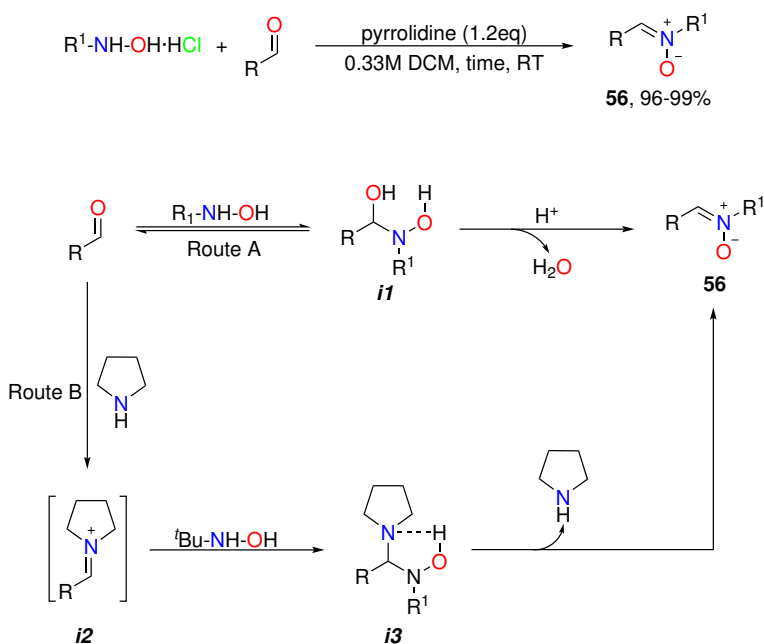
Considering the interesting biological and computational results obtained with the 3-alkyl

isoxazolines previously reported, we decided to synthesise this scaffold in enantiomerically pure form in order to evaluate the activity of the single enantiomers.

In the literature,  $\Delta^2$ - and  $\Delta^4$ -isoxazolines are widely common as scaffold or building block in the synthesis of several types of compounds<sup>98,129</sup> providing many examples of enantioselective synthesis of these molecules, in particular using the 1,3-dipolar cycloaddition (1,3-DC) reaction, well known as Huisgen reaction.<sup>227,228</sup>

*Aléman* and coworkers have already reported the synthesis of 3-aryl isoxazolines by organocatalytic 1,3-DC between a nitron, conveniently *N*-protected and obtained from aryl aldehydes, and an aldehyde;<sup>229</sup> therefore, inspired by his work, we tried to apply the same conditions to the synthesis of isoxazoline-based integrin ligands.<sup>98</sup>

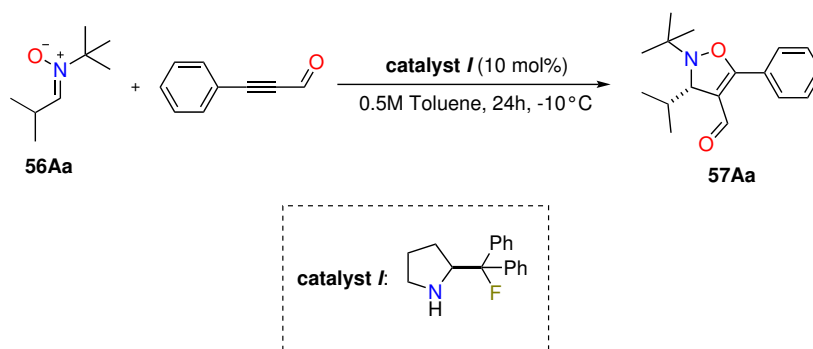
To this purpose, we had to preliminary synthesise the nitrones **56**, by reacting a series of hydrochloric hydroxylamines with a series of proper aldehydes. In fact, due to the poor stability of the free hydroxylamine, the common condensation's strategy employ the corresponding hydrochloride salt and the reaction's conditions involve the use of a base to release the hydroxylamine. The methodology employed for this reaction has been recently reported in the literature<sup>230</sup> and envisage the synthesis of a broad range of  $C=N-R^1$  compounds via iminium ion catalysis by means of pyrrolidine as catalyst (Scheme 2.13).



**Scheme 2.13:** Synthesis of **56** and influence of pyrrolidine in the reaction mechanism.

The Route B provides high yields for the synthesis of several nitrones avoiding the use of metals or Lewis acids (Route A) and employing mild conditions ( $Y \Rightarrow 95\%$ ). Starting from the preliminary results, the researchers discovered that pyrrolidine accelerates the first synthetic step through the formation of an iminium ion **i2**, more reactive than the corresponding aldehyde, easily converted into the aminal **i3**. Moreover, the catalytic effect

provided by the use of pyrrolidine has been considered more important due to its role in facilitating the second step. It has been hypothesised that the higher basicity of N in the intermediate *i3*, compared to *i1*, could increase the proton transfer in acid-free condition, leading to an easier elimination of pyrrolidine from *i3* rather than H<sub>2</sub>O from *i1*. Consequently, we coupled nitron 56Aa and 3-phenylpropionaldehyde in toluene using 10 mol% of I as catalyst for 24h at -10°C (Scheme 2.14).



Scheme 2.14: Synthesis of 57Aa using model conditions.<sup>229</sup>

This synthesis proceeds via an iminium ion catalysis applied to a Huisgen cycloaddition reaction in which the dipolarophile *i1*, obtained through the condensation of the catalyst *I* with 3-phenylpropionaldehyde, reacts with the dipole **56** providing the intermediate *i2*; subsequently to an hydration step, the desired product is released and the catalyst *I* regenerated (Figure 2.29).

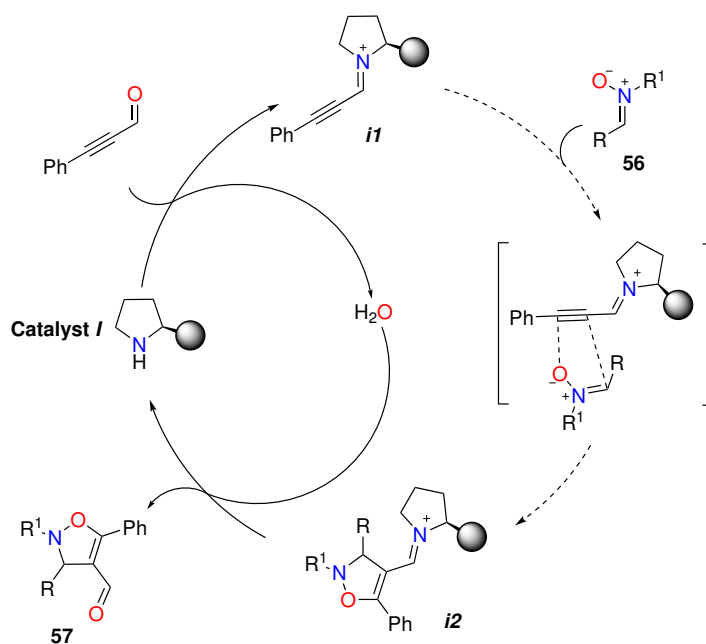
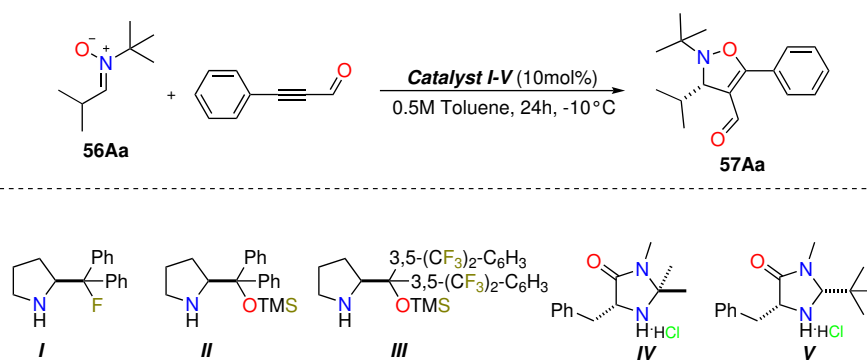


Figure 2.29: Proposed catalytic cycle for 1,3-DC of nitrones to alkyne.

Unfortunately, the poor results in terms of enantioselectivity prompted us to screen the most common secondary amine catalysts in order to find the suitable one for our scope. First of all, we decided to use in the same conditions the more classic *Hayashi* catalyst **II**, bearing an OTMS group instead of the fluoride, and *Jorgensen* catalyst **III** due to their similarity to the catalyst reported in the literature for the similar scope (Scheme 2.15). Also in this case, the high conversion results were clouded by formation of racemic mixtures. Moreover, we decided to test *MacMillan* imidazolidinones thinking that a more hindered catalyst could provide better results. In order to improve the results reported by *Aléman* and coworkers using the catalyst **V** without HCl, we decided to use an acidic co-catalyst as suggested by *MacMillan's* papers.<sup>228</sup>



Scheme 2.15: Catalysts **I-V** screening for the synthesis of **57Aa**.

Entry	Catalyst	er
1 <sup>a</sup>	<b>I</b>	48:52
2 <sup>a</sup>	<b>II</b>	48:52
3 <sup>a</sup>	<b>III</b>	45:55
4 <sup>a</sup>	<b>IV</b>	42:58
5 <sup>a</sup>	<b>V</b>	40:60

<sup>a</sup> Reference conditions<sup>229</sup>;

er: enantiometric ratio

Table 2.3: Catalysts **I-V** screening for the synthesis of **57Aa**.

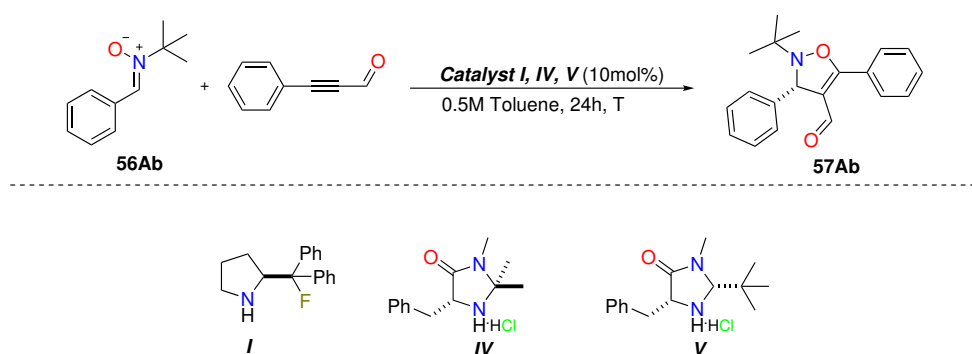
In fact, in these studies the co-catalyst is considered to be a key factor affecting the rate and the selectivity of the process; moreover, an increase in reactivity (in terms of reaction half-life) and selectivity is reported with increasing acidity of the co-catalyst. Initially we tested the commercially available first generation of *MacMillan* imidazolidinone with HCl as co-catalyst, confirming that the more acid HCl provided better, but still unsatisfactory results (entry 4). Finally, we employed the second generation of *MacMillan* imidazolidinone salifying the commercially available free catalyst with a 1M solution of HCl in diethyl ether.



Unfortunately, also in this case the desired product was obtained as a nearly racemic mixture of the two enantiomers, even if this result was the best of this serie (entry 5).

At this point, before planning a new synthetic stragety or modifying the isoxazoline scaffold to improve the ee of the reaction, we rationalised the obtained results by means of the DFT calculation provided in the literature for very similar structures. Our idea was that the free rotation energy of the alkyl chain in position 3 was low enough at  $-10^{\circ}\text{C}$  to overcome the steric hindrance produced by the iminium ion intermediate, leading to the indiscriminate formation of the two enantiomers.

Since the main goal of our work was the synthesis of an enantiopure core for its biological applications, we decided to modify the structure of our target ligand compared to the ones already reported. Since in literature high enantioselectivity has been reported using aryl nitrones, we decided to design the new ligand starting from this key point (Scheme 2.16).



Scheme 2.16: Synthesis of **57Ab** catalysed by catalysts **I**, **IV** and **V**.

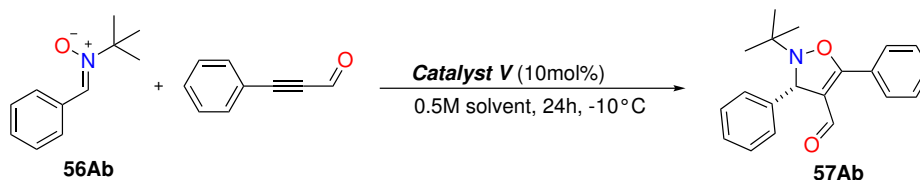
Entry	Catalyst	T/ $^{\circ}\text{C}$	C%	er
1 <sup>a</sup>	<b>I</b>	-10	>99	4:96
2	<b>IV</b>	-10	>99	10:90
3	<b>IV</b>	RT	>99	13:87
4	<b>V</b>	-10	>99	1:99
5	<b>V</b>	RT	>99	3:97

<sup>a</sup> Reference conditions<sup>229</sup>; C: conversion;  
er: enantiomeric ratio

Table 2.4: Synthesis of **57Ab** catalysed by catalysts **I**, **IV** and **V**.

As reported in Table 2.4, starting from the results obtained by *Aléman* (Entry 1), we have decided to employ in the same conditions the *MacMillan* catalysts **IV** and **V**. As expected, the ee observed in these cases were better than those obtained with the previous approach (Entry 2 and 4 Table 2.4 vs Entry 4 and 5 table in Figure 2.15) due to the aromatic nature of the nitrono substituent; in particular, catalyst **V** in toluene both at  $-10^{\circ}\text{C}$  and room

temperature provided results slightly better than those already reported in literature in terms of enantiopurity (Entry 1 vs Entry 4 and 5, Table 2.4). Even if the conversion and ee obtained in these conditions were very high, we have decided to screen the reaction solvent in order to verify the effectiveness of this synthetic system in different media (Scheme 2.17).



Scheme 2.17: Solvent screening for the synthesis of **57Ab** by catalyst **V**.

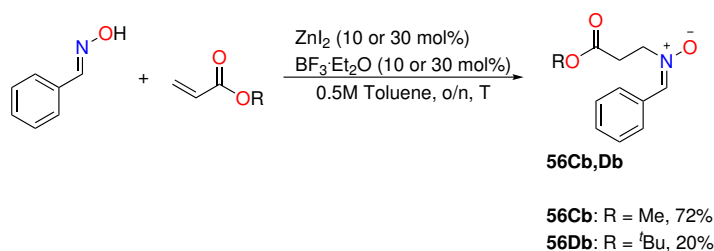
Entry	Solvent	Yield%	er
1	DCM	83	1:99
2	CHCl <sub>3</sub>	79	2:98
3	toluene	>99	1:99
4	AcOEt	83	3:97
5	<sup>t</sup> PrOH	83	12:88

er: enantiomeric ratio

Table 2.5: Solvent screening for the synthesis of **57Ab** by catalyst **V**.

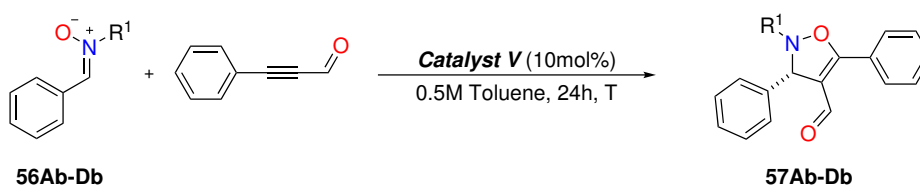
Thus, we have searched in the literature the most employed solvents in 1,3-dipolar cycloaddition reactions matching this selection with those most employed with the second generation of *MacMillan* catalyst. For this purpose, we identified four further solvents in addition to toluene (CH<sub>2</sub>Cl<sub>2</sub>, CHCl<sub>3</sub>, AcOEt and <sup>t</sup>PrOH). As reported in Scheme 2.17, we have obtained very high and similar results in CH<sub>2</sub>Cl<sub>2</sub>, CHCl<sub>3</sub>, toluene and AcOEt concerning the ee (Entry 1-4), whereas the performance <sup>t</sup>PrOH was slightly lower in terms of enantioselectivity (Entry 5). On the other hand, concerning the conversion, we have obtained a wider spectrum of results confirming toluene as best performing medium (Entry 3). Once identified the suitable catalyst and solvent, we extended the scope of the reaction including three different *N*-substitutions in the nitron's structure. Even though for the synthesis of *N*-benzyl nitron we followed the same procedure presented above, for the synthesis of compounds **56Cb** and **56Db** we had to follow a different approach. *Ritter* and coworkers have reported the synthesis of nitrones **56Cb**, **56Db** by means of a synergical catalysis based on ZnI<sub>2</sub>/BF<sub>3</sub>·Et<sub>2</sub>O in which the success of the reaction is obtained through a 1:1 mixture of the two catalysts (Scheme 2.18).<sup>231</sup>

The reaction between oxime and methyl- and <sup>t</sup>Bu- acrylate was carried out with 30% and 10% catalysts loading, respectively, in order to minimise side reactions, such as the hydrolysis of the oxime to benzaldehyde or the cleavage of nitrones.<sup>231</sup> Once prepared the three



Scheme 2.18: Synthesis of 56Cb, 56Db.

new starting materials, we have carried out the Huisgen reaction between nitrones 56Ab-Db and 3-phenylpropiolaldehyde using the conditions previously optimised (Scheme 2.19).



Scheme 2.19: Synthesis of 57Ab-Db.

As reported in Table 2.6, we have obtained *N*-benzyl isoxazoline 57Bb (Entry 3 and 4) with high conversion and very good enantiomeric ratio, even if not comparable to those reported for the synthesis of *N*-<sup>t</sup>Bu isoxazoline 57Ab.

Entry	57	T/°C	R <sub>1</sub>	C(%)	er
1	57Ab	-10	<sup>t</sup> Bu	>99	1:99
2	57Ab	RT	<sup>t</sup> Bu	>99	3:97
3	57Bb	-10	Bn	>99	9:91
4	57Bb	RT	Bn	>99	12:88
5	57Cb	-10	CH <sub>2</sub> CH <sub>2</sub> COOMe	>99	14:86
6	57Cb	RT	CH <sub>2</sub> CH <sub>2</sub> COOMe	>99	22:78
7	57Db	-10	CH <sub>2</sub> CH <sub>2</sub> COO <sup>t</sup> Bu	>99	9:91
8	57Db	RT	CH <sub>2</sub> CH <sub>2</sub> COO <sup>t</sup> Bu	>99	19:81

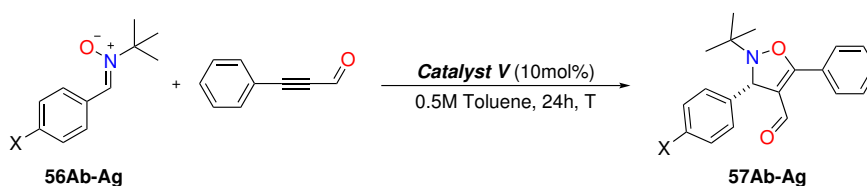
C: conversion; er: enantiomeric ratio

Table 2.6: Effect of *N*-substituent on isoxazoline 57Ab-Db synthesis.

On the other hand, the synthesis of *N*-(methyl propionate) isoxazoline 57Cb and *N*-(<sup>t</sup>Bu propionate) isoxazoline 57Db have provided quite different results; although both isoxazolines have been obtained with low enantiomeric ratio at room temperature (Entry 6 and 8), the stereochemical results at -10°C have surprisingly increased (Entry 5 and 7). We have supposed that the *N*-alkyl functionalisations on these substates could be affected by the temperature more than <sup>t</sup>Bu- or benzyl-group due to the length of the chain. In fact,

the enantiomeric ratio in the synthesis of *N*-<sup>t</sup>Bu isoxazoline **57Ab** was poorly dependent by temperature with a little gain in terms of enantioselectivity (94% ee vs 98% ee, Entry 1 and 2 Table 2.6); on the contrary, the enantiomeric ratio in the synthesis of *N*-(methyl propionate) isoxazoline **57Cb** and *N*-(<sup>t</sup>Bu propionate) isoxazoline **57Db** was highly dependent by temperature with a remarkable gain in terms of enantioselectivity (5% ee vs 72% ee for *N*-(methyl propionate) isoxazoline **57Cb** and 62% ee vs 82% ee for *N*-(<sup>t</sup>Bu propionate) isoxazoline **57Db**, Entry 5-8 Table 2.6). Our hypothesis was that in the *N*-(methyl propionate) isoxazoline **57Cb** and **57Db**, the free rotation of the chains were strongly reduced by the low temperature compared to other *N*-groups; moreover, the better results obtained in the synthesis of **57Db** compared to **57Cb** was probably due to the more hindered <sup>t</sup>Bu group compared to the methyl group.

After the screening of the *N*-substitution, we have decided to evaluate different aryl aldehydes in order to extend the scope of the reaction and, in a second time, use the functionalisation as a derivatisation starting point. Hence, we have synthesised a small library of nitrones using the pyrrolidine-catalysed procedure and we have prepared the corresponding isoxazolines following the general procedure already employed (Scheme 2.20, Table 2.7).



Scheme 2.20: Synthesis of **57Ab-Ag**.

In this way, we have synthesised all the corresponding *p*-halo, *p*-NO<sub>2</sub> and *p*-CN derivatives of the isoxazoline **57Ab-Ag** obtaining high enantioselectivity (9:91 ÷ 3:97, Entry 3-12 Table 2.7), but with a wider spectrum of yields (63 ÷ 92%, Entry 3-12 Table 2.7) compared to the reference synthesis.

Moreover, we have decided to investigate the absolute configuration of C3. Since the presence of heavy atoms is an useful requisite for an optimal crystallisation and its physical appearance seemed naturally suitable, we have decided to characterize isoxazoline **57Ae**, bearing the *p*-I phenyl chain in position 3, by X-Ray crystallography. In fact, this compound did not need to be derivatised to obtain a single crystal compared to other RX studies carried on related compounds (Figure 2.30).<sup>229</sup>

Entry	57	T/°C	X	Yield(%)	er
1	57Ab	-10	H	>99	1:99
2	57Ab	RT	H	>99	3:97
3	57Ac	-10	Cl	80	3:97
4	57Ac	RT	Cl	92	4:96
5	57Ad	-10	Br	82	3:97
6	57Ad	RT	Br	84	7:93
7	57Ae	-10	I	78	3:97
8	57Ae	RT	I	81	5:95
9	57Af	-10	NO <sub>2</sub>	67	3:97
10	57Af	RT	NO <sub>2</sub>	74	8:92
11	57Ag	-10	CN	63	6:94
12	57Ag	RT	CN	70	9:91

er: enantiomeric ratio

Table 2.7: Effect of aromatic substituent in the synthesis of isoxazolines 57Ab-Ag.

As depicted in Figure 2.30, by X-ray studies conducted by Prof. *Monari* and coworkers (Department of Chemistry "Giacomo Ciamician", University of Bologna) employing Apex III CCD instrument and improving the data with SHELXTL software, we were able to attribute the absolute *S* configuration to the C3 in accordance with the literature.<sup>229</sup>

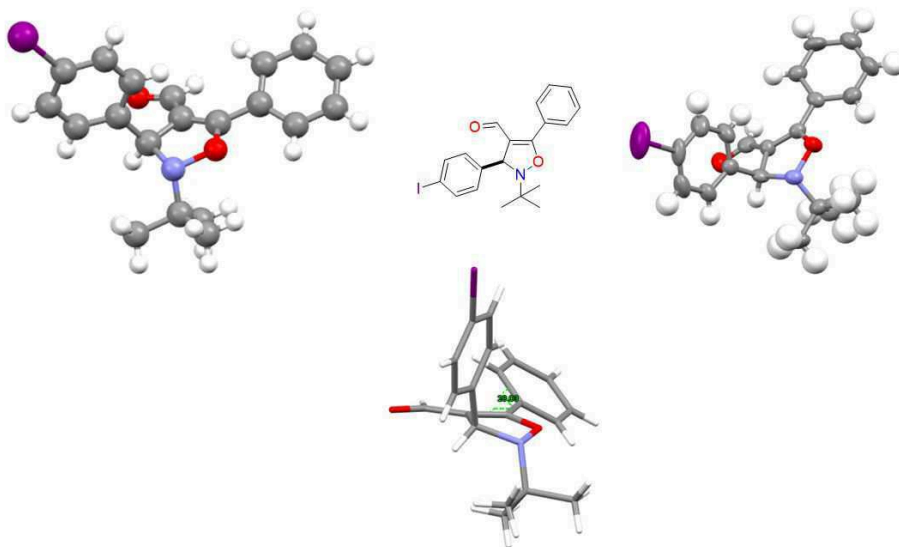


Figure 2.30: X-ray analysis of 57Ae conducted by *Monari* and coworkers.

Once identified a general synthetic procedure for the enantioselective synthesis of isoxazoline rings, we have developed a retrosynthetic strategy for the synthesis of the integrin ligand that was the main aim of our project (Figure 2.31).

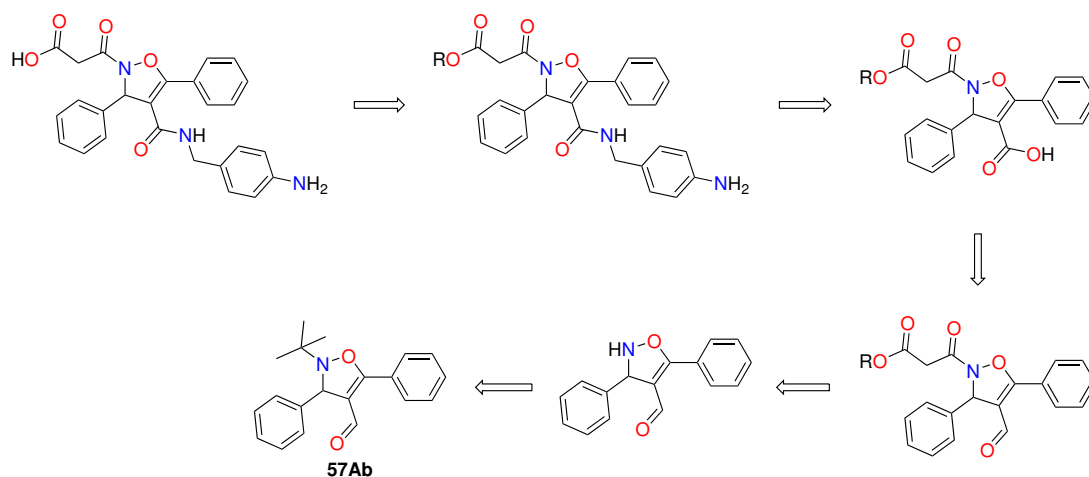


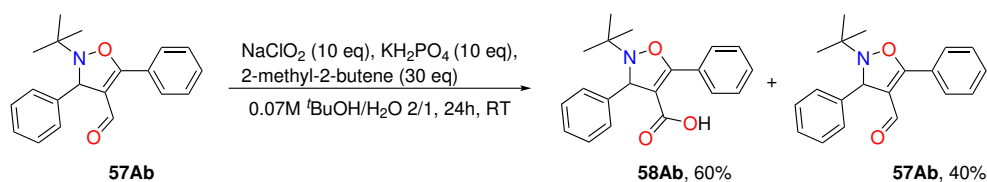
Figure 2.31: Retrosynthetic approach of the synthesis of isoxazoline target ligand.

Due to the high value of the enantiopure isoxazoline, we have decided to perform the peptidomimetic synthesis working on the racemic mixture with the aim to extend the optimised reactions also to enantiopure substrates.

Initially, we have focused our attention on the removal of the *N*-*t*Bu and *N*-benzyl protecting groups from the reference isoxazoline **57Ab** and **57Bb** in order to obtain an intermediate suitable for the insertion of the acidic moiety to mimic the Asp residue in RGD peptidomimetic. First of all we have spent our efforts on the *N*-*t*Bu protecting group which provided the best result in terms of enantiomeric excess (98% ee). In literature, several examples have been reported regarding this kind of deprotection, but unfortunately no one on our substrates or similar one. Hence, we have applied two different approaches that are widely used in these cases: the first was a radical approach<sup>232</sup> using radical initiator and UV light, while the second was an ionic approach using strong acids and scavenger mixtures.<sup>233</sup> Despite different protocols and the screening of several reaction parameters were applied (radical initiator, temperature, wavelength, the nature of acid, etc), we have not obtained the desired product even though in some cases we could recover the starting material. Thus, we have decided to focus our attention on the isoxazoline bearing the *N*-benzyl protecting group. It is well known that this protecting group is easily removed by hydrogenolysis, but it is equally well known that isoxazoline rings are rather sensitive to these conditions when particularly strong. For this reason, we have decided to use mild hydrogenolysis conditions<sup>234</sup> in order to minimise side reactions leading to ring opening byproducts. To carry out this procedure, we have prepared freshly Pd black starting from Pd(OAc)<sub>2</sub>. Adding HCO<sub>2</sub>H to Pd(OAc)<sub>2</sub>, Pd black was prepared in situ with the development of H<sub>2</sub> and CO<sub>2</sub> at low pressure level. Even though in literature related compounds to our substrate were deprotected with high efficacy, in this case we have obtained only the ring opening byproduct, highlighting the sensitivity of this scaffold also to mild hydrogenolysis conditions. Finally, to overcome these drawbacks, we have introduced the synthesis of *N*-(*t*Bu propionate) isoxazoline **57Db**, in

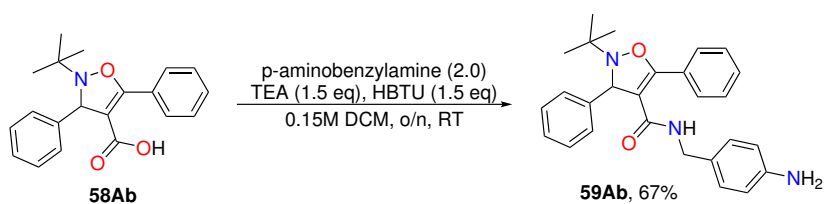
which the *N*-protecting group was introduced to obtain an intermediate closely related to the desired product. By this strategy it was possible to obtain the product avoiding at least one synthetic step in the overall synthesis, that is to say the troublesome *N*-deprotection. However, this approach limits the possibility to introduce further functionalisation on the nitrogen of the heterocycle.

At the same time, working on the *N*-*t*Bu isoxazoline we explored the derivatisation of the aldehyde in position C4 of the reference isoxazoline **57Ab** to prepare the basic moiety to mimic the Arg residue in RGD peptidomimetic. To do this, first of all we needed to oxidise the aldehyde to carboxylic acid and within the broad panorama of oxidation reactions, Pinnick's reaction is certainly one of the most used in organic chemistry for this scope (Scheme 2.21).<sup>235</sup>



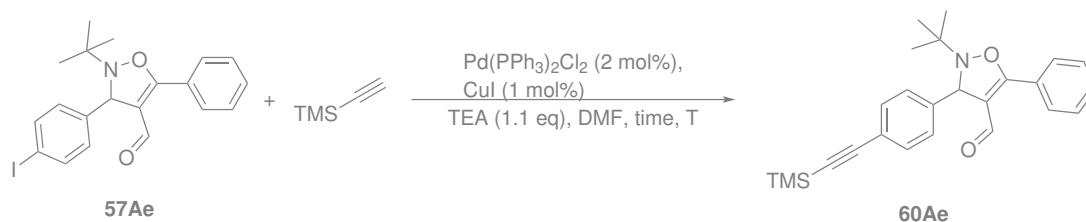
Scheme 2.21: Synthesis of **58Ab**.

Unfortunately, the carboxylic acid was obtained only with the 60% of conversion despite several modification to the reaction conditions, such as concentration, salts equivalents, etc. On the other hand, the remaining 40% was starting material therefore it was possible to recover the aldehyde to repeat again the oxidation step. Then, the intermediate **58Ab** was coupled with *p*-aminobenzylamine using the general procedure employed for the synthesis of related compound **59Ab** with 67% yield (Scheme 2.22).



Scheme 2.22: Synthesis of **59Ab**.

Finally, our future purpose will be the derivatisation of the *p*-substituents of the aryl moiety in position C3. Without further functionalisations, the obtained isoxazoline scaffold could be employed as integrin ligand per se; however, we are interested in its use as imaging biomarkers or carrier in drug delivery systems. Hence, the choice of *p*-halo substituents was not accidental; in fact, our group has recently reported<sup>236</sup> a green approach in Heck-Cassar-Sonogashira (HCS) coupling reaction and our idea was to introduce this strategy in the derivatisation of isoxazoline **57Ae** (Scheme 2.23).



Scheme 2.23: Synthesis of 60Ae.

As depicted in Scheme 2.23, our idea is to perform the coupling reaction on the isoxazoline **57Ae** with trimethylsilylacetylene following the greener procedure already developed. Successively, the removal of TMS protecting group will reveal the alkyne moiety, already presented as a suitable anchorage group for imaging scaffolds and/or drugs.

## 2.5 Conclusions

In the context of the synthesis of bioactive molecules, in particular integrin ligands, we explored the preparation of several rigid scaffolds as core structures for more complex molecules.

The synthesis of  $\alpha/\beta$  dipeptides containing linear or cyclic  $\alpha$ -dehydro- $\beta$ -amino acids has been obtained via Ir-catalyzed allylic amination. Starting from alkylidene acetacetamides, we synthesized differently hindered carbonates that were submitted to allylic amination. The regiochemistry of this class of reactions is known to depend on several factors. For allylic carbonates deriving from  $\alpha$ -amino acids, as compounds **16** and **17**, a strong influence of the carbonate size and the amino acid side chain was observed. For carbonates deriving from amino acids possessing a methylene unit in  $\beta$  position, the expected SN2' amination was exclusively observed. Moreover the presence of a carbamate moiety linked to the amide nitrogen allowed to obtain peptidomimetics containing polyfunctionalized dihydropyrimidine-2,4-dione via spontaneous intramolecular cyclization. Concerning  $\beta$ -branched amino acid-deriving methyl carbonates, competition between SN2 and SN2' pathway occurred, affording mixtures of  $\alpha$ -dehydro- $\beta$ -amino acid-containing dipeptides. By increasing the size of the carbonate, complete regiocontrol was anyway restored. Moreover, by inverting the order of reduction/acylation steps on the starting alkylidene acetoacetamides, the formation of polyfunctionalized 1,3-oxazinane-2,4-dione was obtained. These novel rigid scaffolds may be easily exploited for the preparation of bioactive peptidomimetics.

On the other hands, the synthesis of a small library of ligands, obtained by conjugation of polyfunctionalised linkers to isoxazoline ring via Huisgen-click reaction, allowed to verify the possibility to use these scaffolds as  $\alpha_V\beta_3$  and  $\alpha_5\beta_1$  targeting motifs, with the aim to use them as "shuttles" for selective delivery of therapeutics and diagnostics to cancer cells. The different behavior of the members of the library seems to suggest a correlation between the terminal moiety of the linker chain and the cell adhesion inhibition or activation,



even if a rationale in structure-activity relationship is not predictable and needs further investigation. Compound **42b**, that showed excellent potency towards  $\alpha_5\beta_1$  integrin in the nanomolar range as antagonist, was selected for further investigation to establish the effect on fibronectin induced ERK phosphorylation. It was able to prevent fibronectin-induced  $\alpha_5$ -integrin-mediated ERK1/2 intracellular signaling activation and  $\alpha_5$ -integrin internalisation. Moreover, compound **55**, FITC-conjugated isoxazoline derived from compound **42b**, confirmed the possibility to exploit these integrin ligands as "shuttles" for the selective delivery of therapeutics and diagnostics as consequence of its internalisation only inside integrin expressing cells. The stability in water solution at different values of pH and in bovine serum was verified in order to confirm the potential exploitation of these peptidomimetic molecules for pharmaceutical applications.

Finally, in order to synthesise in enantioselective manner the isoxazolines already presented, a synthetic procedure has been optimised. In particular, the high efficiency and the broad feasibility of the second generation of *MacMillan catalyst V* have been demonstrated, both at RT and  $-10^\circ\text{C}$ . Employing this catalyst, a substantial number of isoxazoline bearing three different *N*-protecting group and six different *p*-substituents on aryl moiety in position C3 have been synthesised in good yields (up to  $>99\%$ ) and high enantioselectivity (up to  $>98\%$ ). Even though several attempts have been spent to the removal of *N*-*t*Bu and *N*-benzyl protecting groups with no profitable results, the synthesis of the *N*-propanate isoxazolines **57Cb** and **57Db** allowed to introduce in the scaffold a suitable precursor of the Asp mimetic group. Furthermore, the aldehyde oxidation and the subsequent coupling with *p*-aminobenzylamine have furnished the compound **60Ae** bearing the suitable functionalities able to mimic the RGD pharmacophores.

## 2.6 Experimental Procedures

### 2.6.1 General Methods

All chemicals were purchased from commercial suppliers and were used without further purification. Microwave-assisted reactions were carried out in a Milestone Mycosynth apparatus, with a dual magnetron system with a pyramid-shaped diffuser, 1000 W maximum power output, and temperature monitor and control by optical fiber up to a vessel temperature of  $250^\circ\text{C}$ . Flash chromatography was carried out on silica gel (230-400 mesh). Flash chromatography was performed on silica gel (230-400 mesh). NMR Spectra were recorded with Varian Mercury Plus 400 or Unity Inova 600 MHz spectrometers. Chemical shifts were reported as  $\delta$  values (ppm) relative to the solvent peak of  $\text{CDCl}_3$  set at  $\delta = 7.27$  ppm ( $^1\text{H}$  NMR) or  $\delta = 77.0$  ppm ( $^{13}\text{C}$  NMR),  $\text{CD}_3\text{OD}$  set at  $\delta = 3.31$  ppm ( $^1\text{H}$  NMR) or  $\delta = 49.0$  ppm ( $^{13}\text{C}$  NMR),  $\text{D}_2\text{O}$  set at  $\delta = 4.79$  ppm ( $^1\text{H}$  NMR),  $\text{CD}_3\text{CN}$  set at  $\delta = 1.93$  ppm ( $^1\text{H}$  NMR) or  $\delta = 117.7$  ppm ( $^{13}\text{C}$  NMR),  $(\text{CD}_3)_2\text{CO}$  set at  $\delta = 2.04$  ppm ( $^1\text{H}$  NMR) or  $\delta = 29.8$  ppm

( $^{13}\text{C}$  NMR). Coupling constants are given in Hertz. LC-MS analyses were performed on an HP1100 liquid chromatograph coupled with an electrospray ionization-mass spectrometer using a Phenomenex Gemini C18-3 $\mu$ -110 column,  $\text{H}_2\text{O}/\text{CH}_3\text{CN}$  as neutral solvent at  $25^\circ\text{C}$  or  $\text{H}_2\text{O}/\text{CH}_3\text{CN}$  with 0.2% formic acid as acid solvents (positive scan 100-500 m/z, fragmentor 70 eV). Another set of experiments has been performed on an HP1100 liquid chromatograph coupled with an electrospray ionization-ion trap mass spectrometer MSD1100 using a Phenomenex Zorbax C18-3.5 $\mu$ -80 column,  $\text{H}_2\text{O}/\text{CH}_3\text{CN}$  with 0.08% trifluoroacetic acid as acid solvents (positive scan 100-500 m/z, fragmentor 70 eV).

## 2.6.2 Synthesis and Characterisation

### General procedure for Luche's reduction on unsaturated acetacetamides.

In a 2-necked round-bottom flask, equipped to perform reaction under  $\text{N}_2$  flow, the unsaturated acetacetamide **14** or **20** was dissolved in a mixture of  $\text{THF}:\text{MeOH}=9:1$  (0.2 M) and  $\text{CeCl}_3\cdot\text{H}_2\text{O}$  (1.1 eq) was added. The mixture was stirred at room temperature for 30 min, then it was cooled at  $-30^\circ\text{C}$  and  $\text{NaBH}_4$  (1.1 eq) was added. After 45 min of stirring at  $-30^\circ\text{C}$ , the reaction was quenched with water and the crude extracted with  $\text{EtOAc}$ . Purification of the products was performed by flash chromatography on silica gel.

( $\pm$ )-(**Z**)-**15a**: Purified by flash chromatography on silica gel, 80:20=Cy:EtOAc; Yield 92%;  $^1\text{H}$  NMR (400 MHz,  $\text{CDCl}_3$ )  $\delta$ (ppm): 6.69 (bs, 1H), 5.57 (d,  $J = 10.0$  Hz), 4.40 (bq,  $J = 6.4$  Hz, 1H), 4.08 (dd,  $J = 5.6, 18.4$  Hz, 1H), 3.97 (dd,  $J = 5.6, 18.4$  Hz, 1H), 2.88 (m, 1H), 2.62 (bs, 1H), 1.49 (s, 9H), 1.39 (d,  $J = 6.4$  Hz, 3H), 1.04 (d,  $J = 6.6$  Hz, 3H), 1.02 (d,  $J = 6.6$  Hz, 3H);  $^{13}\text{C}$  NMR (100 MHz,  $\text{CDCl}_3$ )  $\delta$ (ppm): 169.0, 168.7, 141.8, 136.3, 82.2, 70.9, 41.8, 35.7, 27.9, 22.9, 22.8, 21.7; LC-MS-ESI: rt 5.75 min, m/z 272 [M+1], 294 [M+23], 565 [2M+23].

( $\pm$ )-(**Z**)-**15b**: (60/40 mixture of diastereoisomers) Purified by flash chromatography on silica gel, 80:20=Cy:EtOAc; Yield 85%;  $^1\text{H}$  NMR (400 MHz,  $\text{CDCl}_3$ )  $\delta$ (ppm): 7.06 (d, 0.4H,  $J=8.0$  Hz, NH major), 7.00 (d,  $J=8.4$  Hz, 0.6H), 5.33 (d,  $J=10.1$  Hz, 1H), 4.43 (m, 1H), 4.17 (q,  $J=6.4$  Hz, 1H), 3.99 (bs, 1H), 3.53 (s, 3H), 2.40-2.80 (m, 1H), 1.18-1.55 (m, 3H), 1.16 (d,  $J=6.4$  Hz, 3H, minor), 1.11 (d,  $J=6.4$  Hz, 3H, major), 0.69-0.82 (m, 12H),  $^{13}\text{C}$  NMR (100 MHz,  $\text{CDCl}_3$ )  $\delta$ (ppm): 172.9, 168.3, 141.2, 136.1, 70.0, 51.6, 50.1, 40.5, 27.5, 24.4, 22.4, 22.3, 21.3, 21.1. LC-MS rt 6.67 min (major), 7.91 min (minor) m/z 286 [M+1], 308 [M+23].

( $\pm$ )-(**Z**)-**15c**: (60/40 mixture of diastereoisomers) Purified by flash chromatography on silica gel, 85:15=Cy:EtOAc; Yield 94%;  $^1\text{H}$  NMR (400 MHz,  $\text{CDCl}_3$ )  $\delta$ (ppm): 7.37-7.10 (m, 5H), 6.57/6.49 (d,  $J = 7.6$  Hz, 1H), 5.50 (d,  $J = 9.6$  Hz, 1H), 4.97 (m, 1H), 4.31 (m, 1H), 3.76/3.77 (s, 3H), 3.27 (dd,  $J = 14.0, 5.6$  Hz, 1H), 3.09 (dd,  $J = 14.0, 7.2$  Hz, 1H), 2.65 (m, 1H), 2.42/2.46 (d,  $J = 6.2$  Hz, 1H), 1.22/1.32 (d,  $J = 6.8$  Hz, 3H), 0.90 (d,  $J = 6.6$  Hz, 6H);  $^{13}\text{C}$  NMR (100 MHz,  $\text{CDCl}_3$ )  $\delta$ (ppm): major isomer, 172.0, 168.3, 141.5, 136.0, 135.9, 129.0, 128.5, 127.0, 70.9, 52.8, 52.3, 37.7, 28.0, 22.8, 22.7, 21.7; minor isomer 172.0, 168.5, 141.6, 136.0, 135.8, 129.0, 128.5, 127.0, 70.7, 53.0, 52.3, 37.6, 28.0, 22.7, 22.6, 21.5; LC-MS-ESI: rt 6.90 min, m/z

320 [M+1], 661 [2M+23].

(±)-(Z)-15d: (60/40 mixture of diastereoisomers) Purified by flash chromatography on silica gel, 80:20=Cy:EtOAc; Yield 75%; <sup>1</sup>H NMR (400 MHz, CDCl<sub>3</sub>) δ(ppm): 7.13 (d, J = 7.6 Hz, 1H, major), 6.76 (d, J = 8.0 Hz, 1H, minor), 5.55 (d, J = 10.4 Hz, 1H), 4.90 (m, 1H), 4.31 (q, J = 13.2 Hz, 1H, major), 3.96 (m, 1H, minor), 3.77 (s, 3H), 3.68 (s, 3H), 3.08-2.81 (m, 3H), 2.33 (bs, 1H), 1.32/1.42 (d, J = 6.8 Hz, 3H), 0.86-0.98 (m, 6H); <sup>13</sup>C NMR (100 MHz, CDCl<sub>3</sub>) δ(ppm): major isomer, 174.7, 171.4, 168.4, 141.6, 136.1, 70.6, 68.6, 52.0, 50.9, 35.9, 26.8, 22.8, 21.7, 19.5; minor isomer 174.6, 171.3, 168.4, 141.7, 136.1, 70.8, 68.8, 52.8, 52.7, 36.0, 28.1, 22.7, 21.7, 19.8; LC-MS-ESI: rt 3.45 min, m/z 302 [M+1], 324 [M+23], 625 [2M+23].

(±)-(Z)-15e: (50/50 mixture of diastereoisomers) Purified by flash chromatography on silica gel, 85:15=Cy:EtOAc; Yield 72%; <sup>1</sup>H NMR (400 MHz, CDCl<sub>3</sub>) δ(ppm): 6.73/6.72 (d, J = 7.8 Hz, 1H), 5.57/5.56 (d, J = 10.1 Hz, 1H), 4.63/4.62 (dd, J = 4.6 Hz, 7.8 Hz, 1H), 4.39 (m, 1H), 3.76 (s, 3H), 2.85 (m, 1H), 2.24 (m, 1H), 1.39/1.37 (d, J = 6.8 Hz, 3H), 0.86-0.98 (m, 6H); <sup>13</sup>C NMR (100 MHz, CDCl<sub>3</sub>) δ(ppm): major isomer, 174.4/172.3, 168.7, 141.8/141.7, 136.3, 71.3/70.9, 68.6, 52.1/51.0, 30.9, 28.1, 22.9/22.8, 22.7, 21.8/21.7, 19.2/19.1, 17.8/17.7; LC-MS-ESI: rt 4.99 min, m/z 272 [M+1], 294 [M+23], 565 [2M+23].

(±)-(Z)-15f: (50/50 mixture of diastereoisomers) Purified by flash chromatography on silica gel, 80:20=Cy:EtOAc; Yield 83%; <sup>1</sup>H NMR (400 MHz, CDCl<sub>3</sub>) δ(ppm): 6.70/6.63 (d, 1H, J = 9.2 Hz), 5.57/5.56 (d, J = 10.4 Hz, 1H), 4.55 (m, 1H), 4.40 (m, 1H), 4.27 (m, 1H), 3.75/3.72 (s, 3H), 2.91 (m, 1H), 2.48 (bs, 1H), 1.42/1.38 (d, J = 6.8 Hz, 3H), 1.03 (d, J = 6.6 Hz, 6H), 1.24 (s, 9H), 1.03 (d, J = 6.6 Hz, 3H); <sup>13</sup>C NMR (100 MHz, CDCl<sub>3</sub>) δ(ppm): 171.3/171.1, 169.6/169.4, 140.2/139.9, 136.9, 74.1/74.0, 70.8/70.4, 69.0/68.6, 67.1/67.0, 57.7/57.5, 52.1/51.0, 35.8/35.1, 28.2/28.1, 23.7/23.3, 21.4/21.3, 21.2/21.1, 20.0/19.1; LC-MS-ESI: rt 8.30 min, m/z 330 [M+1], 352 [M+23], 681 [2M+23].

(±)-(Z)-22a: Purified by flash chromatography on silica gel, 95:5=Cy:EtOAc; Yield 86%; <sup>1</sup>H NMR (400 MHz, CDCl<sub>3</sub>) δ(ppm): 6.02 (d, 1H, J = 10.0 Hz, CH=), 4.97 (q, J = 6.4 Hz, 1H), 4.48 (d, J = 16.8 Hz, 1H), 4.42 (d, J = 16.8 Hz, 1H), 3.50 (m, 1H), 1.59 (d, J = 6.4 Hz, 3H), 1.47 (s, 9H), 1.05 (d, J = 6.4 Hz, 6H); <sup>13</sup>C NMR (100 MHz, CDCl<sub>3</sub>) δ(ppm): 170.1, 161.3, 154.6, 149.2, 124.8, 81.8, 74.7, 42.9, 35.2, 28.7, 22.6, 18.8; LC-MS-ESI: rt 10.44 min, m/z 298 [M+1].

(±)-(Z)-22b: (60/40 mixture of diastereoisomers) Purified by flash chromatography on silica gel, 90:10=Cy:EtOAc; Yield 58%; <sup>1</sup>H NMR (400 MHz, CDCl<sub>3</sub>) δ(ppm): major isomer 6.02 (d, J = 9.6 Hz, 1H), 5.22 (dd, J = 9.2, 5.2 Hz, 1H), 4.94 (m, 1H), 3.71 (s, 3H), 3.48 (m, 1H), 2.03 (m, 3H), 1.54 (d, J = 6.4 Hz, 3H), 1.05 (d, J = 6.8 Hz, 6H), 0.94 (d, J = 6.8 Hz, 6H), minor isomer 6.03 (d, J = 10.0 Hz, 1H), 5.26 (dd, J = 9.2, 5.2 Hz, 1H), 4.94 (m, 1H), 3.71 (s, 3H), 3.48 (m, 1H), 2.03 (m, 3H), 1.55 (d, J = 6.4 Hz, 3H), 1.06 (d, J = 6.8 Hz, 6H), 0.95 (d, J = 6.8 Hz, 6H); <sup>13</sup>C NMR (100 MHz, CDCl<sub>3</sub>) δ(ppm): 170.4, 162.6, 153.2, 150.8, 123.6, 75.4, 53.4, 52.8/52.4, 37.6, 29.6, 27.7, 25.3, 22.7, 22.2, 22.1/22.0, 19.1/18.9; LC-MS-ESI: rt 10.48 min (major), m/z 312 [M+1], 334 [M+23], 645 [2M+23].

(±)-(Z)-22c: (50/50 mixture of diastereoisomers) Purified by flash chromatography on silica gel, 95:5=Cy:EtOAc; Yield 62%; <sup>1</sup>H NMR (400 MHz, CDCl<sub>3</sub>) δ(ppm): 7.30-7.15 (m, 5H), 5.89/5.91 (d, J = 10.8 Hz, 1H), 5.57/5.59 (dd, J = 10.8, 5.2 Hz, 1H), 4.65/4.59 (q, J = 6.6 Hz, 1H), 3.78 (s, 3H), 3.58/3.59 (dd, J = 14.0, 5.2 Hz, 1H), 3.42 (dd, J = 14.0, 10.8 Hz, 1H), 3.33/3.28 (m, 1H), 1.19/1.29 (d, J = 6.6 Hz, 3H), 1.00/1.03 (d, J = 6.8 Hz, 3H), 0.95/0.99 (d, J = 6.8 Hz, 3H); <sup>13</sup>C NMR (100 MHz, CDCl<sub>3</sub>) δ(ppm): 169.5, 162.3, 155.1, 150.9, 136.2, 128.6, 127.6, 126.0, 125.6, 70.9, 54.6, 52.3, 35.7, 29.5, 22.2, 18.9; LC-MS-ESI: 10.69 min, m/z 346 [M+1], 368 [M+23], 713 [2M+23].

(±)-(Z)-22d: (50/50 mixture of diastereoisomers) Purified by flash chromatography on silica gel, 85:15=Cy:EtOAc; Yield 74%; <sup>1</sup>H NMR (400 MHz, CDCl<sub>3</sub>) δ(ppm): 6.06 (d, J = 10.4 Hz, 1H), 5.70/5.66 (dd, J = 6.0, 8.0 Hz, 1H), 4.95 (q, J = 7.6 Hz, 1H), 3.75 (s, 3H), 3.70 (s, 3H), 3.52 (m, 1H), 3.35/3.36 (dd, J = 16.4, 6.0 Hz, 1H), 2.91 (dd, J = 16.4, 8.0 Hz, 1H), 1.56 (d, J = 7.6 Hz, 3H), 1.07 (d, J = 6.8 Hz, 3H), 1.06 (d, J = 6.8 Hz, 3H); <sup>13</sup>C NMR (100 MHz, CDCl<sub>3</sub>) δ(ppm): 170.4, 169.4, 162.4, 153.9, 148.7, 127.6, 75.0, 57.2, 52.3/52.2, 51.6/51.4, 34.6, 27.6/27.4, 22.7/22.6, 22.2/22.1, 19.4/18.8; LC-MS-ESI: rt 8.7 min, m/z 328 [M+1], 345 [M+18], 677 [2M+23].

(±)-(Z)-23a: Purified by flash chromatography on silica gel, 80:20=Cy:EtOAc; Yield 96%; <sup>1</sup>H NMR (400 MHz, CDCl<sub>3</sub>) δ(ppm): 5.35 (d, J = 10.0 Hz, 1H), 4.59-4.29 (m, 3H), 3.76 (bs, 1H, OH), 2.42 (m, 1H), 1.46 (s, 9H), 1.44 (s, 9H), 1.33 (d, J = 6.6 Hz, 3H), 0.94 (d, J = 6.6 Hz, 3H), 0.92 (d, J = 6.6 Hz, 3H); <sup>13</sup>C NMR (100 MHz, CDCl<sub>3</sub>) δ(ppm): 169.4, 167.9, 152.7, 134.4, 133.9, 81.6, 79.4, 72.4, 45.6, 29.6, 27.9, 27.7, 22.9, 22.8, 21.8; LC-MS-ESI: rt 10.5 min, m/z 372 [M+1], 394 [M+23], 765 [2M+23].

#### General procedure for N,O-protection with methylchloroformate.

In a 2-necked round bottom flask, equipped to perform reaction under N<sub>2</sub> flow, compound **14** or **15** was dissolved in THF at -78°C. LiHMDA (1.5 eq for **14** or 2.5 eq for **15**) was added and the mixture was stirred for 30 min. Methyl chloroformate (2 eq for **14** or 4 eq for **15**) was added dropwise and the mixture was stirred for 1.5 h at -78°C. The reaction was quenched with water and the crude extracted with EtOAc. The product was purified by flash chromatography on silica gel.

(±)-(Z)-16a: Purified by flash chromatography on silica gel, 90:10=Cy:EtOAc; Yield 79%; <sup>1</sup>H NMR (400 MHz, CDCl<sub>3</sub>) δ(ppm): 5.53 (d, J = 10.4 Hz, 1H), 5.43 (q, J = 6.4 Hz, 1H), 4.50-4.29 (m, 2H), 3.77 (s, 3H), 3.75 (s, 3H), 2.49 (m, 1H), 1.47 (d, J = 6.6 Hz, 3H), 1.46 (s, 9H), 0.97 (d, J = 6.8 Hz, 6H); <sup>13</sup>C NMR (100 MHz, CDCl<sub>3</sub>) δ(ppm): 169.4, 167.2, 155.0, 153.6, 138.9, 134.3, 82.0, 73.8, 54.6, 53.7, 45.9, 28.0, 22.3, 22.1, 19.2; LC-MS-ESI: rt 10.8 min, m/z 410 [M+23], 426 [M+39].

(±)-(Z)-16b: (50/50 mixture of diastereoisomers) Purified by flash chromatography on silica gel, 90:10=Cy:EtOAc; Yield 81%; <sup>1</sup>H NMR (400 MHz, CDCl<sub>3</sub>) δ(ppm): 5.50-5.42 (m, 2H), 5.21/5.30 (m, 1H), 3.84/3.78 (s, 3H), 3.77/3.76 (s, 3H), 3.72/3.70 (s, 3H), 2.50 (m, 1H), 2.00 (m, 1H), 1.78 (m, 1H), 1.57 (m, 1H), 1.44/1.42 (d, J = 6.4 Hz, 3H), 0.97-0.80 (m, 6H); <sup>13</sup>C NMR (100 MHz, CDCl<sub>3</sub>) δ(ppm): 171.2, 169.3, 155.0, 153.9, 137.1, 134.7, 74.3, 57.3, 54.6, 54.1, 52.3, 38.6, 29.7, 28.6, 23.0, 22.9, 21.8, 21.7, 19.5. LC-MS-ESI: rt 10.6 min, m/z 401 [M+1], 424 [M+23].

(±)-(Z)-16c: (60/40 mixture of diastereoisomers) Purified by flash chromatography on silica gel, 95:5=Cy:EtOAc; Yield 78%; <sup>1</sup>H NMR (400 MHz, CDCl<sub>3</sub>) δ(ppm): 7.29-7.19 (m, 5H), 5.56 (m, 1H), 5.39 (d, J = 10.4 Hz), 5.29 (q, J = 6.4 Hz, 1H), 3.77/3.76 (s, 6H), 3.65 (s, 3H), 3.56/3.53 (dd, J = 13.6, 4.8 Hz, 1H), 3.27/3.25 (dd, J = 13.6, 10.8 Hz, 1H), 2.60/2.34 (m, 1H), 1.36 (d, J = 6.8 Hz, 3H), 0.91-0.81 (m, 6H); <sup>13</sup>C NMR (100 MHz, CDCl<sub>3</sub>) δ(ppm): 170.1, 169.2, 155.0, 153.9, 142.3, 137.0, 135.8, 129.5, 128.5, 126.8, 72.6, 57.2, 54.6, 53.6, 52.5, 35.5, 30.2, 22.3, 22.4, 19.6. LC-MS-ESI: rt 11.0 min, m/z 458 [M+23].

(±)-(Z)-16d: (60/40 mixture of diastereoisomers) Purified by flash chromatography on silica gel, 85:15=Cy:EtOAc; Yield 65%; <sup>1</sup>H NMR (400 MHz, CDCl<sub>3</sub>) δ(ppm): 5.66/5.64 (m, 1H), 5.50 (d, J = 10.4 Hz, 1H), 5.40 (m, 1H), 3.80/3.78 (s, 6H), 3.74/3.69 (s, 3H), 3.71/3.67 (s, 3H), 3.30 (dd, 1H, J = 16.8, 6.4 Hz, major), 3.26 (dd, 1H, J = 16.4, 7.2 Hz, minor), 2.79 (dd, 1H, J = 16.8, 7.2 Hz, major), 2.69 (dd, 1H, J = 16.4, 6.4 Hz, minor), 2.46 (m, 1H), 1.44 (d, J = 7.2 Hz, 3H), 0.96 (d, J = 6.8 Hz, 3H), 0.92-0.86 (m, 3H); <sup>13</sup>C NMR (100 MHz, CDCl<sub>3</sub>) δ(ppm): 169.7, 168.1, 167.4, 167.3, 167.2, 142.9, 133.6, 75.7, 54.7, 52.9, 52.6, 50.9, 50.7, 28.2, 25.7, 22.6, 19.5. LC-MS-ESI: rt 9.1 min, m/z 418 [M+1], 440 [M+23], 858 [2M+23].

(±)-(Z)-16e: (50/50 mixture of diastereoisomers) Purified by flash chromatography on silica gel, 90:10=Cy:EtOAc; Yield 79%; <sup>1</sup>H NMR (400 MHz, CDCl<sub>3</sub>) δ(ppm): 6.58/6.51 (d, J = 7.6 Hz, 1H), 5.67/5.66 (d, J = 10.4 Hz, 1H), 5.26 (m, 1H), 4.62 (m, 1H), 3.79 (s, 3H), 3.76 (s, 3H), 2.78 (m, 1H), 2.25 (m, 1H), 1.49/1.47 (d, J = 6.8 Hz, 3H), 1.41 (s, 9H), 1.20-1.01 (m, 6H), 1.01 (m, 6H), 0.94 (d, J = 6.8 Hz, 3H); <sup>13</sup>C NMR (100 MHz, CDCl<sub>3</sub>) δ(ppm): 171.2/171.1, 167.5/167.4, 155.0/154.9, 142.9/142.6, 134.5/134.2, 76.0/75.9, 56.9, 54.7, 52.0, 30.9/30.8, 28.3, 22.6/22.5, 20.0/19.5, 19.1/19.0, 17.5/17.4; LC-MS-ESI: rt 8.7 min, m/z 330 [M+1].

(±)-(Z)-16f: (50/50 mixture of diastereoisomers) Purified by flash chromatography on silica gel, 85:15=Cy:EtOAc; Yield 76%; <sup>1</sup>H NMR (400 MHz, CDCl<sub>3</sub>) δ(ppm): 6.63/6.59 (d, J = 9.2 Hz, 1H), 5.64/5.62 (d, J = 10.4 Hz, 1H), 5.32 (m, 1H), 4.53 (m, 1H), 4.24 (m, 1H), 3.75 (s, 3H, OCH<sub>3</sub>), 3.73 (s, 3H, OCH<sub>3</sub>), 2.88 (m, 1H, CH-CH=), 1.48/1.47 (d, J = 6.8 Hz, 3H, CH<sub>3</sub>-CHOCO<sub>2</sub>Me), 1.41 (s, 9H, tBu), 1.20-1.01 (m, 6H), 0.91 (d, J = 6.4 Hz, 3H); <sup>13</sup>C NMR (100 MHz, CDCl<sub>3</sub>) δ(ppm): 171.1/171.1, 167.8/167.7, 155.1/154.9, 142.2/141.9, 134.2/134.0, 75.9/75.7, 73.9, 67.2/67.1, 57.7/57.6, 54.5/52.0, 50.3/49.9, 28.3, 22.8/22.7, 22.7/22.6, 21.2/21.1, 19.7/19.2; LC-MS-ESI: rt 10.3 min, m/z 388 [M+1], 410 [M+23], 797 [2M+23].

**(Z)-20a:** Purified by flash chromatography on silica gel, 95:5=Cy:EtOAc; Yield 88%;  $^1\text{H}$  NMR (400 MHz,  $\text{CDCl}_3$ )  $\delta$ (ppm): 6.41 (d, 1H,  $J = 11.6$  Hz), 4.48 (m, 2H), 3.75 (s, 3H), 2.62 (m, 1H), 2.35 (s, 3H), 1.48 (s, 9H), 1.08 (d, 6H,  $J = 6.8$  Hz);  $^{13}\text{C}$  NMR (100 MHz,  $\text{CDCl}_3$ )  $\delta$ (ppm): 194.8, 167.9, 167.0, 151.0, 147.6, 138.9, 81.2, 52.6, 45.0, 28.8, 27.6, 25.5, 21.5; LC-MS-ESI: rt 9.53 min,  $m/z$  345 [M+18], 677 [2M+23].

**(Z)-20b:** Purified by flash chromatography on silica gel, 95:5=Cy:EtOAc; Yield 85%;  $^1\text{H}$  NMR (400 MHz,  $\text{CDCl}_3$ )  $\delta$ (ppm): 6.33 (d,  $J = 10.4$  Hz, 1H), 5.31 (m, 1H), 3.70 (s, 3H), 3.68 (s, 3H), 2.54 (m, 1H), 2.29 (s, 3H), 1.96 (m, 1H), 1.85 (m, 1H), 1.67 (m, 1H), 1.05 (d,  $J = 7.2$  Hz, 3H), 1.02 (d,  $J = 7.2$  Hz, 3H), 0.98 (d,  $J = 6.8$  Hz, 6H);  $^{13}\text{C}$  NMR (100 MHz,  $\text{CDCl}_3$ )  $\delta$  (ppm): 195.6, 170.9, 168.4, 153.7, 148.2, 139.3, 53.8, 52.3, 38.3, 30.9, 29.2, 25.7, 24.9, 23.2, 21.9, 21.8, 21.7; LC-MS-ESI: rt 9.6 min,  $m/z$  342 [M+1], 364 [M+23].

**(Z)-20c:** Purified by flash chromatography on silica gel, 95:5=Cy:EtOAc; Yield 83%;  $^1\text{H}$  NMR (400 MHz,  $\text{CDCl}_3$ )  $\delta$ (ppm): 7.40-7.10 (m, 5H), 6.28 (d,  $J = 10.8$  Hz, 1H), 5.64 (m, 1H), 3.78 (s, 3H), 3.64 (s, 3H), 3.25 (m, 2H), 2.28 (s, 3H), 2.15 (m, 1H), 0.93 (d,  $J = 6.8$  Hz, 6H);  $^{13}\text{C}$  NMR (100 MHz,  $\text{CDCl}_3$ )  $\delta$ (ppm): 194.8, 171.7, 168.3, 153.3, 147.6, 138.4, 135.3, 129.0, 128.3, 127.0, 56.8, 53.1, 52.2, 37.8, 28.8, 26.8, 22.0, 21.8. LC-MS-ESI: rt 9.52 min,  $m/z$  376 [M+1], 398 [M+23].

**(Z)-20d:** Purified by flash chromatography on silica gel, 90:10=Cy:EtOAc; Yield 87%;  $^1\text{H}$  NMR (400 MHz,  $\text{CDCl}_3$ )  $\delta$ (ppm): 6.38 (d,  $J = 10.4$  Hz, 1H), 5.65 (m, 1H), 3.78 (s, 3H), 3.74 (s, 3H), 3.73 (s, 3H), 3.35 (dd,  $J = 16.4, 6.8$  Hz, 2H), 2.83 (dd,  $J = 16.4, 6.4$  Hz, 2H), 2.56 (m, 1H), 2.31 (s, 3H), 1.07 (d, 3H,  $J = 6.8$  Hz), 1.06 (d, 3H,  $J = 6.8$  Hz);  $^{13}\text{C}$  NMR (100 MHz,  $\text{CDCl}_3$ )  $\delta$ (ppm): 195.4, 170.9, 169.3, 168.1, 153.2, 148.8, 138.7, 54.1, 52.7, 52.6, 52.0, 34.6, 29.1, 26.9, 25.6, 21.8 (2C); LC-MS-ESI: rt 7.5 min,  $m/z$  358 [M+1], 375 [M+23], 737 [2M+23].

#### General procedure for N,O-protection with di-*tert*-butyldicarbonate.

For the reaction on **14a**: In a 2-necked round bottom flask, equipped to perform reaction under  $\text{N}_2$  flow, compound **14a**, TEA (2 eq) and DMAP (0.2 eq) were dissolved in THF at room temperature.  $(\text{BOC})_2\text{O}$  (2.6 eq) was added and the mixture was left stirring at  $65^\circ\text{C}$  for 2h. The reaction was quenched with water and the crude extracted with DCM. The product was purified by flash chromatography (silica gel, 85:15=Cy:EtOAc).

For the reaction on **15**: In a 2-necked round bottom flask, equipped to perform reaction under  $\text{N}_2$  flow, compound **15** TEA (4.6 eq) and DMAP (0.5 eq) were dissolved in THF at RT.  $(\text{BOC})_2\text{O}$  (6.0 eq) was added and the mixture was left stirring at  $65^\circ\text{C}$  for 2h. The reaction was quenched with water and the crude extracted with DCM. The product was purified by flash chromatography (silica gel, 95:5=Cy:EtOAc).

**(±)-(Z)-17a:** Purified by flash chromatography on silica gel, 90:10=Cy:EtOAc; Yield 88%;  $^1\text{H}$  NMR (400 MHz,  $\text{CDCl}_3$ )  $\delta$ (ppm): 5.46 (d,  $J = 10.0$  Hz, 1H), 5.38 (q,  $J = 6.4$  Hz, 1H), 4.40 (d, 1H,  $J = 13.2$  Hz), 4.24 (m, 1H), 2.48 (m, 1H), 1.48 (s, 9H), 1.46 (s, 9H), 1.44 (s, 9H), 1.42

(d, J = 6.6 Hz, 3H), 0.96 (d, J = 6.4 Hz, 3H), 0.95 (d, J = 6.4 Hz, 3H);  $^{13}\text{C}$  NMR (100 MHz,  $\text{CDCl}_3$ )  $\delta$ (ppm): 169.6, 167.4, 151.7, 151.2, 136.9, 135.1, 82.5, 81.6, 81.4, 72.7, 45.7, 29.5, 27.7, 28.6, 27.6, 22.3, 18.8; LC-MS-ESI: rt 16.1 min, m/z 494 [M+23].

( $\pm$ )-(Z)-17b: (60/40 mixture of diastereoisomers): Purified by flash chromatography on silica gel, 90:10=Cy:EtOAc; Yield 84%;  $^1\text{H}$  NMR (400 MHz,  $\text{CDCl}_3$ )  $\delta$ (ppm): 5.70 (d, J=10.0 Hz, 0.6H, major), 5.68 (d, J=10.2 Hz, 0.4, minor), 5.18 (m, 1H), 4.68 (m, 1H), 3.71 (s, 3H), 2.53 (m, 1H), 1.55-1.75 (m, 3H), 1.49 (s, 9H), 1.42 (s, 9H), 1.45 (d, J=7.2 Hz, 3H), 0.98-1.15 (m, 12H),  $^{13}\text{C}$  NMR (100 MHz,  $\text{CDCl}_3$ )  $\delta$ (ppm): 171.3, 169.7, 152.9, 150.9, 142.5, 135.4(135.3), 84.0, 81.9, 72.9, 52.0, 51.9, 38.8, 27.8 (3C), 27.6 (3C), 26.8, 25.2, 22.7, 22.3, 22.0, 21.9, 19.3 (19.5); LC-MS rt 15.1 min m/z 486 [M+1], 508 [M+23].

( $\pm$ )-(Z)-17c: (50/50 mixture of diastereoisomers) Purified by flash chromatography on silica gel, 95:5=Cy:EtOAc; Yield 82%;  $^1\text{H}$  NMR (400 MHz,  $\text{CDCl}_3$ )  $\delta$ (ppm): 7.32-7.13 (m, 5H), 5.62 (m, 1H), 5.36 (d, J = 10.8 Hz, 1H), 5.25 (q, J = 6.4 Hz, 1H), 3.74/3.73 (s, 3H), 3.54 (dd, J = 14.8, 5.6 Hz, 1H), 3.27 (dd, J = 14.8, 10.8 Hz, 1H), 1.80 (m, 1H), 1.47 (s, 9H), 1.44/1.41 (s, 9H), 1.31 (d, J = 6.6 Hz, 3H), 0.89 (d, J = 7.2 Hz, 3H), 0.83 (d, J = 7.2 Hz, 3H);  $^{13}\text{C}$  NMR (1010 MHz,  $\text{CDCl}_3$ )  $\delta$ (ppm): 170.6, 169.5, 152.8, 150.9, 136.8, 135.8, 135.7, 129.4, 128.4, 126.6, 84.5, 81.7, 73.0, 56.6, 52.2, 35.6, 27.8, 22.5, 22.4, 19.2. LC-MS-ESI: rt 16.3 min, m/z 542 [M+23].

( $\pm$ )-(Z)-17d: (50/50 mixture of diastereoisomers) Purified by flash chromatography on silica gel, 90:10=Cy:EtOAc; Yield 66%;  $^1\text{H}$  NMR (400 MHz,  $\text{CDCl}_3$ )  $\delta$ (ppm): 5.78/5.62 (m, 1H), 5.44/5.42 (d, J = 10.4 Hz, 1H), 5.38 (m, 1H), 3.68 (s, 3H), 3.67 (s, 3H), 3.24/3.20 (dd, J = 15.2, 7.2 Hz, 1H, major), 2.68/2.64 (dd, J = 15.2, 7.2 Hz, 1H, major), 2.44 (m, 1H), 1.45 (d, J = 6.8 Hz, 3H), 1.42 (s, 9H), 1.41 (s, 9H), 0.98-0.91 (m, 6H);  $^{13}\text{C}$  NMR (100 MHz,  $\text{CDCl}_3$ )  $\delta$ (ppm): 170.8, 170.0, 169.8, 169.6, 169.3, 152.9/150.8, 136.7/134.9, 84.5, 81.8, 72.7/72.6, 52.4/52.3, 51.9/51.8, 47.3/46.8, 35.1/34.8, 28.4/27.8, 27.8/27.7, 26.0/25.9, 23.5/22.3, 18.9/17.5; LC-MS-ESI: rt 12.6 min, m/z 523 [M+23], 1025 [2M+23].

( $\pm$ )-(Z)-17e: (50/50 mixture of diastereoisomers) Purified by flash chromatography on silica gel, 95:5=Cy:EtOAc; Yield 69%;  $^1\text{H}$  NMR (400 MHz,  $\text{CDCl}_3$ )  $\delta$ (ppm): 6.84/6.69 (d, J = 9.0 Hz, 1H), 5.64/5.63 (d, J = 10.2 Hz, 1H), 5.17 (m, 1H), 4.60 (m, 1H), 3.75 (s, 3H), 2.79 (m, 1H), 2.27 (m, 1H), 1.49/1.47 (d, J = 6.8 Hz, 3H), 1.47 (s, 9H), 1.04-0.97 (m, 9H), 0.93 (d, J = 6.8 Hz, 3H);  $^{13}\text{C}$  NMR (100 MHz,  $\text{CDCl}_3$ )  $\delta$ (ppm): 172.1/171.9, 167.8/167.7, 152.8/152.6, 142.5/141.9, 135.3/134.7, 82.3/82.2, 76.7/74.6, 52.0/51.9, 30.8/30.7, 28.3/28.2, 27.7/27.6, 22.6/22.5, 22.4, 21.8, 19.5/19.1, 19.1/19.0, 17.5/17.4; LC-MS-ESI: rt 10.9 min, m/z 372 [M+1], 394 [M+23], 765 [2M+23].

( $\pm$ )-(Z)-17f: (50/50 mixture of diastereoisomers) Purified by flash chromatography on silica gel, 90:10=Cy:EtOAc; Yield 72%;  $^1\text{H}$  NMR (400 MHz,  $\text{CDCl}_3$ )  $\delta$ (ppm): 6.74/6.71 (d, J = 9.2 Hz, 1H), 5.64/5.60 (d, J = 10.4 Hz, 1H), 5.25/5.22 (m, 1H), 4.53 (dd, J = 9.2, 1.7 Hz, 1H), 4.26 (m, 1H), 3.69 (s, 3H), 2.90 (m, 1H), 1.47 (s, 9H), 1.46 (s, 9H), 1.47/1.44 (d, J = 6.2 Hz, 3H), 1.21 (d, J = 6.4 Hz, 3H) 1.03-1.01 (d, J = 6.8 Hz, 3H), 1.00-0.99 (d, J = 6.8 Hz, 3H);  $^{13}\text{C}$  NMR (100 MHz,  $\text{CDCl}_3$ )  $\delta$ (ppm): 171.1, 168.1, 153.9, 141.3/141.1, 135.0/134.9, 81.9, 74.1, 73.9/73.8,

67.1, 57.7, 52.0, 28.3, 27.7, 22.8/22.7, 21.2/21.1, 20.0, 19.3; LC-MS-ESI: rt 12.5 min, m/z 430 [M+1], 452 [M+23], 881 [2M+23].

**(Z)-21a:** Purified by flash chromatography on silica gel, 95:5=Cy:EtOAc; Yield 95%; <sup>1</sup>H NMR (400 MHz, CDCl<sub>3</sub>) δ(ppm): 6.21 (d, 1H, J = 10.8 Hz, CH=), 4.24(m, 2H), 2.43 (m, 1H), 2.14 (s, 3H), 1.31 (s, 9H), 1.27 (s, 9H), 0.89 (d, J = 6.8 Hz, 6H); <sup>13</sup>C NMR (100 MHz, CDCl<sub>3</sub>) δ(ppm): 194.6, 168.2, 167.4, 152.3, 149.2, 137.9, 83.4, 81.2, 45.2, 29.4, 28.1, 27.5, 27.3, 25.2, 21.9. LC-MS-ESI: rt 11.3 min, m/z 370 [M+1], 392 [M+23], 761 [2M+23].

**General procedure for the SN2' with 4-amino-benzylamine.** A solution of [Ir(COD)Cl]<sub>2</sub> (2 mmol%) and phosphorous ligand (8 mmol%) in EtOH (0.2 M) under nitrogen atmosphere was stirred for 20 min at RT, then 4-amino-benzylamine (1 eq) was added and the mixture stirred for further 20 min. Then a second portion of 4-amino-benzylamine (4 eq) was added together with carbonate **16** or **17**. The solution was stirred under refluxing conditions and monitored by TLC. After removal of the solvent under reduced pressure, the residue was diluted with ethyl acetate. The organic solution was washed three times with water then dried over Na<sub>2</sub>SO<sub>4</sub>, filtered and concentrated under reduced pressure. The products were isolated by flash chromatography (silica gel, 80:20 =Cy:EtOAc).

**(±)-(Z)-19a:** Purified by flash chromatography on silica gel, 85:15=Cy:EtOAc; Yield 62%; <sup>1</sup>H NMR (400 MHz, CDCl<sub>3</sub>) δ(ppm): 7.09 (d, 2H, J = 8.6 Hz), 6.98 (q, J = 6.8 Hz, 1H), 6.69 (d, J = 8.6 Hz, 2H), 5.54 (d, J = 10.8 Hz, 2H), 4.44 (d, J = 10.8 Hz, 2H), 4.07-3.91 (m, 3H), 2.00 (m, 1H), 1.36 (d, J = 7.2 Hz, 3H), 1.24 (s, 9H), 1.01 (d, J = 6.4 Hz, 3H), 0.99 (d, J = 6.4 Hz, 3H); <sup>13</sup>C NMR (100 MHz, CDCl<sub>3</sub>) δ(ppm): 169.0, 168.6, 152.9, 147.0, 136.2, 129.0, 128.2, 126.9, 114.5, 82.3, 58.5, 53.3, 42.9, 32.8, 22.7, 18.5, 14.1; LC-MS-ESI: rt 9.5 min, m/z 424 [M+23].

**(±)-(Z)-19b:** (60/40 mixture of diastereoisomers) Purified by flash chromatography on silica gel, 85:15=Cy:EtOAc; Yield 58%; <sup>1</sup>H NMR (400 MHz, CDCl<sub>3</sub>) δ(ppm): 7.00/6.97 (d, J = 8.4 Hz, 2H), 6.86/6.81 (q, J = 7.2 Hz, 1H), 6.64/6.63 (d, J = 8.4 Hz, 2H), 5.33/5.35 (d, J = 15.0 Hz, 1H), 5.28/5.30 (dd, J = 9.6, 4.2 Hz, 1H), 3.95/3.89 (d, J = 15.0 Hz, 1H), 3.80/3.78 (d, J = 7.8 Hz/8.4 Hz, 1H), 3.71/3.68 (s, 3H), 2.17-2.01 (m, 2H), 1.93 (m, 1H), 1.59 (m, 1H), 1.52 (d, J = 7.2 Hz, 3H), 1.00 (d, J = 6.6 Hz, 3H), 0.95 (m, 6H), 0.84/0.83 (d, J = 6.6 Hz, 3H); <sup>13</sup>C NMR (100 MHz, CDCl<sub>3</sub>) δ(ppm): 171.2/171.3, 165.1/164.5, 152.7/152.1, 146.0, 137.1/137.6, 128.7/128.8, 128.1/127.7, 125.7, 115.0/114.9, 56.8/56.7, 52.7, 52.0/51.8, 50.9/50.7, 38.6/37.9, 33.0/33.1, 25.4/25.3, 22.9/22.8, 18.3/19.2, 13.9/14.0; LC-MS-ESI: rt 9.9 min, m/z 416 [M+1], 438 [M+23], 853 [2M+23].

**(±)-(Z)-19c:** (60/40 mixture of diastereoisomers) Purified by flash chromatography on silica gel, 90:10=Cy:EtOAc; Yield 55%; <sup>1</sup>H NMR (400 MHz, CDCl<sub>3</sub>) δ(ppm): major isomer: 7.24-7.10 (m, 5H), 6.99/6.89 (d, J = 6.8 Hz/8.0 Hz, 2H), 6.80-6.70 (m, 3H), 5.71/5.64 (dd, J = 10.8/10.4, 6.4/6.0 Hz, 1H), 5.32 (d, J = 14.4 Hz, 1H), 4.09 (d, J = 14.4 Hz, 1H), 3.98/3.99 (d, J = 7.4 Hz, 1H), 3.76/3.72 (s, 3H), 3.38-3.60 (m, 2H), 2.03 (m, 1H), 1.44 (d, J = 7.2



Hz, 3H), 0.80/0.74 (d, J = 6.8 Hz, 3H), 0.58/0.50 (d, J = 6.6 Hz, 3H);  $^{13}\text{C}$  NMR (100 MHz,  $\text{CDCl}_3$ )  $\delta$ (ppm): major isomer: 170.8, 165.1/164.4, 153.0/152.7, 147.8/147.0, 138.4/137.7, 137.2/136.9, 135.9, 129.2, 129.0, 128.8, 128.4, 126.4/124.7, 119.1/117.2, 66.8/64.6, 57.9/57.0, 54.8/53.7, 51.4/51.1, 35.2/34.0, 31.9/31.4, 22.9/22.6, 20.0/19.7, 14.1; LC-MS-ESI: rt 9.8 min, m/z 450[M+1], 472[M+23], 921[2M+23].

(±)-(Z)-19d: (60/40 mixture of diastereoisomers) Purified by flash chromatography on silica gel, 85:15=Cy:EtOAc; Yield 58%;  $^1\text{H}$  NMR (400 MHz,  $\text{CDCl}_3$ )  $\delta$ (ppm): major isomer: 7.01/6.98 (d, J = 8.0 Hz, 2H), 6.90/6.83 (q, J = 7.2 Hz/7.6 Hz, 1H), 6.64 (d, J = 8.0 Hz, 2H), 5.75 (t, J = 6.8 Hz, 1H), 5.29 (d, J = 14.8 Hz, 1H), 3.89 (d, J = 14.8 Hz, 1H), 3.80 (m, 1H), 3.74/3.71 (s, 3H), 3.70/3.68 (s, 3H), 3.37 (dd, J = 16.0, 6.8 Hz, 1H), 2.85 (dd, J = 16.0, 6.8 Hz, 1H), 2.06 (m, 1H), 1.57/1.55 (d, J = 7.2 Hz/7.6 Hz, 3H), 0.98/0.83 (d, J = 7.2 Hz, 3H), 0.58/0.50 (d, J = 6.6 Hz, 3H);  $^{13}\text{C}$  NMR (100 MHz,  $\text{CDCl}_3$ )  $\delta$ (ppm): major isomer: 171.3, 169.7, 164.4, 155.8, 154.9, 140.2, 139.0/138.3, 129.7/128.6, 125.2/125.1, 120.2, 61.9/61.1, 58.2, 52.7/52.0, 50.8/50.5, 48.4, 34.5, 33.4, 23.4/22.5, 19.5, 14.5/14.1; LC-MS-ESI: rt 8.4 min, m/z 432[M+1], 885[2M+23].

(±)-(Z)-18a: Purified by flash chromatography on silica gel, 85:15=Cy:EtOAc; Yield 54%;  $^1\text{H}$  NMR (400 MHz,  $\text{CDCl}_3$ )  $\delta$ (ppm): 7.00 (d, J=7.6 Hz, 2H), 6.65 (m, 1H), 6.59 (d, J =7.6 Hz, 2H), 4.57 (bd, 1H), 4.46 (d, J = 12.4 Hz, 1H), 4.31 (m, 1H), 3.87 (dd, J = 18.0, 5.6 Hz, 1H), 3.70 (m, 1H), 3.58 (bs, 2H), 2.68 (m, 1H), 1.84 (d, J =6.6 Hz, 3H), 1.47 (s, 18H), 0.89 (d, J =6.6 Hz, 3H), 0.83 (d, J =6.6 Hz, 3H);  $^{13}\text{C}$  NMR (100 MHz,  $\text{CDCl}_3$ )  $\delta$ (ppm): 167.5, 164.8, 156.4, 145.9, 137.0, 129.8, 129.0, 126.0, 118.8, 81.8, 81.5, 60.7, 57.0, 50.9, 31.8, 28.2, 27.9, 20.2, 20.8, 14.1; LC-MS rt 11.0 min m/z 476[M+1], 498[M+23], 514[M+39], 973[2M+23].

(±)-(Z)-18b: Purified by flash chromatography on silica gel, 85:15=Cy:EtOAc; Yield 52%;  $^1\text{H}$  NMR (400 MHz,  $\text{CDCl}_3$ )  $\delta$ (ppm): 7.70 (bd, J= 8.6 Hz, 1H), 7.14 (d, J = 8.0 Hz, 2H), 6.68 (m, 1H), 6.64 (d, J = 8.0 Hz, 2H), 5.39 (m, 1H), 4.29 (m, 1H), 3.69 (s, 3H) 3.61 (bs, 2H), 2.51 (m, 1H), 1.99 (m, 4H), 1.67-1.88 (m, 2H), 1.46 (s, 9H), 0.92-1.03 (m, 12H);  $^{13}\text{C}$  NMR (100 MHz,  $\text{CDCl}_3$ )  $\delta$ (ppm): 171.5, 163.4, 151.3, 145.0, 134.6, 130.5(130.4), 129.2, 129.1, 114.8, 83.7, 72.9, 62.0, 51.9, 50.0, 38.7, 28.3 (3C), 27.7, 24.9, 23.2, 23.1, 21.9, 21.8, 19.4; LC-MS rt 10.3 min m/z 490 [M+1], 512 [M+23].

(±)-(Z)-18c: Purified by flash chromatography on silica gel, 90:10=Cy:EtOAc; Yield 46%;  $^1\text{H}$  NMR (400 MHz,  $\text{CDCl}_3$ )  $\delta$ (ppm): 7.54 (d, J = 8.6 Hz, 2H), 7.37-7.18 (m, 5H), 6.62 (d, J = 8.6 Hz, 2H), 6.60 (m, 1H), 5.01 (m, 1H), 4.40 (m, 1H), 4.35-4.10 (m, 2H), 3.77 (s, 3H), 3.60 (bs, 2H) 3.00-3.21 (m, 2H), 2.35 (m, 1H), 1.66 (d, J =6.6 Hz, 3H), 1.43 (s, 9H), 0.88 (m, 6H);  $^{13}\text{C}$  NMR (100 MHz,  $\text{CDCl}_3$ )  $\delta$ (ppm): 168.3, 164.5, 152.8, 143.7, 138.1, 134.6, 132.4, 130.0, 128.8, 128.7, 128.1, 125.8, 117.2, 82.1, 64.3, 58.7, 52.6, 52.0, , 36.4, 31.9, 28.3, 20.1, 19.9, 14.8; LC-MS rt 9.0 min m/z 524[M+1], 546[M+23], 1071 [2M+23].

(±)-(Z)-18d: Purified by flash chromatography on silica gel, 90:10=Cy:EtOAc; Yield 20%;  $^1\text{H}$  NMR (400 MHz,  $\text{CDCl}_3$ )  $\delta$ (ppm): 7.16 (d, J=7.8 Hz, 2H), 6.87 (d, J =7.8 Hz, 2H), 6.73/6.67 (m, 1H), 5.76/5.56 (t, J =7.0/6.8 Hz, 1H), 4.66/4.50 (m, 1H), 4.20-4.05 (m, 2H), 3.68 (s, 3H),

3.60 (s, 3H), 3.16 (dd,  $J = 7.0, 15.2$  Hz, 2H), 2.90-2.75 (m, 2H), 2.54 (m, 1H), 1.50 (d,  $J = 7.6$  Hz, 3H), 1.42 (s, 9H), 1.25/1.22 (m, 3H), 0.88/0.86 (m, 3H);  $^{13}\text{C}$  NMR (100 MHz,  $\text{CDCl}_3$ )  $\delta$ (ppm): 169.2, 168.8, 164.1, 154.0, 146.6, 138.2, 134.9, 132.0, 128.7, 116.4, 81.9, 72.3, 59.1, 52.0, 51.7, 36.5, 34.9, 28.6, 20.3, 19.8, 15.0; LC-MS rt 8.8 min  $m/z$  506[M+1], 1033 [2M+23].

( $\pm$ )-(*E*)-24e: (50/50 mixture of diastereoisomers) Purified by flash chromatography on silica gel, 80:20=Cy:EtOAc; Yield 47%;  $^1\text{H}$  NMR (400 MHz,  $\text{CDCl}_3$ )  $\delta$ (ppm): 7.02 (d,  $J = 7.6$  Hz, 2H), 6.70 (m, 3H); 5.77 (m, 1H), 4.47 (bd, 1H), 4.05-4.21 (m, 2H), 3.78 (s, 3H), 3.40 (m, 1H), 2.78 (m, 1H), 2.15 (d,  $J = 8.4$  Hz, 1H), 2.05 (m, 1H), 0.84-1-04 (m, 12H);  $^{13}\text{C}$  NMR (100 MHz,  $\text{CDCl}_3$ )  $\delta$ (ppm): 171.3, 166.8, 144.0, 138.4, 136.1, 129.9, 128.6, 117.3, 61.6, 58.5, 54.2, 51.7, 32.6, 28.4, 22.3, 22.0, 19.3, 19.2, 14.7; LC-MS rt 3.76 min  $m/z$  376[M+1], 773[2M+23].

( $\pm$ )-(*Z*)-24e: (50/50 mixture of diastereoisomers) Purified by flash chromatography on silica gel, 80:20=Cy:EtOAc; Yield 47%;  $^1\text{H}$  NMR (400 MHz,  $\text{CDCl}_3$ )  $\delta$ (ppm): 7.51 (d,  $J = 8.0$  Hz, 2H), 6.95 (m, 1H), 6.72 (m, 3H); 4.53 (m, 1H), 4.05-4.21 (m, 2H), 3.65 (s, 3H), 3.54 (m, 1H), 2.66 (m, 1H), 2.05 (m, 1H), 1.84 (d,  $J = 7.8$  Hz, 1H), 0.84-1-04 (m, 12H);  $^{13}\text{C}$  NMR (100 MHz,  $\text{CDCl}_3$ )  $\delta$ (ppm): 171.6, 166.9, 146.3, 138.2, 136.0, 130.2, 128.7, 116.8, 61.2, 59.2, 53.1, 51.6, 32.5, 29.1, 22.4, 22.1, 19.6, 19.2, 14.9; LC-MS rt 3.90 min  $m/z$  376[M+1], 773[2M+23].

( $\pm$ )-(*E*)-24f: (50/50 mixture of diastereoisomers) Purified by flash chromatography on silica gel, 80:20=Cy:EtOAc; Yield 35%;  $^1\text{H}$  NMR (400 MHz,  $\text{CDCl}_3$ )  $\delta$ (ppm): 9.44 (bd,  $J = 7.6$  Hz, 1H), 7.00 (d,  $J = 8.0$  Hz, 2H), 6.95 (d,  $J = 8.0$  Hz, 2H), 5.83 (m, 1H), 4.54 (bd, 1H), 4.65 (m, 1H), 4.20 (s, 2H), 3.78 (s, 3H), 3.58 (m, 1H), 2.74 (m, 1H), 2.01 (d,  $J = 6.6$  Hz, 3H), 0.90-1.15 (m, 9H);  $^{13}\text{C}$  NMR (100 MHz,  $\text{CDCl}_3$ )  $\delta$ (ppm): 171.3, 164.7, 145.1, 138.2, 135.9, 130.0, 128.7, 116.8, 79.6, 73.7, 60.1, 58.2, 55.7, 51.8, 30.9, 28.9, 22.4, 22.3, 19.2, 15.0; LC-MS rt 8.9 min  $m/z$  434[M+1], 472 [M+39], 889[2M+23].

( $\pm$ )-(*Z*)-24f: (50/50 mixture of diastereoisomers) Purified by flash chromatography on silica gel, 80:20=Cy:EtOAc; Yield 35%;  $^1\text{H}$  NMR (400 MHz,  $\text{CDCl}_3$ )  $\delta$ (ppm): 9.05 (bd,  $J = 7.6$  Hz, 1H), 7.12 (d,  $J = 8.0$  Hz, 2H), 6.94 (m, 1H), 6.88 (d,  $J = 8.0$  Hz, 2H), 4.63 (m, 1H), 4.55 (m, 1H), 4.21 (s, 2H), 3.65 (s, 3H), 3.47 (m, 1H), 2.53 (m, 1H), 1.99 (d,  $J = 6.8$  Hz, 3H), 0.90-1.15 (m, 9H);  $^{13}\text{C}$  NMR (100 MHz,  $\text{CDCl}_3$ )  $\delta$ (ppm): 170.7, 168.6, 143.9, 140.1, 136.9, 132.0, 128.7, 115.0, 80.2, 76.1, 61.5, 58.9, 52.7, 51.3, 33.4, 28.6, 22.4, 22.2, 19.3, 14.7; LC-MS rt 8.0 min  $m/z$  434[M+1], 472 [M+39], 889[2M+23].

( $\pm$ )-(*Z*)-25e: (50/50 mixture of diastereoisomers) Purified by flash chromatography on silica gel, 80:20=Cy:EtOAc; Yield 62%;  $^1\text{H}$  NMR (400 MHz,  $\text{CDCl}_3$ )  $\delta$ (ppm): 7.04 (d,  $J = 7.6$  Hz, 2H), 6.80 (d,  $J = 8.6$  Hz, 1H), 6.69 (m, 3H); 4.59 (bd, 1H), 4.27 (m, 2H), 3.77 (s, 3H), 3.55 (m, 1H), 2.75 (m, 1H), 2.25 (m, 1H), 1.35 (d,  $J = 6.6$  Hz, 3H), 0.84-1-04 (m, 12H);  $^{13}\text{C}$  NMR (100 MHz,  $\text{CDCl}_3$ )  $\delta$ (ppm): 170.9, 164.6, 155.9, 145.3, 132.4, 129.6, 128.7, 118.1, 61.2, 57.3, 57.0, 52.1, 31.6, 27.9, 22.2, 21.9, 19.0, 18.6, 18.4; LC-MS rt 5.76 min  $m/z$  376[M+1], 398[M+23].

( $\pm$ )-(*Z*)-25f: (50/50 mixture of diastereoisomers) Purified by flash chromatography on silica gel, 80:20=Cy:EtOAc; Yield 20%;  $^1\text{H}$  NMR (400 MHz,  $\text{CDCl}_3$ )  $\delta$ (ppm): 7.03 (d,  $J = 8.4$  Hz, 2H), 6.95 (m, 3H), 6.61 (d,  $J = 9.0$  Hz, 1H), 4.54 (bd, 1H), 4.25 (m, 2H), 3.76 (s, 3H), 3.56 (m,

1H), 2.83 (m, 1H), , 1.42 (d, J =6.6 Hz, 3H), 0.95-1.15 (m, 9H); <sup>13</sup>C NMR (100 MHz, CDCl<sub>3</sub>) δ(ppm): 170.6, 165.8, 156.0, 145.2, 131.9, 129.6, 128.6, 118.4, 75.8, 73.7, 60.7, 57.8, 56.8, 51.9, 31.0, 28.5, 22.3, 22.0, 19.8, 19.2; LC-MS rt 4.1 min m/z 434[M+1], 456 [M+23], 889 [2M+23].

**General procedure for the synthesis of 26 and 35.** In a 2-neck round bottom flask, equipped to perform reaction under N<sub>2</sub> atmosphere, a solution of dimethyl sulfoxide (2.3 eq) in DCM (4.0 M) was added at -78°C to a solution of oxalyl chloride (1.2 eq) in DCM (0.5 M), and the mixture was stirred for 5 min. After this time, the alcohol in DCM (0.9 M) was added dropwise in 5 min and the solution was then stirred for 15 min. TEA dry (5 eq) was added dropwise and the mixture was stirred further at room temperature for 10 min. The mixture was diluted with Et<sub>2</sub>O and water. The organic layer, after dilution with Et<sub>2</sub>O, was washed with NH<sub>4</sub>Cl sat. (20 mLx3). It was then dried over Na<sub>2</sub>SO<sub>4</sub> and evaporated under reduced pressure to give the product as a yellow oil and used without further purifications. **26:** Yield >99%. <sup>1</sup>H NMR (400 MHz, CDCl<sub>3</sub>) δ(ppm): 9.79 (t, J = 1.3 Hz, 1H), 2.59 (dt, J = 1.3, 7.2 Hz, 2H), 2.26 (dt, J = 2.6, 7.2 Hz, 2H), 1.96 (t, J = 2.6 Hz, 1H), 1.84 (m, 2H); <sup>13</sup>C NMR (100 MHz, CDCl<sub>3</sub>) δ(ppm): 200.1, 82.2, 68.6, 45.2, 20.0, 16.7.

**tert-butyl-2-acetyloct-2-en-7-ynoate 27.** In a one-neck round bottom flask, **26**, *tert*-butyl acetoacetate (1 eq) and piperidine (15 mol%) were stirred at room temperature for 24h. The mixture was diluted with EtOAc and washed with water. The organic layer was dried over Na<sub>2</sub>SO<sub>4</sub> and then evaporated. The crude was purified with flash chromatography (silica gel, 99/1 cyclohexane/EtOAc) to obtain the product as a 1/4 mixture of *Z/E* isomers.

**27:** Yield = 40%. <sup>1</sup>H NMR (400 MHz, CDCl<sub>3</sub>) δ(ppm): 6.77 (t, J = 8.0 Hz, 1H, *E* isomer), 6.74 (t, J = 7.6 Hz, 1H, *Z* isomer), 2.42 (dt, J = 7.6, 7.2 Hz, 2H), 2.29 (s, 3H), 2.23 (dt, J = 2.4, 6.8 Hz, 2H), 1.96 (t, J = 2.4 Hz, 1H), 1.72 (m, 2H), 1.53 (s, 9H); <sup>13</sup>C NMR (100 MHz, CDCl<sub>3</sub>) δ(ppm): 194.8, 165.5, 145.1, 138.6, 83.2, 82.1, 69.2, 28.6, 28.0, 27.0, 26.8, 18.0; LC-MS: rt=9.1 min, m/z: 259 [M+23], 275 [M+39], 495 [2M+23].

**tert-butyl 2-acetyl-8-(trimethylsilyl)oct-2-en-7-ynoate 36.** A 1 M solution of TiCl<sub>4</sub> in DCM (2.0 eq) was added dropwise to THF (0.5 M) at 0°C and the mixture was stirred for few minutes. Then *tert*-butyl acetoacetate (1.0 eq) in THF (2.3 M) and **35** in THF (2.3M) were added at 0°C; the mixture was stirred for 75 min. A solution of pyridine (4.0 eq) in THF (6 M) was then added dropwise in 90 min and the mixture stirred overnight. The solution was diluted with Et<sub>2</sub>O and washed with water and brine. The organic layer was dried over Na<sub>2</sub>SO<sub>4</sub>, filtered and concentrated under reduced pressure. The crude product was purified by flash chromatography (silica gel, 98/2 cyclohexane/EtOAc) to obtain the product as a 1/4 mixture of *Z/E* isomers.

**36:** Yield = 83%.  $^1\text{H}$  NMR (400 MHz,  $\text{CDCl}_3$ )  $\delta$ (ppm): 6.75 (t,  $J$  = 8.0 Hz, 1H, *E* isomer), 6.73 (t,  $J$  = 7.6 Hz, 1H, *Z* isomer), 2.39 (dt,  $J$  = 7.6, 7.6 Hz, 2H), 2.28 (s, 3H), 2.24 (m, 2H), 1.68 (m, 2H), 1.53 (s, 9H), 0.12 (s, 9H);  $^{13}\text{C}$  NMR (100 MHz,  $\text{CDCl}_3$ )  $\delta$ (ppm): 201.0 (E), 194.8 (Z), 165.5 (Z), 163.3 (E), 145.8 (E), 145.4 (Z), 138.4 (Z), 137.9 (E), 105.9 (Z+E), 85.2 (Z+E), 82.1 (Z), 81.7 (E), 28.7 (Z+E), 28.0 (Z), 27.9 (E), 27.8 (E), 27.4 (E), 27.2 (Z), 26.8 (Z), 19.5 (Z), 19.3 (E), 0.0 (Z+E); LC-MS:  $t_r$ =12.5 min,  $m/z$ : 331 [M+23], 347 [M+39], 639 [2M+23].

**General procedure for the synthesis of isoxazolidine ring 28 and 37.** In a 2-necked round bottom flask, equipped to perform reaction under  $\text{N}_2$  atmosphere,  $\text{Yb}(\text{OTf})_3$  (5 mol%) was added to a solution of **27** or **36** in DCM (0.05 M), and the mixture stirred for 10 min at RT. After this time, *N,O*-bistrimethylsilyl hydroxylamine (2.0 eq) was added at  $0^\circ\text{C}$  and the mixture stirred for 30 min. The solution was diluted with DCM and washed with water, giving the crude product as yellow oil used without further purifications.

**General procedure for the synthesis of acylated isoxazolidine ring 29 and 38.** In two-necked round bottom flask, equipped to perform reaction under  $\text{N}_2$  atmosphere, TEA (1.5 eq) and methyl malonyl chloride (1.5 eq) were added at  $0^\circ\text{C}$  to a solution of **28** or **37** in DCM (0.2 M). The mixture was stirred at room temperature for 2,5 h. The mixture was washed with water. The crude product was purified with flash chromatography (silica gel, 80/20 cyclohexane/EtOAc). The product was isolated as a yellow oil.

**(±)-29:** Yield = 51% (over two steps).  $^1\text{H}$  NMR (400 MHz,  $\text{CDCl}_3$ )  $\delta$ (ppm): 4.65 (dt,  $J$  = 6.8, 7.4 Hz, 1H), 3.72 (s, 3H), 3.59 (d,  $J$  = 15.5 Hz, 1H), 3.53 (d,  $J$  = 15.6 Hz, 1H), 2.86 (d,  $J$  = 7.4 Hz, 1H), 2.28-2.19 (m, 2H), 1.92 (t,  $J$  = 2.4 Hz, 1H), 1.83-1.74 (m, 2H), 1.63 (s, 3H), 1.64-1.52 (m, 2H), 1.46 (s, 9H);  $^{13}\text{C}$  NMR (100 MHz,  $\text{CDCl}_3$ )  $\delta$ (ppm): 169.3, 168.4, 167.5, 105.3, 83.7, 82.6, 68.7, 61.6, 59.1, 52.3, 40.7, 33.9, 27.8, 24.6, 22.8, 17.8. LC-MS:  $t_r$ =8.3 min,  $m/z$ : 370 [M+1], 392 [M+23], 761 [2M+23].

**(±)-38:** Yield = 50% (over two steps).  $^1\text{H}$  NMR (400 MHz,  $\text{CDCl}_3$ )  $\delta$ (ppm): 4.64 (dt,  $J$  = 6.8, 7.2 Hz, 1H), 3.67 (s, 3H), 3.50 (s, 2H), 2.82 (d,  $J$  = 7.2 Hz, 1H), 2.21 (dt,  $J$  = 6.8, 6.0 Hz, 2H), 1.72 (m, 2H), 1.62 (s, 3H), 1.59-1.47 (m, 2H), 1.42 (s, 9H), 0.07 (s, 9H);  $^{13}\text{C}$  NMR (100 MHz,  $\text{CDCl}_3$ )  $\delta$ (ppm): 169.2, 168.5, 167.6, 106.7, 105.4, 84.8, 82.6, 61.7, 59.2, 52.4, 40.8, 34.0, 27.9, 24.8, 22.9, 19.4, 0.1. LC-MS:  $t_r$ =11.3 min,  $m/z$ : 442 [M+1], 464 [M+23], 905 [2M+23].

**Synthesis of isoxazoline 30 from 29 and isoxazoline 39 from 38.** In a two-necked round bottom flask, equipped to perform reaction under  $\text{N}_2$  atmosphere, TEA (2.0 eq) and methanesulfonyl chloride (2.0 eq) were added to a solution of **29** or **38** in DCM (0.24 M) at  $0^\circ\text{C}$ , and the mixture stirred at room temperature for 24h. The mixture was diluted with DCM and washed with water. The organic layer was dried over  $\text{Na}_2\text{SO}_4$ , filtered and concentrated under reduced pressure. The crude product was purified by flash chromatography (silica gel, 80/20 cyclohexane/EtOAc) giving the product as a white solid.

(±)-**30**: Yield = 51%. <sup>1</sup>H NMR (400 MHz, CDCl<sub>3</sub>) δ(ppm): 5.30 (m, 1H), 3.72 (s, 3H), 3.58 (d, J = 15.9 Hz, 1H), 3.46 (d, J = 15.9 Hz, 1H), 2.29- 2.14 (m, 2H), 2.20 (s, 3H), 1.99 (m, 1H), 1.92 (t, J = 2.4 Hz, 1H), 1.76 (m, 1H), 1.64-1.53 (m, 2H), 1.48 (s, 9H); <sup>13</sup>C NMR (100 MHz, CDCl<sub>3</sub>) δ(ppm): 166.8, 162.0, 161.0, 105.8, 83.8, 80.9, 68.4, 62.8, 52.2, 40.4, 32.4, 28.0, 26.7, 23.6, 17.8, 11.1. LC-MS: LC-MS: rt=10.1 min, m/z: 352 [M+1], 374 [M+23], 725 [2M+23].

(±)-**39**: Yield = 87%. <sup>1</sup>H NMR (400 MHz, CDCl<sub>3</sub>) δ(ppm): 5.30 (m, 1H), 3.72 (s, 3H), 3.58 (d, J = 15.9 Hz, 1H), 3.46 (d, J = 15.9 Hz, 1H), 2.24 (dt, J = 3.2, 7.2 Hz, 2H), 2.20 (s, 3H), 1.92 (m, 1H), 1.71 (m, 1H), 1.64-1.53 (m, 2H), 1.48 (s, 9H), 0.12 (s, 9H); <sup>13</sup>C NMR (100 MHz, CDCl<sub>3</sub>) δ(ppm): 167.0, 167.9, 162.2, 161.1, 106.9, 106.0, 84.6, 81.1, 63.1, 52.4, 40.6, 32.8, 28.2, 23.9, 19.5, 11.3, 0.1; LC-MS: rt= 13.2 min, m/z: 424 [M+1], 446 [M+23], 462 [M+39].

**Synthesis of isoxazoline ring 30 from 39 by TMS protecting group removal.** To a solution of **39** in THF (0.5 M), tetrabutylammonium fluoride trihydrate (1.9 eq) was added and the mixture stirred overnight at room temperature. After adding water, THF was removed and the solution diluted with 10mL of DCM. The organic layer was washed with water, dried over Na<sub>2</sub>SO<sub>4</sub>, filtered and concentrated under reduced pressure. The crude product was purified by flash chromatography (silica gel, 8/2 cyclohexane/EtOAc) to obtain the product as a yellow oil. Yield of **30**: 53%.

**Removal of *tert*-butyl ester: synthesis of acid 31.** In one-necked round bottom flask, to a solution of **30** in DCM (0.03 M) trifluoroacetic acid (15 eq) was added and the mixture stirred for 24h. The solution was evaporated to obtain the desired product as brown oil.

(±)-**31**: Yield >99%. <sup>1</sup>H NMR (400 MHz, CDCl<sub>3</sub>) δ(ppm): 5.36 (m, 1H), 3.73 (s, 3H), 3.63 (d, J = 15.9 Hz, 1H), 3.50 (d, J = 16.0 Hz, 1H), 2.27 (s, 3H), 2.20 (m, 2H), 2.03 (m, 1H), 1.93 (t, J = 2.6 Hz, 1H), 1.78 (m, 1H), 1.65-1.52 (m, 2H); <sup>13</sup>C NMR (100 MHz, CDCl<sub>3</sub>) δ(ppm): 168.3, 167.9, 167.0, 164.4, 104.2, 83.7, 68.7, 62.9, 52.6, 40.4, 32.3, 23.6, 18.0, 11.8; LC-MS: rt= 5.0 min, m/z: 296 [M+1], 318 [M+23], 334 [M+39], 613 [2M+23].

**Synthesis of isoxazoline- 4-amino benzylamide 32.** In two-necked round bottom flask, equipped to perform reaction under N<sub>2</sub> atmosphere, TEA (1.5 eq) and HBTU (1.5 eq) were added to a solution of **31** in DCM, and the mixture was stirred at room temperature for 5 min. 4-aminobenzylamine (2.0 eq) was then added and the mixture stirred for further 4h. The mixture was diluted with DCM and washed with water. The organic layer was dried over Na<sub>2</sub>SO<sub>4</sub>, filtered and concentrated under reduced pressure. The crude product was purified by flash chromatography (silica gel, 80/20 cyclohexane/EtOAc) giving the product as a yellow oil.

(±)-**32**: Yield = 76%. <sup>1</sup>H NMR (400 MHz, CDCl<sub>3</sub>) δ(ppm): 7.06 (d, J = 8.0 Hz, 2H), 6.63 (d, J = 8.0 Hz, 2H), 5.62 (bs, 1H), 5.27 (m, 1H), 4.41 (dd, J = 5.6, 14.0 Hz, 1H), 4.29 (dd, J = 5.2, 14.0 Hz, 1H), 3.70 (s, 3H), 3.58 (d, J = 15.9 Hz, 1H), 3.44 (d, J = 16.0 Hz, 1H), 2.38 (m, 1H),

2.21 (m, 1H), 2.02 (s, 3H), 1.97 (m, 1H), 1.65 (m, 1H), 1.58-1.51 (m, 2H);  $^{13}\text{C}$  NMR (100 MHz,  $\text{CDCl}_3$ )  $\delta$ (ppm): 168.5, 166.9, 162.0, 159.0, 145.9, 129.1, 127.6, 115.1, 106.5, 83.7, 69.3, 61.6, 52.4, 43.1, 40.5, 38.5, 32.6, 23.0, 17.3, 11.3; LC-MS: rt= 1.4 min, m/z: 400 [M+1], 422 [M+23], 438 [M+39], 821 [2M+23].

**General procedure for the hydrolysis of malonyl methyl ester. Synthesis of 33, 42a, 42b, 45a, 45b, 48, 50.** In a one-necked round bottom flask,  $\text{LiOH}\cdot\text{H}_2\text{O}$  (1.0 eq) was added to a solution of ester in a 2/1 mixture of THF/ $\text{H}_2\text{O}$  (0.007 M). The reaction was stopped after disappearance of the starting material, following the evolution by TLC. The solution was neutralized adding dropwise HCl 1M solution and then water was evaporated. The product was purified by flash chromatography (C18 reverse phase silica gel, 8/2 water/ $\text{CH}_3\text{CN}$ ).

( $\pm$ )-33: Yield = 99%.  $^1\text{H}$  NMR (400 MHz, Methanol- $d_4$ )  $\delta$ (ppm): 7.04 (d, J = 8.2 Hz, 2H), 6.66 (d, J = 8.2 Hz, 2H), 5.43 (m, 1H), 4.84 (m, 2H), 4.36 (d, J = 14.6 Hz, 1H), 4.17 (d, J = 14.6 Hz, 1H), 2.22-2.11 (m, 2H), 2, 18 (s, 3H), 1.87 (bs, 1H), 1.86 (m, 1H), 1.66 (m, 1H), 1.57-1.48 (m, 2H);  $^{13}\text{C}$  NMR (400 MHz, Methanol- $d_4$ )  $\delta$ (ppm): 172.4, 172.0, 163.6, 158.3, 146.4, 128.3, 128.1, 115.2, 106.6, 83.2, 68.5, 62.3, 42.3, 39.9, 32.8, 23.5, 17.3, 10.0. LC-MS: rt= 1.6 min, m/z: 386 [M+1], 400 [M+23], 771 [2M+1].

( $\pm$ )-42a: Yield = 80%.  $^1\text{H}$  NMR (400 MHz, Methanol- $d_4$ )  $\delta$ (ppm): 7.64 (s, 1H), 7.61 (bs, 1H), 7.01 (d, J = 8.3 Hz, 2H), 6.90 (bs, 1H), 6.65 (d, J = 8.3 Hz, 2H), 5.45 (m, 1H), 4.85 (m, 2H), 4.39-4.32 (m, 3H), 4.18 (d, J = 14.4 Hz, 1H), 3.45 (t, J = 5.6 Hz, 2H), 2.67 (t, J = 8.0 Hz, 2H), 2.17 (s, 3H), 1.87-1.53 (m 4H), 1.37 (s, 9H).  $^{13}\text{C}$  NMR (400 MHz, Methanol- $d_4$ )  $\delta$ (ppm): 169.7, 163.4, 163.0, 161.9, 158.5, 147.3, 144.9, 129.3, 129.0, 121.9, 115.4, 107.3, 79.8, 61.3, 49.8, 42.7, 40.5, 38.8, 32.4, 28.3, 24.4, 23.2, 11.3; LC-MS: rt= 1.6 min, m/z: 572 [M+1].

( $\pm$ )-42b: Yield = 87%.  $^1\text{H}$  NMR (400 MHz, Methanol- $d_4$ )  $\delta$ (ppm): 7.69 (s, 1H), 7.00 (d, J = 8.0 Hz, 2H), 6.64 (d, J = 8.0 Hz, 2H), 5.45 (m, 1H), 4.35-4.31 (m, 3H), 4.17 (d, J = 14.6 Hz, 1H), 3.46 (d, J = 14.8 Hz, 1H), 3.21 (d, J = 14.8 Hz, 1H), 3.01 (t, J = 6.0 Hz, 2H), 2.67 (t, J = 7.2 Hz, 2H), 2.17 (s, 3H), 2.01-1.98 (m, 2H), 1.86-1.61 (m, 4H), 1.40 (s, 9H);  $^{13}\text{C}$  NMR (400 MHz, Methanol- $d_4$ )  $\delta$ (ppm): 171.9, 169.5, 163.6, 161.7, 158.3, 147.4, 146.4, 135.7, 128.2, 122.0, 115.1, 106.5, 78.7, 62.3, 48.2, 42.2, 37.1, 32.8, 30.1, 29.2, 27.3, 24.3, 24.1, 10.0. LC-MS: rt= 1.6 min, m/z: 586 [M+1], 608[M+23].

( $\pm$ )-45a: Yield = 75%.  $^1\text{H}$  NMR (400 MHz,  $\text{CDCl}_3$ )  $\delta$ (ppm): 7.76 (s, 1H), 7.47 (bs, 1H), 7.41 (d, J = 8.0 Hz, 2H), 7.28 (d, J = 8.0 Hz, 2H), 5.51 (m, 1H), 5.20 (s, 2H), 4.50 (d, J = 15.2 Hz, 2H), 4.39 (d, J = 15.2 Hz, 2H), 2.76-2.69 (m, 2H), 2.20 (s, 3H), 1.85-1.60 (m, 4H), 1.45 (s, 9H);  $^{13}\text{C}$  NMR (100 MHz,  $\text{CDCl}_3$ )  $\delta$ (ppm): 173.6, 171.2, 169.9, 169.2, 167.2, 147.0, 146.8, 134.1, 128.2, 122.4, 115.3, 106.6, 82.4, 61.0, 51.4, 43.2, 34.0, 33.3, 27.8, 24.6, 24.0, 11.0; LC-MS (acid eluents): rt= 9.4 min, m/z: 543 [M+1], 565 [M+23].

( $\pm$ )-45b: Yield = 75%.  $^1\text{H}$  NMR (400 MHz,  $\text{CDCl}_3$ )  $\delta$ (ppm): 7.82 (bs, 1H), 7.80 (s, 1H), 7.44 (d, J = 8.0 Hz, 2H), 7.34 (d, J = 8.0 Hz, 2H), 5.50 (m, 1H), 4.61-4.56 (m, 3H), 4.46 (d, J = 12.4 Hz, 1H), 2.90-2.85 (m, 2H), 2.75-2.71 (m, 2H), 2.20 (s, 3H), 1.86-1.65 (m, 4H), 1.38 (s, 9H);  $^{13}\text{C}$

NMR (100 MHz, CDCl<sub>3</sub>)  $\delta$ (ppm): 173.6, 170.8, 170.2, 169.6, 167.5, 147.0, 146.2, 133.8, 128.6, 122.0, 115.1, 106.4, 80.9, 60.7, 48.2, 43.4, 35.4, 33.9, 30.8, 27.6, 24.8, 24.2, 11.5; LC-MS(acid eluents): rt= 10.0 min, m/z: 557 [M+1], 579 [M+23].

(±)-**48**: Yield = 40%. <sup>1</sup>H NMR (400 MHz, Methanol-d<sub>4</sub>)  $\delta$ (ppm): 7.80 (s, 1H), 7.43 (d, J = 8.0 Hz, 2H), 7.35 (d, J = 8.0 Hz, 2H), 5.52 (m, 1H), 4.51 (d, J = 15.0 Hz, 1H), 4.22-4.35 (m, 3H), 3.18-3.13 (m, 2H), 2.78-2.68 (m, 2H), 2.63-2.57 (m, 2H), 2.48-2.44 (m, 2H), 2.21 (s, 3H), 2.08-2.03 (m, 2H), 1.98-1.94 (m, 1H), 1.87-1.83 (m, 1H), 1.76-1.59 (m, 4H), 1.41 (s, 9H); <sup>13</sup>C NMR (400 MHz, Methanol-d<sub>4</sub>)  $\delta$ (ppm): 172.5, 172.2, 172.0, 169.1, 165.6, 162.7, 147.0, 146.5, 135.2, 128.6, 122.1, 115.3, 106.2, 80.8, 62.0, 48.4, 42.8, 37.0, 33.1, 31.2, 30.8, 29.4, 28.8, 28.0, 24.4, 24.0, 11.0; LC-MS (acid eluents): rt= 9.4 min, m/z: 642 [M+1], 664 [M+23].

(±)-**50**: Yield = 40%. <sup>1</sup>H NMR (400 MHz, Methanol-d<sub>4</sub>)  $\delta$ (ppm): 7.73 (s, 1H), 7.03 (d, J = 8.4 Hz, 2H), 6.67 (d, J = 8.4 Hz, 2H), 5.47 (m, 1H), 4.82 (m, 2H), 4.51 (t, J = 5.2 Hz, 2H), 4.37 (d, J = 14.6 Hz, 1H), 4.20 (d, J = 14.6 Hz, 1H), 3.87 (t, J = 5.2 Hz, 2H), 3.60-3.57 (m, 4H), 3.46 (t, J = 5.6 Hz, 2H), 3.19 (t, J = 6.0 Hz, 2H), 2.71 (t, J = 6.8 Hz, 2H), 2.20 (s, 3H), 1.85-1.58 (m, 4H), 1.42 (s, 9H); <sup>13</sup>C NMR (400 MHz, Methanol-d<sub>4</sub>)  $\delta$ (ppm): 175.4, 172.4, 170.3, 168.2, 158.2, 156.9, 147.3, 146.4, 128.4, 128.2, 122.5, 115.1, 107.1, 78.7, 70.0, 69.8, 69.6, 69.0, 49.8, 42.2, 42.1, 39.8, 33.3, 29.3, 27.3, 24.9, 10.3 LC-MS(acid eluents): rt= 9.9 min, m/z: 660 [M+1], 682 [M+23].

**General procedure for the synthesis of azides 40a and 40b.** In two-necked round bottom flask, equipped to perform reaction under N<sub>2</sub> atmosphere, to a solution of 2-bromoethylamine hydrobromide or 3-bromo-propylamine hydrobromide (1.1 eq) in DCM (0.2 M), Boc<sub>2</sub>O and TEA (1.5 eq) were added at 0°C and the mixture stirred at room temperature overnight. The mixture was then washed with NH<sub>4</sub>Cl saturated solution, NaHCO<sub>3</sub> saturated solution, brine and evaporated to afford the *N*-Boc-bromo amine intermediate as a colourless oil that was used without further purifications. The intermediate was dissolved in DMF (0.8 M) and NaN<sub>3</sub> (1.2 eq) was added in one portion. The mixture was stirred at 60°C for 4h and then diluted with EtOAc and washed with water. The organic layer was dried over Na<sub>2</sub>SO<sub>4</sub>, filtered and concentrated under reduced pressure to give the azides as yellow oils.

**40a**: Yield = 70%. <sup>1</sup>H NMR (400 MHz, CDCl<sub>3</sub>)  $\delta$ (ppm): 4.79 (bs, 1H), 3.40 (t, J = 5.7 Hz, 2H), 3.28 (m, 2H), 1.43 (s, 9H). <sup>13</sup>C NMR (100 MHz, CDCl<sub>3</sub>)  $\delta$ (ppm): 155.8, 79.9, 50.8, 39.8, 28.2; LC-MS: rt= 6.5 min, m/z: 209 [M+23], 372 [2M+1], 395 [2M+23]. **40b**: Yield = 90%. <sup>1</sup>H NMR (400 MHz, CDCl<sub>3</sub>)  $\delta$ (ppm): 4.63 (bs, 1H), 3.33 (t, J = 8.0 Hz, 2H), 3.18 (m, 2H), 1.71-1.77 (m, 2H), 1.41 (s, 9H). <sup>13</sup>C NMR (100 MHz, CDCl<sub>3</sub>)  $\delta$ (ppm): 162.2, 78.4, 48.7, 36.1, 31.0, 28.0; LC-MS: rt= 7.4 min, m/z: 223 [M+23], 423 [2M+23].

**tert-butyl 4-((3-bromopropyl)amino)-succinate.** In two-necked round bottom flask, equipped to perform reaction under N<sub>2</sub> atmosphere, to a solution of mono *tert*-butyl pentandioic acid in DCM (0.14 M), HBTU (1.5 eq), TEA (1.5 eq) and 3-bromo propylamine hydrobromide (1.1

eq) were added and the mixture stirred at RT for 4h. The mixture was diluted with DCM, washed with water, dried over  $\text{Na}_2\text{SO}_4$ , filtered and concentrated under reduced pressure. The crude product was purified by flash chromatography. Yield= 50%.  $^1\text{H}$  NMR (400 MHz,  $\text{CDCl}_3$ )  $\delta$ (ppm): 5.93 (bs, 1H), 3.43-3.36 (m, 4H), 2.62-2.52 (m, 2H), 2.40 (t, J = 6.8 Hz, 2H), 2.07 (m, 2H), 1.44 (s, 9H);  $^{13}\text{C}$  NMR (100 MHz,  $\text{CDCl}_3$ )  $\delta$ (ppm): 172.3, 172.2, 80.8, 38.0, 32.2, 31.1, 30.8, 30.7, 27.9 ; LC-MS: rt= 6.6 min, m/z: 316 [M+23], 609 [2M+23].

**General procedure for the synthesis of 43a, 43b, 46, 51.** Bromo derivative was dissolved in DMF (0.7 M) and  $\text{NaN}_3$  (1.1 eq) was added. The mixture was stirred at 60°C for 4h and then diluted with EtOAc and washed with water.

**43a:** Yield = 45%.  $^1\text{H}$  NMR (400 MHz,  $\text{CDCl}_3$ )  $\delta$ (ppm): 3.72 (s, 2H); 1.48 (s, 9H);  $^{13}\text{C}$  NMR (100 MHz,  $\text{CDCl}_3$ )  $\delta$ (ppm): 167.2, 82.6, 50.6, 27.7. LC-MS: rt= 8.2 min, m/z: 180 [M+23].

**43b:** Yield = 45%.  $^1\text{H}$  NMR (400 MHz,  $\text{CDCl}_3$ )  $\delta$ (ppm): 3.50 (t, J = 6.4 Hz, 2H); 2.48 (t, J = 6.8 Hz, 2H); 1.45 (s, 9H);  $^{13}\text{C}$  NMR (100 MHz,  $\text{CDCl}_3$ )  $\delta$ (ppm): 169.7, 80.7, 46.6, 35.9, 27.6. LC-MS: rt= 8.8 min, m/z: 194 [M+23].

**46:** Yield = 90%.  $^1\text{H}$  NMR (400 MHz,  $\text{CDCl}_3$ )  $\delta$ (ppm): 6.00 (bs, 1H), 3.36-3.30 (m, 4H), 2.56 (t, J = 6.8 Hz, 2H); 2.40 (t, J = 6.8 Hz, 2H), 1.80-1.72 (m, 2H), 1.43 (s, 9H);  $^{13}\text{C}$  NMR (100 MHz,  $\text{CDCl}_3$ )  $\delta$ (ppm): 172.4, 172.0, 80.8, 49.2, 37.0, 31.2, 30.8, 28.8, 28.0; LC-MS: rt= 6.0 min, m/z: 279 [M+23], 535 [2M+23].

**51:** Yield = 85%.  $^1\text{H}$  NMR (400 MHz,  $\text{CDCl}_3$ )  $\delta$ (ppm): 4.10 (q, J = 7.2 Hz, 2H), 3.27 (t, J = 6.4 Hz, 2H), 2.31 (t, J = 6.8 Hz, 2H), 1.73-1.57 (m, 4H), 1.23 (t, J = 7.2 Hz, 3H);  $^{13}\text{C}$  NMR (100 MHz,  $\text{CDCl}_3$ )  $\delta$ (ppm): 172.9, 60.2, 50.9, 33.5, 28.2, 22.0, 14.1; LC-MS: rt= 8.0 min, m/z: 172 [M+1], 194 [M+23].

**Ethyl 2-(2-(2-azidoethoxy)ethoxy)acetate 53.** [2-(2-azidoethoxy)ethoxy]acetic acid cyclohexylamine salt was dissolved in  $\text{Et}_2\text{O}$  (1.0 M) and  $\text{BF}_3 \cdot \text{Et}_2\text{O}$  (1.0 eq) was added at 0°C. The mixture was refluxed for 3h and then evaporated. The crude product was purified by flash chromatography (silica gel, 1/1 EtOAc/cyclohexane) affording the pure product as a colourless oil.

**53:** Yield = 40%.  $^1\text{H}$  NMR (400 MHz,  $\text{CDCl}_3$ )  $\delta$ (ppm): 4.20 (q, J = 7.2 Hz, 2H), 4.14 (s, 2H); 3.75-3.72 (m, 2H), 3.70-3.66 (m, 4H), 3.38 (q, J = 5.2 Hz, 2H), 1.27 (q, J = 7.2 Hz, 3H);  $^{13}\text{C}$  NMR (100 MHz,  $\text{CDCl}_3$ )  $\delta$ (ppm): 170.2, 70.8, 70.7, 70.5, 68.6, 60.6, 50.5, 14.0. LC-MS: rt= 5.4 min, m/z: 218 [M+1], 240[M+23].

**General procedure for the Huisgen reaction between methyl ester 32 and azides: 41a, 41b, 44a, 44b, 47, 49.** In one-necked round bottom flask, in a mixture of  $t\text{BuOH}:\text{H}_2\text{O}=1:1$  (0.15 M) TEA (1.0 eq) and HCl 1M (1.0 eq) were added and stirred for 2 min. **32**, Cu(0) (10 mol%) and azide (1.0 eq) were added and the mixture stirred at room temperature following the reaction by TLC. The mixture was filtered through celite to remove the copper



powder and evaporated. The crude was purified by flash chromatography (silica gel, 9/1 EtOAc/cyclohexane).

(±)-**41a**: Yield = 57%.  $^1\text{H}$  NMR (400 MHz,  $\text{CDCl}_3$ )  $\delta$ (ppm): 7.44 (bs, 1H), 7.29 (s, 1H), 7.13 (d,  $J = 8.2$  Hz, 2H), 6.66 (d,  $J = 8.2$  Hz, 2H), 5.45 (m, 1H), 5.09 (bs, 1H), 4.42-4.35 (m, 4H), 3.69 (s, 3H), 3.56 (d,  $J = 16.0$  Hz, 1H), 3.51 (m, 2H), 3.46 (d,  $J = 16.0$  Hz, 1H), 2.72-2.67 (m, 2H), 2.24 (s, 3H), 1.85 (m, 1H), 1.75 (m, 1H), 1.61-1.55 (m, 2H), 1.39 (s, 9H);  $^{13}\text{C}$  NMR (100 MHz,  $\text{CDCl}_3$ )  $\delta$ (ppm): 168.9, 167.1, 162.2, 158.9, 155.9, 147.3, 144.9, 129.3, 129.0, 121.9, 115.4, 107.3, 79.8, 61.2, 52.4, 49.8, 42.7, 40.5, 32.3, 29.6, 28.3, 24.4, 23.2, 11.3; LC-MS: rt= 5.6 min, m/z: 586 [M+1], 608 [M+23].

(±)-**41b**: Yield = 67%.  $^1\text{H}$  NMR (400 MHz,  $\text{CDCl}_3$ )  $\delta$ (ppm): 7.50 (bs, 1H), 7.35 (s, 1H), 7.12 (d,  $J = 7.9$  Hz, 2H), 6.72 (d,  $J = 7.9$  Hz, 2H), 5.52 (m, 1H), 4.88 (bs, 1H), 4.42 (m, 2H), 4.27 (t,  $J = 6.9$  Hz, 2H), 3.71 (s, 3H), 3.58 (d,  $J = 16.0$  Hz, 1H), 3.48 (d,  $J = 15.9$  Hz, 1H), 3.10-3.05 (m, 2H), 2.68 (m, 2H), 2.24 (s, 3H), 1.99-1.95 (m, 2H), 1.75-1.84 (m, 2H), 1.63-1.53 (m, 2H), 1.43 (s, 9H);  $^{13}\text{C}$  NMR (100 MHz,  $\text{CDCl}_3$ )  $\delta$ (ppm): 168.9, 167.1, 162.2, 158.9, 156.1, 147.2, 145.1, 129.2, 128.9, 121.4, 115.3, 107.3, 79.4, 61.2, 52.4, 47.4, 42.7, 40.5, 37.4, 32.3, 30.5, 28.4, 24.4, 23.0, 11.3; LC-MS: rt= 6.3 min, m/z: 600 [M+1], 622 [M+23].

(±)-**44a**: Yield = 20%.  $^1\text{H}$  NMR (400 MHz,  $\text{CDCl}_3$ )  $\delta$ (ppm): 7.54 (s, 1H), 7.02 (d,  $J = 8.4$  Hz, 2H), 6.92 (bs, 1H), 6.58 (d,  $J = 8.4$  Hz, 2H), 5.39 (m, 1H), 4.26 (d,  $J = 6.0$  Hz, 2H), 3.67 (s, 3H), 3.58 (d,  $J = 16.4$  Hz, 1H), 3.50 (d,  $J = 16.4$  Hz, 1H), 2.81-2.70 (m, 2H), 2.17 (s, 3H), 1.81-1.51 (m, 6H), 1.46 (s, 9H);  $^{13}\text{C}$  NMR (100 MHz,  $\text{CDCl}_3$ )  $\delta$ (ppm): 173.9, 171.0, 169.1, 167.3, 163.9, 147.1, 146.4, 134.0, 128.6, 122.2, 115.1, 106.3, 82.2, 60.8, 52.1, 51.6, 43.8, 33.4, 31.5, 27.9, 24.8, 24.3, 11.8; LC-MS: rt= 6.8 min, m/z: 557 [M+1], 1135 [2M+23]. (±)-**44b**: Yield = 34%.  $^1\text{H}$  NMR (400 MHz,  $\text{CDCl}_3$ )  $\delta$ (ppm): 7.50 (s, 1H), 7.02 (d,  $J = 8.4$  Hz, 2H), 7.29 (bs, 1H), 6.65 (d,  $J = 8.4$  Hz, 2H), 5.47 (m, 1H), 4.55 (bs, 1H), 4.38-4.34 (m, 3H), 4.18 (d,  $J = 14.4$  Hz, 1H), 3.67 (s, 3H), 3.58 (d,  $J = 16.0$  Hz, 1H), 3.47 (d,  $J = 16.0$  Hz, 1H), 2.80 (t,  $J = 6.4$  Hz, 2H), 2.72 (m, 1H), 2.39 (m, 1H), 2.10 (s, 3H), 1.78-1.54 (m, 4H), 1.38 (s, 9H);  $^{13}\text{C}$  NMR (100 MHz,  $\text{CDCl}_3$ )  $\delta$ (ppm): 173.7, 170.9, 169.6, 167.6, 164.2, 147.3, 146.6, 133.7, 128.4, 122.0, 115.3, 106.1, 81.3, 60.6, 52.3, 48.8, 43.6, 35.4, 31.9, 30.4, 27.9, 24.6, 24.2, 11.6. LC-MS: rt= 6.7 min, m/z: 571 [M+1], 593 [M+23].

(±)-**47**: Yield = 75%.  $^1\text{H}$  NMR (400 MHz,  $\text{CDCl}_3$ )  $\delta$ (ppm): 7.67 (s, 1H), 7.07 (m, 1H), 7.00 (d,  $J = 8.4$  Hz, 2H), 6.58 (d,  $J = 8.4$  Hz, 2H), 5.39 (m, 1H), 4.50 (m, 2H), 4.26 (d,  $J = 5.6$  Hz, 2H), 3.67 (s, 3H), 3.29 (m, 2H), 3.16 (m, 2H), 2.70-2.66 (m, 2H), 2.53-2.48 (m, 2H), 2.41-2.38 (m, 2H), 2.17 (s, 3H), 2.07-2.00 (m, 2H), 1.83-1.57 (m, 4H), 1.41 (s, 9H);  $^{13}\text{C}$  NMR (100 MHz,  $\text{CDCl}_3$ )  $\delta$ (ppm): 172.0, 168.5, 166.8, 161.9, 158.5, 146.9, 145.0, 128.7, 128.5, 121.4, 114.8, 107.0, 80.4, 61.0, 60.0, 52.1, 47.1, 42.3, 40.2, 36.1, 32.0, 30.7, 30.3, 29.6, 27.7, 24.1, 13.8, 10.9; LC-MS: rt= 6.0 min, m/z: 656 [M+1], 678 [M+23].

(±)-**49**: Yield = 79%.  $^1\text{H}$  NMR (400 MHz,  $\text{CDCl}_3$ )  $\delta$ (ppm): 7.53 (bs, 1H), 7.45 (s, 1H), 7.17 (d,  $J = 8.4$  Hz, 2H), 6.72 (d,  $J = 8.4$  Hz, 2H), 5.59 (m, 1H), 4.95 (bs, 1H), 4.47-4.45 (m, 4H), 3.82 (t,  $J = 5.2$  Hz, 2H), 3.71 (s, 3H), 3.61-3.46 (m, 6H), 3.28-3.26 (m, 2H), 3.08 (m, 1H), 2.72

(m, 1H), 2.27 (s, 3H), 1.93-1.76 (m, 2H), 1.63-1.54 (m, 2H), 1.42 (s, 9H), 1.27-1.22 (m, 2H);  $^{13}\text{C}$  NMR (100 MHz,  $\text{CDCl}_3$ )  $\delta$ (ppm): 169.0, 167.0, 162.5, 162.2, 159.0, 155.9, 147.1, 145.2, 129.3, 129.1, 122.2, 115.2, 107.4, 70.5, 70.2, 70.0, 69.5, 61.2, 52.4, 50.1, 42.7, 40.6, 36.4, 32.3, 29.6, 28.4, 24.6, 11.3; LC-MS: rt= 6.4 min, m/z: 674 [M+1], 696 [M+23].

**General procedure for the Huisgen reaction between acid 33 and azides: 52 and 54.**

In one-necked round bottom flask, in a mixture of  $t\text{BuOH:H}_2\text{O}=6:4$  (0.016 M) compound 33,  $\text{Cu}(\text{OAc})_2$  (20 mmol%), Na-ascorbate (40 mmol%) and azide (1.0 eq) were added and the mixture was stirred at room temperature following the reaction by TLC. The mixture was filtered through celite and evaporated. The product was purified by flash chromatography (C18 reverse phase silica gel, 8/2 water/ $\text{CH}_3\text{CN}$ ).

( $\pm$ )-52: Yield = 20%.  $^1\text{H}$  NMR (400 MHz, Methanol- $d_4$ )  $\delta$ (ppm): 7.43 (s, 1H), 7.24 (bs, 1H), 7.04 (d, J = 8.0 Hz, 2H), 6.64 (d, J = 8.0 Hz, 2H), 5.46 (m, 1H), 4.85 (m, 2H), 4.35-4.31 (m, 3H), 4.18 (d, J = 15.0 Hz, 1H), 4.08 (q, J = 7.6 Hz, 2H), 3.19-3.14 (m, 2H), 2.72-2.64 (m, 2H), 2.32-2.30 (m, 2H), 2.20-2.15 (m, 2H), 2.13 (s, 3H), 2.01-1.98 (m, 2H), 1.87-1.78 (m, 2H), 1.71-1.52 (m, 2H), 1.28 (t, J = 7.6 Hz, 3H);  $^{13}\text{C}$  NMR (400 MHz, Methanol- $d_4$ )  $\delta$ (ppm): 173.5, 172.9, 171.8, 169.4, 164.2, 147.2, 146.6, 133.9, 128.3, 122.2, 115.4, 106.1, 61.4, 60.2, 49.2, 43.9, 36.4, 33.5, 30.5, 28.2, 24.5, 24.2, 22.0, 14.1, 10.2; LC-MS (acid eluents): rt= 9.0 min, m/z: 557 [M+1], 579 [M+23].

( $\pm$ )-54: Yield = 40%.  $^1\text{H}$  NMR (400 MHz, Methanol- $d_4$ )  $\delta$ (ppm): 7.82 (bs, 1H), 7.27 (s, 1H), 7.07 (d, J = 8.4 Hz, 2H), 6.62 (d, J = 8.4 Hz, 2H), 5.48 (m, 1H), 4.86 (m, 2H), 4.56-4.47 (m, 3H), 4.40 (m, 1H), 4.18 (q, J = 7.2 Hz, 2H), 4.11-4.05 (m, 2H), 3.88-3.85 (m, 2H), 3.75-3.56 (m, 4H), 2.70 (m, 1H), 2.34 (m, 1H), 2.20 (s, 3H), 1.87-1.53 (m, 4H), 1.26 (t, J = 7.2 Hz, 2H);  $^{13}\text{C}$  NMR (400 MHz, Methanol- $d_4$ )  $\delta$ (ppm): 175.5, 172.6, 170.5, 170.0, 168.5, 147.1, 146.4, 128.6, 128.1, 122.4, 115.3, 107.2, 71.8, 70.8, 70.3, 68.6, 61.6, 60.5, 49.8, 42.3, 39.7, 33.2, 29.3, 24.8, 11.3, 14.0. LC-MS: rt= 1.6 min, m/z: 603 [M+1].

**Synthesis of FITC-conjugated ligand 55.** In one-necked round bottom flask, trifluoroacetic acid (15.0 eq) was added to a solution of 41b in DCM (0.2 M) and the mixture stirred for 2h. The solution was evaporated to obtain the desired intermediate as an orange oil. It was dissolved in DCM (0.07 M) and TEA (4.0 eq) was added dropwise. After 10 min, FITC (1.0 eq) was added and the mixture stirred overnight at room temperature. The solvent was removed under vacuum and the crude used without further purifications. It was dissolved in a 2/1 mixture of THF/ $\text{H}_2\text{O}$  (0.01 M) and  $\text{LiOH}\cdot\text{H}_2\text{O}$  (1.0 eq) was added to a solution of ester. The reaction was stopped after disappearance of the starting material, following the evolution by HPLC-MS. The solution was neutralized adding dropwise HCl 1M solution and then water was evaporated. The crude was purified by preparative HPLC, affording 10 mg of the desired product. LC-MS: rt= 27.4 min, m/z: 875 [M+1], 897 [M+23].

## Pharmacology

**Cell Culture.** SK-MEL-24 (American Tissue Culture Collection, ATCC, Rockville, MD) were routinely grown in minimum essential medium (MEM, Cambrex, Walkersville, MD) supplemented with 10% fetal bovine serum (FBS), nonessential amino acids, and sodium pyruvate. K-562 (ATCC, Rockville, MD) were maintained as a stationary suspension culture in RPMI-1640 and L-glutamine with 10% FBS (Invitrogen (Carlsbad, CA). Cells were kept at 37°C in a 5% CO<sub>2</sub> humidified atmosphere. Forty hours before experiments, K-562 were treated with 25 ng/mL PMA (Sigma-Aldrich SRL, Milan, Italy) to induce differentiation and to increase expression of cell surface antigens.<sup>237</sup>

**Cell Adhesion Assays.** Plates (96 wells) (Corning Costar, Celbio, Milan, Italy) were coated by passive adsorption with fibronectin (10 µg/mL) or poly-L-lysine (0.002%) (Sigma-Aldrich SRL) overnight at 4°C. Cells were counted with a haemocytometer and pre-incubated with different concentrations of each compound or with the vehicle (methanol) for 30 min at room temperature to reach a ligand-receptor equilibrium. Stock solutions (10<sup>-2</sup> M) of the assayed compounds were prepared in phosphate-buffered saline (PBS). At the end of the incubation time, the cells were plated (50000 cells/well) and incubated at room temperature for 1 h. Then, all the wells were washed with PBS to remove nonadherent cells, and 50 µL of hexosaminidase [4-nitrophenyl *N*-acetyl-β-D-glucosaminide dissolved at a concentration of 7.5 mM in 0.09M citrate buffer solution (pH = 5) and mixed with an equal volume of 0.5% Triton X-100 in water] was added. This product is a chromogenic substrate for β-*N*-acetylglucosaminidase that is transformed in 4-nitrophenol whose absorbance can be measured at 405 nm. As previously described,<sup>238</sup> there is a linear correlation between absorbance and enzymatic activity. Therefore, it is possible to identify the number of adherent cells among treated wells, interpolating the absorbance values of unknowns in a calibration curve. The reaction was blocked by addition of 100 µL of a stopping solution [50 µM glycine and 5 µM EDTA (pH = 10.4)], and the plates were read in an EnSpire Multimode Plate Reader (PerkinElmer, Waltham, MA, USA). Experiments were carried out in quadruplicate and repeated at least three times. Data analysis and IC<sub>50</sub>/EC<sub>50</sub> values were calculated using Graph-Pad Prism 5.0 (GraphPad Software, San Diego, CA).

**Western blotting analysis.** K562 cells were incubated in RPMI-1640 with 1% FBS for 16 h. Plates were coated with 10 µg/mL of fibronectin and blocked with 1% BSA (Sigma-Aldrich SRL). Subsequently, 4x10<sup>6</sup> cells were pre-incubated with different concentrations of compounds for 30 minutes. Cells were allowed to adhere for 1 hour on fibronectin in RPMI-1640 with 1% FBS. Cells treated with agonists were not incubated with fibronectin. Then, the cells were lysed in M-PER Mammalian Protein Extraction Reagent; (M-PER Pierce, Rockford, IL, USA) supplemented with phosphatase inhibitor (Sigma-Aldrich SRL) for 10 min at 4°C by gently shaking. Cell debris were removed by centrifugation (14,000xg for 15 minutes at 4°C) and protein concentrations were estimated by BCA assay (Pierce, Rockford, IL, USA).

Protein extracts (100  $\mu\text{g}$ ) were denatured at 95°C for 3 min before being loaded and separated in 12% SDS-PAGE gels. The membranes were blocked in 1% BSA and incubated for 2 hours with anti-phospho-ERK 1/2 (extracellular signal-regulated kinase 1/2) (1:2500) or anti-total ERK 1/2 antibodies (1:5000) (Promega, Madison, WI, USA) and, thereafter with anti-rabbit peroxidase-conjugated secondary antibody. Digital images were acquired and analyzed following previously reported methods.<sup>239</sup>

*Confocal laser scanning microscopy.* HEK293 cells (not expressing  $\alpha_5$  but endogenously expressing  $\beta_1$  integrin<sup>222,223</sup>) were plated in 6 well plates and at 50-60% confluence were transiently transfected with  $\alpha_5$ -EGFP plasmid using Lipofectamine2000 transfection reagent (LifeTechnologies). After 48 h from transfection, HEK293+ $\alpha_5$ -EGFP cells were assessed to verify integrins expression by flow cytometry (data not shown).  $\alpha_5$ -EGFP integrin plasmid was a kind gift from Michael Davidson (Addgene plasmid #56423). HEK293+ $\alpha_5$ -EGFP cells were treated at 4°C with fibronectin (10  $\mu\text{g}/\text{ml}$ ) or the agonist 24 (1  $\mu\text{M}$ ) in MEM for 1 hour. Cells exposed to the antagonist **42b** (1  $\mu\text{M}$ ), before the addition of fibronectin, were pre-incubated with the compound for 20 minutes at 4°C. After 1 h incubation with fibronectin or compound 24, cells were moved to 37°C for 15 minutes. Then, the cells were washed twice with PBS and fixed with paraformaldehyde (3% in PBS, pH = 7.4, 10 min). Thereafter, the cover slips were washed twice with 0.1 M glycine in PBS and twice with 1% BSA (bovine serum albumin) in PBS. In another set of experiments, to study the localization of FITC-conjugated integrin ligand **55**, K562 cancer cells or HEK293 cells transfected or not with  $\alpha_5$  subunit coding plasmid (pCB7 alpha5) or with  $\alpha_V$ <sup>240</sup> and  $\beta_3$  subunit coding plasmids were treated with compound **55** (0.1-1  $\mu\text{M}$ ) for 60 minutes, moved to 37°C for 15 minutes and then fixed as previously described. Monensin (2  $\mu\text{M}$ , 2h) was employed as an inhibitor of integrin trafficking, and was added 1 h before compound **55** addition to K562 cells. As K562 were grown in suspension and they could not be grown attached to glass coverslip, for confocal microscopy experiments cells were treated and fixed as described above and then centrifuged using cytospin technique (1200 rpm 5 min; 1ml/sample of 0.5 mil cells/mL solution). Nuclei were counterstained with 4',6-diamidino-2-phenylindole dilactate (DAPI, Sigma). pCB7  $\alpha_5$  was a gift from Filippo Giancotti (Addgene plasmid #16041<sup>241</sup>).  $\alpha_V$  integrin plasmid was a kind gift from Michael Davidson (Addgene plasmid no.57345), while  $\beta_3$  subunit coding plasmid was a kind gift of Prof. S.J.Shattil. Specimens were embedded in Mowiol and analyzed using a Nikon C1s confocal laser-scanning microscope, equipped with a Nikon PlanApo 60X, 1.4-NA oil immersion lens. The images have elaborated using NIS-Elements C Software. For internalization analysis of ligand **55**, the mean fluorescence intensity was related to the background; the relative fluorescence intensity is reported in the graph in (Figure 2.27).

### Computational studies

All calculations were performed using the Schrödinger Suite through the Maestro graphical interface [Maestro, version 10.5, Schrödinger, LLC, New York, NY, 2016].

*Ligand preparation.* Ionized carboxylate and neutral aniline are suggested by the Epik module [Epik version 3.5, Schrödinger, LLC, New York, NY, 2016] as the relevant protonation states at pH = 7 for the acid and basic pharmacophoric groups of isoxazoline derivatives according to predicted pKa values of 3.3 (carboxylic acid) and 4.6 (phenyl anilinium derivative). These protonation states were considered for computational studies of the isoxazoline-containing compounds. Ionized carboxylate and protonated guanidinium groups have been employed for the cyclic RGD integrin ligands.

*Protein Preparation.* The crystal structure of the extracellular domain of the integrin  $\alpha_5\beta_1$  in complex with the disulfide-bonded cyclic peptide ACRGDGWC (PDB code 4WK4) and the crystal structure of the extracellular domain of the integrin  $\alpha_V\beta_3$  in complex with the cyclic pentapeptide RGDf(NMe)V Cilengitide (PDB code 1L5G) were used for docking studies. The  $\alpha_5\beta_1$  integrin structure was set up for docking as previously reported (residues 40-351 for chain  $\alpha_5$  and 121-358 for chain  $\beta_1$ ,  $Mg^{2+}$  ion at MIDAS)<sup>242</sup> The  $\alpha_V\beta_3$  integrin structure was truncated to residue sequences 1-438 for chain  $\alpha_V$  and 107-354 for chain  $\beta_3$ , and all the bivalent cations were modeled as  $Mn^{2+}$  ions. Then, the Protein Preparation Wizard using the OPLS2005 force field was run to get the final structures.

*Molecular docking.* Docking calculations were performed using Glide version 7.0 [Glide version 7.0, Schrödinger, LLC, New York, NY, 2016] in the SP (Standard Precision) mode. Receptor grids were generated on the extracellular fragments of  $\alpha_5\beta_1$  and  $\alpha_V\beta_3$  integrin prepared as described in Protein Preparation. The settings of the docking step were defined as previously reported.<sup>208,239</sup> The GlideScore function was used to select 20 poses for each ligand after a post-minimization of the ligand structure within the binding site. The flexible-ligand docking method was selected and the SP mode was used with the option for amide bonds set to 'Penalize non planar conformation'. No Epik state penalty was added to the docking score. Each docking protocol was initially tested for its ability to reproduce the X-ray binding mode of the cyclic RGD ligand in the receptor crystal structure. Glide was successful in reproducing the experimentally determined binding mode of the cyclic peptide ACRGDGWC in  $\alpha_5\beta_1$  integrin and of Cilengitide in  $\alpha_V\beta_3$  integrin, as they correspond to the best-scored poses in the two docking runs.

*Molecular Dynamics simulations.* Short MD simulations were run for selected derivatives to investigate the reliability of docking poses while allowing partial receptor flexibility. MD simulations were performed starting from the docking best poses and using MacroModel version 11.1 [MacroModel version 11.1, Schrödinger, LLC, New York, NY, 2016]. The following protocol was employed: OPLS2005 force field, implicit GB/SA water model, temperature 300 K, 1.0 fs integration step, 10 ps equilibration time and 10 ns simulation time. Variable degrees of freedom were assigned to the different moieties of the ligand-

receptor complex, constraining the position of the atoms that are farthest from the receptor binding site and removing the interactions which are likely to have a negligible influence on the results. The ligand-integrin complex employed in the docking calculations is divided into four substructures according to the following scheme: the ligand is allowed to freely move, residues within 10 from the ligand are constrained at the crystal positions with a force constant  $K=100 \text{ kJ mol}^{-1} \text{ }^{-2}$ , residues within 5 from the second shell are constrained at the crystal positions with a force constant  $K=200 \text{ kJ mol}^{-1} \text{ }^{-2}$ , residues within 10 from the third shell are frozen in their respective crystal positions. The remaining residues are not considered in the calculation. Each structure has undergone a TNCG minimization step and, after the equilibration at 300 K, 2.000 structures from each simulation were saved for the analysis.

**General procedure for the synthesis of nitrones 56Aa, 56Ab, 56Ac, 56Ad, 56Ae, 56Af, 56Ag and 56Bb.** According to the literature,<sup>230</sup> to a solution of an equimolar amount of the suitable *N*-protected hydroxylamine (1.0 eq) and the corresponding aldehyde in DCM (0.33 M), pyrrolidine (1.2 eq) was added. The mixture was stirred at room temperature during the time indicated in each case. Then, the reaction was filtered through a short pad of either silica gel or basic  $\text{Al}_2\text{O}_3$  using a glass frit with  $\text{EtOAc}$ <sup>243</sup> to obtain the final nitrones without any further purification. It is worth noting that pyrrolidinium chloride stays trapped in either silica gel or in basic  $\text{Al}_2\text{O}_3$  during filtration. Silica gel was used for filtration of aromatic nitrones and basic  $\text{Al}_2\text{O}_3$  was used for the aliphatic and  $\alpha,\beta$ -unsaturated ones.

**56Aa:** Reaction time: 3 min. Yield >99%.  $^1\text{H NMR}$  (400 MHz,  $\text{CDCl}_3$ )  $\delta$ (ppm): 6.64 (d,  $J = 6.8 \text{ Hz}$ , 1H), 3.23-3.15 (m, 1H), 1.50 (s, 9H), 1.11 (d,  $J = 7.6$ , 6H).

**56Ab:** Reaction time: 15 min. Yield >99%.  $^1\text{H NMR}$  (400 MHz,  $\text{CDCl}_3$ )  $\delta$ (ppm): 8.31-8.29 (m,  $J = 7.6$ , 2H), 7.55 (s, 1H), 7.45-7.39 (m, 3H), 1.63 (s, 9H);  $^{13}\text{C NMR}$  (100 MHz,  $\text{CDCl}_3$ )  $\delta$ (ppm): 130.7, 129.6, 129.4, 128.4, 128.0, 70.4, 27.9. LC-MS-ESI: rt 11.1 min,  $m/z$  178 [M+1], 355 [2M+1].

**56Ac:** Reaction time: 20 min. Yield = 98%.  $^1\text{H NMR}$  (400 MHz,  $\text{CDCl}_3$ )  $\delta$ (ppm): 8.25 (d,  $J = 8.6 \text{ Hz}$ , 2H), 7.53 (s, 1H), 7.38 (d,  $J = 8.6 \text{ Hz}$ , 2H), 1.61 (s, 9H). LC-MS-ESI: rt 13.4 min,  $m/z$  212 [M+1], 423 [2M+1].

**56Ad:** Reaction time: 25 min. Yield >99%.  $^1\text{H NMR}$  (400 MHz,  $\text{CDCl}_3$ )  $\delta$ (ppm): 8.16 (d,  $J = 8.0 \text{ Hz}$ , 2H), 7.58-7.53 (m, 3H), 1.61 (s, 9H). LC-MS-ESI: rt 14.2 min,  $m/z$  257 [M+1], 513 [M+1].

**56Ae:** Reaction time: 25 min. Yield >99%.  $^1\text{H NMR}$  (400 MHz,  $\text{CDCl}_3$ )  $\delta$ (ppm): 8.04 (d,  $J = 8.4 \text{ Hz}$ , 2H), 7.76 (d,  $J = 8.4 \text{ Hz}$ , 2H), 7.50 (s, 1H), 1.62 (s, 9H);  $^{13}\text{C NMR}$  (100 MHz,  $\text{CDCl}_3$ )  $\delta$ (ppm): 137.2, 130.2, 129.8, 128.6, 95.5, 70.9, 28.0. LC-MS-ESI: rt 14.6 min,  $m/z$  304 [M+1], 607 [2M+1], 629 [2M+23].

**56Af:** Reaction time: 35 min. Yield >99%.  $^1\text{H NMR}$  (400 MHz,  $\text{CDCl}_3$ )  $\delta$ (ppm): 8.45 (d,  $J = 9.0$  Hz, 2H), 8.25 (d,  $J = 9.1$  Hz, 2H), 7.71 (s, 1H), 1.64 (s, 9H). LC-MS-ESI: rt 13.1 min,  $m/z$  223 [M+1].

**56Ag:** Reaction time: 30 min. Yield = 96%.  $^1\text{H NMR}$  (400 MHz,  $\text{CDCl}_3$ )  $\delta$ (ppm): 8.35 (d,  $J = 8.0$  Hz, 2H), 7.67 (d,  $J = 8.0$  Hz, 2H), 7.61 (s, 1H), 1.61 (s, 9H). LC-MS-ESI: rt 11.9 min,  $m/z$  203 [M+1].

**56Bb:** Reaction time: 10 min. Yield = 96%.  $^1\text{H NMR}$  (400 MHz,  $\text{CDCl}_3$ )  $\delta$ (ppm): 8.21-8.17 (m, 2H), 7.48-7.45 (m, 2H), 7.41-7.37 (m, 7H), 5.05 (s, 2H).

**General procedure for the synthesis of nitrones 56Cb, 56Db.** Benzaldoxime and acrylate (2.0 eq) were placed in a round bottom flask and dissolved in toluene (0.5 M). Zinc iodide (10 or 30 mol%) and boron trifluoride diethyl etherate (10 or 30 mol%) were added. The flask was closed with a plug and the reaction mixture was heated overnight. The solvent was evaporated, the crude product dissolved in DCM and filtered through a short celite pad. The crude was purified by column chromatography over silica gel (ethyl acetate/petrol ether 1:1).

**56Cb:** Yield = 72%.  $^1\text{H NMR}$  (400 MHz,  $\text{CDCl}_3$ )  $\delta$ (ppm): 8.12-8.10 (m, 2H), 7.54 (s, 1H), 7.29-7.22 (m, 3H), 4.16 (t,  $J = 6.0$  Hz, 2H), 3.52 (s, 3H), 2.91 (t,  $J = 6.0$  Hz, 2H);  $^{13}\text{C NMR}$  (100 MHz,  $\text{CDCl}_3$ )  $\delta$ (ppm): 171.2, 138.7, 131.2, 129.5, 129.2, 128.3, 61.2, 51.8, 31.1. LC-MS-ESI: rt 9.3 min,  $m/z$  208 [M+1], 230 [M+23], 437 [2M+23].

**56Db:** Yield = 20%.  $^1\text{H NMR}$  (400 MHz,  $\text{CDCl}_3$ )  $\delta$ (ppm): 8.26-8.21 (m, 2H), 7.50 (s, 1H), 7.44-7.40 (m, 3H), 4.19 (t,  $J = 6.4$  Hz, 2H), 2.97 (t,  $J = 16.0$  Hz, 2H), 1.43 (s, 9H);  $^{13}\text{C NMR}$  (100 MHz,  $\text{CDCl}_3$ )  $\delta$ (ppm): 170.0, 135.1, 130.33, 130.28, 128.5, 128.4, 81.3, 62.1, 32.9, 27.9. LC-MS-ESI: rt 12.8 min,  $m/z$  250 [M+1], 521 [2M+23].

**General Procedure for the synthesis of 2,3-dihydroisoxazoles 57.** According to the literature,<sup>229</sup> to a cooled (-10 °C) or RT solution of nitrone and catalyst **V** (10 mol%) in toluene (0.5 M), aldehyde (1.2 eq) was added. When the reaction was completed, the crude product was filtered through a short pad of silica with EtOAc and purified by flash chromatography.

**57Aa:** Yield = 58% (-10 °C). The ee was determined by HPLC using a Chiralpak IC column [hexane/*i*PrOH (90:10)]; flow rate 1.0 mL/min;  $\tau_{\text{minor}} = 9.6$  min,  $\tau_{\text{major}} = 11.3$  min (e.r. = 40:60).  $^1\text{H NMR}$  (400 MHz,  $\text{CDCl}_3$ )  $\delta$ (ppm): 9.70 (s, 1H), 7.67 (d,  $J = 7.2$  Hz, 1H), 7.60-7.56 (m, 2H), 7.52-7.49 (m, 2H), 4.43 (d,  $J = 3.2$ , 1H), 2.05-1.97 (m, 1H), 1.18 (s, 9H), 0.99 (d,  $J = 6.4$  Hz, 3H), 0.94 (d,  $J = 6.4$  Hz, 3H).

**57Ab:** Yield >99% (-10 °C) and Yield >99% (RT). The ee was determined by HPLC using a Chiralpak IC column [hexane/*i*PrOH (90:10)]; flow rate 1.0 mL/min;  $\tau_{\text{minor}} = 7.0$ , min,  $\tau_{\text{major}} = 8.8$  min (e.r. = 1:99 at -10°C and e.r. = 3:97 at RT).  $^1\text{H NMR}$  (400 MHz,  $\text{CDCl}_3$ )  $\delta$ (ppm): 9.69 (s, 1H), 7.71 (d,  $J = 6.8$  Hz, 2H), 7.61-7.48 (m, 5H), 7.34 (t,  $J = 7.6$  Hz, 2H), 7.26 (t,  $J = 6.8$  Hz, 1H), 5.60 (s, 1H), 1.25 (s, 9H);  $^{13}\text{C NMR}$  (100 MHz,  $\text{CDCl}_3$ )  $\delta$ (ppm): 185.0,

168.9, 142.6, 132.0, 129.1, 128.9, 128.4, 127.4, 127.3, 126.2, 117.7, 66.1, 61.8, 25.0.

**57Ac:** Yield = 80% (-10 °C) and Yield = 92% (RT). The ee was determined by HPLC using a Chiralpak IC column [hexane/iPrOH (90:10)]; flow rate 1.0 mL/min;  $\tau_{\text{minor}} = 5.7$ , min,  $\tau_{\text{major}} = 6.8$  min (e.r. = 3:97 at -10°C and e.r. = 4:96 at RT).  $^1\text{H}$  NMR (400 MHz,  $\text{CDCl}_3$ )  $\delta$ (ppm): 9.68 (s, 1H), 7.70 (d, J = 6.8 Hz, 2H), 7.63-7.48 (m, 3H), 7.49 (d, J = 8.5 Hz, 2H), 7.32 (d, J = 8.5 Hz, 2H), 5.59 (s, 1H), 1.25 (s, 9H);  $^{13}\text{C}$  NMR (100 MHz,  $\text{CDCl}_3$ )  $\delta$ (ppm): 184.9, 168.9, 141.2, 133.5, 132.2, 129.0, 129.0, 128.7, 128.5, 126.0, 117.4, 65.5, 61.8, 24.9.

**57Ad:** Yield = 82% (-10 °C) and Yield = 84% (RT). The ee was determined by HPLC using a Chiralpak IC column [hexane/iPrOH (90:10)]; flow rate 1.0 mL/min;  $\tau_{\text{minor}} = 7.2$ , min,  $\tau_{\text{major}} = 9.0$  min (e.r. = 3:97 at -10°C and e.r. = 7:93 at RT).  $^1\text{H}$  NMR (400 MHz,  $\text{CDCl}_3$ )  $\delta$ (ppm): 9.64 (s, 1H), 7.68-7.65 (m, 2H), 7.51-7.49 (m, 2H), 7.45-7.42 (m, 5H), 5.54 (s, 1H), 1.21 (s, 9H).

**57Ae:** Yield = 78% (-10 °C) and Yield = 81% (RT). The ee was determined by HPLC using a Chiralcel IC column (25cm), [hexane/iPrOH (90:10)]; flow rate 1.0 mL/min;  $\tau_{\text{minor}} = 6.4$  min,  $\tau_{\text{major}} = 8.0$  min, (e.r. = 3:97 at -10°C and e.r. = 5:95 at RT).  $^1\text{H}$  NMR (400 MHz,  $\text{CDCl}_3$ )  $\delta$ (ppm): 9.67 (s, 1H), 7.70-7.67 (m, 4H), 7.61-7.52 (m, 3H), 7.32-7.30 (m, 2H), 5.56 (s, 1H), 1.24 (s, 9H);  $^{13}\text{C}$  NMR (100 MHz,  $\text{CDCl}_3$ )  $\delta$ (ppm): 185.0, 169.0, 142.4, 137.5, 132.2, 129.4, 129.1, 125.9, 117.3, 93.1, 65.7, 61.9, 25.0.

**57Af:** Yield = 67% (-10 °C) and Yield = 74% (RT). The ee was determined by HPLC using a Chiralpak IC column [hexane/iPrOH (90:10)]; flow rate 1.0 mL/min;  $\tau_{\text{minor}} = 16.3$ , min,  $\tau_{\text{major}} = 19.3$  min (e.r. = 3:97 at -10°C and e.r. = 8:92 at RT).  $^1\text{H}$  NMR (400 MHz,  $\text{CDCl}_3$ )  $\delta$ (ppm): 9.63 (s, 1H), 7.68-7.63 (m, 5H), 7.52-7.49 (m, 2H), 7.29-7.26 (m, 2H), 5.52 (s, 1H), 1.21 (s, 9H);  $^{13}\text{C}$  NMR (100 MHz,  $\text{CDCl}_3$ )  $\delta$ (ppm): 185.0, 169.2, 149.7, 132.5, 129.13, 129.06, 128.3, 125.6, 123.7, 116.8, 65.6, 62.0, 24.9.

**57Ag:** Yield = 63% (-10 °C) and Yield = 70% (RT). The ee was determined by HPLC using a Chiralpak IC column [hexane/iPrOH (90:10)]; flow rate 1.0 mL/min;  $\tau_{\text{minor}} = 20.6$ , min,  $\tau_{\text{major}} = 26.4$  min (e.r. = 6:94 at -10°C and e.r. = 9:91 at RT).  $^1\text{H}$  NMR (400 MHz,  $\text{CDCl}_3$ )  $\delta$ (ppm): 9.77 (s, 1H), 7.83-7.69 (m, 7H), 7.64 (d, J = 7.7 Hz, 2 H) 5.76 (s, 1H), 1.35 (s, 9H);  $^{13}\text{C}$  NMR (100 MHz,  $\text{CDCl}_3$ )  $\delta$ (ppm): 184.9, 169.2, 147.8, 132.5, 132.3, 129.2, 129.1, 128.2, 125.7, 118.9, 116.9, 111.2, 65.8, 62.0, 25.0.

**57Bb:** Yield = 63% (-10 °C) and Yield = 70% (RT). The ee was determined by HPLC using a Chiralpak IC column [hexane/iPrOH (90:10)]; flow rate 1.0 mL/min;  $\tau_{\text{minor}} = 10.0$ , min,  $\tau_{\text{major}} = 12.1$  min (e.r. = 9:91 at -10°C and e.r. = 12:88 at RT).  $^1\text{H}$  NMR (400 MHz,  $\text{CDCl}_3$ )  $\delta$ (ppm): 9.61 (s, 1H), 7.77 (d, J = 6.9 Hz, 2H), 7.68-7.36 (m, 13H), 5.55 (s, 1H), 4.58 (d, J = 13.0 Hz, 1H), 4.30 (d, J = 13.0 Hz, 1H).

**57Cb:** Yield = 40% (-10 °C) and Yield = 48% (RT). The ee was determined by HPLC using a Chiralpak IC column [hexane/iPrOH (80:20)]; flow rate 1.0 mL/min;  $\tau_{\text{minor}} = 16.8$ , min,  $\tau_{\text{major}} = 19.3$  min (e.r. = 14:86 at -10°C and e.r. = 22:78 at RT).  $^1\text{H}$  NMR (400 MHz,  $\text{CDCl}_3$ )  $\delta$ (ppm): 9.79 (s, 1H), 7.70-7.68 (m, 2H), 7.62-7.58 (m, 1H), 7.54-7.45 (m, 4H), 7.38-7.34 (m,



2H), 7.31-7.28 (m, 1H), 5.34 (s, 1H), 3.69 (s, 3H), 3.62-3.55 (m, 1H), 3.36-3.29 (m, 1H), 2.86-2.82 (m, 2H);  $^{13}\text{C}$  NMR (100 MHz,  $\text{CDCl}_3$ )  $\delta$ (ppm): 185.5, 171.9, 168.0, 140.0, 132.3, 129.4, 129.0, 128.6, 127.9, 127.0, 126.0, 116.7, 73.0, 55.6, 51.8, 32.6.

**57Db:** Yield = 32% (-10 °C) and Yield = 37% (RT). The ee was determined by HPLC using a Chiralpak IC column [hexane/*i*PrOH (80:20)]; flow rate 1.0 mL/min;  $\tau_{\text{minor}} = 10.3$ , min,  $\tau_{\text{major}} = 11.7$  min (e.r. = 9:91 at -10°C and e.r. = 19:81 at RT).  $^1\text{H}$  NMR (400 MHz,  $\text{CDCl}_3$ )  $\delta$ (ppm): 9.80 (s, 1H), 7.71-7.68 (m, 2H), 7.62-7.42 (m, 5H), 7.38-7.29 (m, 3H), 5.28 (s, 1H), 3.50-3.44 (m, 2H), 3.25-3.20 (m, 2H), 1.40 (s, 9H).

**Synthesis of 58Ab.** To a cooled solution (0°C) of aldehyde in  $t\text{BuOH}$  (0.07 M), a solution of  $\text{NaH}_2\text{PO}_4$  (10.0 eq) and  $\text{NaClO}_2$  (10.0 eq) in  $\text{H}_2\text{O}$  (1.5 M) was added. Successively, 2-methyl-2-butene (30.0 eq) was added, the solution was warmed up to RT and stirred 24h. The mixture was quenched with  $\text{NH}_4\text{Cl}$  and extracted with  $\text{AcOEt}$ .

**58Ab:** Yield: 60%.  $^1\text{H}$  NMR (400 MHz,  $\text{CDCl}_3$ )  $\delta$ (ppm): 8.07-8.04 (m, 2H), 7.85-7.82 (m, 2H), 7.51-7.46 (m, 4H), 7.25-7.30 (m, 2H), 5.50 (s, 1H), 1.25 (s, 9H).

**Synthesis of 59Ab.** In two-necked round bottom flask, equipped to perform reaction under  $\text{N}_2$  atmosphere, TEA (1.5 eq) and HBTU (1.5 eq) were added to a solution of **58Ab** in DCM (0.15 M), and the mixture was stirred at room temperature for 5 min. 4-aminobenzylamine (2.0 eq) was then added and the mixture stirred for further 4h. The mixture was diluted with DCM and washed with water. The organic layer was dried over  $\text{Na}_2\text{SO}_4$ , filtered and concentrated under reduced pressure. The crude product was purified by flash chromatography.

**59Ab:** Yield: 67%.  $^1\text{H}$  NMR (400 MHz,  $\text{CDCl}_3$ )  $\delta$ (ppm): 7.66-7.62 (m, 4H), 7.57-7.54 (m, 2H), 7.41-7.32 (m, 4H), 7.02 (d,  $J = 8$  Hz, 2H), 6.64 (d,  $J = 8$  Hz, 2H), 5.54 (s, 1H), 5.27 (t,  $J = 5.6$  Hz), 4.41 (dd,  $^1J = 3.6$ ,  $^2J = 5.6$  Hz, 2H) 1.17 (s, 9H).

## Chiral HPLC spectra.

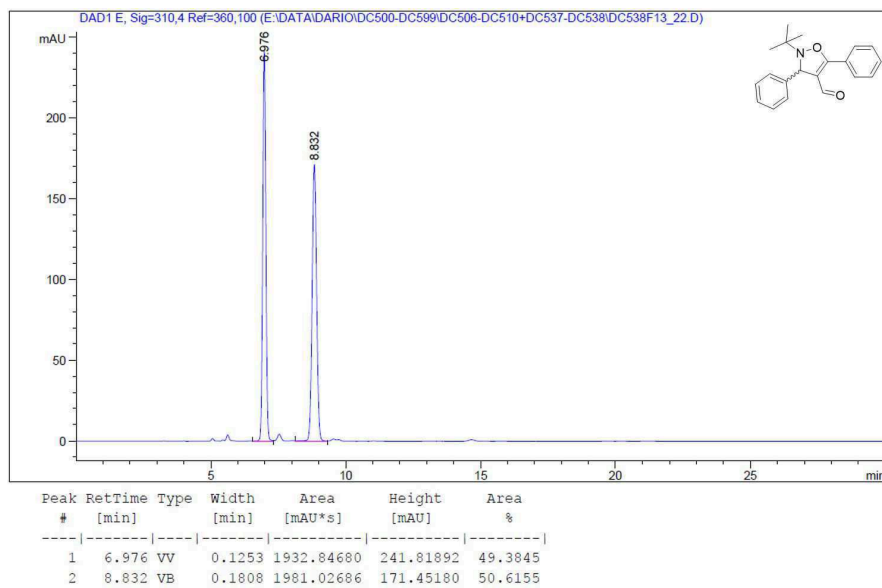


Figure 2.32: Chiral HPLC of the racemic mixture of compound 57Ab.

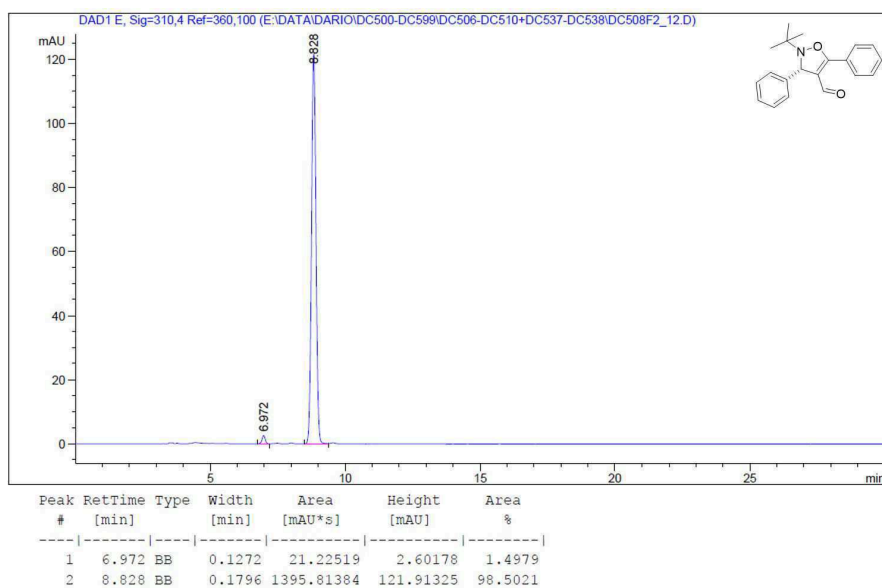


Figure 2.33: Chiral HPLC of compound 57Ab; conditions reported in entry 1 Table 2.7.

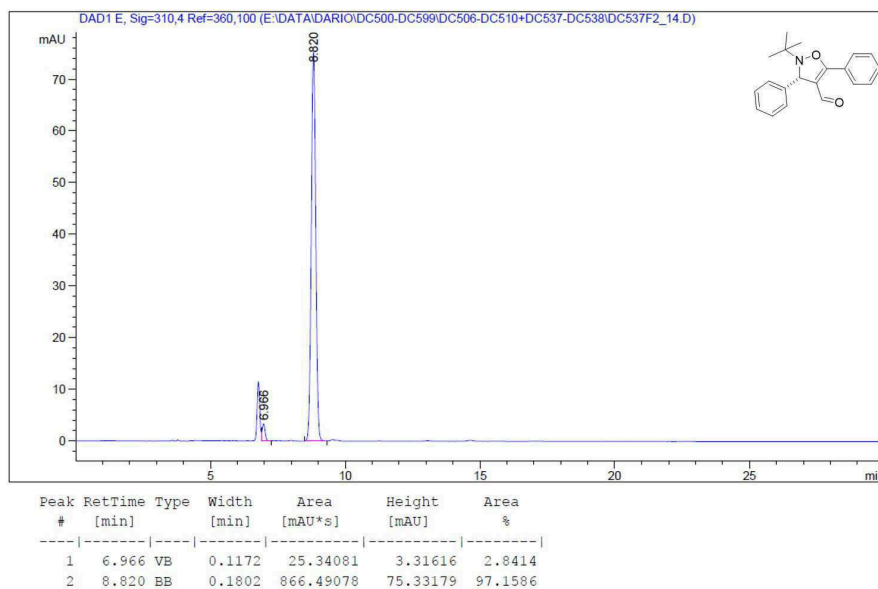


Figure 2.34: Chiral HPLC of compound 57Ab; conditions reported in entry 2 Table 2.7.

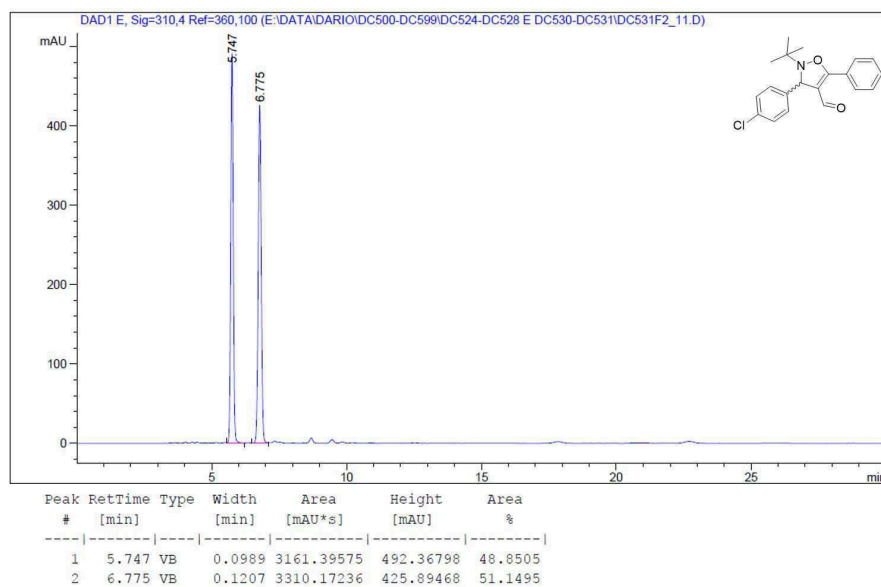


Figure 2.35: Chiral HPLC of the racemic mixture of compound 57Ac.

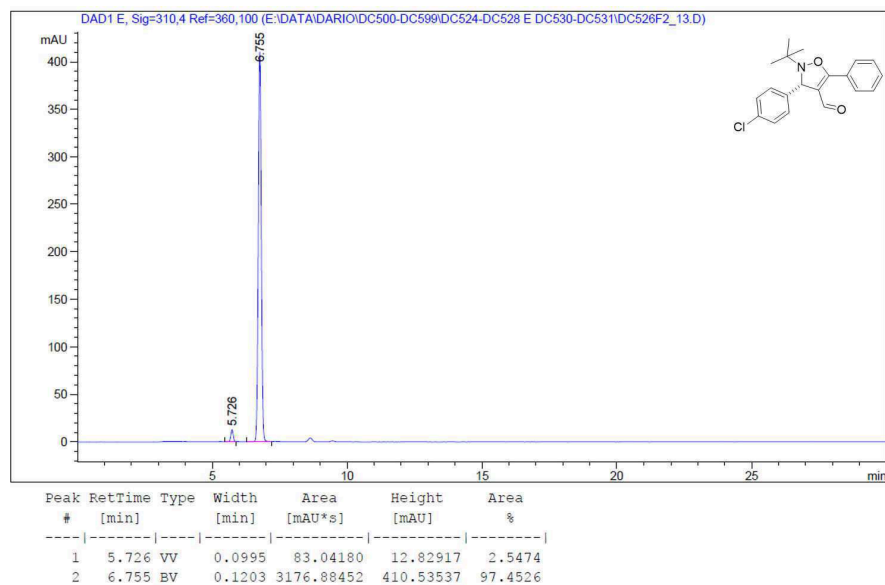


Figure 2.36: Chiral HPLC of compound 57Ac; conditions reported in entry 3 Table 2.7.

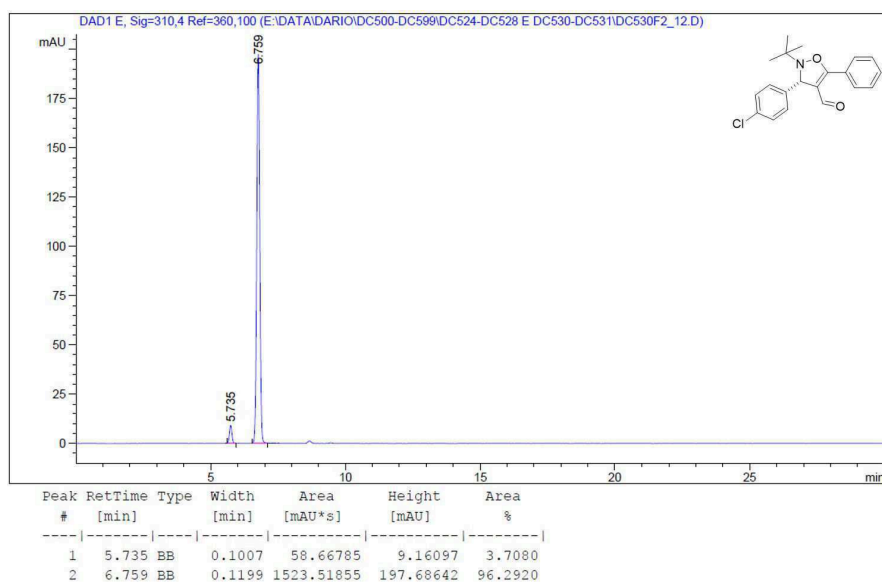


Figure 2.37: Chiral HPLC of compound 57Ac; conditions reported in entry 4 Table 2.7.

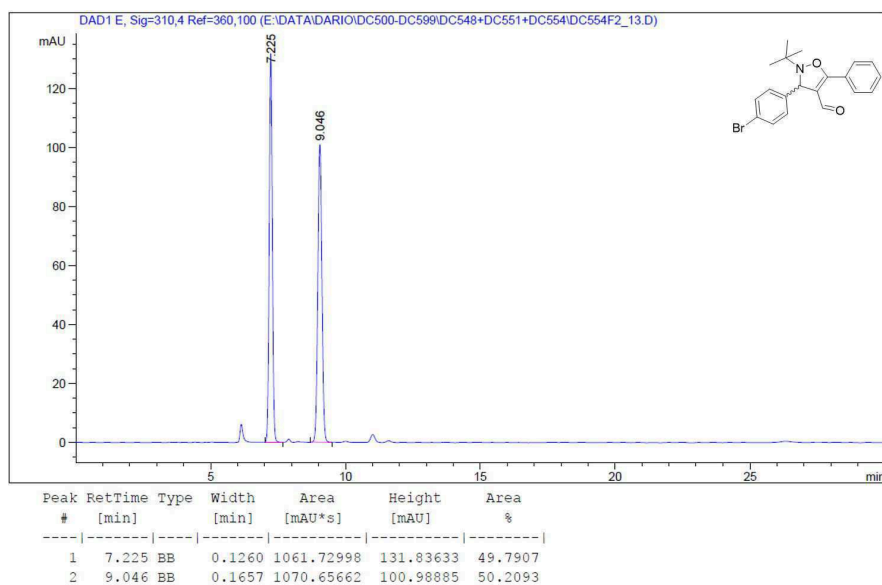


Figure 2.38: Chiral HPLC of the racemic mixture of compound 57Ad.

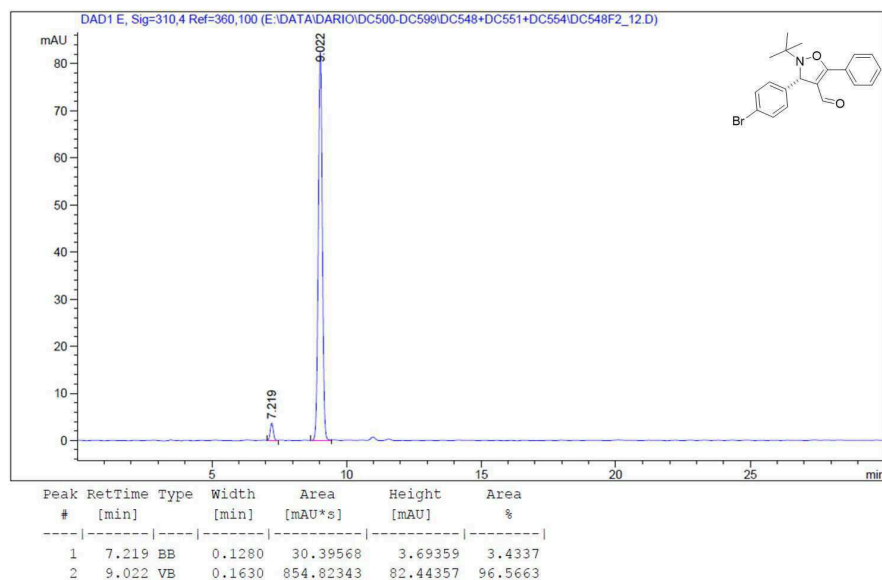


Figure 2.39: Chiral HPLC of compound 57Ad; conditions reported in entry 5 Table 2.7.

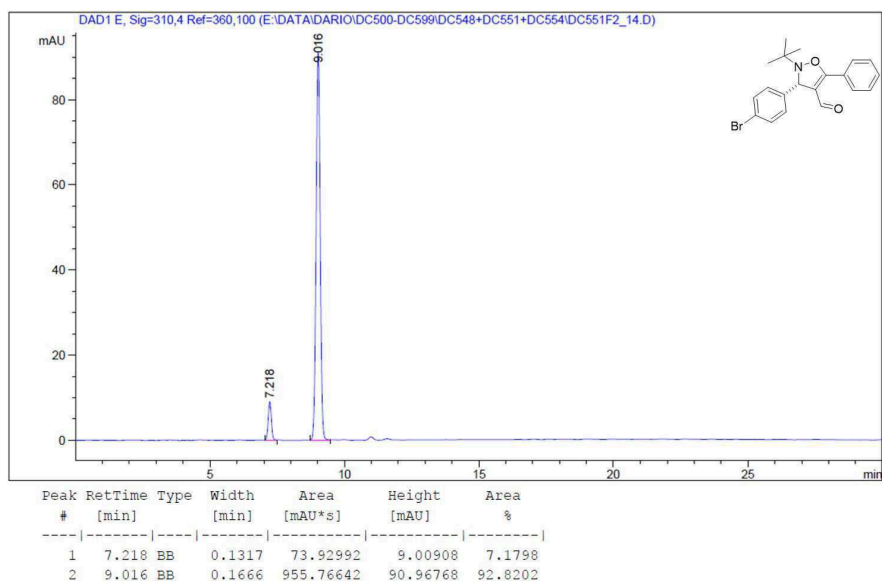


Figure 2.40: Chiral HPLC of compound 57Ad; conditions reported in entry 6 Table 2.7.

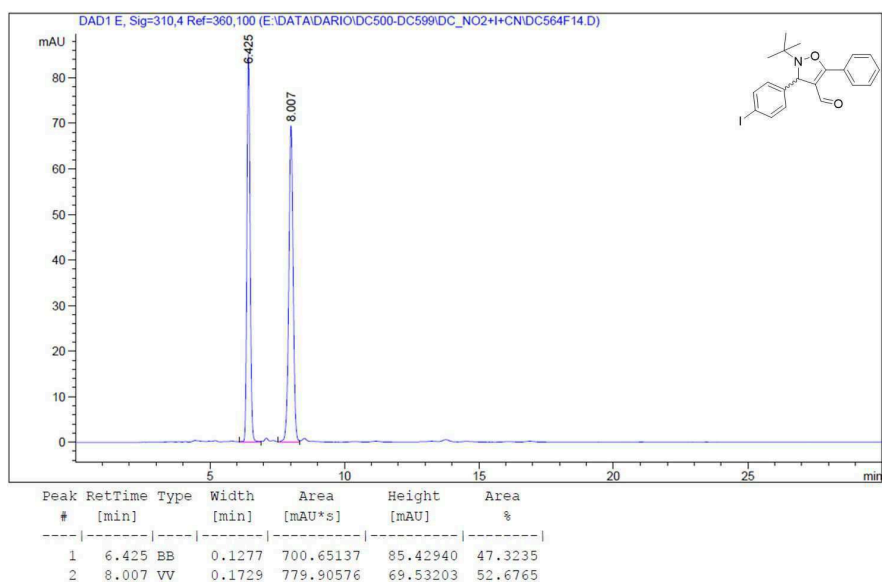


Figure 2.41: Chiral HPLC of the racemic mixture of compound 57Ae.

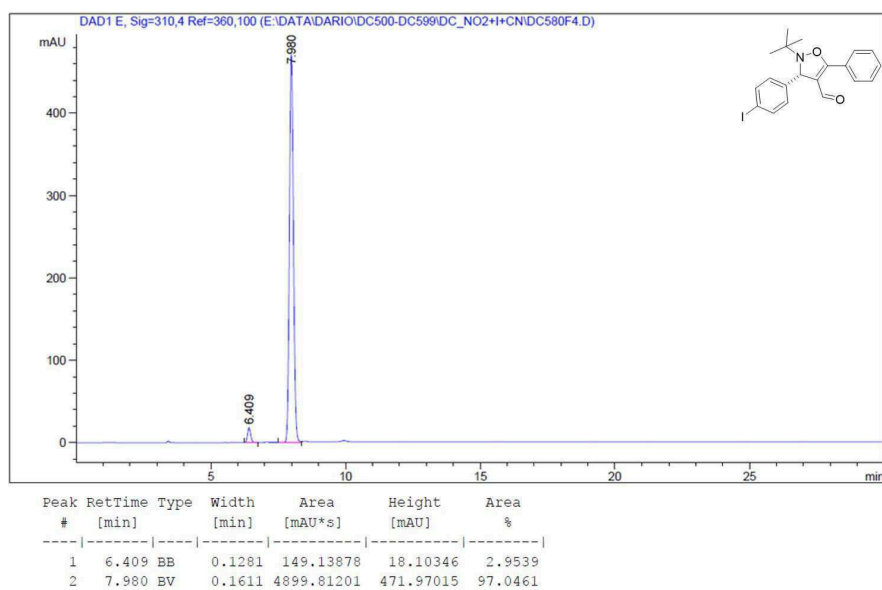


Figure 2.42: Chiral HPLC of compound 57Ae; conditions reported in entry 7 Table 2.7.

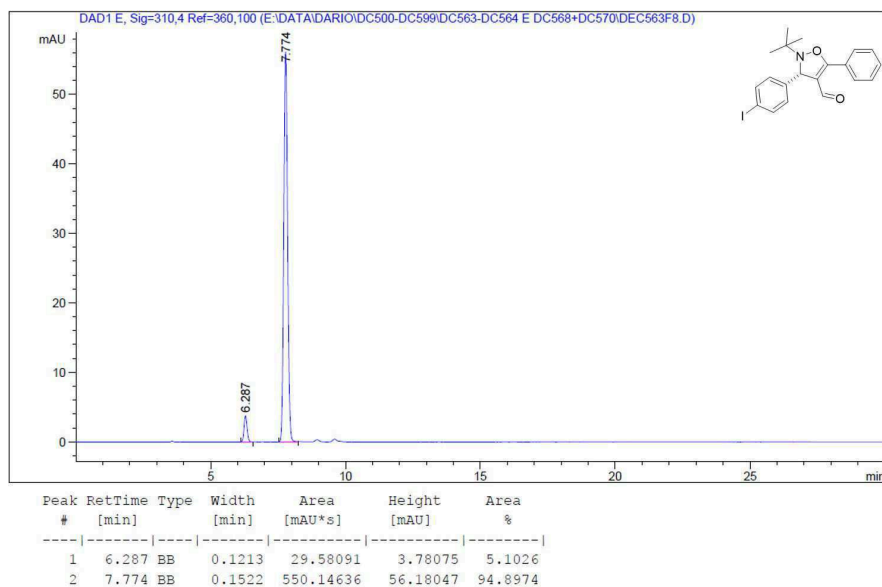


Figure 2.43: Chiral HPLC of compound 57Ae; conditions reported in entry 8 Table 2.7.

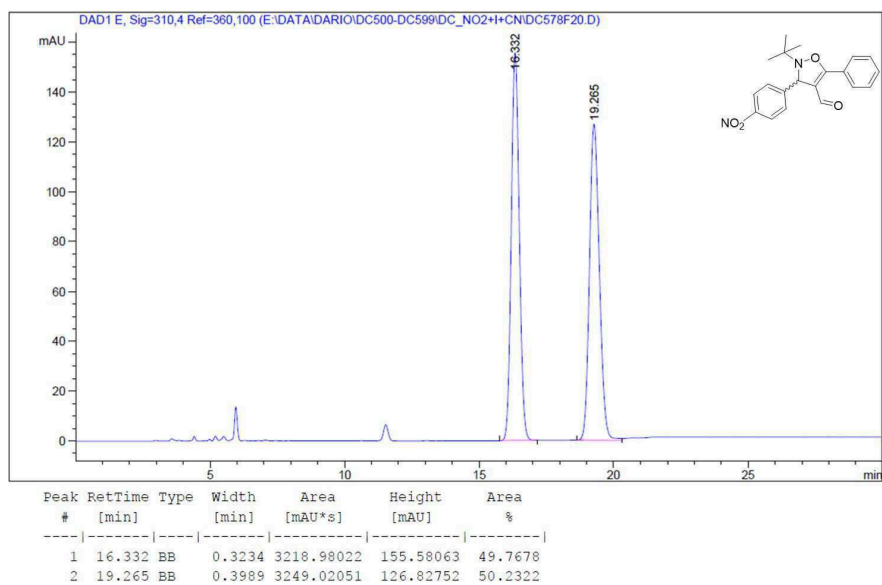


Figure 2.44: Chiral HPLC of the racemic mixture of compound 57Af.

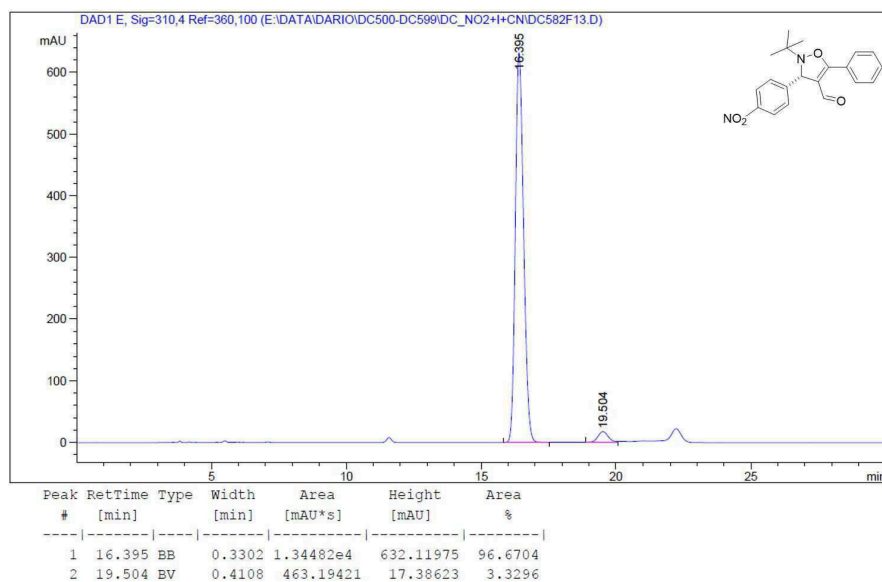


Figure 2.45: Chiral HPLC of compound 57Af; conditions reported in entry 9 Table 2.7.



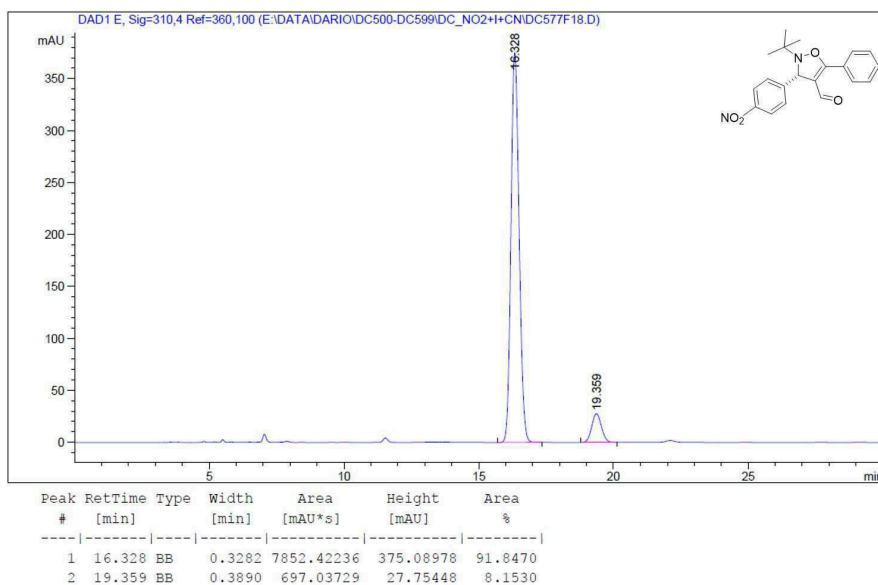


Figure 2.46: Chiral HPLC of compound 57Af; conditions reported in entry 10 Table 2.7.

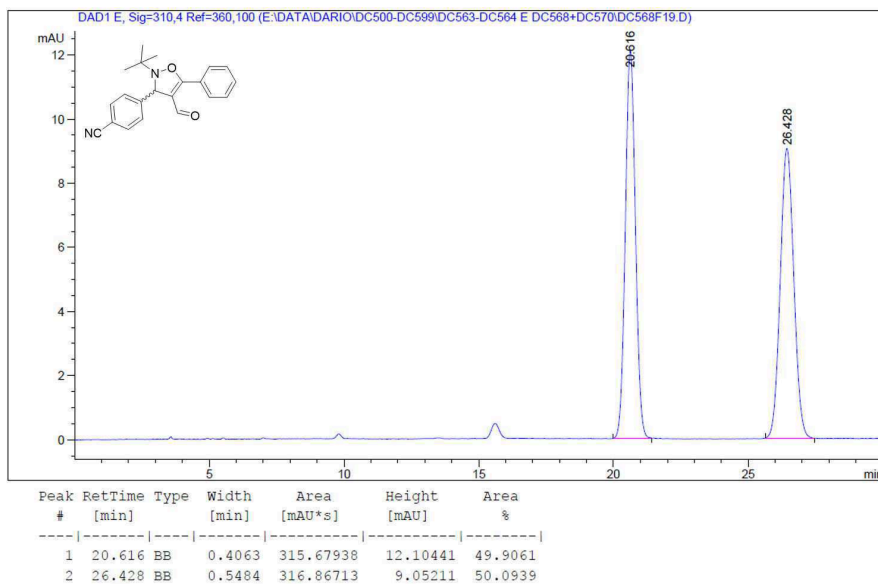


Figure 2.47: Chiral HPLC of the racemic mixture of compound 57Ag.

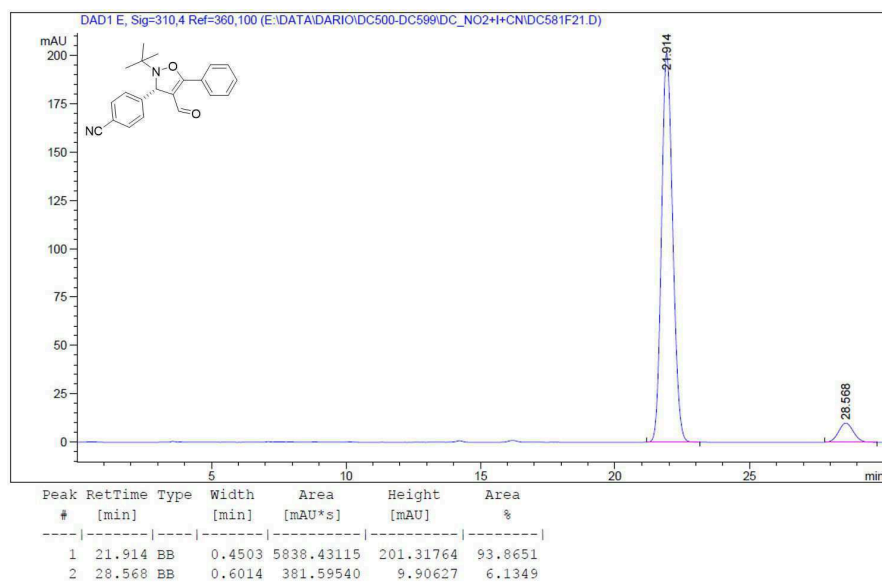


Figure 2.48: Chiral HPLC of compound 57Ag; conditions reported in entry 11 Table 2.7.

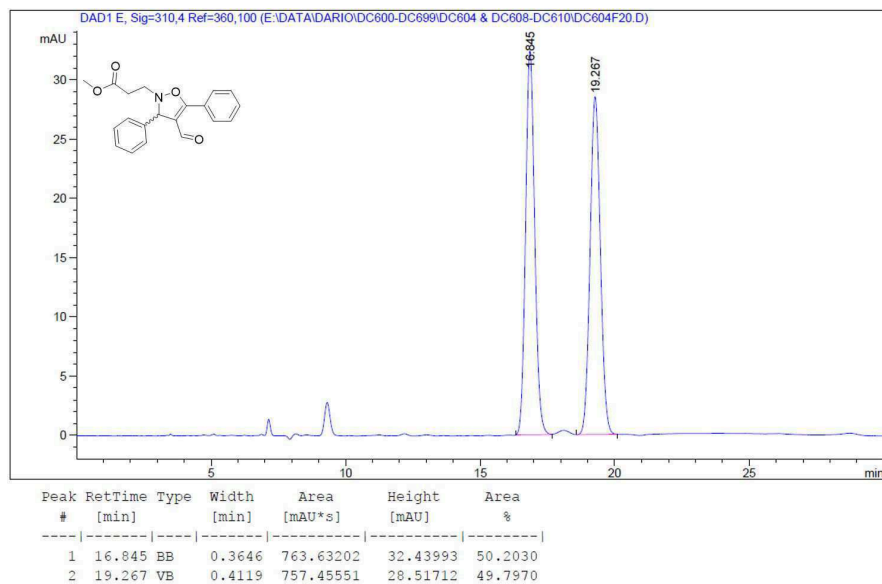


Figure 2.49: Chiral HPLC of the racemic mixture of compound 57Cb.

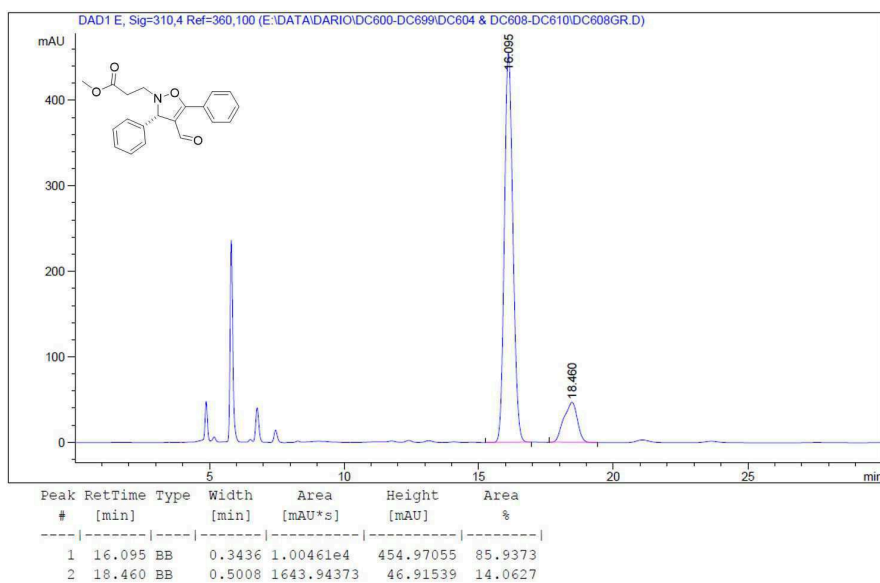


Figure 2.50: Chiral HPLC of compound 57Cb; conditions reported in entry 5 Table 2.6.

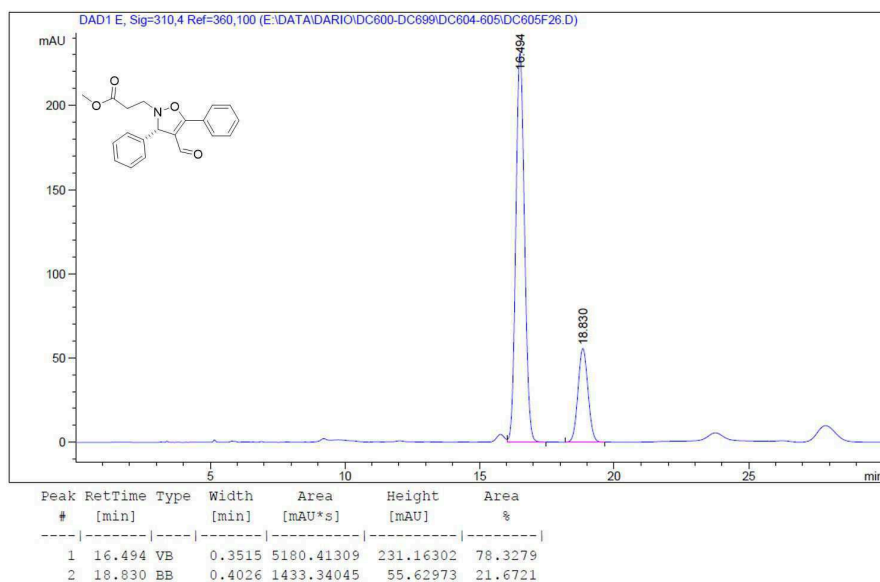


Figure 2.51: Chiral HPLC of compound 57Cb; conditions reported in entry 6 Table 2.6.

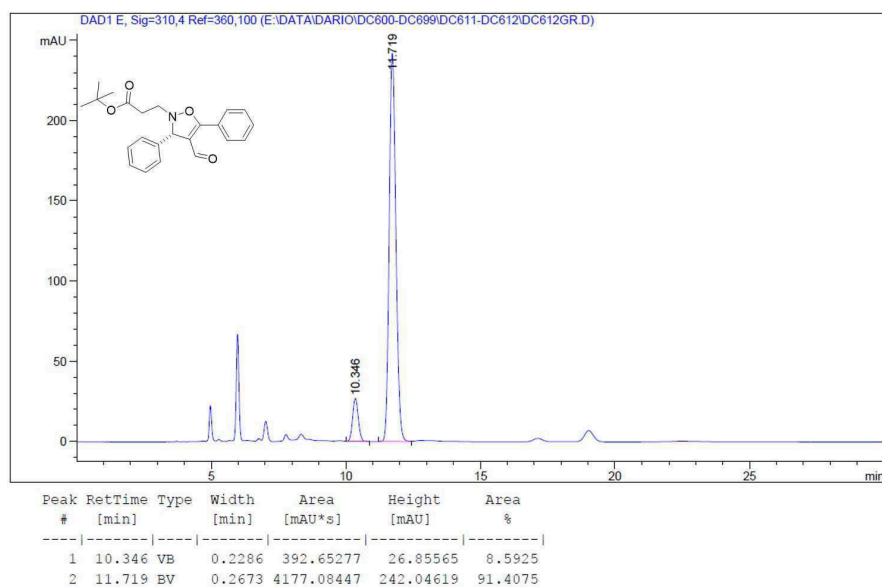


Figure 2.52: Chiral HPLC of compound 57Db; conditions reported in entry 7 Table 2.6.

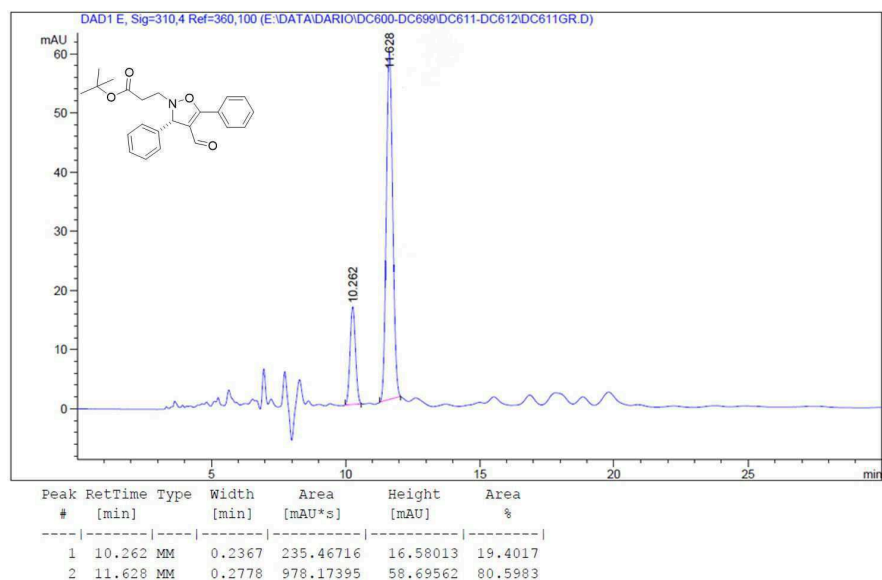


Figure 2.53: Chiral HPLC of compound 57Db; conditions reported in entry 8 Table 2.6.

## Chapter3

---

### Reporting Drug Delivery System (RDDS)

---

#### 3.1 Introduction

Nowadays, one of the most important challenges in the pharmacological approach of diseases is the *selectivity*. In tumour therapy, the treatments involve the administration of cytotoxic agents (e.g. chemical compounds capable of killing cells) that interfere with events in cancerogenic cells growth and proliferation. However, their benefic effects are often limited by their indiscriminate activity towards both unhealthy and healthy cells.<sup>244</sup> In fact, the systemic administration of cytotoxic agents often leads to severe side effects, limiting therapeutic benefits. Several approaches have been investigated to overcome the drawbacks of traditional chemotherapy, pointing to target the cytotoxic agent to cancer cells more selectively in order to minimise side effects.<sup>245</sup> For decades, the researchers have investigated the way to improve the pharmacological effects of cytotoxic agents with a concomitant decrease of systemic toxicity, mainly by means of the development of different tumor-targeted prodrugs able to enhance the drug accumulation mainly at the tumor site.<sup>246</sup> In order to achieve the delivery of the molecules, it is possible to employ a *passive targeting*,<sup>247</sup> in which the extravasation of nanocarriers into cancer tissues is easier as a consequence of the interstitial gaps between endothelial cells in blood microvasculature of tumour and cells of healthy tissues (~200-1200 nm). This enhanced permeation and retention (EPR) effect of endothelial blood microvasculature leads to a greater accumulation and a longer tumour exposure to the drug. Since this permeation is passive, it is not necessary to use a target ligand to selectively drive the drug.

On the other hand, the evidence that tumors often express different receptors, enzymes and other proteins in higher amounts than normal tissues, has paved the way to the so-called "active drug targeting" strategies. In this case, recognition of tumor cells is made possible through the covalent temporary conjugation of cytotoxic agents to targeting carriers (e.g. monoclonal antibodies, vitamins, peptides and substrate analogues) that are able to bind specific tumor antigens (Figure 3.1).

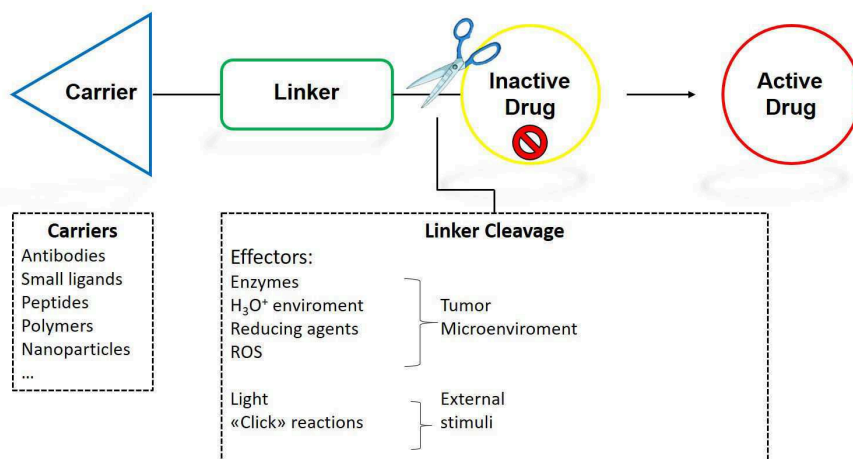


Figure 3.1: Schematic representation of tumor-targeted prodrugs.

Depending on the exact localisation of the receptor, different active targeting approaches have been introduced:

- active targeting to cancer cells: the target is expressed on the plasma membrane of tumor cells. Generally, the transmembrane receptor promotes the internalization of the drug by means of receptor-mediated endocytosis. This strategy is particularly useful to improve the cellular uptake of a specific payload;
- active targeting to endothelial cells: the target is highly expressed on cells of tumor blood vessels (e.g. endothelial cells). This strategy overcomes the need for extravasation and penetration into the tumor mass. As a result of the cytotoxic action, the tumor is deprived of oxygen, nutrients and other growth factors, which are required for cancer progression. Moreover, upon binding to tumor blood vessels, the payload can also diffuse within the tumor vasculature, thus enabling low molecular weight drugs to penetrate deeply into the tumor environment.<sup>247</sup>

The general structure of this second class of systems is reported in Figure 3.1 and it consists in a "head" containing a carrier moiety that directs the nanosystem to the target, and a "tail" containing a cleavable linker and the cargo. This second portion of the molecule has to be stable in the circulation *in vivo* until it reaches its destination, and just in that moment it has to release the payload drug in an active form. These systems can be employed also as imaging tools; in this case, the bridge between the selective ligand and the cargo is stable and the cargo consists in an imaging agent rather than a drug. The insertion of the imaging agents is necessary to detect and localise the malignant tissues, and to perform pharmacokinetic studies on the nanoscale systems.

In this field, **antibody-drug conjugates (ADCs)**<sup>248</sup> represent the most clinically validated technology, with five products currently available on the market. The concept behind the ADC strategy is the necessity to bind selectively transmembrane tumor antigens, by exploiting the cancer recognition displayed by monoclonal antibodies (mAbs). In fact, it has

been postulated that ADCs (and more generally the active-targeting therapeutics) should bind to tumor receptors and release the cytotoxic agent inside the targeted cancer cell by folding and endocytosis of the ADC-receptor complex into membrane vesicles.<sup>249</sup> The environmental conditions (e.g. acidic pH, high expression of proteases, high concentration of antioxidants) are responsible for the linker cleavage. Finally, the released drug is free to enter the cytoplasm and to bind its molecular target, resulting in cell cycle arrest and apoptosis.<sup>250</sup> However, it has been demonstrated that targeted cytotoxic cargo specific to non-internalising antigens allowing the extracellular drug release and its passive diffusion within the tumor microenvironment may increase the treatment efficacy.<sup>251</sup>

Although the great results obtained, ADCs suffer from several drawbacks such as the inability of the majority of therapeutics to end up in the tumor. This pitfall is due to the dimensions of the antibody carrier, that leads to a delayed extravasation and results in a poor drug accumulation.<sup>252</sup> Moreover, ADCs are a family of compounds bearing varying number of drugs attached to the antibody, thanks to the employed synthetic chemistry, resulting in wide spectrum of pharmacokinetic properties. In addition, the large-scale production of ADCs is very expensive because of sterile manufacturing and the necessity to work with high concentration of cytotoxic compounds.<sup>253</sup> Finally, possible side immune response that alters the activity of the system may occur.

Although ADCs are the most advanced technology in tumor treatment, the above-mentioned drawbacks prompted the development of smaller devices with better pharmacokinetic and pharmacodynamic behaviours, a different in vivo/in vitro stability and the ability to preserve the tumor-targeting features of mAbs.<sup>254</sup> For these reasons, a growing emerging family of delivery systems is represented by **small molecule-drug conjugates (SMDCs)**. As smaller targeting vehicles, they would easily extravasate and penetrate deeply in the tumor mass and show different rate of excretion. Particles smaller than  $\sim 40$  kDa are extracted from the bloodstream by glomeruluses that drive rapidly the wastes to the kidneys that excrete them into the urine.<sup>100</sup> Particles above this threshold (especially higher than  $\sim 100$  kDa) are ejected with greater difficulty from the blood by cells and can be better accumulated in the liver tissues than in the unhealthy targeted ones.<sup>255</sup>

Moreover, SMDCs would be suitable for hit-to-lead optimisations as well as be more economical in terms of production costs.<sup>256</sup> However, SMDCs and ADCs present several structural similarities: linker and drug fragments are attached to a targeting carrier (SMCs, a small ligand; ADCs, an antibody), which binds tumor antigens with high affinity; the conjugate construct allows the employment of ultrapotent cytotoxic agents due to the inactivation of the drug, which would result too toxic to be administered for therapy as free drugs; the drug release requires a suitable spacer (Spacer 2, Figure 3.2) to install proper functional groups for conjugation chemistry and to improve the kinetic of drug release. It is important to highlight that the ligand and linker fragments in SMDCs may be not sufficiently hydrophilic to solubilise the cytotoxic agent (which is usually highly lipophilic). Therefore, the water sol-

ubility is often improved introducing hydrophilic spacers (e.g. PEG chains or short peptide sequences bearing hydrophilic residues), which are commonly installed between the ligand and the drug modules (Spacer 1 in Figure 3.2).<sup>257,258</sup>

For all these reasons and features, these sort of "magic bullets" are called **drug delivery systems (DDSs)**.<sup>259</sup>

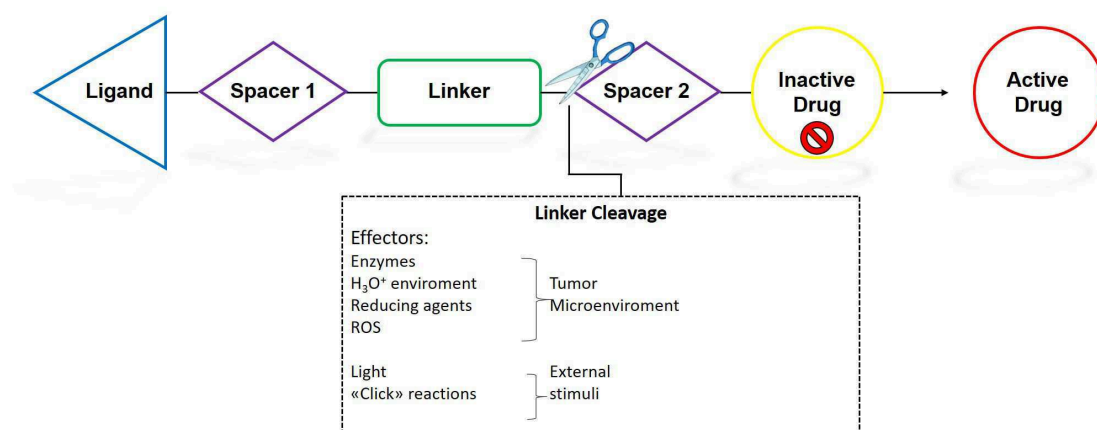


Figure 3.2: DDS structure and pathways to enter into the cell.

In order to obtain a successful DDS, it is necessary to evaluate some general requirements that have to be satisfied.

**-Receptor:** it must be overexpressed on the cancer tissue (at least threefold overexpression) and it must be accessible to the drug. Commonly, DDS enters into the cells by receptor-mediated endocytosis and is driven to a compartment of uncoupling of receptor and ligand (CURL) where the release of the cargo and the degradation/recycling of the receptor occur (Figure 3.2). Thus, choosing the suitable receptor, its recycling and resynthesis rate should be taken into account, in order to have new receptors able to recruit other DDSs.

**-Carrier:** It is fundamental to develop an optimal molecular design in order to enhance the binding affinity and to reduce the amount of drug necessary to the treatment. The "head" of the DDS has to recognise only the desired receptor among the others of the same family, in order to maintain its tumour specificity and consequently to reduce the risk of unwanted drug release; for this purpose, carriers are designed to recognise a specific tumour isoform, or, alternately, to recognise an allosteric site of the receptor. In fact, these sites differ one from another more than the orthosteric sites do. Designing the ligand, the necessity to have a peripheral functionalisable position is a crucial point in order to conjugate the "tail" with a robust moiety (carbamates, oximes, amides, esters, carbonates, disulphides, triazoles etc).

**-Linker:** The spacer and the linker don't play a passive role in the overall behaviour, being fundamental for both the stability of the intact nanosystem in the blood stream and for the drug release. In particular, the possible weakness of the linker can cause a poor stability of the construct in the blood stream, resulting in premature drug release and lowering the



therapeutic efficacy. Moreover, the physico-chemical properties of the whole conjugate, can be improved by a smart design of the chemical linker nature. For example, it is possible to enhance the solubility in the physiological environment of the drug and to reduce the nonspecific adsorption. The moieties generally used with this purpose are PEGs, polysaccharides, peptidoglycans or hydrophilic amino acids.<sup>100</sup> Most important, the linker is responsible for the controlled release of the payload. As touched on above, the linker must remain intact during the migration to the target, reacting rapidly just in the presence of cancer cells and releasing the cytotoxic molecule in an active form. On the basis of the specific environmental conditions, different linker moieties have been developed to release the cargo: in acidic conditions, characterising many extracellular environments, acetals, hydrazones and esters can be hydrolysed; in case of tumour hypoxia - generated by an increased metabolic rate of cancer cells - linkers based on indolequinone and nitroaromatics can be cleaved by specific hypoxia activated-enzymes; in abnormal enzyme expression conditions, amide and ester bonds can be cleaved, as well.

Moreover, when a bulky drug is coupled with a ligand, the insertion of a spacer lightens the resulting steric hindrance due to the proximity of these two fragments that could partially inhibit the binding between the receptor and the ligand.<sup>257</sup> Finally, it should be underlined the importance of the nature of the linker to be coupled to the drug since after the cascade process for drug-uncaging, no atoms from the linker have to remain bounded to the cytotoxic agent.

As mentioned in the scope of this thesis, the RDDS of our interest is built up on a selective integrin ligand, a spacer, a dipeptide linker coupled with a self immolative spacer, a second spacer, a latent fluorophore and a cytotoxic agent (Figure 1.15). Since the selective carrier has already been discussed in Chapter 2, here we will focus our attention on the remaining part of the device, in particular on the activation of the linker and the fluorophore system.

### 3.2 Enzyme-Activable Linkers

Peptide sequences or carbohydrate moieties are employed as linkers representing a large subset of targeted therapeutics which can be cleaved by tumor-associated enzymes. Generally, systems thus designed show remarkable stability in serum, minimizing nonspecific payload release. Until now, intracellular proteases (e.g. cathepsins,<sup>260</sup> legumain<sup>261</sup>) and glycosidases ( $\beta$ -glucuronidase,<sup>262</sup>  $\beta$ -galactosidase<sup>263</sup>) have been deeply investigated; in particular, cathepsins are involved in phenomena such as DNA replication and transcription, cell proliferation, differentiation and apoptosis, or angiogenesis. As a consequence, cathepsins are optimal enzymatic cleavers for selective activation of prodrugs due to their localised overexpression and involvement in the onset of diseases such as cancer or Alzheimer's dis-

ease.<sup>264</sup> For example, cysteine cathepsins are intracellular lysosomal proteases activated in acidic conditions and overexpressed in several forms of cancer, making these enzymes useful as pathological biomarkers. On the other hand, small molecule-drug conjugates (SMDC) may be targeted towards metastatic sites that express **cathepsin B** or cathepsin L, paving the way to several studies on structural requirement for enzyme sensitive linkers.<sup>265</sup> In the panorama of the selective **cathepsin B**-cleavable linkers, *Val-Cit* dipeptide (Figure 3.3) can be considered the pivotal subset, being included in several marketed conjugates, as well as in other ADCs undergoing clinical evaluation.<sup>266</sup>

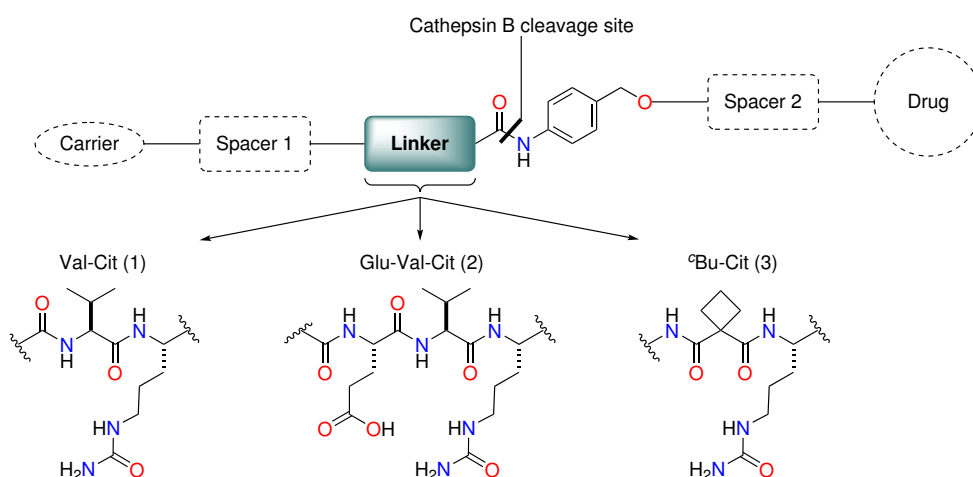


**Figure 3.3:** Cathepsin B-cleavable linkers (adapted from *Dal Corso A. et al.*<sup>267</sup>)

Deep research activities have started from the success obtained employing these linkers, especially at the industrial level, aiming to find new tumor-associated enzymes as potential drug release mediators. In particular, a suboptimal stability of the *Val-Cit* linker (despite the excellent overall results) was observed causing the premature release of the cargo and the onset of side pathologies.<sup>268</sup> On this topic, researchers at Pfizer have highlighted how the mouse carboxylesterase 1C (*Ces1C*) may be responsible for the low *Val-Cit* stability in rodent serum, lowering the reliability of the ADCs in the pre-clinical development.<sup>269</sup> In the light of these results, they have modified the N-terminus linker to improve the substrate stability towards *Ces1C*, without affecting the drug release kinetics in the presence of cathepsin B. These studies led to the identification of the *Glu-Val-Cit* linker (Linker 2, Figure 3.3), in which the addition of a *Glu* residue imparted high plasma stability. In *in vivo* tumor therapy experiments, *Glu-Val-Cit* linker displayed superior therapeutic activity than the traditional *Val-Cit*, even when the linker was stressed with more harsh enzymatic degradation conditions.<sup>270</sup> While linker 2 represents an example of improved drug release specificity by means of hindering the enzymatic action of competitor enzymes, another strategy is evaluation of available crystallographic data to design the linker structure and enhance the specificity towards the target enzyme.<sup>271</sup> Recently, Genentech researchers have reached this purpose replacing the *Val* residue in the *Val-Cit* dipeptide with a cyclobutane-1,1-dicarboxamide mo-

ity (linker 3, Figure 3.3).<sup>272</sup> This peptidomimetic linker showed similar stability in blood stream, but higher cathepsin B specificity than the Val-Cit standard, enabling superior therapeutic performances.

Several groups have deeply investigated the cathepsin B-cleavable peptide sequence; for example, *Firestone* and coworkers<sup>273</sup> have performed a systematic evaluation of different dipeptides in order to understand the general features required to fit properly in the specific enzymatic pockets (normally defined as S1 for C-terminus amino acid and S2 for N-terminus one): basic or strongly hydrogen bonding amino acids (Lys, Arg) are suitable to occupy position S<sub>1</sub>, while in position S<sub>2</sub> hydrophobic amino acids (Phe or Val) are recommended (Figure 3.4).<sup>273</sup> Finally, the opportunity to functionalise the N-term, in particular with hydrophobic moieties, induces a good fit to the S<sub>3</sub> site in the binding pocket, showing good activity in enzyme assay.

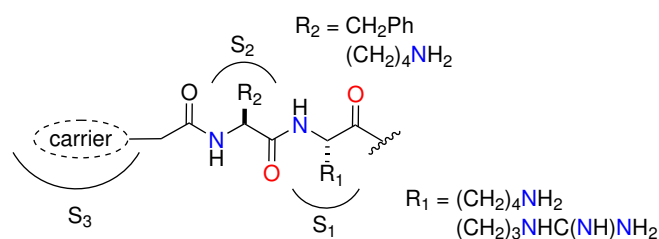


Figure 3.4: General structure of Cathepsin B-cleavable linkers.

Fortunately (or unfortunately due to the complexity of the active sites) the dipeptides presented by *Firestone* are just a general guideline. In fact, several amino acid sequences are reported in literature as efficient cathepsin sensitive linkers, such as Val-Ala,<sup>274</sup> Arg-Arg, Ala-Leu, Ala-Leu-Ala-Leu,<sup>275</sup> Ala-Phe-Lys,<sup>276</sup> Gly-Leu-Phe-Gly, and Gly-Phe-Leu-Gly.<sup>277</sup> In recent years, new enzymes have been identified as suitable effectors for the cleavage of linkers in DDSs. Among these, the intracellular protease *caspase 3* is one of the most interesting ones, involved in the apoptotic pathway. Under stress conditions, this pro-enzyme is activated by another caspase subtype and its proteolytic activity contributes to interrupt ATP synthesis.<sup>278</sup> Owing to its stringent specificity, the Asp-Glu-Val-Asp linker (DEVD) sequence has been recently identified as a caspase 3-cleavable linker and employed in different therapeutic/diagnostic constructs (Figure 3.5).

As observed for cathepsin B-cleavable dipeptides, also this linker is cleaved at C terminus and various payloads can be conjugated through the well-known *p*-aminobenzyl carbamate spacer (PABC).

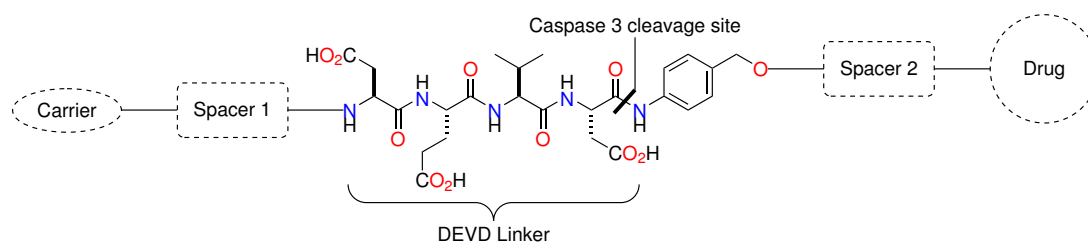


Figure 3.5: Caspase 3-cleavable linker DEVD (adapted from *Dal Corso A. et al.*<sup>267</sup>)

Recently, several evidences have demonstrated that cathepsin B and other primarily intracellular enzymes can be expressed also in extracellular compartments. Indeed, lysosomally cleavable linkers have shown to efficiently release cytotoxic payloads at the tumor site also when installed together with non-internalizing carriers, certain monoclonal antibodies<sup>279</sup> and small ligands.<sup>280</sup> On the other hand, extracellular enzymes have also been considered for the release of cytotoxic payloads from different carriers. For instance, the *serine protease elastase* has been selected as a mediator of drug release in extracellular space. In 2002, Bayer researchers have been the first to report an in vitro evaluation of a tumor-targeted conjugate featuring a novel elastase-cleavable linker, based on an Asn-Pro-Val (NPV) tripeptide. Almost 20 years later, *Gennari*<sup>281</sup> and coworkers have used the NPV linker to activate the release of paclitaxel from the peptidomimetic compound cyclo(DKPRGD), a non-internalizing ligand of the tumor receptor integrin  $\alpha_V\beta_3$ , and preliminary assays have shown promising results for its use in vivo therapeutic trials.

### 3.3 Self-Immolative Spacer

As discussed in the previous section, the cleavage of a specific chemical bond at the linker moiety should release the payload in its active form. However, there could be several structural limitations in the direct connection of the linker to the drug (e.g. the anchoring points at the drug site may not be compatible with a specific linker, steric hindrance may limit drug conjugation and linker cleavage, etc..).

Therefore, spacers between drug and linker fragments are often installed, either to lower the steric hindrance around the cleavable bond or acting as chemical adaptors. Moreover, several spacers can be coupled in series since the self-propagation of the electronic cascade allow to obtain an enhanced separation between the payload and the linker, also improving the efficiency of the device. These moieties are usually called "**self-immolative**" spacers.<sup>282</sup> These systems are designed such that the cleavage of a terminus (usually at the enzymatic cleavage site) uncages an activate moiety that undergoes a series of cascade reactions leading to the decomposition of the spacer to small molecules and the release of the activated form of the drug. The ideal structures for the generation of self immolative spacers are

represented by aromatic moieties and conjugated  $\pi$ -systems. The *p*-aminobenzyl alcohol (PABA), described by *Katzenellenbogen* in 1981,<sup>283</sup> can be considered the pivotal structure in this context (Figure 3.6). After the cleavage, the free aniline moiety undergoes a fast 1,6-elimination, affording an azaquinone methide and releasing different functional groups from the benzylic position (A in Figure 3.6).

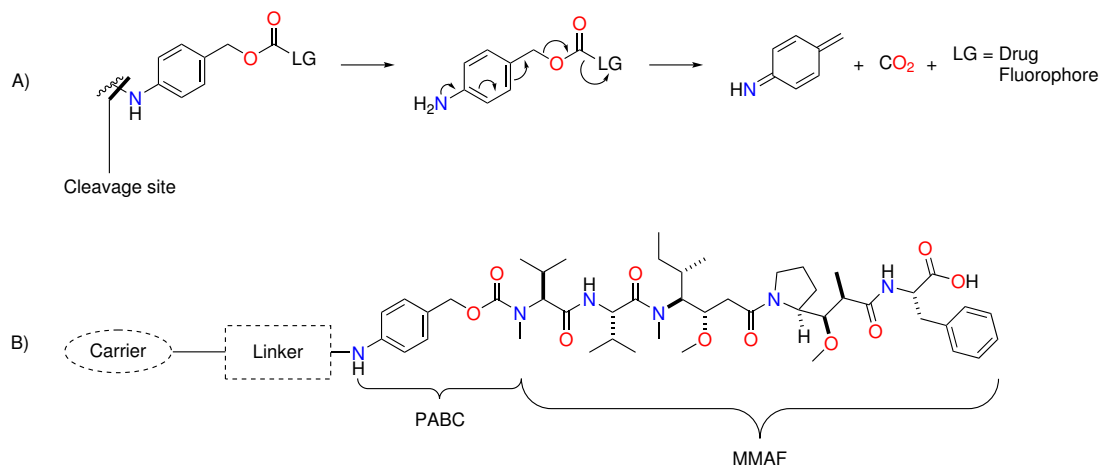


**Figure 3.6:** A) Mechanism of the disassembly of electronic cascade linkers; B) model compound containing a PABC moiety and MMAF.

Currently, a large number of ADCs (undergoing clinical evaluations) contain a *p*-aminobenzyl carbamate (PABC) spacer in their structures; for instance, the compound **B** (Figure 3.6) after the cleavage releases an amine-bearing drug which proceeds through the electronic cascade previously described, resulting in the loss of CO<sub>2</sub> and the unlock of the drug (MMAF, in this case).<sup>284</sup> *Genentech* researchers have recently reported an evolution of the traditional PABC spacer, with the development of the *p*-aminobenzyl quaternary ammonium salt (PABQ) spacer (**A** in Figure 3.7).<sup>285</sup>

This is obtained converting the benzyl alcohol of PABC into the corresponding benzyl chloride, which is then coupled with a tertiary or heteroaryl amine moiety of different payloads. In this way, *Genentech* researchers have expanded the scope of the traditional PABC, which could be used only to conjugate primary and secondary amines. Then, they incorporated this spacer in ADCs and tested it in mice, observing optimal stability in circulation and high therapeutic efficacy. Moreover, the same group adopted this strategy to conjugate phenol-bearing drugs. However, the resulting *p*-aminobenzyl ether (PABE) spacer (**B** in Figure 3.7) showed poor drug release in presence of electron-donating groups on the phenol. On the contrary, it was observed an improved release rate by means of the introduction of payloads bearing highly acidic phenolic groups.<sup>286</sup>

Traditionally, the conjugation of bioactive molecules at hydroxyl groups to the *p*-aminobenzyl alcohol (PABA) consists in the insertion in between of an ethylenediamine moiety, which is

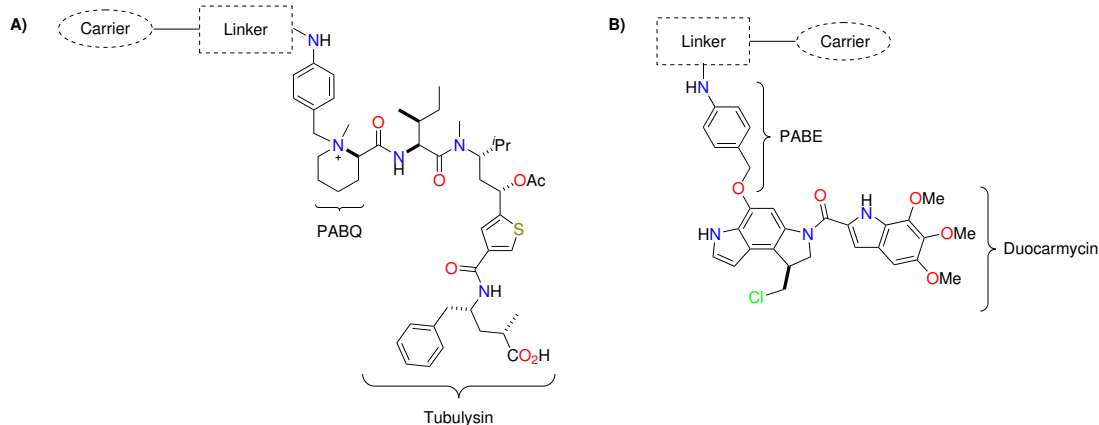


**Figure 3.7:** A) model compound containing a PABQ moiety and Tubulysin; B) model compound containing a PABE moiety and Duocarmycin.

coupled to the PABA spacer by a second carbamate bond (A in Figure 3.8). In this case, the 1,6-elimination of PABC moiety is followed by amine cyclisation of intermediate A1 into cyclic urea A2, releasing the free drug. In the reported mechanism, the amine cyclisation is the rate-limiting step, which can be further slowed down employing acidic conditions.<sup>281</sup>

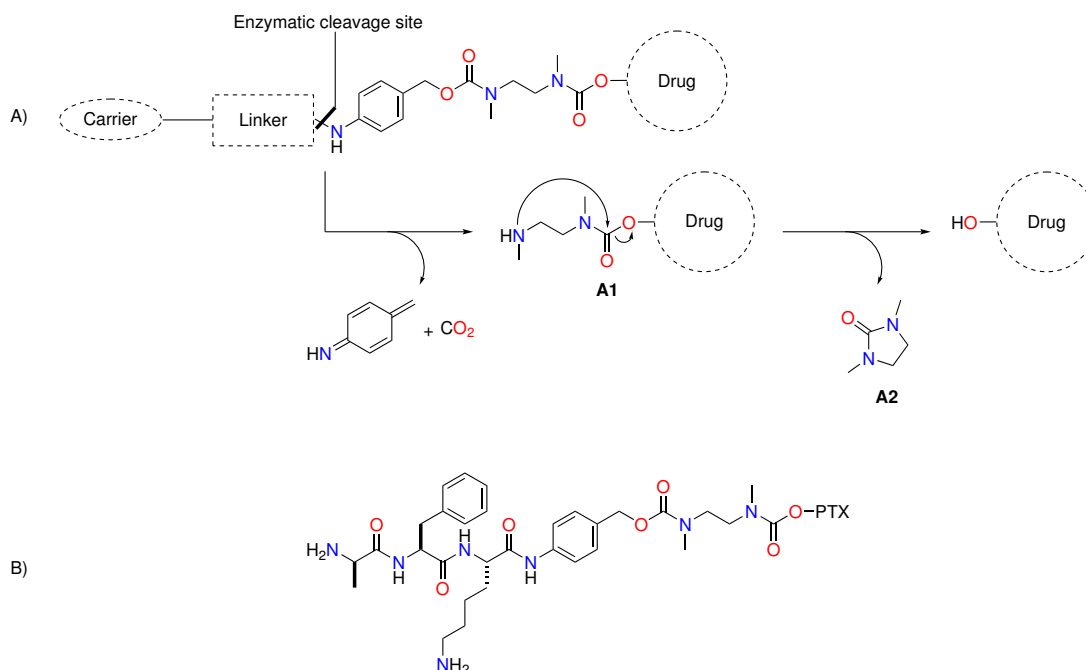


**Figure 3.8:** A) Example of common spacers PABC+ethylenediamine based for the release of HO-bearing drugs and its drug release mechanisms; B) Structure of the first enzymatic triggered DDS.

In 2001, *de Groot* and coworkers<sup>287</sup> were the first who incorporated PABC self-immolative spacers in combination with the ethylenediamine moiety between a specific cleavable sequence and a prodrug, in that case Paclitaxel (PTX) and Doxorubicin (DOX) (B in Figure 3.8). Moreover, several groups have reported the use of this intervening spacer for the conjuga-

tion of many drugs bearing phenolic,<sup>288</sup> primary,<sup>289</sup> secondary,<sup>281</sup> and tertiary<sup>290</sup> hydroxyl groups to the carrier-linker construct. In 2016, *Seattle Genetics*<sup>291</sup> reported a new methodology for the release of OH-bearing drugs based on a N-methylene-alkoxy group instead of the previously discussed ethylenediamine, employing a *p*-hydroxybenzyl alcohol for the connection of the linker to the N-methylene-alkoxy group (A in Figure 3.9). Although this approach had been previously reported in the literature,<sup>292</sup> only in 2016 the N-methylene-alkoxy spacer was first employed in the ADC therapy.<sup>291</sup> As depicted in Figure 3.9, upon cleavage of the linker a 1,6-elimination occurs to the *p*-hydroxybenzyl alcohol, releasing a hemiaminal derivative of formaldehyde (A1 in Figure 3.8) and, subsequently, the cytotoxic payload.<sup>293</sup> In the same year, *Daiichi Sankyo* researchers independently reported the use of the N-methylene-alkoxy spacer to directly connect a drug bearing a primary alcohol group to the C terminus of a peptide linker (B in Figure 3.9).<sup>294</sup>

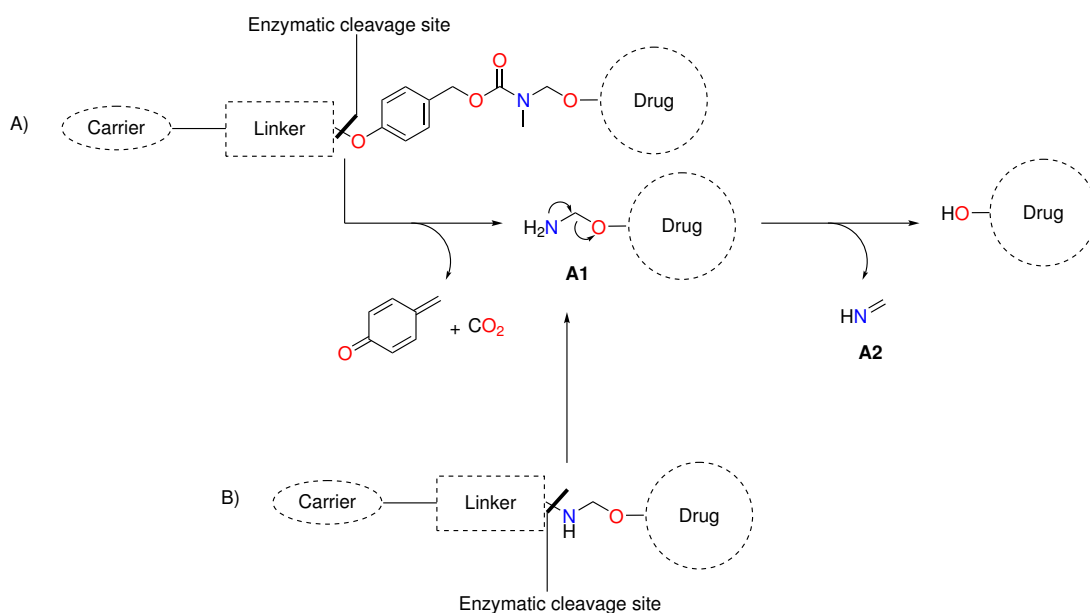


**Figure 3.9:** Examples of common spacers used for release of HO-bearing drugs and their drug release mechanisms. A) PHBC+N-methylene-alkoxy combination; B) direct use of N-methylene-alkoxy spacer.

The efficacy of these new self-immolative spacers was confirmed by in vivo clinical assays, which demonstrated the efficacy of the methylene alkoxy spacer for the delivery of OH-bearing payloads.

Finally, *Merck* researchers have recently proposed an innovative approach to connect OH-bearing drugs to linkers. Despite the self-immolative spacer strategy aims to release the payload spontaneously, they have developed enzymatically cleavable substrates as spacers between drug and linker. In fact, researchers have applied this strategy to a new ADC construct in which the primary hydroxy group of the drug was connected to a linker-PAB module through a phosphate or a diphosphate group (Figure 3.10), leading to an overall increased hydrophilicity of the linker-payload module. Moreover, this construct presented

high plasma stability, while the release of free drug (specifically Budesonide) in rat lysosomal lysates was preserved by the efficient phosphatase-mediated hydrolysis of P-O bond.<sup>295</sup>

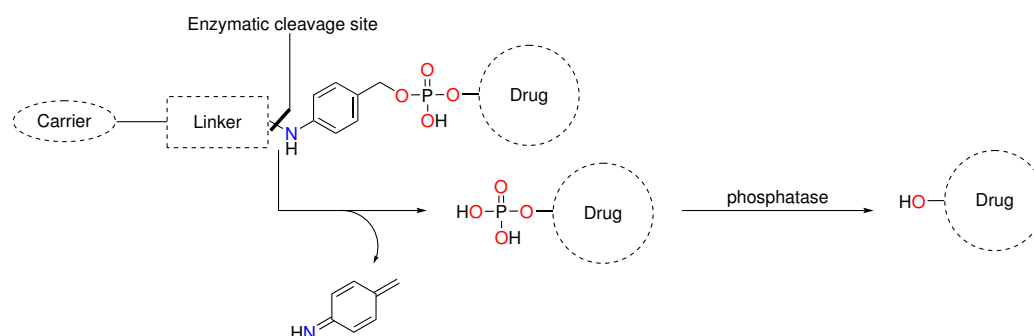


**Figure 3.10:** Example of new PABA-phosphate based spacer for the release of HO-bearing drugs and its drug release mechanisms.

### 3.4 Latent Fluorophore

Before introducing a drug as cargo in a delivery system, reporting studies employing fluorescent species were carried out. In fact, molecular fluorescence is a key tool for the visualisation of biologically relevant molecules or activities, since it offers an enhanced spectroscopic response and, in many cases, can be detected with non-invasive procedures.<sup>296</sup> In this context, **latent fluorophores (LFs)** are sophisticated and powerful instruments. LFs are molecules in which the fluorescence is inhibited by the conjugation with a quencher by means of a cleavable bond; due to the presence of the quencher, electronic properties of the fluorophore are altered, modifying the photophysical behaviour of the molecule. Removing the quencher unmasks the fluorophore and its original properties are restored (Figure 3.11).<sup>297</sup>

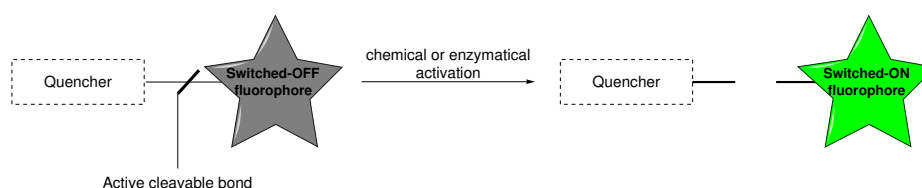


**Figure 3.11:** Mechanism of action of latent fluorophores (LFs).

Applying this reporting chemistry to the general principle of prodrug design, it is possible to develop imaging probes composed by a target identification unit, a specific linker, a self-immolative spacer and a LF. In these systems, the fluorophore release occurs upon the specific cleavage of the chemical bond at linker site, followed by the decomposition of the intervening moiety (Figure 3.12).



Generally, the triggering portion is designed to be recognised by proteases owing to their common overexpression on malignant or inflamed tissues. However, other enzymes can be used as promoter of the activation cascade, such as glycosidases, phosphatases, lactamases or even metal ions.

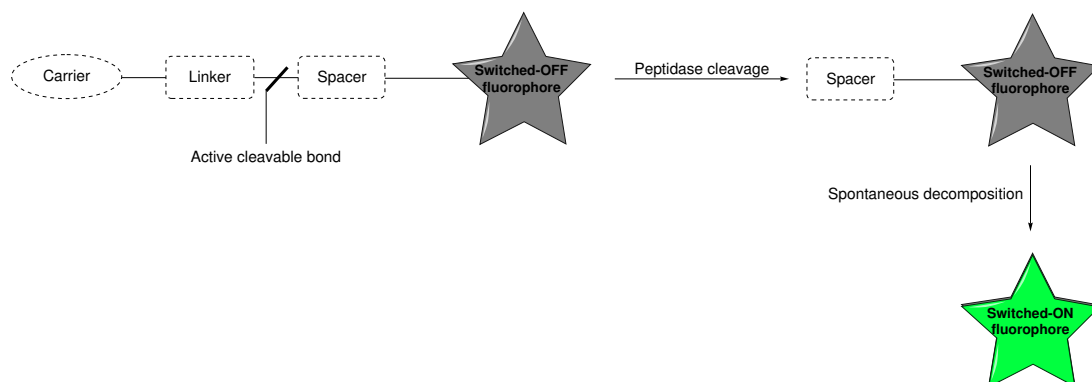


Figure 3.12: Mechanism of action of latent fluorophores (LFs).

In 2006, Jones<sup>297</sup> and coworkers proposed a series of imaging systems following this approach; the reported compounds contain a proteinogenic substrate for prostate specific antigen (PSA, a serine protease), a spacer and aminomethyl coumarin (7-AMC), disperse orange 11 or rhodamine 110 as fluorophore (Figure 3.13). These fluorescent molecules, such as other phenol-, aniline- and thiophenol-based compounds, are good leaving fragments suitable for multistep cascade.

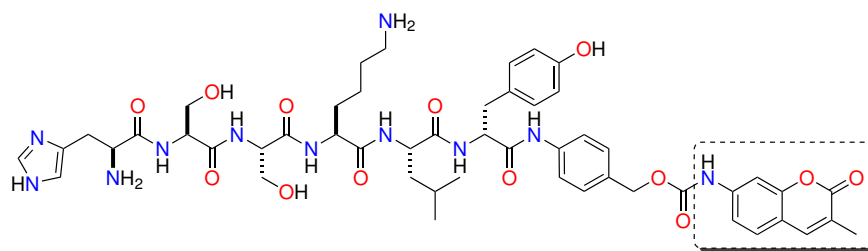


Figure 3.13: Imaging system proposed by Jones and coworkers bearing 7-AMC as LF.

As highlighted, the incorporation of cytotoxic agents in drug delivery systems (DDS) have drastically improved the therapeutic index of anticancer drugs, but this approach has an undeniable lack of direct data on time, location and extent of the drug release. To overcome this limitation, it is possible to insert a reporting signal element associated with the cargo release phenomenon. Previously mentioned LFs are attracting candidates for this purpose: if a single chemical cascade would be able both to turning on of the fluorescent signal and to releasing a drug, it should be possible to obtain real-time information about the overall phenomenon by developing an efficient theranostic platform. The use of LFs is even

more attractive since their detection is possible also in a non-invasive manner making this systems suitable for in vivo assays. Constructs with this behaviour are called **reporting drug delivery systems (RDDSs)** (Figure 3.14).<sup>298</sup>

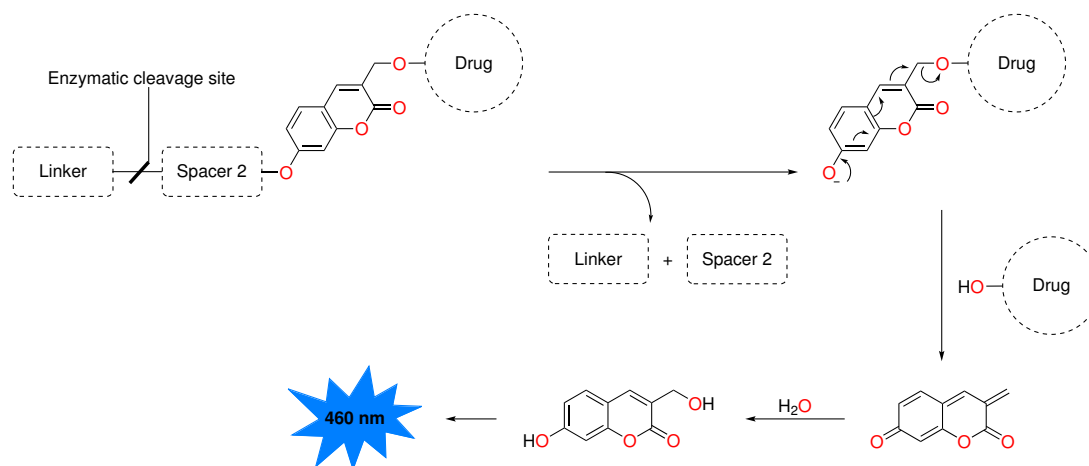


Figure 3.14: Proposed disassembly mechanism of coumarin-based RDDS.

Fluorophores employed for RDDSs must possess at least two functionalisable sites: one is necessary for the anchorage of the linker/spacer moiety, the other is devoted to connect the reporting system to the payload. Since the fluorophore is inserted between the self-immolative linker and the drug, it has to act as a self-immolative linker analogue, spreading the cascade reaction until the drug release. Finally, the disassembly mechanism that involves the activation of the reporting moiety must be the only one involved in the release of the payload; in this manner, by means of the measuring of fluorescence response, it would be also possible to indirectly quantify the amount, the time and the location of the drug release (Figure 3.14). The coumarin scaffold is a perfect candidate to play the role of the latent fluorophore in RDDSs. In fact, the first example reported of these constructs was based on a 3-hydroxymethyl-7-hydroxy coumarin linker in which the phenolic group was connected to a triggering-substrate for cathepsin B and the hydroxymethyl function binds to the drug unit (Figure 3.15).

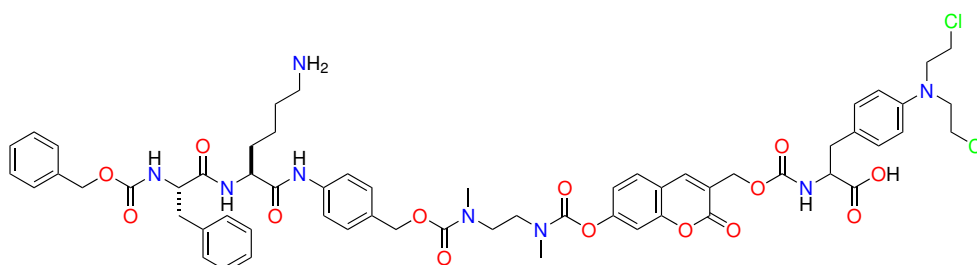
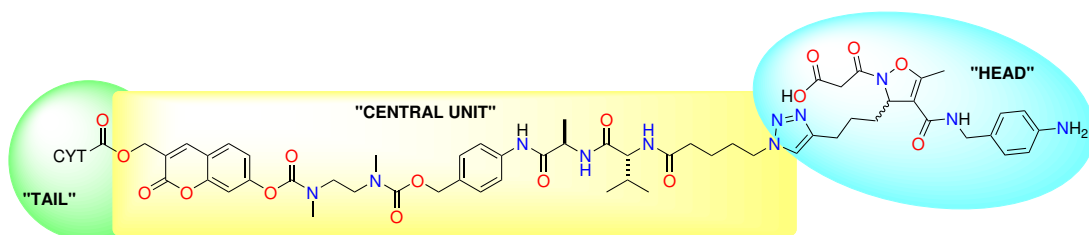


Figure 3.15: Chemical structure of a synthetic coumarin-based RDDS.

On the bases of these considerations, we assumed that this disassembly cascade would be the suitable strategy for our RDDS target purpose.

### 3.5 Results and Discussion

Up today, drug delivery systems targeted to  $\alpha_V\beta_3/\alpha_5\beta_1$  integrins have either drugs or imaging agents as cargo. Those labelled with a fluorophore permit to perform pharmacokinetics analyses, whereas those labelled with a drug permit a therapeutic treatment of the disease. Unfortunately, none of them reports direct information about the drug release from the vehicle. On the contrary, the compounds we have designed should be potentially able to report this event by way of a fluorescent signal. Our target product is composed of three portions with different purposes (Figure 3.16):



**Figure 3.16:** RDDS planned for a selective interaction with  $\alpha_V\beta_3$  and  $\alpha_5\beta_1$  integrin receptors.

- the "head", devoted to give effective ligand-receptor interaction;
- the central unit, composed by a spacer, a dipeptide linker, a self-immolative spacer and a latent fluorophore;
- the "tail" made up by a prodrug unit.

Here the components of the central unit, whose synthesis will be deeply discussed below are summarily presented. The first spacer is made up by an alkylic chain, necessary to relieve the steric hindrance between the carrier and the dipeptide. The  $C_5$  chain has been chosen due to the necessity of an hydrophobic moiety that would fit the  $S_3$  binding pocket of cathepsin B. Furthermore, as reported in Chapter 2, this functionalised integrin ligand was one of the most active derivatives tested on  $\alpha_V\beta_3$  integrins (compound **33**,  $\alpha_V\beta_3$   $IC_{50}/EC_{50} = 0.83 \pm 0.05 \mu M$ ). To avoid deprotection problems, easily occurring in the use of amino acids bearing basic functionalities in the side chains, we selected Val-Ala dipeptide since it is the most simple alkylic sequence recognised by this protease. As self-immolative portion, we selected a combination of PABA group and a diamine, directly linked at the C-terminus of the dipeptide. We followed this strategy in order to couple a phenolic fluorescent (such as 7-hydroxy coumarin) to the self-immolative linker by means of a carbamate moiety preferable to a weaker carbonate moiety. The use of this imaging agent makes the reporting drug delivery system suitable for in vitro application, since the generated wavelength of 460 nm is too short to be detected using procedures adapted for in vivo analysis. Finally, the methylenoxy function in position 3 of the coumarin scaffold is a perfect anchorage point for the coupling with a drug. Indeed, this function is actively involved in the cascade decomposition allowing the release of the latent fluorophore and the active form of the

cytotoxic agent (CYT) (Figure 3.17).

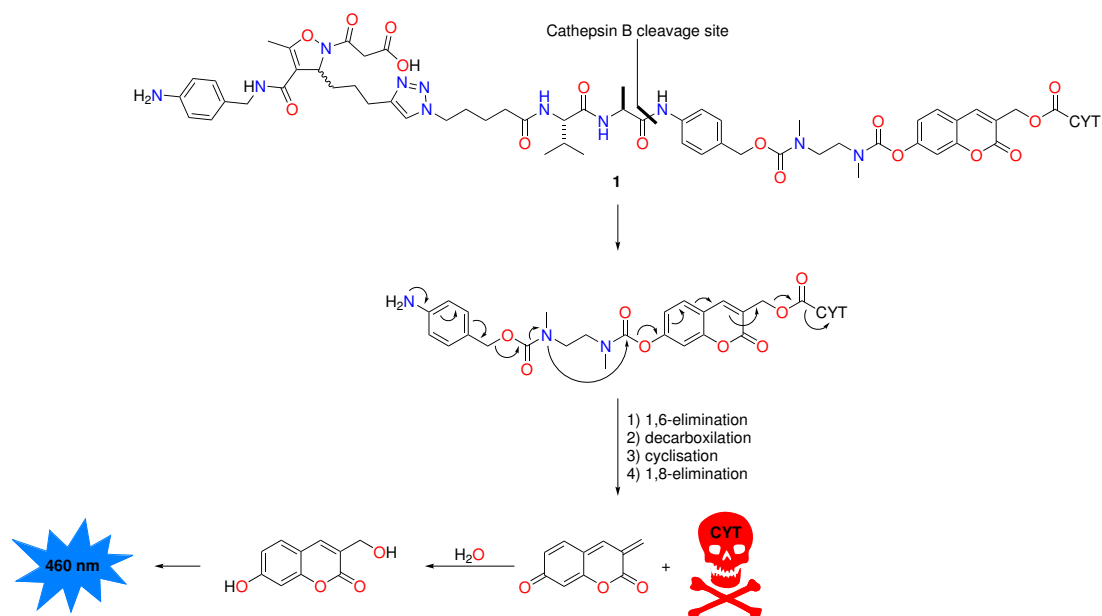


Figure 3.17: Proposed mechanism for the cascade disassembly of compound 1.

According to the literature,<sup>298</sup> the disassembly cascade starts with the enzymatic cleavage at the C-terminus of the dipeptide; upon this event, a spontaneous decomposition cascade occurs involving the aniline derivative (1,6-elimination and decarboxylation), the diamine spacer (cyclisation) and the fluorophore (1,8-elimination). Finally, the process leads to the free CYT and the generation of a quinone methide derivative which is hydrated by the environment, leading to the final formation of the high fluorescent coumarin derivative.

In the preliminary stages of the design of the synthetic pathway we performed a retrosynthetic analysis of the molecule and we opted for a convergent approach dividing the molecule in smaller intermediates due to the complexity of the target products. We have highlighted three points of disconnection: the triazole ring, the diamine spacer and the cytotoxic agent (Figure 3.18).

We have already discussed the synthesis of the isoxazoline ring and [1,2,3]-triazole moiety used to connect **fragments A** and **B**, therefore to avoid redundancy we refer to the subsection entitled "Synthesis of new isoxazoline-based integrin ligands" in Chapter 2. The self-immolative spacer has been divided in two distinct intermediates that will be then assembled forming the carbamate moiety. Thus, the synthesis of **fragment B** involves four consecutive peptide coupling reactions in which the central unit is constituted by the selective cathepsin B-cleavable dipeptide. Finally, the third point of disconnection that we have identified is the carbonate moiety between **fragment C** and the cytotoxic agent. In this way it is possible to insert the drug in the last stages of the synthesis, avoiding excessive following steps that could damage it.

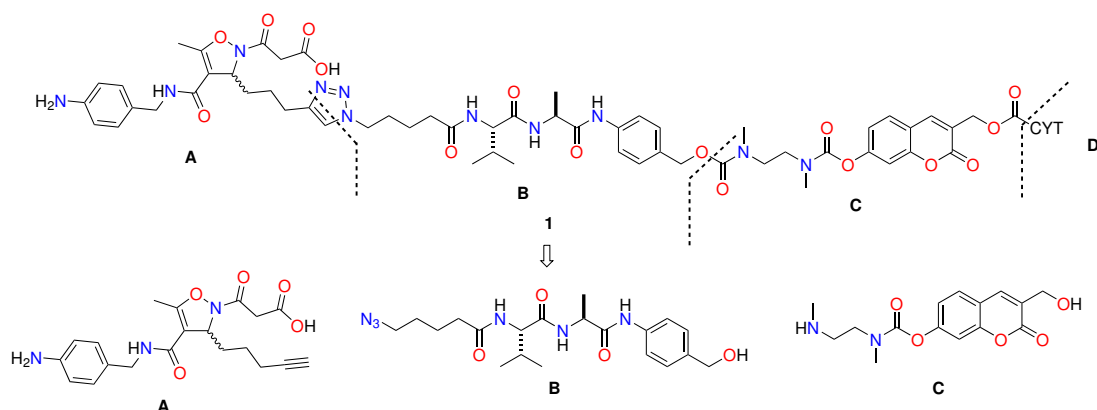


Figure 3.18: Retrosynthetic analysis of compounds 1

### 3.5.1 Synthesis of Fragment B

For the synthesis of **fragment B** we carried out in parallel the synthesis of the 5-azidovaleric acid **2** and Val-Ala dipeptide **3** (Figure 3.19), that will be discussed separately here.

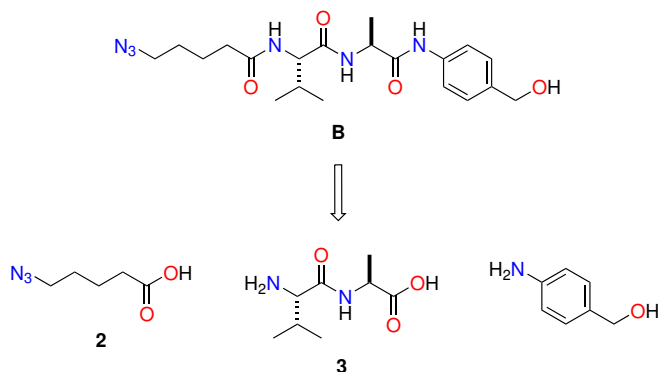
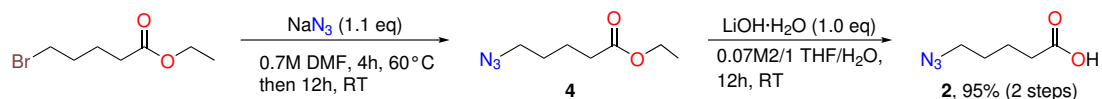


Figure 3.19: Retrosynthetic analysis of fragment B

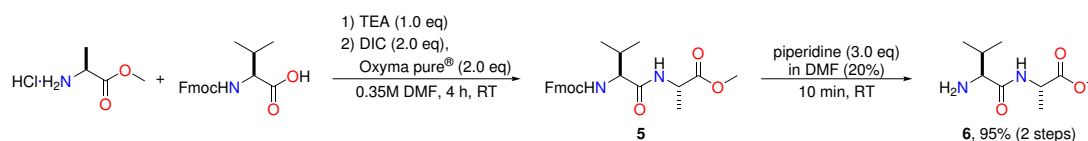
In order to obtain compound **2**, ethyl 5-bromovalerate was submitted to nucleophilic substitution in presence of  $\text{NaN}_3$ , carrying out the reaction at  $60^\circ\text{C}$  for 4 hours and overnight at RT in DMF. Then, the ester **4** was hydrolysed to the corresponding acid in basic conditions using  $\text{LiOH}\cdot\text{H}_2\text{O}$  obtaining the desired product **2** in 95% overall yield (Scheme 3.1).



Scheme 3.1: Synthesis of compound 2

On the other hand, the first step for the synthesis of the compound **3** was the coupling reaction between L-alanine methyl ester hydrochloride and N-Fmoc-Valine, employing TEA to release the amine functionality and DIC/Oxyma pure<sup>®</sup> as coupling reagents. The N-Fmoc

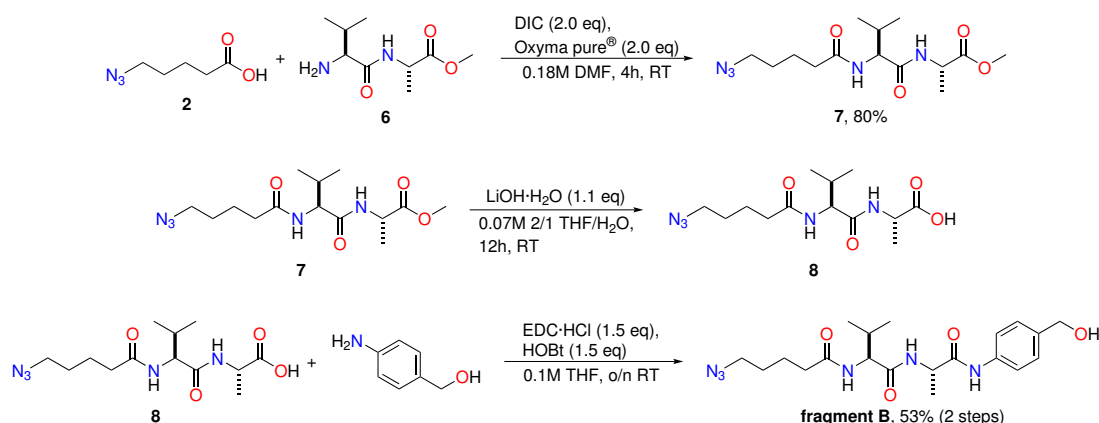
protection was removed from intermediate **5** in presence of a 20% piperidine solution in DMF, providing the desired compound **6** in 95% yield over two steps (Scheme 3.2).



Scheme 3.2: Synthesis of intermediate **6**

With intermediates **2** and **6** in hand, we were ready to couple the spacer **1** and the cathepsin B-selective linker of our RDDS. To do this, we employed again DIC and Oxyma pure<sup>®</sup> as coupling reagents, obtaining the intermediate **7** in good yield (80%).

To complete the synthesis of fragment B, hydrolysis of compound **7** in basic conditions was performed, obtaining the corresponding acid **8**. Then, **8** was coupled with p-aminobenzyl alcohol (PABA) with an excess of EDC·HCl and HOBT as coupling reagents. In this way, the target **fragment B** was obtained in good yield (53% over two steps) (Scheme 3.3).



Scheme 3.3: Synthesis of **fragment B**

### 3.5.2 Synthesis of Fragment C

For the synthesis of **fragment C** we carried out at the same time the synthesis of the diamine spacer **9** and 7-hydroxy coumarin **10**, focusing particularly on the synthesis and optimisation of the latter (Figure 3.20).

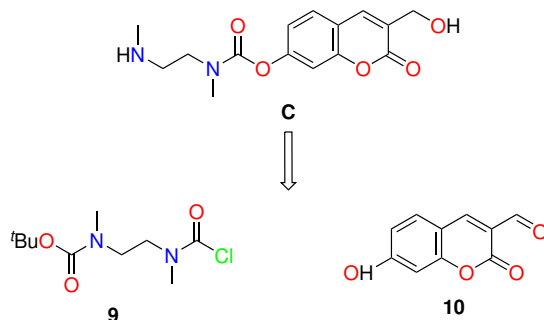
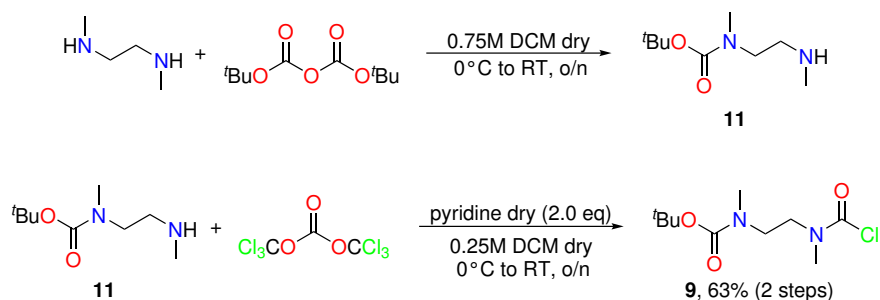


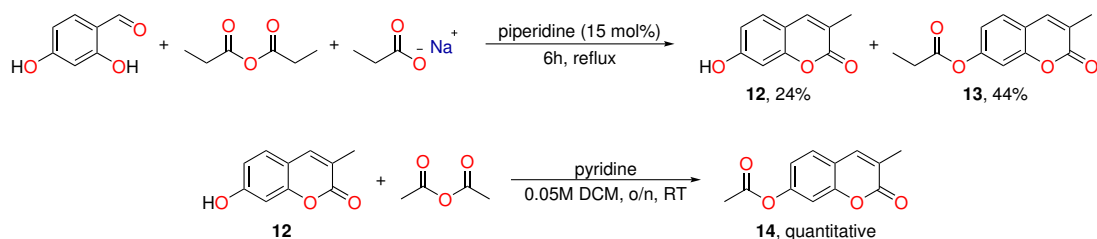
Figure 3.20: Retrosynthetic analysis of fragment C

In order to obtain compound 9, *N,N'*-dimethylethylenediamine was protected only at one of the two nitrogen atoms using a lack of Boc-anhydride; then, the mono-protected diamine 11 was activated towards coupling reaction converting the free amine function in a carbamoyl chloride group using triphosgene as carbonyl source (Scheme 3.4).



Scheme 3.4: Synthesis of compound 11

On the other hand, regarding the synthesis of the latent fluorophore, we decided to use the aldehyde as a sort of protecting group of the benzylic alcohol to avoid interferences during the synthesis of the carbamate moiety of **fragment C**. Focusing our attention on the synthesis of 10, a common reaction used for the synthesis of coumarin scaffold is the *Perkin* reaction (evolution of Pechmann condensation), the most widespread method employed for the synthesis of substituted coumarins (Scheme 3.5).

Scheme 3.5: A) Scheme of the *Perkin* reaction; B) Scheme of the protection of the phenoxy group

This reaction was discovered as an efficient method for pursuing the aldol condensation on aromatic aldehydes, but, if the aromatic ring is properly functionalized with a hydroxyl func-

tion in ortho position, it is possible to proceed to the lactonization that gives the coumarin as product. We adopted the classical procedure for this reaction in which 2,4-dihydroxybenzaldehyde was coupled with propionic anhydride and sodium propionate in the presence of piperidine in a one-pot two-steps reaction (Figure 3.21). The reaction crude was then treated with HCl to give a mixture of 3-methyl-7-hydroxy coumarin **12** and 3-methyl-7-propionate coumarin **13** (1:2 ratio) both suitable intermediates for the synthesis of the compound **10** (Scheme 3.5). In fact, to proceed in the synthesis of the target, it is necessary to protect the 7-hydroxy function; the propionate intermediate **13** already presents the necessary protection, whereas we had to protect the intermediate **12** by acetylation using acetic anhydride to obtain **14** in quantitative yield.

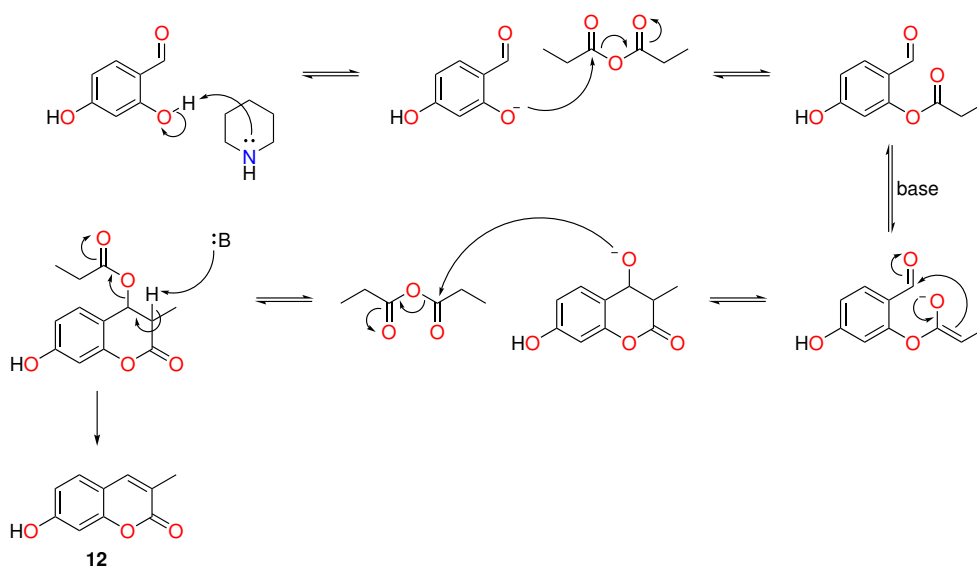
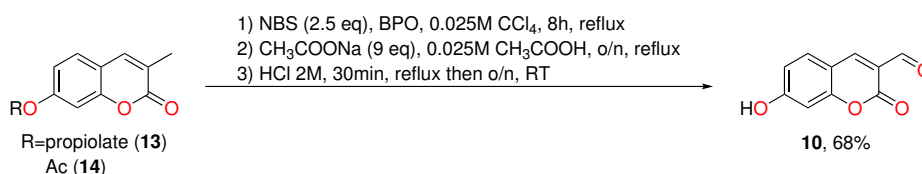


Figure 3.21: Mechanism of the *Perkin* reaction.

Successively, both compounds **13** and **14** were oxidised to the corresponding aldehyde in a one-pot two-steps reaction using an excess of NBS and traces of benzoyl peroxide (BPO) as radical initiator to achieve a double bromination. Then acetic acid and sodium acetate were added to transform the resulting allyl bromide to the corresponding aldehyde in the second step (Scheme 3.6).



Scheme 3.6: Synthesis of compound **12**

Before proceeding with the synthesis, it is interesting focusing our attention on the reaction mechanism for the synthesis of **10** (Figure 3.22). As stated before, firstly the substrate



undergoes to a double geminal bromination with a radical mechanism: once BPO is activated by heating (steps a and b), the radical attacks the carbonyl of NBS that releases Br as free radical (step c). The radical bromine then subtracts the hydrogen from the allylic position of **12/13**, starting the radical cascade that leads to the first intermediate of the synthesis (steps d, e, f and g). Once acetic acid and sodium acetate are added, the dibrominated adduct undergoes double nucleophilic substitution giving an acetal (step h). Finally, adding HCl the acetal is hydrolysed to the desired product **10** (step i).

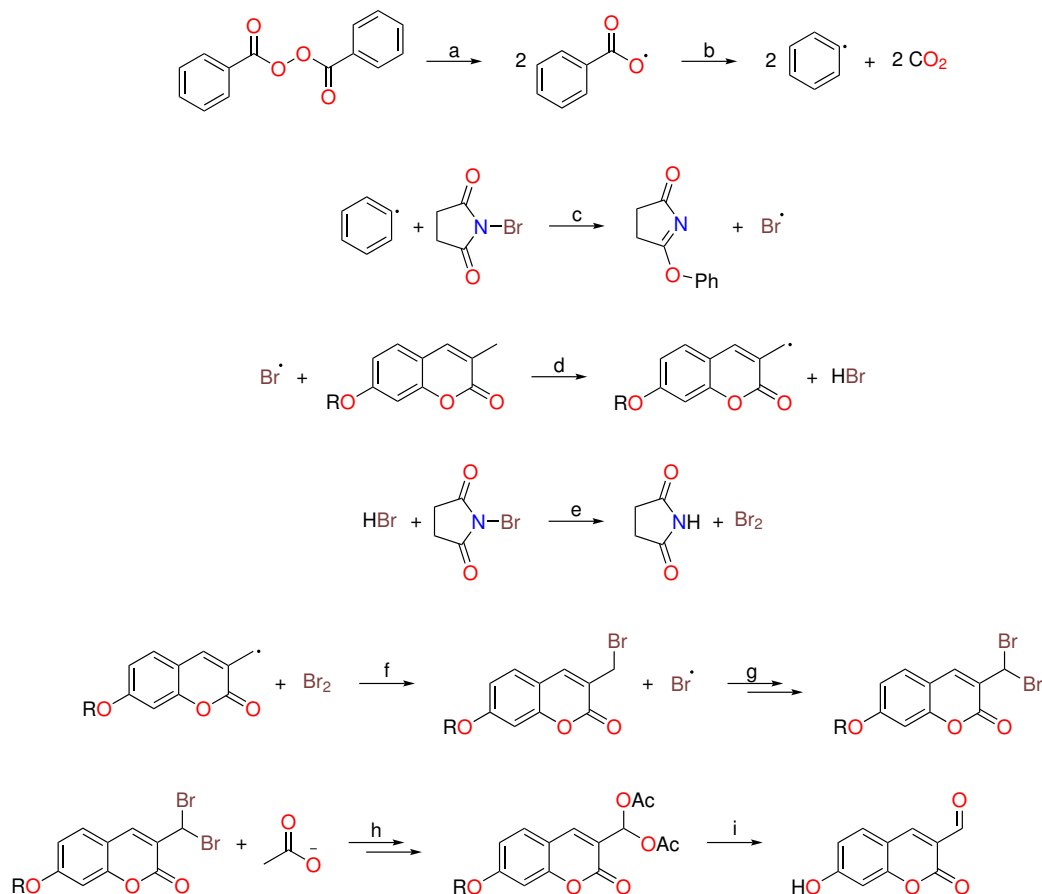
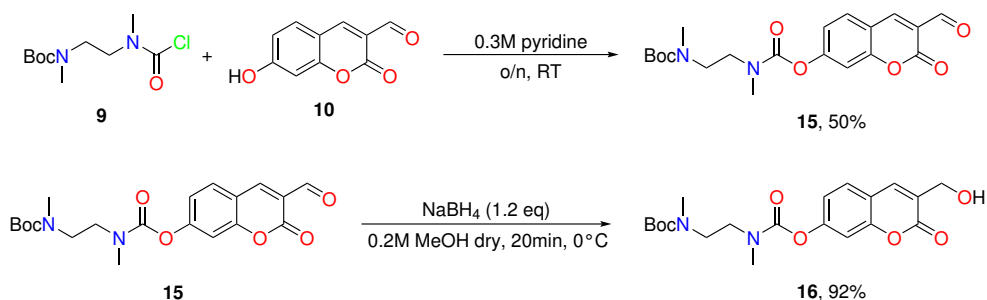


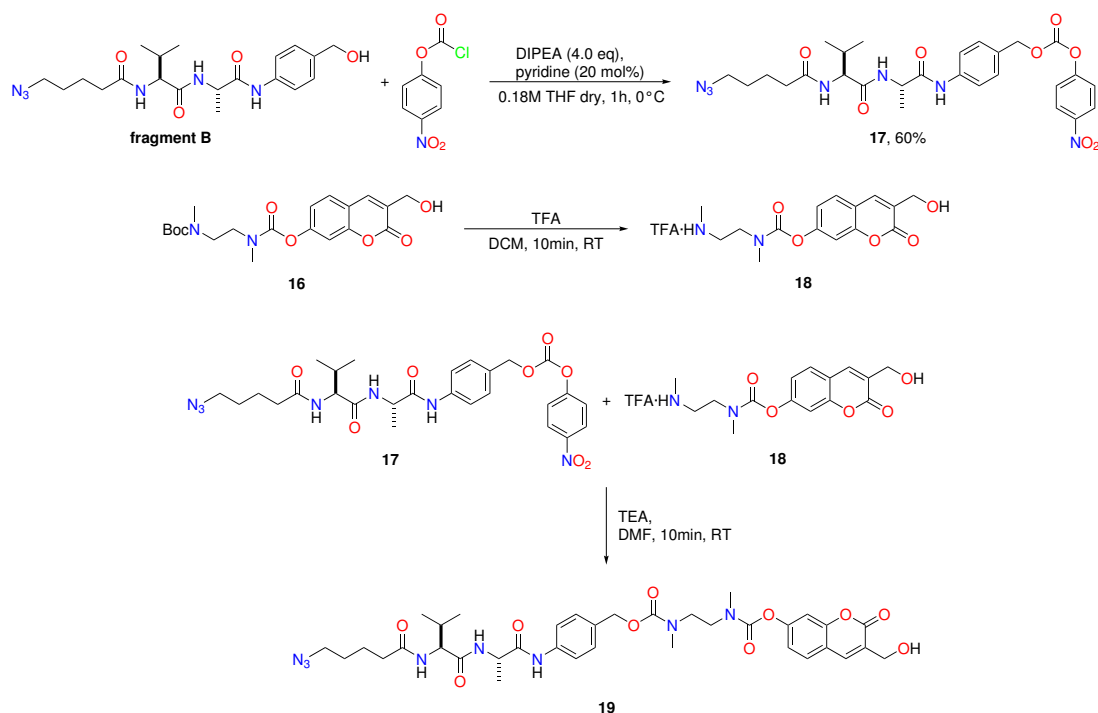
**Figure 3.22:** Mechanism of the one-pot two-steps oxidation for the synthesis of **12**

Once obtained coumarin **10**, it was reacted with the activated diamine **9** in presence of pyridine. Successively, the aldehyde group was reduced to the corresponding alcohol using  $\text{NaBH}_4$  in MeOH providing the **fragment C** precursor **16** in good yield (46% over 2 steps) (Scheme 3.7).



Scheme 3.7: Synthesis of 18 (precursor of fragment C)

At this point, with **fragment B** and compound 16 in hand, we opted for the initial activation of benzyl alcohol on **fragment B** by means of the formation of a carbonate moiety, having a good leaving group such as *p*-nitrophenate, and the subsequent formation of the carbamate by addition of **fragment C**, previously deprotected on the terminal Boc-protected amine. In particular, the employment of *p*-nitrophenate as leaving group in this type of process is widely reported, making these reaction conditions free from interference with other functional groups (Scheme 3.8).

Scheme 3.8: Coupling of **fragment B** and **fragment C**

For this purpose, first of all **fragment B** was activated as carbonate with 4-nitrophenyl chloroformate in presence of DIPEA and pyridine in THF. For the following coupling with 16 we decided to pursue a one-pot two-steps reaction, involving the initial removal of Boc group on the terminal amine using trifluoroacetic acid and then the addition of the carbonate previously formed, with TEA and DMF as solvent. This first attempt was performed just

in explorative scale and although traces of the desired product were obtained, HPLC-MS analysis has highlighted the presence of the self-immolative products (cyclic urea and fluorophore). With this goal in mind, we have also investigated in which conditions and at which state of the process the self-immolative cascade partially occurs, observing that the treatment of **18** with TEA is sufficient to permit the starting of the cascade. Moreover, we have investigated if the presence of the alcohol on the coumarin scaffold could activate the system towards the self-immolative process. Again, treating **16** initially with TFA and then with TEA (without other reaction partners) we have observed the formation of the cyclic urea and the fluorophore even in its tautomeric forms (Figure 3.23).

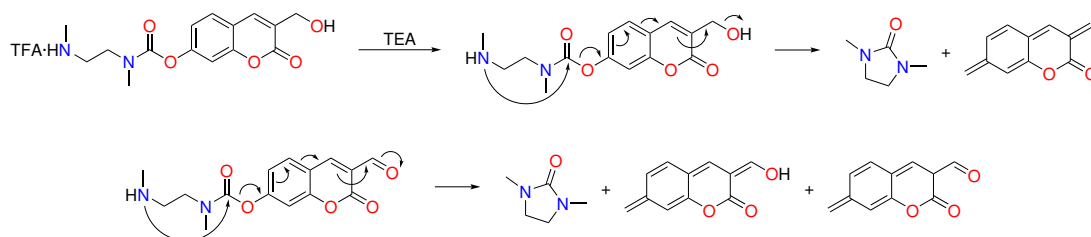


Figure 3.23: Electronic cascade on compound **20** that release cyclic urea and fluorophore

Nevertheless, this first experiment makes us confident that the procedure elected will allow us to obtain the desired product after further optimisation studies.

### 3.6 Conclusions

In conclusion, we have designed the first example of RDDS devoted to the treatment or visualisation of biological process involving  $\alpha_V\beta_3$  and  $\alpha_5\beta_1$  integrins. We have demonstrated the feasibility of the preparation of compound **1** by means of a convergent synthesis between **fragments A**, **B** and **C**. While the synthesis of **fragment A** has been already discussed in Chapter 2, the synthesis of **fragment B** has been obtained through a series of peptide couplings between a hydrophobic spacer, two amino acids and a self-immolative spacer. Finally, **fragment C** was prepared starting from a diamine spacer and 7-hydroxy coumarin obtained using the *Perkin* reaction and a variant of *Wohl-Ziegler* bromination. Even if some issues in the last steps of the synthesis were observed, we are confident that deeper optimisations will allow to complete the entire synthesis of the RDDS as a proof of concept of this innovative theranostic approach.

## 3.7 Experimental Procedures

### 3.7.1 General Methods

All chemicals were purchased from commercial suppliers and were used without further purification. Flash chromatography was carried out on silica gel (230-400 mesh). Flash chromatography was performed on silica gel (230-400 mesh). NMR Spectra were recorded with Varian Mercury Plus 400 or Unity Inova 600 MHz spectrometers. Chemical shifts were reported as  $\delta$  values (ppm) relative to the solvent peak of  $\text{CDCl}_3$  set at  $\delta = 7.27$  ppm ( $^1\text{H}$  NMR) or  $\delta = 77.0$  ppm ( $^{13}\text{C}$  NMR),  $\text{CD}_3\text{OD}$  set at  $\delta = 3.31$  ppm ( $^1\text{H}$  NMR) or  $\delta = 49.0$  ppm ( $^{13}\text{C}$  NMR),  $\text{D}_2\text{O}$  set at  $\delta = 4.79$  ppm ( $^1\text{H}$  NMR),  $\text{CD}_3\text{CN}$  set at  $\delta = 1.93$  ppm ( $^1\text{H}$ -NMR) or  $\delta = 117.7$  ppm ( $^{13}\text{C}$  NMR),  $(\text{CD}_3)_2\text{CO}$  set at  $\delta = 2.04$  ppm ( $^1\text{H}$  NMR) or  $\delta = 29.8$  ppm ( $^{13}\text{C}$  NMR). Coupling constants are given in Hertz. LC-MS analyses were performed on an HP1100 liquid chromatograph coupled with an electrospray ionization-mass spectrometer using a Phenomenex Gemini C18-3 $\mu$ -110 column,  $\text{H}_2\text{O}/\text{CH}_3\text{CN}$  as neutral solvent at 25°C or  $\text{H}_2\text{O}/\text{CH}_3\text{CN}$  with 0.2% formic acid as acid solvents (positive scan 100-500 m/z, fragmentor 70 eV). Another set of experiments has been performed on an HP1100 liquid chromatograph coupled with an electrospray ionization-ion trap mass spectrometer MSD1100 using a Phenomenex Zorbax C18-3.5 $\mu$ -80 column,  $\text{H}_2\text{O}/\text{CH}_3\text{CN}$  with 0.08% trifluoroacetic acid as acid solvents (positive scan 100-500 m/z, fragmentor 70 eV).

### 3.7.2 Synthesis and Characterization

**Synthesis of ethyl 5-azidovalerate 4.** Ethyl 5-bromovalerate was dissolved in DMF (0.7 M) and  $\text{NaN}_3$  (1.1 eq) was added. The mixture was stirred at 60°C for 4h, then cooled down to RT and stirred 12h. The reaction mixture was diluted with EtOAc and washed with water. **2:** Yield = 95%.  $^1\text{H}$  NMR (400 MHz,  $\text{CDCl}_3$ )  $\delta$ (ppm): 4.10 (q, J = 7.2 Hz, 2H), 3.27 (t, J = 6.4 Hz, 2H), 2.31 (t, J = 6.8 Hz, 2H), 1.73-1.57 (m, 4H), 1.23 (t, J = 7.2 Hz, 3H);  $^{13}\text{C}$  NMR (100 MHz,  $\text{CDCl}_3$ )  $\delta$ (ppm): 172.9, 60.2, 50.9, 33.5, 28.2, 22.0, 14.1.

**Synthesis of 5-azidopentanoic acid 2.** **4** was dissolved in a mixture of THF/ $\text{H}_2\text{O}$  (2:1, 0.07 M).  $\text{LiOH}\cdot\text{H}_2\text{O}$  (1.0 eq) was added and the reaction was stirred at RT overnight. The complete conversion of the reaction was checked by TLC. The pH of the solution was then neutralised adding dropwise a solution of 1M HCl, extracted with AcOEt, dried with  $\text{Na}_2\text{SO}_4$ , filtered and concentrated under reduced pressure.

**2:** Yield >99%.  $^1\text{H}$  NMR (400 MHz,  $\text{CDCl}_3$ )  $\delta$ (ppm): 3.39-3.29 (m, 2H), 2.23 (t, J = 7.2 Hz, 2H), 1.69-1.54 (m, 4H);  $^{13}\text{C}$  NMR (100 MHz,  $\text{CDCl}_3$ )  $\delta$ (ppm): 173.0, 60.3, 51.0, 33.6, 28.2, 22.0, 14.1.

**Synthesis of N-Fmoc-Val-Ala-OMe 5.** To a solution of L-Ala methyl ester hydrochloride in DMF (0.35 M) was added TEA (1.0 eq) and stirred for 5 min at RT. At the same time, to a solution of N-Fmoc-L-Val-OH in DMF (1.0 eq, 0.18 M) was added DIC (2.0 eq) and Oxyma pure<sup>®</sup> (2.0 eq) and stirred for 5 min at RT. Then, former solution was added to the second and stirred at RT, checking the reaction with TLC. The reaction mixture was quenched with H<sub>2</sub>O and extracted with AcOEt, dried with Na<sub>2</sub>SO<sub>4</sub>, filtered and concentrated under reduced pressure. The crude residue was purified by flash chromatography to afford compound 5.

5: Yield >99%. <sup>1</sup>H NMR (400 MHz, CDCl<sub>3</sub>) δ(ppm): 7.73 (d, J = 7.3 Hz, 2H), 7.60-7.55(m, 2H), 7.42-7.34 (m, 2H), 7.31-7.24 (m, 2H), 6.67(brs, 1H), 5.59 (d, J = 8.8 Hz, 1H), 4.57 (q, J = 7.4 Hz, 1H), 4.41 (m, 1H), 4.32 (m, 1H), 4.19 (m, 1H), 4.07 (m, 1H), 3.71 (s, 3H), 2.13-2.05 (m, 1H), 1.37 (d, J = 6.8 Hz, 3H), 0.97 (d, J = 6.8 Hz, 3H), 0.94 (d, J = 6.8 Hz, 3H); <sup>13</sup>C NMR (100 MHz, CDCl<sub>3</sub>) δ(ppm): 173.3, 171.1, 156.5, 144.0, 143.9, 141.4, 127.8, 127.2, 125.3, 125.2, 120.1, 67.2, 60.3, 52.6, 48.1, 47.2, 31.6, 19.2, 18.2, 18.1.

**Synthesis of H-Val-Ala-OMe 6.** A solution of piperidine (3.0 eq) in DMF 20% w/w was prepared and added to compound 5. The mixture was stirred at RT until the formation of a white solid. The solid was dissolved in AcOEt and the organic phase was washed three times with water, was dried over Na<sub>2</sub>SO<sub>4</sub>, filtered and concentrated under reduced pressure. The crude product was used directly in the next step.

6: Yield = 95%. <sup>1</sup>H NMR (400 MHz, CDCl<sub>3</sub>) δ(ppm): 4.47 (q, 1H), 3.70 (s, 3H), 3.68 (d, 1H), 2.21 (m, 1H), 1.42 (s, 3H), 1.09 (d, 6H).

**Synthesis of (5-azidopentanoyl)Val-Ala-OMe 7.** To a solution of 5-azidopentanoic acid 2 (1.0 eq) in DMF (0.18 M) was added DIC (2.0 eq), Oxyma pure<sup>®</sup> (2.0 eq) and stirred for 5 min at RT. Then, H-Val-Ala-OMe 6 was added to the activated acid solution and stirred at RT, checking the reaction with TLC. The reaction mixture was quenched with H<sub>2</sub>O and extracted with AcOEt, dried with Na<sub>2</sub>SO<sub>4</sub>, filtered and concentrated under reduced pressure. The crude residue was purified by flash chromatography to afford compound 7.

7: Yield = 80%. <sup>1</sup>H NMR (400 MHz, CDCl<sub>3</sub>) δ(ppm): 6.51 (brs, 1H), 6.11 (brs, 1H), 4.54-4.46 (m, 2H), 3.73 (s, 3H), 3.28 (t, J = 6.8 Hz, 2H), 2.22 (dt, J = 1.6 Hz, 7.3, 2H), 2.19-2.11 (m, 1H), 1.76-1.56 (m, 4H), 1.37 (d, J = 6.8 Hz, 3H), 0.89 (dd, J = 6.8, 10.0 Hz, 6H).

**Synthesis of (5-azidopentanoyl)Val-Ala-OH 8.** 8 was dissolved in a mixture of THF/H<sub>2</sub>O (2:1, 0.07 M). LiOH·H<sub>2</sub>O (1.1 eq) was added and the reaction was stirred at RT overnight. The complete conversion of the reaction was checked by TLC. The pH of the solution was then neutralised adding dropwise a solution of 1M HCl, extracted with AcOEt, dried with Na<sub>2</sub>SO<sub>4</sub>, filtered and concentrated under reduced pressure.

7: Yield = 94%. <sup>1</sup>H NMR (400 MHz, CDCl<sub>3</sub>) δ(ppm): 7.01 (d, J = 8.8 Hz, 1H), 6.64 (d, J =

7.6 Hz, 1H), 4.66-4.59 (m, 1H), 4.52 (dd,  $J = 4.8, 8.4$  Hz, 1H) 3.28 (t,  $J = 6.8$  Hz, 2H), 2.28-2.19 (m, 3H), 1.72-1.56 (m, 4H), 1.35 (d,  $J = 6.8$  Hz, 3H), 0.93 (t,  $J = 6.4$  Hz, 6H).

**Synthesis of fragment B.** In a round bottom flask under  $N_2$  atmosphere, to a solution of **8** in THF dry (0.1 M) were added N-methylmorpholine (2.0 eq), ECD·HCl (1.5 eq), HOBT (1.5 eq) and stirred for 5 min. Then, 4-aminobenzyl alcohol (2 eq) was added and the mixture was stirred overnight. Afterwards the reaction was quenched with water and the solvent was removed under reduced pressure. The aqueous phase was extracted with AcOEt and the collected organic phases were washed with, 1M HCl,  $NaHCO_3$  and brine. The organic phase was dried over  $Na_2SO_4$ , filtered and concentrated under reduced pressure.

**fragment B:** Yield = 56%.  $^1H$  NMR (400 MHz, methanol- $d_4$ )  $\delta$ (ppm): 7.54-7.50 (m, 2H), 7.30-7.26 (m, 2H), 4.53 (s, 2H), 4.41 (q,  $J = 7.2$  Hz, 1H), 4.29 (d,  $J = 7.3$  Hz, 1H), 3.30-3.24 (m, 2H), 2.25 (t,  $J = 7.2$  Hz, 2H), 2.15-2.07 (m, 1H), 1.71-1.53 (m, 4H), 1.33 (d,  $J = 7.2$  Hz, 3H), 0.99 (d,  $J = 6.8$  Hz, 6H);  $^{13}C$  NMR (100 MHz, methanol- $d_4$ )  $\delta$ (ppm): 175.6, 175.2, 171.9, 138.8, 138.5, 128.6, 121.3, 64.8, 60.6, 52.1, 50.4, 36.0, 32.5, 29.4, 24.0, 19.7, 18.8, 17.8

**Synthesis of tert-butyl methyl(2-(methylamino)ethyl)carbamate 11.** In a round bottom flask under  $N_2$  atmosphere, N,N'-dimethylethylenediamine (3 eq) was dissolved in DCM (0.75 M). The solution was cooled at  $0^\circ C$  in ice bath and a solution of  $Boc_2O$  in DCM (0.5 M) was added dropwise. The solution was slowly allowed to reach room temperature and stirred under  $N_2$  atmosphere until complete conversion verified by TLC. The solvent was removed and the crude product was dissolved in AcOEt; the organic layer was washed three times with water and then dried over  $Na_2SO_4$ , filtered and concentrated under reduced pressure. The crude product was used without further purification in the next step.

**11:** Yield = 75%.  $^1H$  NMR (400 MHz,  $CDCl_3$ )  $\delta$ (ppm): 3.32 (t,  $J = 5.8$  Hz, 2H), 2.87 (s, 3H), 2.72 (t,  $J = 5.8$  Hz, 2H), 2.44 (s, 3H), 1.45 (s, 9H);  $^{13}C$  NMR (100 MHz,  $CDCl_3$ )  $\delta$ (ppm): 155.94, 79.44, 49.73, 48.43, 36.32, 34.71, 28.45.

**Synthesis of compound 9.** In a round bottom flask, under  $N_2$  atmosphere and cooled at  $0^\circ C$  in ice bath, a solution of triphosgene (0.37 eq) in DCM (0.5 M) was prepared. A solution of **11** and pyridine (2.0 eq) in DCM (1.0 M) was added dropwise to the former one. The mixture was allowed to reach RT and stirred under  $N_2$  atmosphere for 1 h. The reaction was quenched with 1M HCl and the organic phase was washed twice with 1M HCl. The collected organic phase was dried over  $Na_2SO_4$ , filtered and concentrated under reduced pressure. The crude product was used without further purification in the next step.

**9:** Yield = 84%.  $^1H$  NMR (400 MHz,  $CDCl_3$ )  $\delta$ (ppm): 3.48-3.41 (m, 4H), 3.12 (s, 2H), 3.04 (s, 1H), 2.87-2.85 (m, 3H), 1.43 (s, 9H).  $^{13}C$  NMR (100 MHz,  $CDCl_3$ )  $\delta$ (ppm): 154.95, 145.43, 79.81, 50.52, 48.38, 46.09, 45.29.

**Synthesis of 7-hydroxy-3-methyl-2H-chromen-2-one 12 and 13.** According to the literature,<sup>299</sup> in a round bottom flask were added 2,4-hydroxybenzaldehyde, sodium propionate (2.1 eq), propionic anhydride (2.7 eq) and piperidine (15 mol%). The mixture was heated to reflux and stirred for 6h and the solution was poured into ice water. The aqueous mixture, made acidic with a 0.1N solution of HCl, yielded a precipitate that was filtered and treated under stirring with concentrated H<sub>2</sub>SO<sub>4</sub>. The resulting mixture was poured onto ice again and the crude residue was purified by flash chromatography to afford compound **12** and **13**. **12**: Yield = 24%. <sup>1</sup>H NMR (400 MHz, CDCl<sub>3</sub>) δ(ppm): 7.51 (s, 1H), 7.38 (d, J = 8.5 Hz, 1H), 6.89 (dd, J = 8.5, 2.5 Hz, 1H), 6.85 (d, J = 2.5 Hz, 1H), 2.24 (s, 3H).

**13**: Yield = 44%. <sup>1</sup>H NMR (400 MHz, CDCl<sub>3</sub>) δ(ppm): 7.50 (s, 1H), 7.40 (d, 1H, J = 8 Hz), 7.08 (d, 1H, J = 2 Hz), 7.00 (dd, 1H, J = 8, 2 Hz), 2.64-2.59 (2H), 2.20 (s, 3H), 1.29-1.25 (3H); <sup>1</sup>H NMR (100 MHz, CDCl<sub>3</sub>) δ(ppm): 162.0, 153.8, 152.3, 138.9, 127.7, 125.2, 118.4, 117.4, 110.1, 27.8, 17.2, 9.1.

**Synthesis of 3-methyl-2-oxo-2H-chromen-7-yl acetate 14.** Compound **12** was dissolved in DCM (0.05 M). To the stirring solution was added acetic anhydride (21 eq) and three drops of pyridine. The solution was stirred at RT overnight and the complete conversion was verified by TLC. The solvent was removed under reduced pressure, and the mixture was diluted with DCM. The organic phase was washed three times with water and the organic phase was dried over Na<sub>2</sub>SO<sub>4</sub>, filtered and concentrated under reduced pressure. The crude product was used directly in the next step.

**14**: Yield >99%. <sup>1</sup>H NMR (400 MHz, CDCl<sub>3</sub>) δ(ppm): 7.51 (s, 1H), 7.43 (d, J = 8.4 Hz, 1H), 7.10 (d, J = 2.0 Hz, 1H), 7.03 (dd, J = 8.4, 1.8 Hz, 1H), 2.34 (d, J = 0.4 Hz, 3H), 2.22 (s, 3H); <sup>13</sup>C NMR (100 MHz, CDCl<sub>3</sub>) δ(ppm): 168.8, 161.8, 153.6, 152.0, 138.7, 127.6, 125.1, 118.2, 117.4, 109.9, 21.1, 17.1.

**Synthesis of 7-hydroxy-2-oxo-2H-chromene-3-carbaldehyde 10.** According to the literature,<sup>299</sup> compound **13** or **14** was dissolved in CCl<sub>4</sub> (0.025 M) in a round bottom flask. N-Bromosuccinimide (2.5 eq) and traces of BPO were added. The mixture was heated to reflux and stirred for 8h and the solution became gradually red. Afterwards the solvent was removed under reduced pressure obtaining a yellowish solid; to the flask was added sodium acetate (9.0 eq) and acetic acid (0.025 M) and the yellow solution was heated to reflux and stirred for 12 hours. Subsequently, 2N HCl was added to the hot mixture and the reaction was allowed to continue for 30 min and then cooled to RT. The stirring was continued for 9h until the formation of a white fine solid suspended in an orange solution. Once the solid decanted on the bottom of the flask the liquid phase was removed and the precipitate was washed with water and cold MeOH. The product was obtained as a reddish solid.

**10**: Yield = 68%. <sup>1</sup>H NMR (400 MHz, dmsO-d<sub>6</sub>) δ(ppm): 10.0 (s, 1H), 8.62 (s, 1H), 7.86 (d, J = 8.5 Hz, 1H), 6.92 (dd, J = 8.4, 2.2 Hz, 1H), 6.82 (d, J = 2.2 Hz, 1H); <sup>13</sup>C NMR (100 MHz,

dms<sub>o</sub>-d<sub>6</sub>)  $\delta$ (ppm): 188.2, 165.2, 157.8, 148.6, 147.6, 133.6, 130.5, 117.3, 114.7, 102.6

**Synthesis of compound 15.** According to the literature,<sup>298</sup> to a solution of compound 10 in pyridine (0.3 M), compound 9 (1.2 eq) was added. The solution was stirred at RT and the reaction was monitored to completion (overnight) by TLC. The organic phase was washed twice with 1M HCl, dried over Na<sub>2</sub>SO<sub>4</sub>, filtered and concentrated under reduced pressure. The crude product was used directly in the next step.

15: Yield = 50%. <sup>1</sup>H NMR (400 MHz, dms<sub>o</sub>)  $\delta$ (ppm): 10.02 (s, 1H), 8.68 (s, 1H), 8.01 (d, J = 8.4 Hz, 1H), 7.28 (s, 1H), 7.20 (d, J = 8.4 Hz, 1H), 3.33-3.56 (m, 4H), 2.81-3.07 (m, 6H), 1.29 (s, 9H); <sup>13</sup>C NMR (100 MHz, dms<sub>o</sub>-d<sub>6</sub>)  $\delta$ (ppm): 187.6, 159.9, 156.4, 145.1, 131.5, 128.8, 128.6, 128.5, 128.2, 128.1, 127.2, 127.1, 119.4, 110.3, 77.2, 57.7, 31.9, 30.3, 29.7, 28.4, 22.7.

**Synthesis of compound 16.** According to the literature,<sup>298</sup> to a solution of compound 15 in MeOH (0.2 M), cooled to 0°C, sodium borohydride (1.2 eq) was added slowly. The reaction was monitored to completion (20 min) by TLC. The reaction mixture was diluted with EtOAc, washed once with saturated NH<sub>4</sub>Cl solution, dried over Na<sub>2</sub>SO<sub>4</sub>, filtered and concentrated under reduced pressure. The crude product was used directly in the next step.

16: Yield = 92%. <sup>1</sup>H NMR (400 MHz, dms<sub>o</sub>-d<sub>6</sub>)  $\delta$ (ppm): 7.96 (s, 1H), 7.79 (d, J = 8.4 Hz, 1H), 7.18 (s, 1H), 7.09 (d, J = 8.4 Hz, 1H), 5.31 (t, J = 8.4 Hz, 1H), 4.30 (d, J = 8.4 Hz, 2H), 3.34-3.58 (m, 4H), 2.80-3.05 (m, 6H), 1.29 (s, 9H). <sup>13</sup>C NMR (100 MHz, dms<sub>o</sub>-d<sub>6</sub>)  $\delta$ (ppm): 164.0, 160.0, 159.4, 157.8, 157.4, 141.2, 132.7, 128.3, 123.2, 121.0, 113.8, 83.1, 62.6, 50.9, 50.1, 39.2, 38.3, 32.3.

**Synthesis of compound 17.** In a round bottom flask under N<sub>2</sub> atmosphere, to a solution of **fragment B** in THF (0.18 M) and cooled at 0°C in ice bath, DIPEA (4.0 eq), p-nitrophenyl chloroformate (3.0 eq) and pyridine (20 mol%) were added. The solution was stirred at 0°C and the reaction was monitored to completion (1h) by TLC. The solution was diluted with AcOEt and washed with NH<sub>4</sub>Cl and brine, dried over Na<sub>2</sub>SO<sub>4</sub>, filtered and concentrated under reduced pressure. The crude residue was purified by flash chromatography to afford compound 17.

17: Yield = 60%. <sup>1</sup>H NMR (400 MHz, methanol-d<sub>4</sub>)  $\delta$ (ppm): 8.28 (d, J = 9.2 Hz, 2H), 7.65 (d, J = 8.4 Hz, 2H), 7.44 (d, J = 9.2 Hz, 2H), 7.40 (d, J = 8.4 Hz, 2H), 5.24 (s, 2H), 4.41 (q, J = 7.2 Hz, 1H), 4.29 (d, J = 7.3 Hz, 1H), 3.30-3.24 (m, 2H), 2.27 (t, J = 6.8 Hz, 2H), 1.69-1.56 (m, 5H), 1.34 (d, J = 7.2 Hz, 3H), 0.96 (dd, J = 6.0, 10.4 Hz, 6H).



## Chapter 4

# Total Synthesis of Mycapolyol A

### 4.1 Introduction

One of the most harsh challenges in the modern chemistry is the synthesis of complex structures employing non toxic, easy to handle and versatile starting materials. Among the synthetic tools available in the organic chemistry panorama, **pinacol boronic esters** have risen as pivotal building blocks owing to their peculiar chemical properties. In fact, chiral boronic esters are both chemically and configurationally stable; moreover, since they can be synthesised with very high levels of enantioselectivity, they can be transformed in the corresponding C-C and C-X (X = heteroatom) bonds in high stereocontrolled fashion (Figure 4.1).<sup>300,301</sup>

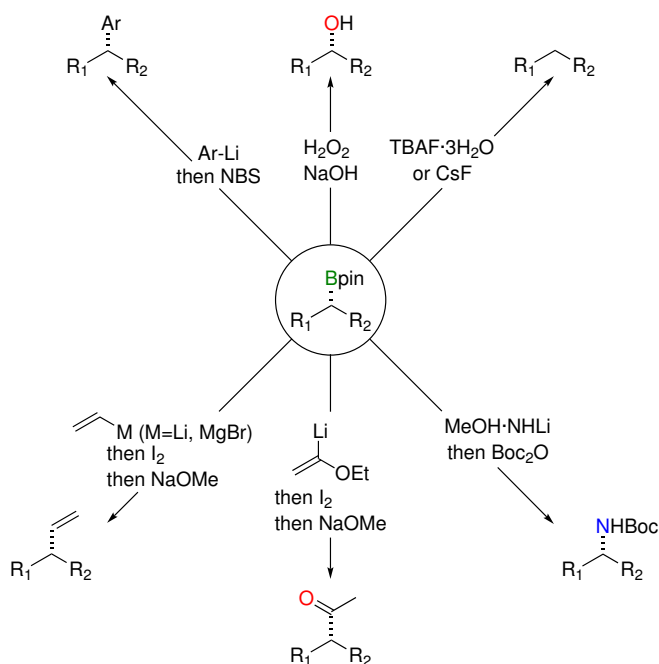


Figure 4.1: Stereospecific transformations of secondary boronic esters

In particular in the last fifteen years, their homologation using lithium carbenoids via 1,2-metallate rearrangement has been recognised as a powerful reaction strategy for chemical diversification.

#### 4.1.1 Lithiation-Borylation: from a Single Homologation to the Assembly-Line Synthesis

In the 1980s, *Matteson*<sup>302</sup> reported a two-step homologation process of boronic esters bearing a chiral diol, using dichloromethyl lithium and Grignard reagents.<sup>302,303</sup> In this approach, the stereochemistry of chiral diol moiety of the boronic ester controls the subsequent transformations generating a **substrate-controlled** process (Figure 4.2). In this approach, the dichloromethyl lithium ( $\text{LiCHCl}_2$ ) is sufficiently nucleophilic to react with the boronic ester, obtaining a chiral boronate species which undergoes 1,2-migration with concomitant expulsion of the chloride providing the  $\alpha$ -chloro boronic ester (Figure 4.2). Successively, the addition of an achiral Grignard reagent (or a general nucleophile) to the  $\alpha$ -chloro boronic ester yields the homologated product (Figure 4.2).

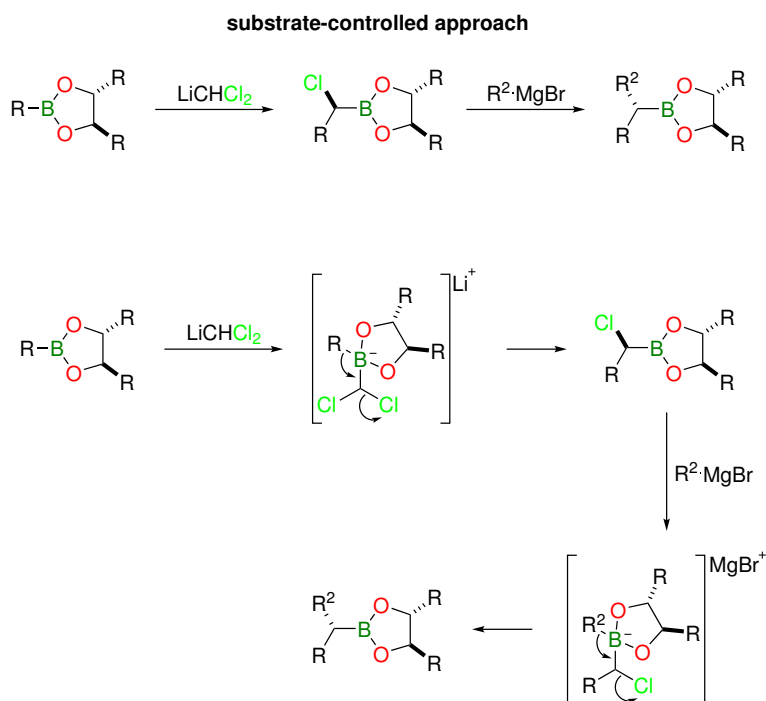
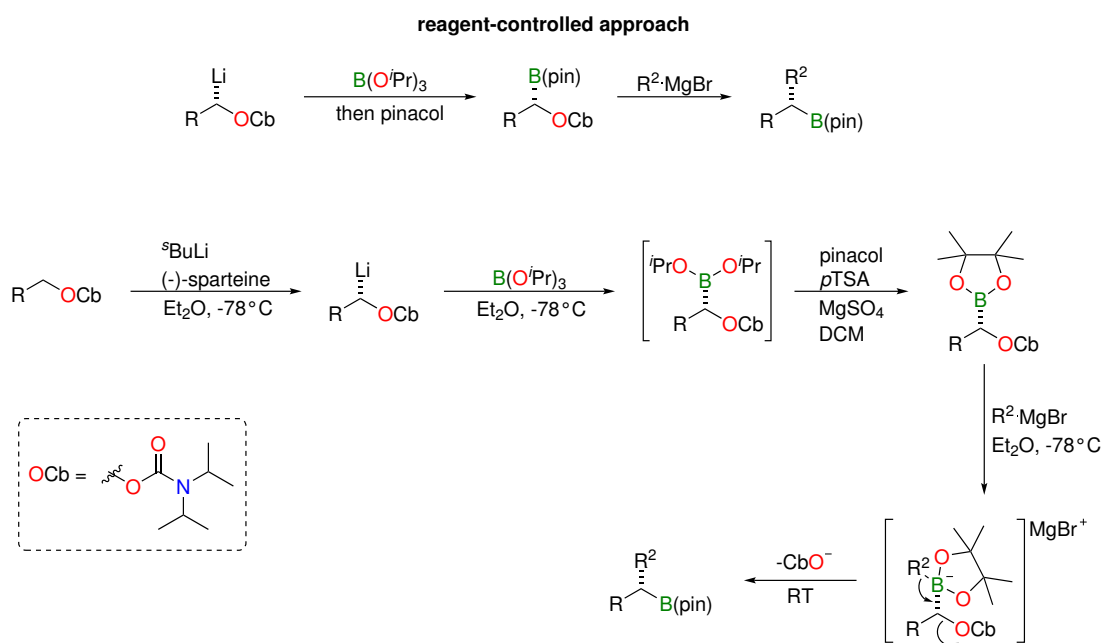


Figure 4.2: Matteson's two step homologation on general substrates

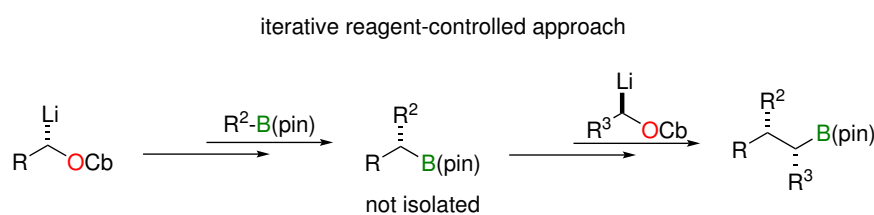
Even though *Matteson's* homologation is a powerful approach in controlling the stereochemical outcome, its poor versatility and feasibility make it a limited strategy. In particular, the stereochemistry of the product is steered by the stereochemistry of the auxiliary diol embedded in the boronic ester and to obtain the opposite stereoisomer product is necessary to employ the opposite chiral diol, a manipulation that is not always viable.<sup>304</sup>

An alternative approach involves to move the chiral information from the boronic esters to

the metal carbenoid reagent to construct the related "ate" complex in enantioselective manner which follows the previously presented 1,2-metallate rearrangement providing the expected chiral boronic ester (**reagent-controlled**). *Hoppe* reported the enantioenriched preparation of lithiated carbamates containing all the features necessary for stereocontrolled homologation of boronic esters (Figure 4.3). Moreover, *Hoppe* showed as the homologation sequence proceeds through two key steps involving chiral lithiated carbamates trapped by  $B(O^iPr)_3$ , successively converted into the stable pinacol boronic esters, analogue of the *Matteson's*  $\alpha$ -chloro boronic ester, and 1,2-metallate rearrangement upon treatment with a Grignard reagent to give the expected product with exquisite stereocontrol.



At the same time, *Aggarwal*<sup>305</sup> and *Kocienski*<sup>306</sup> showed that this type of homologation could proceed by means of in situ reaction between a lithiated carbamate and a pinacol boronic ester, a reaction now usually referred as **lithiation-borylation** (Figure 4.4). In addition, *Aggarwal* demonstrated how this process could be employed in iterative manner in the synthesis of complex molecules containing contiguous stereocenters.<sup>104</sup>



It is possible to identify three main steps in lithiation-borylation processes. The first is the chiral  $\alpha$ -lithiation of a carbamate (OCb) or a hindered benzoate (OTIB). These intermediates have to be obtained in high yield, selectivity and it should be both chemically and configurationally stable under the reaction conditions to avoid decomposition and racemisation.

The second step is the formation of chiral boronate complex by means of an electrophilic trapping. This process has to be absolutely stereospecific (usually with retention of configuration) and faster than the following rearrangement.

Finally, the formation of homologate organoboron intermediate occurs immediately after a 1,2-metallate rearrangement. The *anti* relative arrangement between boron and the leaving group is required for the success of the process and it has to be carried out at higher temperature than the borylation step in order to avoid over-homologations.

The main aspect that it is necessary to highlight is that the organoboron intermediate can undergo other lithiation-borylation cycles in order to elongate the stereodefined chain (Figure 4.5).

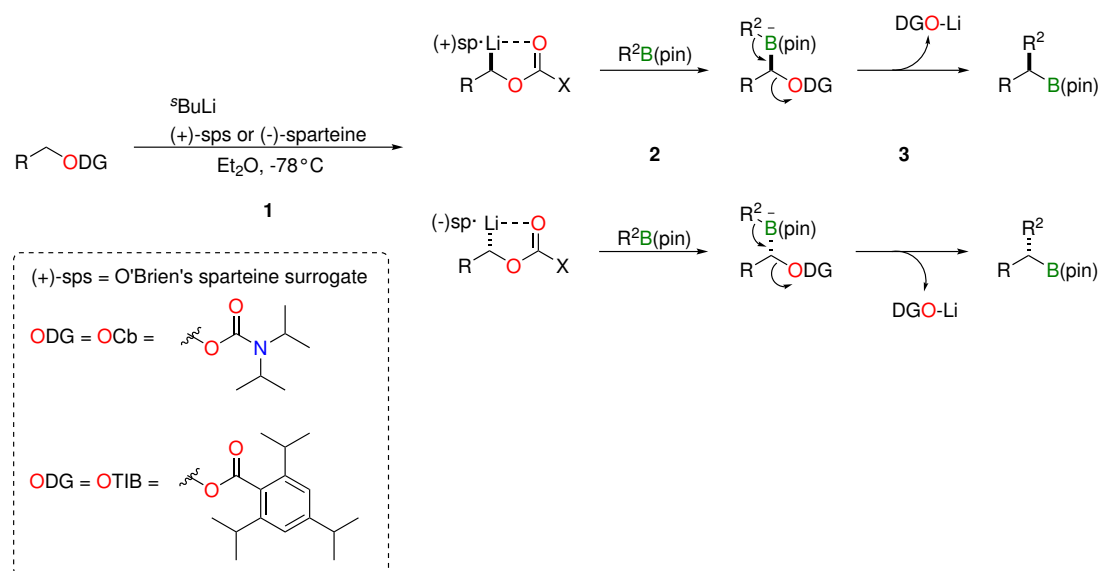
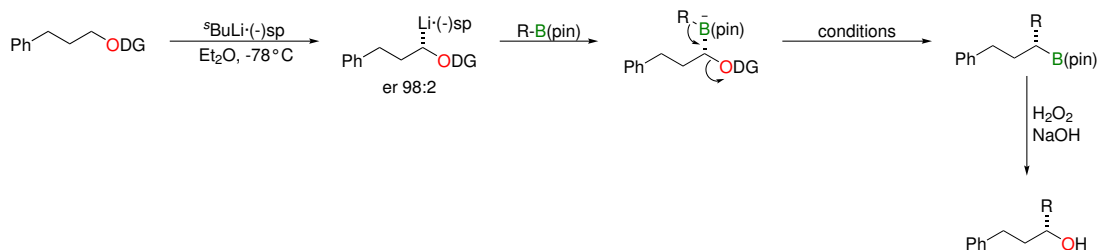


Figure 4.5: Three fundamental steps of the Lithiation-Borylation process

Moreover, during their studies *Aggarwal* and coworkers observed that a combination of steric and electronic effects could reduce the rate of 1,2-metallate rearrangement in the presence of carbamate as leaving-group. In these cases, the process required the addition of a weak Lewis acid ( $\text{MgBr}_2$ ) to yield the product. In particular, boronic esters bearing a migrating methyl group showed a low rate in this rearrangement due to the high energy of the C-B bond, while boronic esters bearing  $\beta$ -EWG [e.g.  $(\text{CH}_2)_2\text{CN}$ ] exhibited the same behaviour due to a decreased nucleophilicity.<sup>307</sup> Inspired by *Beak's* work, *Aggarwal* identified the 2,4,6-triisopropyl benzoates (TIB ester) as a suitable leaving group to overcome the encountered pitfall. After showing that the *Beak's* deprotonation could be carried out in enantioselective way replacing TMEDA with (-)-sparteine, *Aggarwal* and coworkers demonstrated that the

1,2-metallate rearrangement could be accelerated employing this hindered benzoate instead of carbamate. In this manner, the scope of the homologation through lithiation-borylation was significantly expanded including substrates not accessible before and improving the yields avoiding the use of Lewis acid (Table 4.1).



ODG	R	T/°C, time/h	Lewis acid	Yield/%	er <sup>a</sup>
OCb	Ph	reflux, 16	MgBr <sub>2</sub>	90	97:3
OTIB	Ph	reflux, 2	-	79	96:4
OCb	Me	reflux, 16	MgBr <sub>2</sub>	50	95:5
OTIB	Me	reflux, 2	-	76	96:4
OCb	(CH <sub>2</sub> ) <sub>2</sub> CN	reflux, 16	MgBr <sub>2</sub>	0	nd
OTIB	(CH <sub>2</sub> ) <sub>2</sub> CN	reflux, 2	-	46	97:3

<sup>a</sup>er obtained from the corresponding alcohol after oxidation of boronic ester product

**Table 4.1:** Comparison between 1,2-metallate rearrangement on boronates bearing OCb and OTIB as leaving group.

As mentioned before, inspired by the way the nature assembles natural products, *Aggarwal* explored the opportunity to not stop the lithiation-borylation at the first cycle, but to carry on the growth of a stereodefined complex molecule in iterative fashion. His approach, termed **assembly-line synthesis (ALS)**, has all the features that we can find in a natural assembly-line (such as the polyketide synthase) paving the way to the easy introduction of many structural variations in molecular structure.<sup>308</sup>

It is noteworthy that, for a high-performance iterative process, it is fundamental to carry out each iteration with almost perfect diastereocontrol and conversion, in order to avoid a complex mixture of products (Figure 4.6).

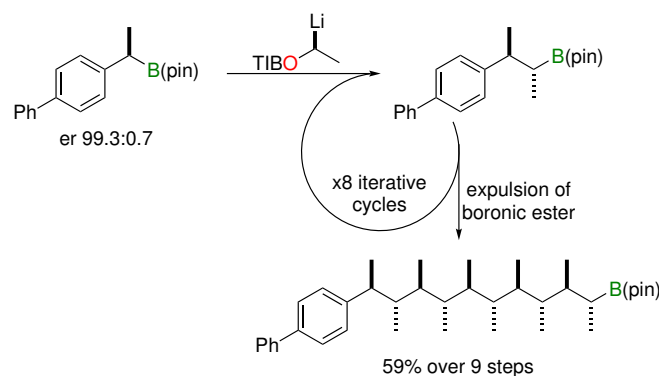


**Figure 4.6:** Assembly-line synthesis(ALS).

To reach this purpose, reagents must be available in enantiopure forms since mixture of enantiomers produces mixture of diastereomers, exacerbating the problem step by step during the synthesis. With the same relevance, it is fundamental to prevent under-homologation by means of complete boronate complex formation and to avoid over-homologation through the decomposition of any excess of carbenoid before the migration step.<sup>308</sup>

#### 4.1.2 Stereocontrolled Synthesis of 1,3-diols

As previously mentioned, boronic esters can be converted in a wide range of functional groups behaving as a mask for following derivatisations. Combining this information with the solid results obtained with assembly-line synthesis, *Aggarwal* focused his attention on the synthesis of molecules containing 1,3-hydroxy moieties due to their presence in many natural products, particularly secondary-secondary and secondary-tertiary 1,3-diols.<sup>309</sup> These scaffolds are easily prepared using ordinary chemistry (such as aldol reactions); however, they can not be prepared from boronic esters with an electronegative group in the beta position since the boronate intermediate employed in the building up of the 1,3-diol can follow two different pathways: the desired 1,2-migration or the undesired  $\beta$ -elimination (Figure 4.7).

To overcome this drawback, it was necessary to change the point of view on the hydroxyl group precursors. Since  $\beta$ -boronic esters do not undergo competitive elimination and boronic ester can stereospecifically be oxidised to the corresponding alcohol, *Aggarwal* and coworkers decided to introduce a second boronic ester for masking the  $\beta$ -alkoxy group. To follow this strategy, the required 1,2-bis(boronic esters) were readily available by means of *Morken/Nishiyama* asymmetric diboration of terminal alkenes.<sup>310–312</sup> Once obtained the vicinal bis(boronic ester) it is fundamental to identify regioselective and stereoselective conditions to homologate this intermediate for the synthesis of more complex molecules. Combining *Morken/Nishiyama* diboration and lithiation-borylation, *Aggarwal's* group developed a selective homologation at the less hindered primary boronic ester to pre-

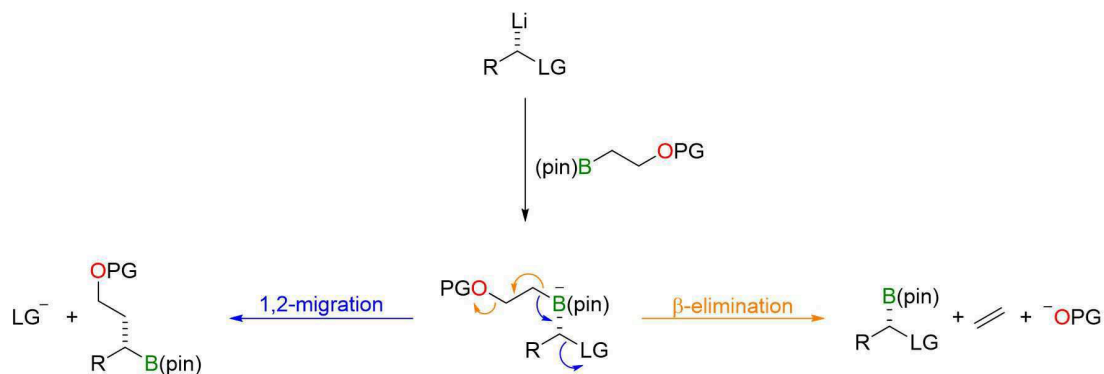


Figure 4.7: Competition between 1,2-metallate rearrangement and  $\beta$ -elimination.

pare 1,3-bis(boronic esters) which can be oxidised at the late stage of the synthetic pathway by using  $H_2O_2/NaOH$  to reveal the target 1,3-diols (Figure 4.8).

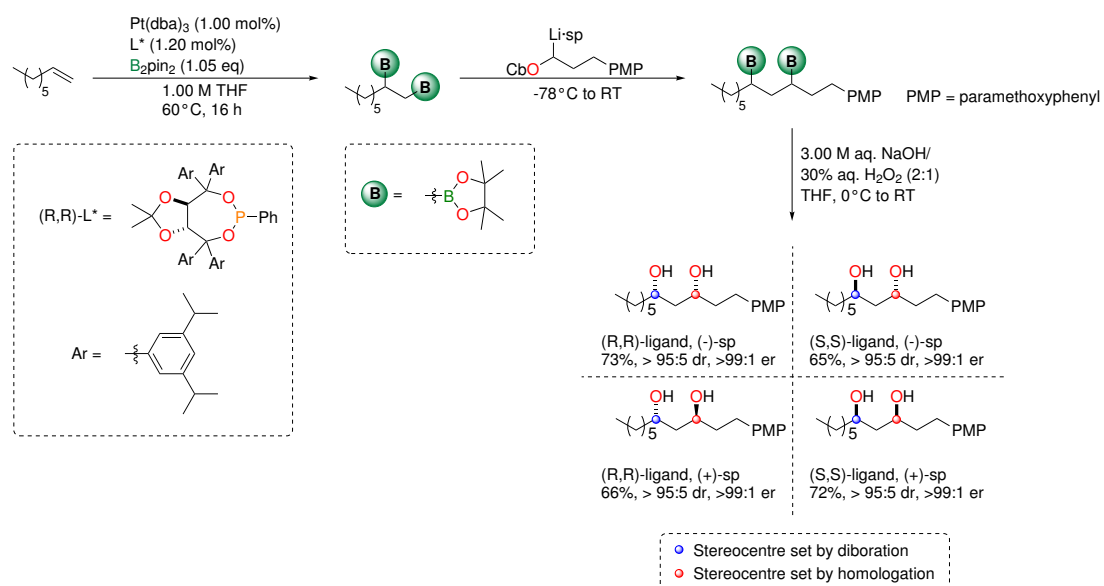
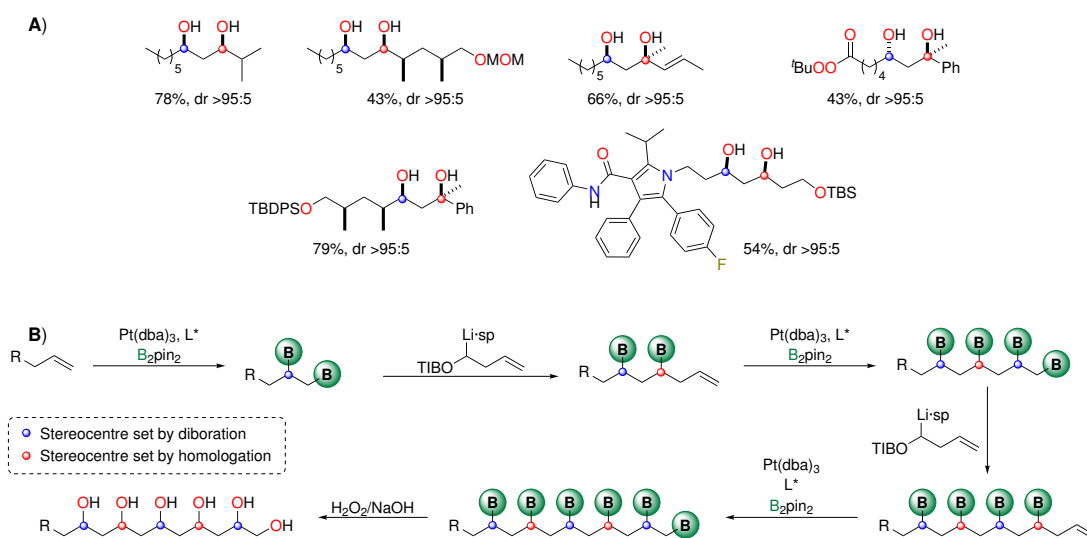


Figure 4.8: Morken asymmetric diboration/lithiation-borylation for stereocontrolled synthesis of 1,3-diols.

Even if the regioselectivity of the homologation step might seem quite predictable, *Aggarwal* and coworkers highlighted a fundamental key point. The competitive reactivity of primary/secondary boronic esters was critically dependent on the nature of the carbenoid. In fact, using less hindered lithiated nucleophiles (either diamine-free or TMEDA-ligated lithiated carbamate or benzoate, or chloro methyl carbenoid) they observed a mixture of starting materials, homologated and over-homologated products. This pitfall was overcome employing the suitable (+)- or (-)-sparteine-ligated lithiated carbenoid or benzoate as nucleophiles, achieving higher regioselectivity for the primary boronic ester over secondary ones.<sup>309</sup> With this knowledge in hand, *Aggarwal's* group prepared the four possible diol isomers setting the stereochemistry of the stereocenter obtained in the diboration step through the proper

enantiomer of the metal ligand, while the stereochemistry of the stereocentre obtained in the lithiation-borylation step was set by changing from (+)- to (-)-sparteine, operating exclusively under reagent control. In all cases, the diols were obtained with the same high diastereo- and enantioselectivity and with comparable yields, highlighting that no matched or mismatched effects occur in the developed synthetic strategy.

The *Morken*-diboration/lithiation-borylation strategy was thus applied for the synthesis of many compounds bearing diol moiety (A in Figure 4.9), but the most attractive goal was the proposed merging of this process with the assembly-line synthesis.



**Figure 4.9:** A) Selected compounds bearing 1,3-diol synthesised using *Aggarwal's* procedure; B) Application of assembly-line synthesis to the preparation of a 1,3-polyol generic compound.

Following this idea, they had access to stereodefined 1,3-polyols employing homoallylic benzoate as nucleophile and avoiding protection/deprotection steps since the stereospecific oxidation of boronic esters can reveal the desired hydroxy functionality (B in Figure 4.9).<sup>309</sup>

#### 4.1.3 Development of New $\alpha$ -Sulfinyl Benzoates as Carbenoid Precursors

Since there was a changing of paradigm in the homologation of boronic esters from a substrate-controlled to a reagent-controlled approach, the synthesis of bench stable carbenoid precursors arised as a crucial necessity. This species should be endowed with certain peculiarities: a) high enantiopurity (if possible, >99:1); b) a substituent that can rapidly and stereospecifically undergo transmetalation (typically with Li or Mg), and c) a suitable leaving group. Furthermore, the entire process has to follow several conditions. In particular, the stereospecific metallation must occur under reaction conditions maintaining high chemical and configurational stability provided by carbenoid precursor; then, the metal-borylation exchange should undergo irreversibly and stereospecifically in quantitative yields using a boronic ester as limiting reactant. Furthermore, the invertive 1,2-metallate rearrangement



has to take place with exquisite stereocontrol and at higher temperature in order to decompose the excess of carbenoid, avoiding overhomologation. Finally, the product should be efficiently isolated for further transformations, or byproduct be quite inactive to allow further homologations in one-pot procedure.<sup>313</sup>

In 2014, *Aggarwal* reported the development of  $\alpha$ -stannyl ethyl benzoate as a bench-stable carbenoid precursor for the assembly-line synthesis of contiguous polymethyl hydrocarbons (Figure 4.6).<sup>308</sup> This precursor could be obtained in very high levels of enantiopurity (er >99.9:0.01) through sparteine-mediated asymmetric metallation of the corresponding ester followed by electrophilic trapping with  $\text{Me}_3\text{SnCl}$ , and then recrystallisation from methanol (Figure 4.10).

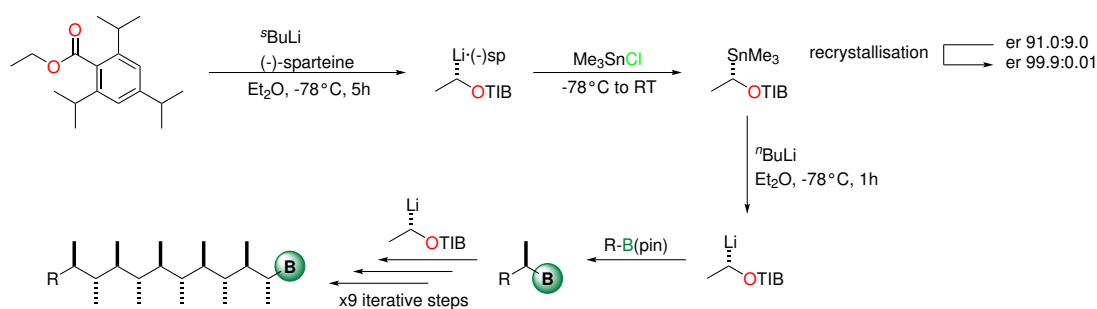
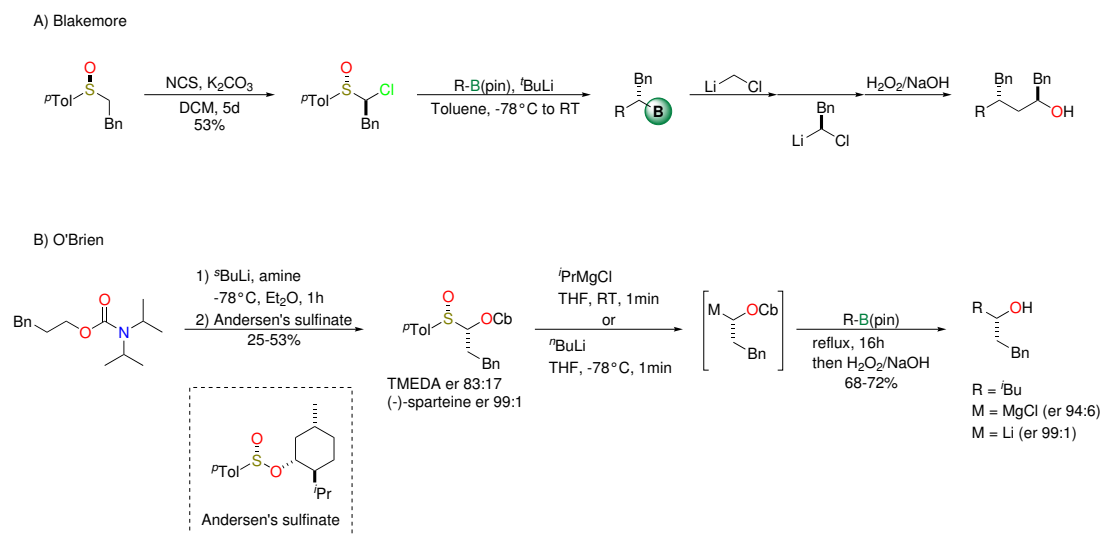


Figure 4.10:  $\alpha$ -stannyl ethyl benzoate synthesis and its application in assembly-line synthesis.

However, several drawbacks were related with the use of these carbenoid precursors; in particular, the toxicity of  $\text{Me}_3\text{SnCl}$  required for their synthesis hinders its approval by the scientific community and only the methyl-substituted precursors are crystalline, making difficult the preparation of other derivatives in high levels of enantiopurity.<sup>314</sup>

Inspired by *Blakemore's* and *O'Brien's* homologations, *Aggarwal* investigated the possibility to use  $\alpha$ -sulfinyl benzoates as building blocks in assembly-line synthesis.<sup>315,316</sup> In fact, *Blakemore* had already demonstrated the feasibility of an  $\alpha$ -chloro sulfoxide as carbenoid precursors in a homologation reaction even if, together with a lower toxicity than corresponding stannyl derivatives, a series of side-reactions were observed (A in Figure 4.11).<sup>317</sup> On the other hand, *O'Brien* changed the perspective for the sulfinyl intermediate preparation; in particular, he discovered that treating an enantioenriched lithiated carbamate (obtained using a chiral nonracemic sparteine or 1,2-diaminocyclohexane derivative) with an enantiomerically pure Andersen's menthol-derived sulfinate, only one diastereomer was synthesised with high levels of stereoselectivity (B in Figure 4.11).<sup>316</sup>



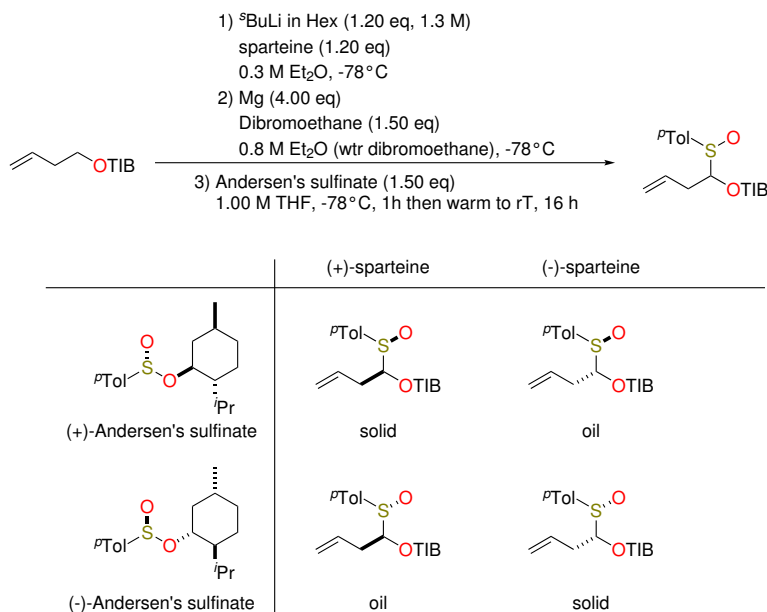
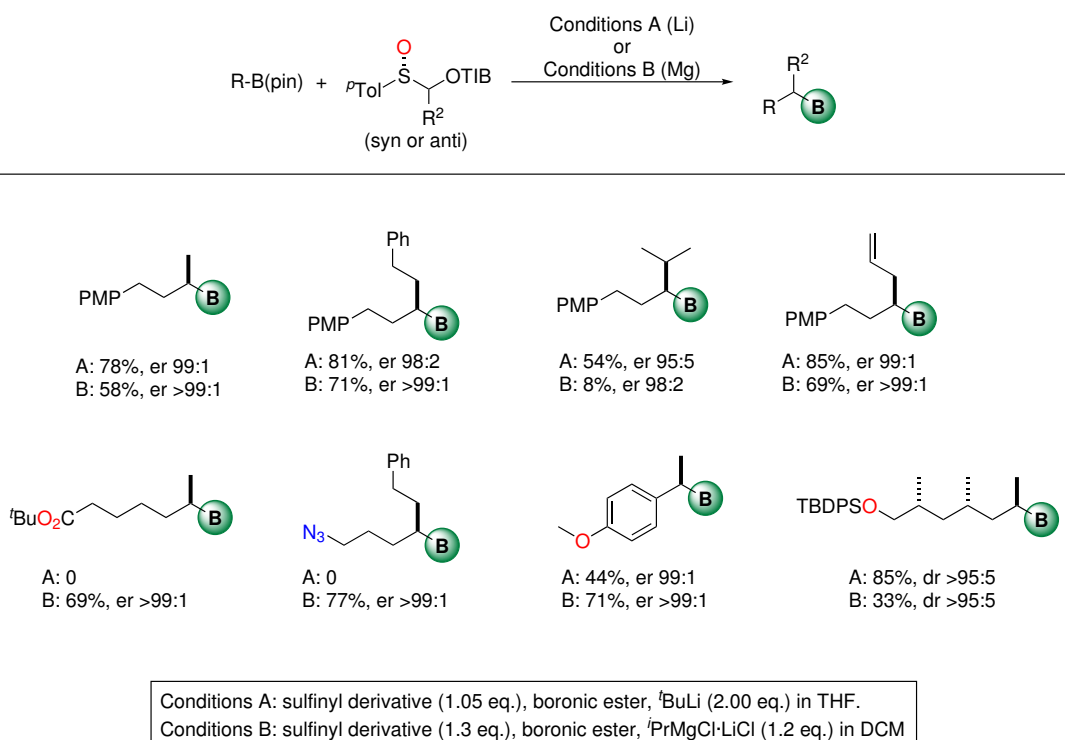
**Figure 4.11:** Synthesis of A) *Blakemore's*  $\alpha$ -sulfinyl chloride and B) *O'Brien*  $\alpha$ -sulfinyl carbamate applied to a homology reaction.

In order to use the acquired knowledge on the benzoate carbenoids,<sup>104</sup> *Aggarwal* and coworkers developed an  $\alpha$ -sulfinyl benzoate carbenoid precursor starting from the corresponding alkyl benzoate which underwent an asymmetric deprotonation with sparteine-ligated  $t\text{BuLi}$ , followed by transmetalation with  $\text{MgBr}_2 \cdot \text{Et}_2\text{O}$  and finally trapping with Andersen's sulfinate.<sup>313</sup> The  $\alpha$ -sulfinyl benzoate diastereomers (whose minor enantiomer derives from lithiation step) thus obtained were isolated through column chromatography with exquisite levels of enantiopurity, in which the stereocontrol was set by the suitable choice of the (+) or (-)-Andersen's sulfinate (Figure 4.12).

Moreover, moving from an achiral diamine (e.g. TMEDA) to a chiral one (e.g. sparteine) it was possible to set the carbenoid carbon stereochemistry, as well. In particular, with the proper choice of both Andersen's sulfinate and sparteine ligand, *Aggarwal's* group could selectively prepare all four possible  $\alpha$ -sulfinyl benzoate isomers with high er (typically >99:1), as an oil or a solid.

Successively, they investigated  $\alpha$ -sulfinyl benzoate effectiveness as carbenoid precursor for the homology of boronic esters using both  $t\text{BuLi}$  and  $i\text{PrMgCl} \cdot \text{LiCl}$  for metal exchange. Focusing their attention on sulfoxide-Li exchange step, they developed a *Barbier*-type conditions reaction in which the addition of  $t\text{BuLi}$  (2.00 eq) to a solution of  $\alpha$ -sulfinyl benzoate (1.05 eq) and boronic ester in THF at  $-78^\circ\text{C}$ , then warmed up to room temperature delivered the desired product in good yields and very high enantiomeric excess (Conditions A, Figure 4.13).

On the other hand, the sulfoxide-Mg exchange step was optimised adding boronic ester to a solution of  $\alpha$ -sulfinyl benzoate (1.30 eq) and  $i\text{PrMgCl} \cdot \text{LiCl}$  in DCM at  $-78^\circ\text{C}$ , leading to desired homologated boronic ester with almost perfect stereocontrol; in this case, employing *Barbier*-

Figure 4.12: Synthesis of all four possible  $\alpha$ -sulfinyl benzoate isomers.Figure 4.13: Homologation of boronic esters with carbenoids derived from  $\alpha$ -sulfinyl benzoates using two different conditions.

type conditions none improvement was obtained (Conditions B, Figure 4.13). As depicted in Figure 4.13, the obtained results highlighted that hindered carbon-carbon bonds were obtained in higher yields when using lithium carbenoids, whereas boronic ester bearing electrophilic functional groups required magnesium carbenoids probably because the organo-

lithium species reacted faster with these groups than the sulfoxide-metal exchange. To overcome potential pitfalls deriving from a slow sulfoxide-Li exchange or an internal quenching of the carbenoid, *Aggarwal* and coworkers<sup>313</sup> developed an improved procedure adding the sterically bulky tridentate amine PMDTA (N,N,N',N',N'',N''-pentamethyldiethylenetriamine).

## 4.2 Mycapolyol A

One of the major sources of bioactive compounds is still the plant kingdom. Among the thousands of plants, sponges are certainly among the most prolific ones; for instance, a variety of bioactive metabolites have been isolated from marine sponges of the genus *Mycale*, including nitrogen-containing polyketides,<sup>102</sup> terpenoid peroxides<sup>318</sup> and nucleosides.<sup>319</sup> In particular, polyketides highlighted highly specific and potent biological activity. Further investigation on the marine sponge *Mycale izuensis*, collected in the Amakusa Islands (southwest of Japan), have led to the isolation of six unusual polyketide synthase metabolites named **Mycapolyols A-F** which exhibited cytotoxicity against HeLa cells ( $IC_{50} = 0.06 \pm 0.90 \mu\text{g/mL}$ ) (Figure 4.14).

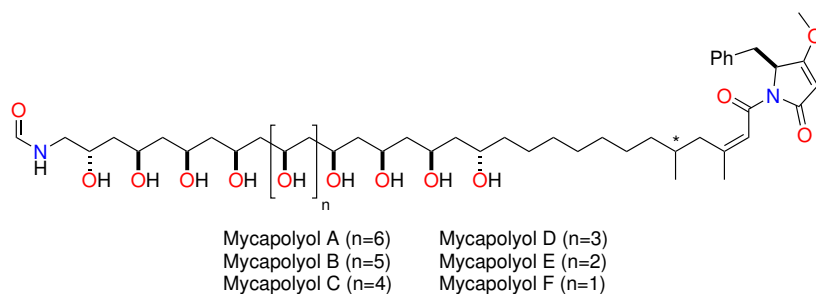


Figure 4.14: Mycapolyol A-F.

Even though a structural characterisation of Mycapolyols A-F was elucidated in 2005 by *Fusetani* and coworkers,<sup>103</sup> there are no reported syntheses of any mycapolyols in the literature to date. For this reason, and since the assembly-line synthesis has proven to be easily applicable for the preparation of 1,3-polyol scaffolds, *Aggarwal* identified **Mycapolyol A** as an attractive challenge for his iterative processes.

As depicted in Figure 4.15, they developed a retrosynthetic approach involving an iterative sequence diboration/homologation already presented in the previous section. This choice allows to avoid the addition of protection/deprotection steps and since both key reactions are carried out with high levels of enantiopurity, this synthesis provides the final 1,3-polyol with high levels of stereocontrol.

In particular, the first step involved the protection of both 1,3-polyol and formamide moiety using acetonide and trityl chloride, respectively. Successively, the disconnection of pyrrole-2,4-dione revealed  $\alpha,\beta$ -unsaturated carboxylic acid which was then reduced and protected using TBS. Finally, the 1,3-hydroxyl functionalities in the polyol chain were masked as pina-

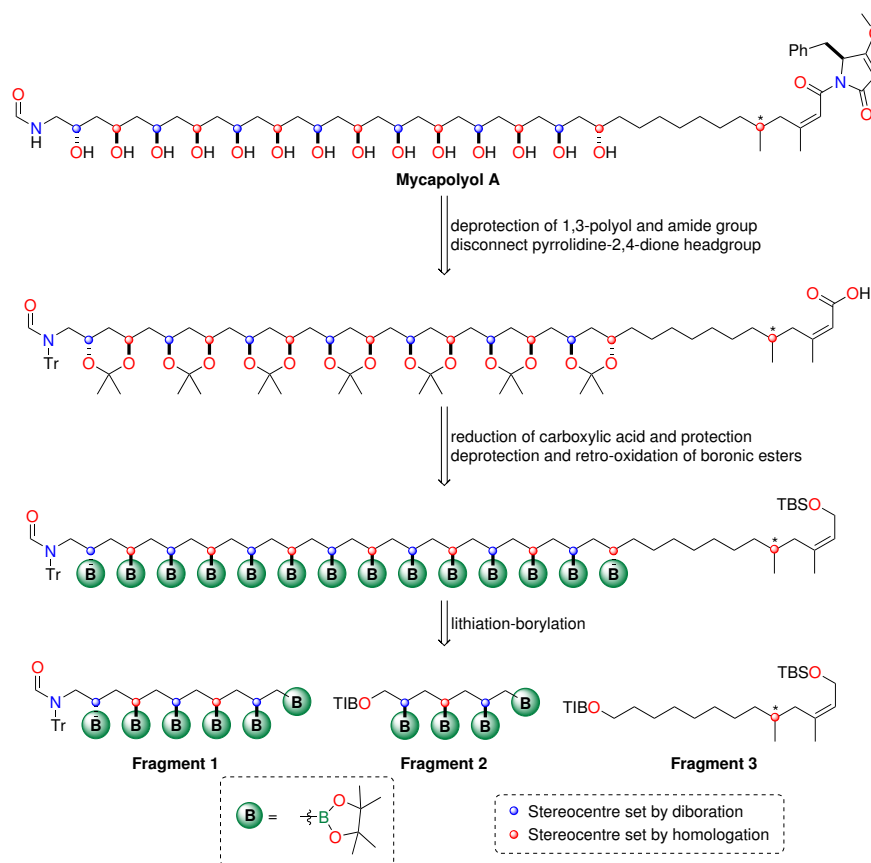


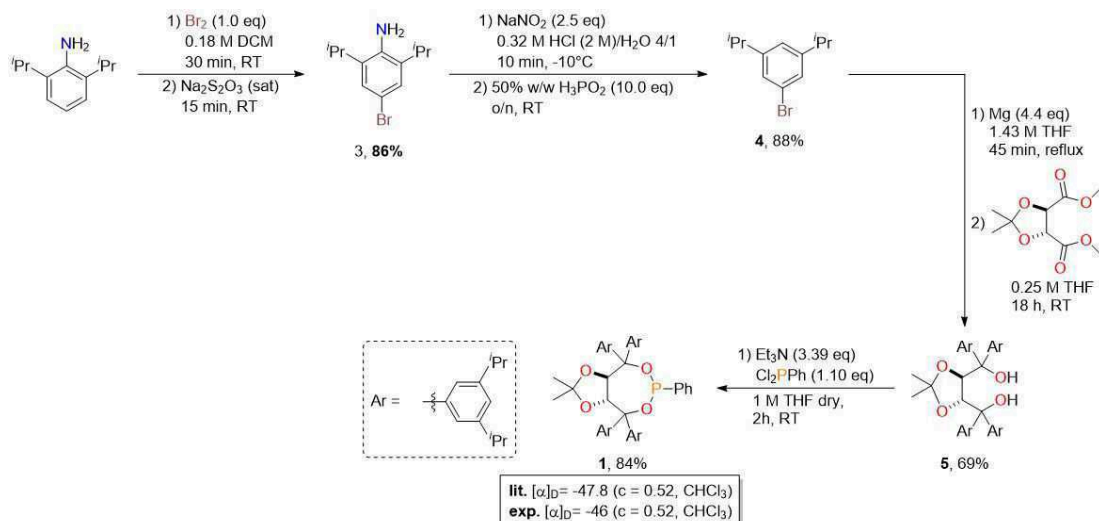
Figure 4.15: Retrosynthetic approach for the synthesis of Mycapolyol A.

col boronic esters and disconnected into three different fragments.

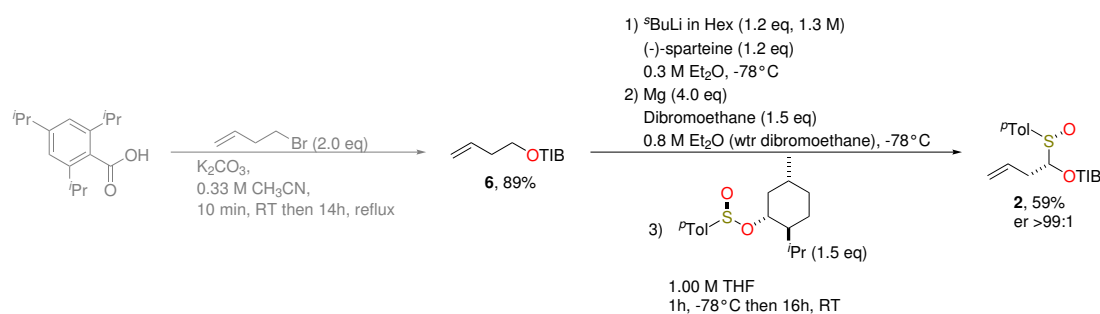
Following the proposed retrosynthetic strategy, mycapolyol A was synthesised employing a modular approach in which fragments 1, 2 and 3 were prepared separately and coupled together, at the end.

Since this assembly-line synthesis is mainly based on *Morken's* diboration and primary boronic ester homologation, before continuing with the synthesis of each fragment, the preparation of ligand 1 and  $\alpha$ -sulfinyl benzoate 2 will be presented.

First of all, 2,6-diisopropyl aniline was brominated and successively reduced to 3,5-diisopropylbromobenzene 4 (76% yield, 2 steps) in order to obtain the substrate for the synthesis of the suitable Grignard reagent. In situ preparation of the Grignard reagent was followed by the double addition on each ester group of tartrate derivative providing the intermediate 5 in good yield (69%). Finally, the addition of  $\text{Cl}_2\text{PPh}$  to the (*R,R*)-diol 5 allowed the synthesis of desired ligand whose stereochemistry was verified by comparing its  $[\alpha]_D$  with that reported in the literature (for the synthesis of the (*S,S*)-ligand the opposite enantiomer of the tartrate was required) (Scheme 4.1).<sup>320,321</sup>

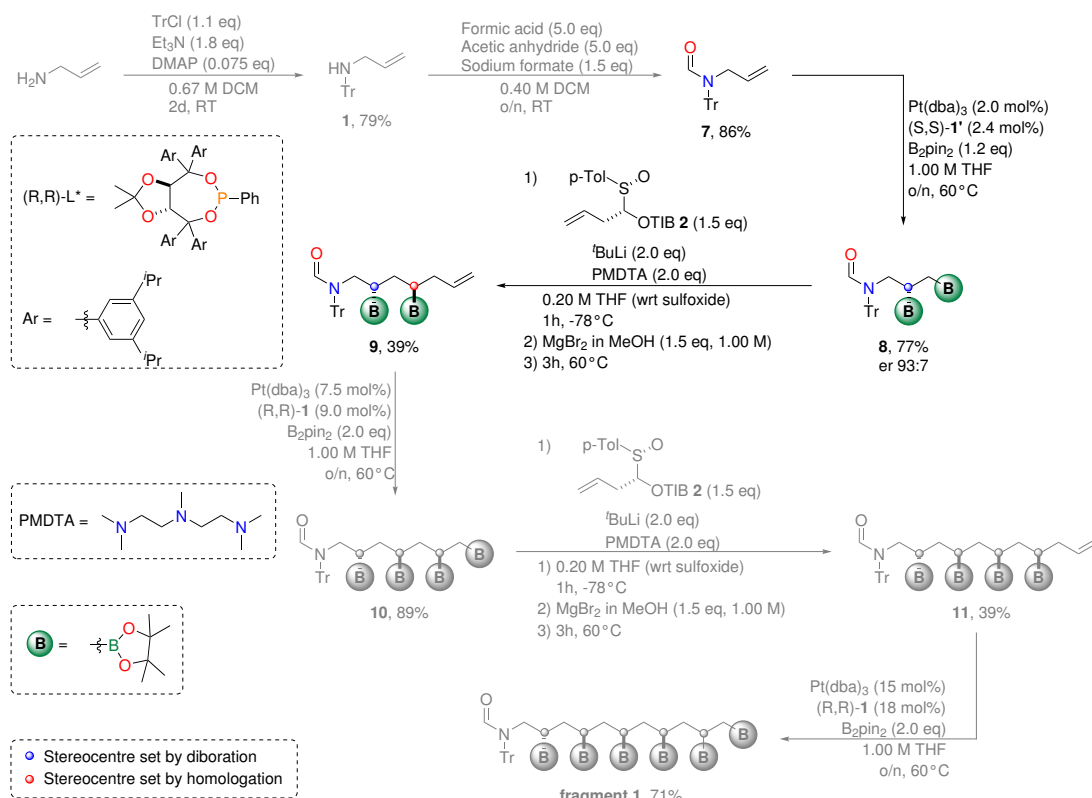
Scheme 4.1: Synthesis of the ligand for *Morcken's* diboration.

On the other hand, the optimisation of the synthesis of  $\alpha$ -sulfinyl benzoate was already discussed in this Chapter (see 4.1.3) therefore the procedure for the preparation of the homoallylic  $\alpha$ -sulfinyl benzoate required in several stages of the iterative homologation-diboration strategy is reported herein. First of all, bulky homoallylic ester **6** was prepared in gram scale from the corresponding bromide; then, the proper choice of the sparteine enantiomer during the lithiation of homoallylic benzoate **6** set the stereochemistry at the metallation center, as previously mentioned. The addition of freshly prepared  $\text{MgBr}_2 \cdot \text{Et}_2\text{O}$  led to the Mg carbenoid and subsequent sulfinylation of the  $\alpha$ -magnesiated precursor afforded the desired  $\alpha$ -sulfinyl benzoate **2** in good yield (59%) (Scheme 4.2).

Scheme 4.2: Synthesis of homoallylic  $\alpha$ -sulfinyl benzoate **2**. N.B.: synthetic steps in grey were carried out by researchers of *Aggarwal's* group.

For our purpose, the lithiation of the homoallylic benzoate **6** was carried out using (-)-sparteine, while the sulfinylation was obtained using (-)-Andersen's sulfinate and the desired  $\alpha$ -sulfinyl benzoate **2** was achieved in high enantiopurity (er >99:1).

The synthesis of **fragment 1** was started from compound **7** previously prepared by researchers of *Aggarwal's* group through a protection and formylation steps (68%, 2 steps) (Scheme 4.3).



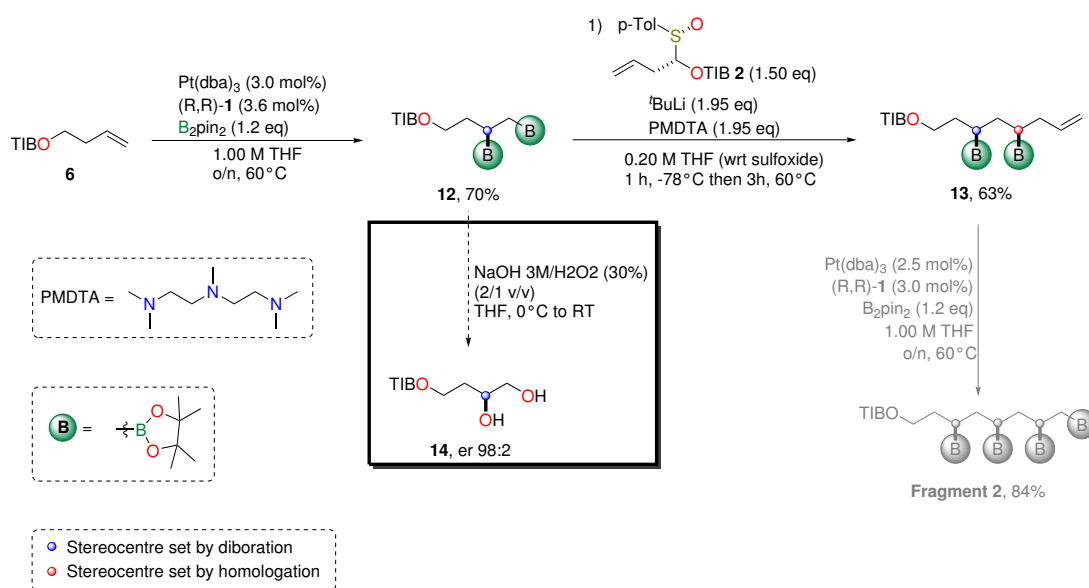
Scheme 4.3: Synthesis of fragment 1. N.B.: synthetic steps in grey were carried out by researchers of Aggarwal's group.

On this substrate, a *Morcken* diboration reaction was carried out in order to obtain compound **8** in good yield and er (77%, er 93:7); successively, diboronic ester **8** underwent homology step with  $\alpha$ -sulfinyl benzoate **2** providing homologated intermediate **9** in good yield as well (39%).

Compared to the previously discussed homology reactions (see 4.1.3), compound **9** required an enhanced amount of  $\alpha$ -sulfinyl benzoate reagent (1.50 eq vs 1.05 eq) and the addition of  $\text{MgBr}_2$  in order to improve the yield, supporting the 1,2-metallate rearrangement unfavored by hindrance of the system. The next three steps followed the assembly-line synthesis concept, involving a diboration, a homology using again compound **2** and a latest diboration providing the desired product in 25% yield over 3 steps (Scheme 4.3). It is noteworthy the need to enhance the catalytic loading in the diboration reactions (from  $\text{Pt(dba)}_3$  2 mol% to 15 mol%) for more electron deficient alkenes.

Also for the synthesis of **fragment 2** an iterative diboration/homology strategy was followed. The homoallylic  $\alpha$ -sulfinyl benzoate **2** (synthesis depicted in Scheme 4.2) was subjected to *Morcken*'s diboration to give bis(boronic ester) **12** in good yield (70%). In order to verify the stereoselectivity of this step, the intermediate **12** were oxidised to the corresponding diol **14** and analysed by chiral HPLC. The data highlighted as this specific batch

of ligand required to enhance the catalyst loading (from 1.00 mol% to 3.00 mol%) to obtain the high enantioselectivity usually achieved (er 98:2) (Scheme 4.4).



Scheme 4.4: Synthesis of fragment 2. N.B.: synthetic steps in grey were carried out by researchers of Aggarwal's group.

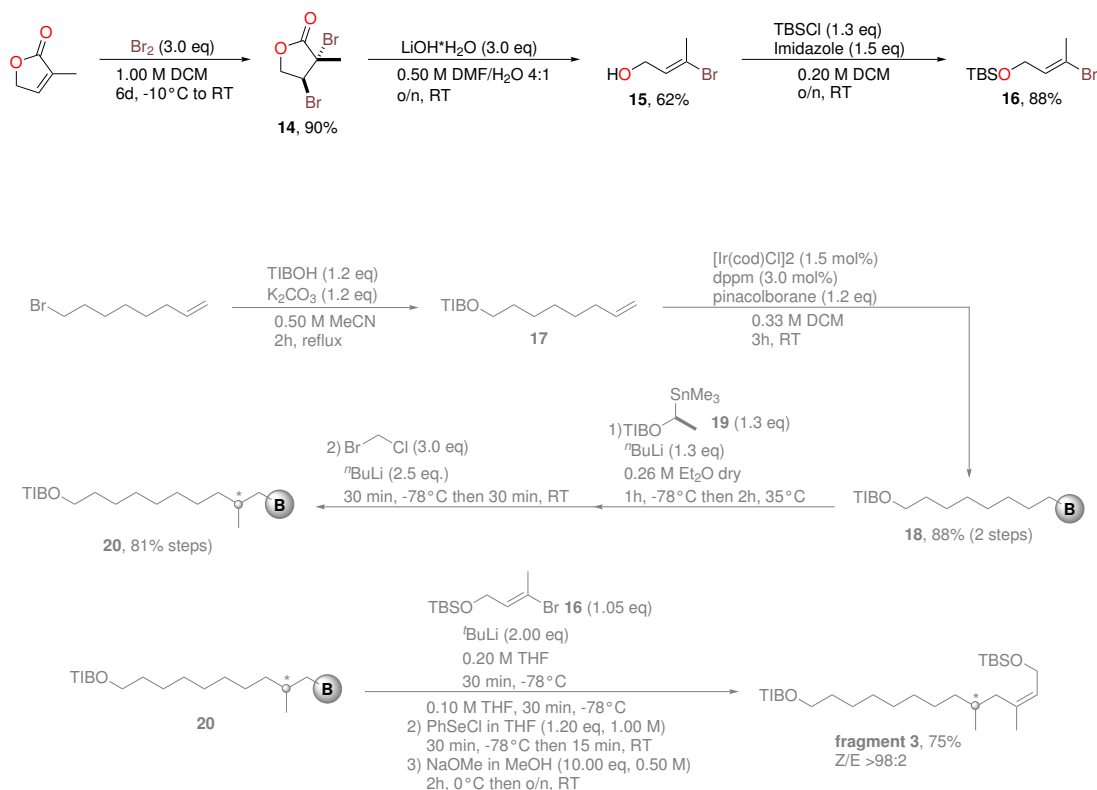
Subsequent optimised homologation with  $\alpha$ -sulfinyl benzoate 2 was carried out on intermediate 12 providing the homologated bis(boronic ester) 13. Finally, compound 13 was subjected to a last *Morken's* diboration in order to synthesise the desired **fragment 2** whose conditions were optimised by *Aggarwal* and coworkers.

The synthesis of **fragment 3** was divided in two parts: the former was the synthesis of the (*E*)-vinyl bromide 16, while the second was the preparation of the primary boronic ester 20; at the end, this two subfragments were coupled together yielding the desired product (Scheme 4.5).

The application of the (*E*)-vinyl bromide was developed by researchers of *Aggarwal* and coworkers<sup>322</sup> in order to optimise the subsequent *Zweifel's* olefination step due to some troubles encountered in the initial reaction performed on (*Z*)-alkene. First of all, 3-methyl butanolide was brominated to intermediate 14 which was subjected to decarboxylative debromination reaction providing in the first trial compound 15 in low yield. This setback was probably caused by the high volatility of this intermediate; in fact, this synthetic step was optimised reaching 62% of yield. Finally, the protection of the allylic alcohol was achieved using TBSCl as silylating agent, affording the desired product 16 (Scheme 4.5).

On the other hand, the synthesis of boronic ester 20 was started from the conversion of 8-Bromo-oct-1-ene into TIB ester following the same procedure used for the synthesis of compound 6; subsequently, this intermediate was subjected to iridium catalysed hydroboration to give compound 18 in 88% yield over 2 steps (Scheme 4.5). Primary boronic ester 18 was then treated with the stannane 19 (to stereospecifically set the methyl group in posi-





Scheme 4.5: Synthesis of fragment 3. N.B.: synthetic steps in grey were carried out by researchers of Aggarwal's group.

tion C5) and bromochloromethane (*Matteson* homologation) carbenoid precursors in a two iterative homologations following the *Aggarwal's* assembly line synthesis procedures. Finally, *Aggarwal's* group optimised the *Zweifel's* olefination between the homologated boronic ester **20** and the (*E*)-vinyl bromide **16** using a bulky silyl chloride protecting group and poorer leaving group (a selenide instead of iodide), reaching good a yield and exquisite Z/E selectivity (75% yield, Z/E >98:2).

*Aggarwal* and coworkers are still working on the optimisation of last steps; however, in order to provide the complete scenario for the total synthesis of Mycapolyol A, in the Figure 4.16 the synthetic strategy they have planned with the support of successful model studies, it is summarily presented.

**Fragment 3** will be subjected to a double sequence of three reactions: 1) a homologation with **fragment 2**, following the already presented procedure; 2) an oxidation of the boronic esters to avoid nucleophilic attack by  $^i\text{BuLi}$  in subsequent homologations, revealing the polyol moiety masked with such groups, and 3) an acetone protection of the polyol intermediate, in order to protect the hydroxyl group from the homologation conditions of the subsequent step. Then, the eight hydroxyl-protected intermediate **21** will be subjected to a last homologation with **Fragment 1**, followed by the oxidation of the six boronic ester

just added and the acetonide protection of the resulting polyol as done previously. The full protected intermediate **22** will be deprotected on the western hydroxy group using TBAF and oxidised previously to aldehyde using *Dess Martin's* reagent, then to carboxylic acid through *Pinnick* oxidation. The ester formation obtained by means of the condensation between intermediate **23** and pentafluorophenol will provide an activated species towards the coupling reaction with pyrrolinone **24**, previously synthesised from N-Boc ethyl ester phenylalanine in three steps. Finally, the simultaneous removal of the trityl and the acetonides protecting groups using TFA will reveal the desired **Mycapolyol A**.

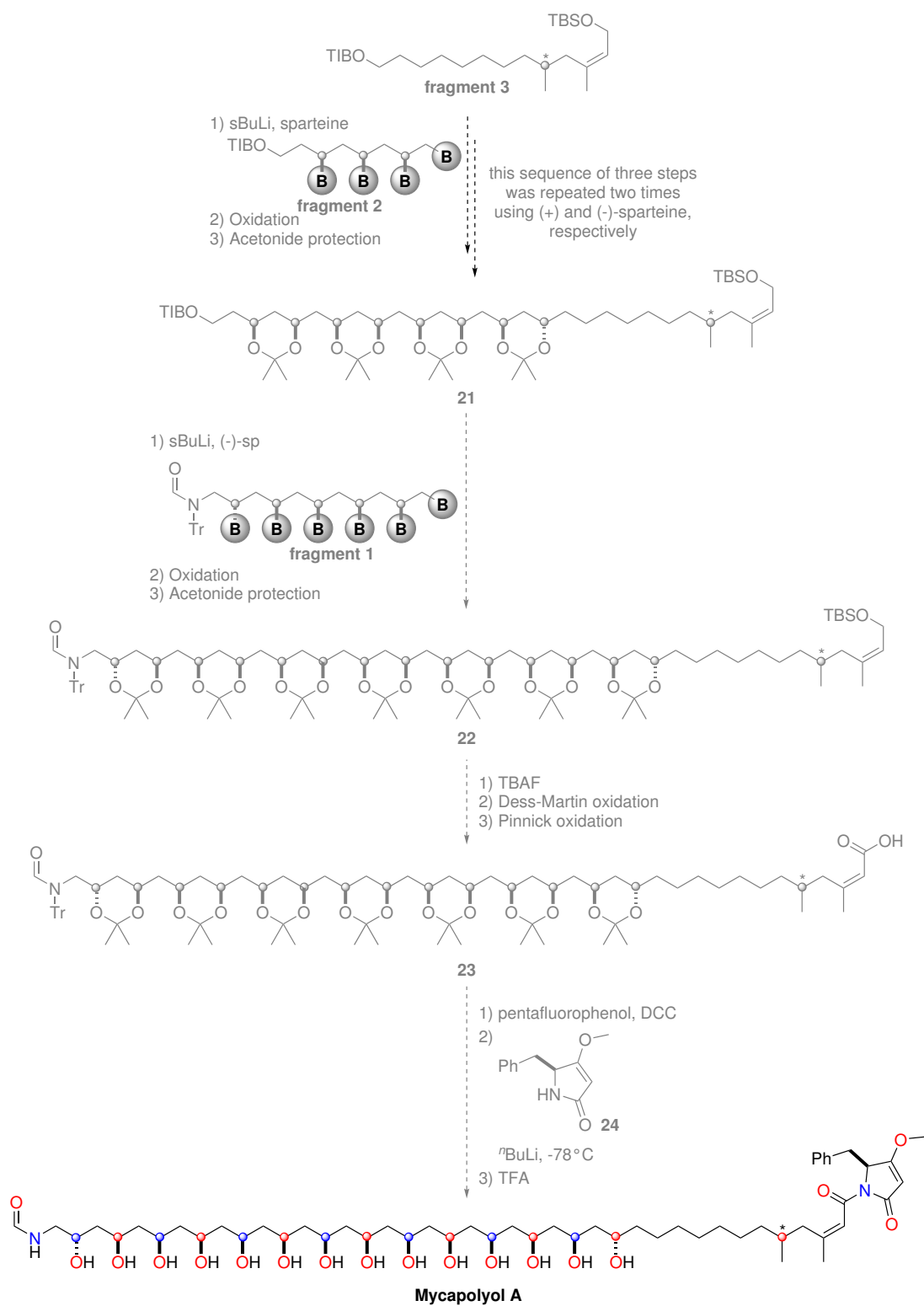


Figure 4.16: Synthetic strategy planned by Aggarwal and coworkers.

### 4.3 Conclusions

*Morken's* asymmetric diboration and *Aggarwal's* lithiation-borylation were merged for the iterative synthesis of the three fragments (**Fragments 1, 2 and 3**) underlying the preparation of **Mycopoliol A**. While asymmetric diboration tended to proceed smoothly according to the literature procedure, *Aggarwal* and coworkers have deeply optimised the homologation step involving allylic  $\alpha$ -sulfinyl benzoate to obtain the stereodefined 1,3-polyol motif into Mycapolyol A. Moreover, owing to the peculiarity of the target material and the synthetic chemistry used to gain such product, other synthetic steps (e.g. *Zeifel's* olefination, the formamide protection) have been further developed.

Regarding the personal objective, or rather, the gram scale synthesis of **Fragments 1, 2, and 3**, it was only partially achieved due to early termination of internship caused by Covid-19 pandemic. Until that moment, compound **9** (Fragment 1 intermediate) was prepared over 1g scale, while compound **13** (Fragment 2 intermediate) and compound **16** (Fragment 3 intermediate) were synthesised in sub gram scale.

### 4.4 Experimental Procedures

#### 4.4.1 General Methods

Reaction mixtures were stirred magnetically. Air- and moisture-sensitive reactions were carried out in flame-dried glassware under a nitrogen atmosphere using standard Schlenk manifold technique. All required fine chemicals were purchased from Acros Organics, Alfa Aesar, Inochem-Frontier Scientific or Sigma-Aldrich and used as received unless otherwise mentioned. *sec*-Butyllithium (<sup>s</sup>BuLi) was received from Acros Organics as a 1.3 M solution in hexanes and *tert*-Butyllithium (<sup>t</sup>BuLi) was received from Sigma Aldrich as a 2.8 M solution in heptane, and the molarity was verified by titration with *N*-benzylbenzamide. 1 M MgBr<sub>2</sub> solutions in MeOH were prepared in advance by adding anhydrous MeOH to solid MgBr<sub>2</sub>. MgBr<sub>2</sub>·Et<sub>2</sub>O was prepared by the slow addition of dibromoethane to magnesium turnings in anhydrous Et<sub>2</sub>O. TMEDA, PMDTA, Et<sub>3</sub>N and TMSCl were distilled over CaH<sub>2</sub> before use. Pinacolborane was distilled before use. (-)-sparteine and (+)-sparteine were isolated from the commercially available sulfate salt following a procedure by Beak. Anhydrous THF, DCM, toluene, hexane, acetonitrile and Et<sub>2</sub>O were obtained by passing commercially available drums of solvent through a modified Grubbs system of alumina columns, manufactured by Anhydrous Engineering, and were transferred under nitrogen via syringes. <sup>1</sup>H Nuclear magnetic resonance (NMR) spectra were recorded in CDCl<sub>2</sub> at 400 or 500 MHz on a Bruker Nano 400, Varian 400-MR or a Bruker Avance III HD 500 Cryo Fourier transform spectrometer. Chemical shifts ( $\delta$ H) are quoted in parts per million (ppm) and referred to the residual proton solvent signals of CHCl<sub>3</sub> (7.26 ppm). <sup>1</sup>H NMR coupling constants are reported in hertz and refer to apparent multiplicities. Data are reported as follows: chemical

shift, multiplicity (s = singlet, br. s = broad singlet, d = doublet, t = triplet, q = quartet, quin = quintet, sext = sextet, sept = septet, m = multiplet, dd = doublet of doublet, etc.), coupling constant, integration, and assignment. Assignment of signals in  $^1\text{H}$  spectra was performed using  $^1\text{H}$ - $^1\text{H}$  COSY,  $^1\text{H}$ - $^{13}\text{C}$  HSQC and  $^1\text{H}$ - $^{13}\text{C}$  HMBC experiments where appropriate.  $^{13}\text{C}$  NMR spectra were recorded at 101 or 126 MHz. Chemical shifts ( $\delta\text{C}$ ) are quoted in ppm referenced to  $\text{CHCl}_3$  (77.16 ppm). Mass spectra were recorded by the University of Bristol, School of Chemistry departmental mass spectrometry service using electrospray ionisation (ESI) or Matrix-assisted Laser Desorption/Ionisation (MALDI) techniques for low- and high-resolution mass spectra. HRMS ESI was performed on either an Esquire 6000, micrOTOF II or Apex IV. HRMS MALDI was performed on either an ABI4700 or UltrafleXtreme. Samples were submitted in DCM. All infrared spectra were recorded on the neat compounds using a PerkinElmer Spectrum One FT-IR spectrometer, irradiating between  $4000\text{ cm}^{-1}$  and  $600\text{ cm}^{-1}$ . Only strong and selected absorbance values ( $\hat{I}_{1/2\text{max}}$ ) are reported. Analytical TLC was performed on aluminium-backed silica plates (Merck, Silica Gel 60 F254, 0.25 mm). Compounds were visualised by UV irradiation or by staining the plates with PMA, acidic p-anisaldehyde or basic  $\text{KMnO}_4$  followed by heating. Flash column chromatography was performed on silica gel (Aldrich, Silica Gel 60, 40-63  $\mu\text{m}$ ). All mixed solvent eluents are reported as v/v solutions. Optical rotations were obtained using a Bellingham + Stanley Ltd. ADP220 polarimeter at 589 nm (Na D-line) in a cell with a path length of 1 dm. Specific rotation values are given in (deg mL)/(g dm). Chiral high performance liquid chromatography (HPLC) separations were performed on an Agilent 1100 Series HPLC unit equipped with UV-Vis diode-array detector monitored at 210.8 nm, by using Daicel Chiralpak ADH, IA, IB or IC columns ( $4.6 \times 250\text{ mm}^2$ , 5  $\mu\text{m}$ ) fitted with respective guards ( $4 \times 10\text{ mm}^2$ ).

#### 4.4.2 Synthesis and Characterization

**Synthesis of 4-Bromo-2,6-diisopropylaniline 3.** According to the literature,<sup>320</sup> a solution of  $\text{Br}_2$  (1.0 eq) in DCM (2.7 M) was slowly added dropwise at  $0^\circ\text{C}$  to a solution of 2,6-diisopropylaniline in DCM (0.19 M). After completed addition, the reaction mixture was stirred at RT for an additional 30 min. Then a saturated solution of  $\text{Na}_2\text{S}_2\text{O}_3$  (100 mL) was added and the mixture was stirred for an additional 15 min. The organic layer was separated, concentrated to half of its original volume and extracted with  $\text{NaOH}$  0.5M and brine. The organic layer was dried over  $\text{MgSO}_4$ , filtered and concentrated under reduced pressure and the crude product was purified by flash chromatography.

3: Yield = 86%.  $^1\text{H}$  NMR (400 MHz,  $\text{CDCl}_3$ )  $\delta$ (ppm): 7.11 (s, 2H), 3.70 (sbr, 2H), 2.88 (sept., J = 6.8 Hz, 2H), 1.26 (d, J = 6.8 Hz, 12H);  $^{13}\text{C}$  NMR (75 MHz,  $\text{CDCl}_3$ )  $\delta$ (ppm): 139.4, 134.7, 125.8, 111.2, 28.1, 22.4.

**Synthesis of 1-Bromo-3,5-diisopropylbenzene 4.** According to the literature,<sup>320</sup> a solution of sodium nitrite (2.50 eq) in water (4.6 M) was added dropwise to a precooled suspension (-10°C) of **3** in HCl 2M (0.39 M). The reaction was allowed to react at -10°C for an additional 10 min., then H<sub>3</sub>PO<sub>2</sub> (50 w%, 10.0 eq) was added. The reaction mixture was stirred for 24h during which time the cooling bath was allowed to slowly warm to RT. The mixture was extracted with Et<sub>2</sub>O. The combined organic layers were washed with NaOH 0.5M and H<sub>2</sub>O, then dried over MgSO<sub>4</sub>, filtered and concentrated under reduced pressure.

**4:** Yield = 88%. <sup>1</sup>H NMR (400 MHz, CDCl<sub>3</sub>) δ(ppm): 7.18 (m, 2H), 6.99 (tt, J = 1.6, 0.5 Hz, 1H) 2.86 (sept., J = 6.9 Hz, 2H), 1.24 (d, J = 6.9 Hz, 12H); <sup>13</sup>C NMR (75 MHz, CDCl<sub>3</sub>) δ(ppm): 151.2, 127.0, 123.8, 122.5, 34.2, 24.0.

**Synthesis of (R,R)-3,5-di-iso-propylphenylTADDOL 5.** According to the literature,<sup>323</sup> to a flame-dried two-neck round-bottomed flask was added crushed magnesium turnings (5.3 eq) under N<sub>2</sub>. The apparatus was flame-dried again, followed by addition of a single crystal of I<sub>2</sub> along with tetrahydrofuran (1.0 M). To a separate flame dried round-bottomed flask was added **4** (5.0 eq) and tetrahydrofuran (0.8 M). The resulting solution was slowly added to the magnesium mixture at RT. The reaction was gently warmed to initiate reflux and stirred 15min. The mixture was heated to reflux for 30min at which time the reaction was cooled to RT, and a solution of (4R,5R)-dimethyl 2,2-dimethyl-1,3-dioxolane-4,5-dicarboxylate in THF (0.25 M) was added slowly. The reaction was allowed to reflux for 18 h, after which it was cooled to RT and quenched with saturated aqueous NH<sub>4</sub>Cl. The organic and aqueous layers were separated and the aqueous layer was further extracted with EtOAc. The combined organics were dried over MgSO<sub>4</sub>, filtered and concentrated under reduced pressure. The crude material was purified by recrystallisation from methanol. The crystallised solid was isolated by filtration, washed with cold methanol, and dried under vacuum to afford compound **5** as white solid.

**5:** Yield = 69%. <sup>1</sup>H NMR (400 MHz, CDCl<sub>3</sub>) δ(ppm): 7.16 (d, J = 1.7 Hz, 4H), 6.95 (d, J = 1.5 Hz, 4H), 6.92 (s, 2H), 6.86 (s, 2H), 4.61 (s, 2H), 3.63 (s, 2H), 2.81 (dq, J = 7.0 Hz, 7.0 Hz, 4H), 2.72 (dq, J = 7.0 Hz, 7.0 Hz, 4H), 1.16 (dd, J = 7.0 Hz, 1.5 Hz, 24H), 1.06 (dd, J = 7.5 Hz, 7.0 Hz, 24H), 0.84 (s, 6H); <sup>13</sup>C NMR (125 MHz, CDCl<sub>3</sub>) δ(ppm): 148.0, 147.3, 145.8, 142.5, 124.5, 123.5, 123.4, 123.2, 108.9, 21.2, 78.5, 34.3, 34.2, 30.3, 27.0, 24.4, 24.0, 23.9.

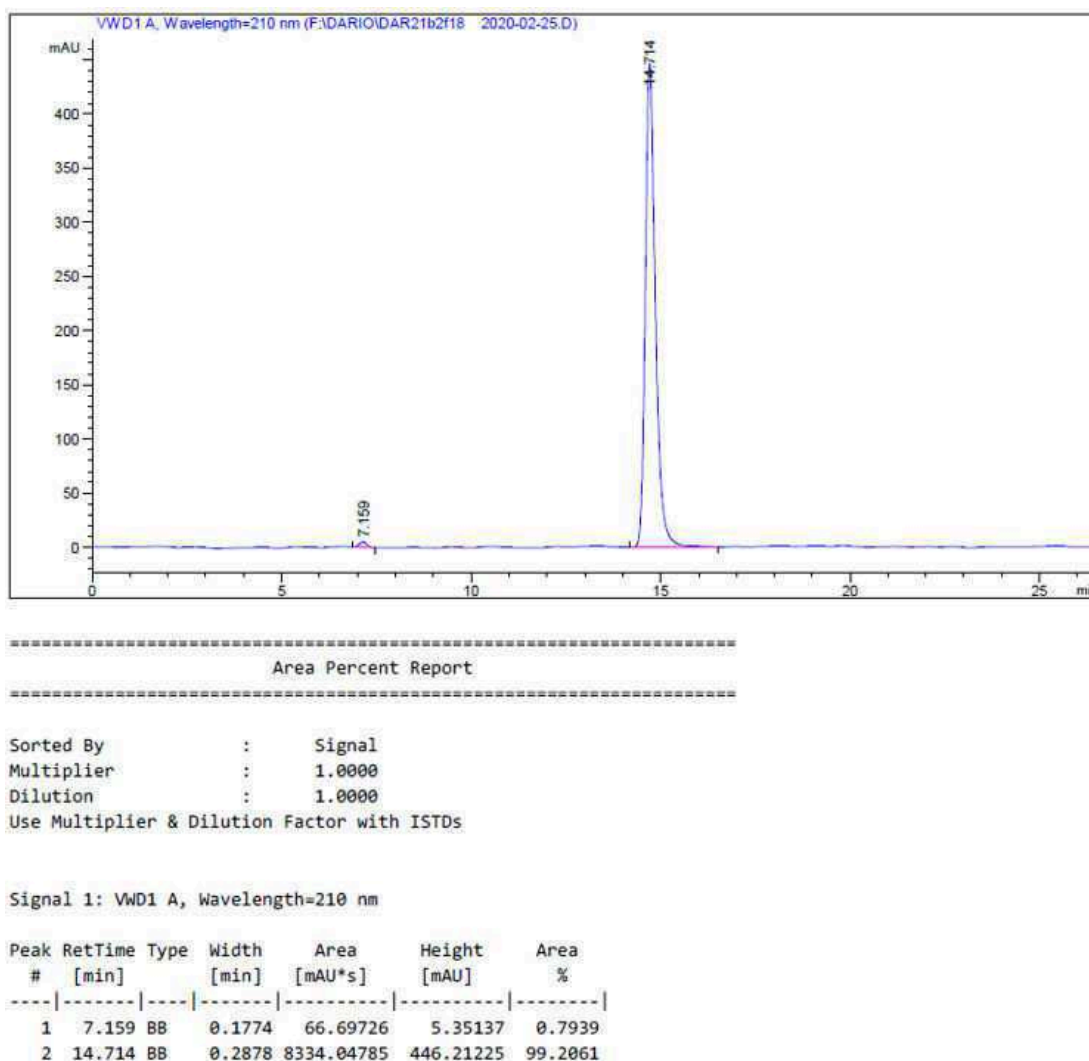
**Synthesis of (R,R)-di-iso-propylphenylTADDOLPh 1.** According to the literature,<sup>323</sup> to a flame dried round bottom flask was added a solution of **5** in THF (1 M) under N<sub>2</sub>. The reaction mixture was cooled to 0°C and dry Et<sub>3</sub>N (3.39 eq) was added. Then, dichlorophenylphosphine (1.1 eq) was added dropwise and the reaction was warmed to RT and was allowed to stir for 2 h. The reaction was diluted with Et<sub>2</sub>O, filtered quickly through celite and concentrated in vacuo. The crude material was purified by silica gel chromatography (1% EtOAc in pentane, with 1% Et<sub>3</sub>N to prevent hydrolysis) to afford compound **1** as white

solid. 1: Yield = 84%.  $^1\text{H}$  NMR (400 MHz,  $\text{CDCl}_3$ )  $\delta$ (ppm): 7.86-7.90 (m, 2H), 7.51 (s, 2H), 7.44-7.47 (m, 3H), 7.34 (s, 2H), 7.18 (brs, 2H), 6.98 (d,  $J = 2.0$  Hz, 2H), 6.94 (s, 1H), 6.91 (s, 2H), 6.83 (s, 1H), 5.58 (dd,  $J = 8.5$  Hz, 4.0 Hz, 1H), 4.91 (d,  $J = 8.5$  Hz, 1H), 2.78-2.84 (m, 8H), 1.51 (s, 3H), 1.10-1.25 (m, 48H), 0.11 (s, 3H);  $^{13}\text{C}$  NMR (125 MHz,  $\text{CDCl}_3$ )  $\delta$ (ppm): 147.9, 147.8, 147.3, 147.1, 146.8, 146.3, 146.2, 142.2, 142.1, 141.7, 141.4, 130.4, 130.1, 129.9, 128.2, 128.1, 125.1, 124.8, 124.7, 123.6, 123.5, 123.4, 123.3, 123.1, 110.4, 84.3, 84.3, 83.9, 83.8, 83.4, 83.2, 82.8, 82.8, 34.4, 34.2, 34.1, 34.0, 28.0, 24.2, 24.1, 24.0, 23.9, 23.9.  $[\alpha]_D^{25} = -46$  ( $c = 0.52$ ,  $\text{CHCl}_3$ ,  $l = 50$  mm).

**Synthesis of (S)-1-((R)-p-tolylsulfinyl)but-3-en-1-yl 2,4,6-triisopropylbenzoate 2.** According to the literature procedure,<sup>313</sup>  $^t\text{BuLi}$  (1.3 M in hexane, 1.2 eq) was added slowly (syringe pump, 0.3 mL/min) to a stirred solution of (-)-sparteine (1.2 eq) and **6** in anhydrous  $\text{Et}_2\text{O}$  (0.3 M) at  $-78^\circ\text{C}$  under  $\text{N}_2$ . The reaction mixture was stirred at  $-78^\circ\text{C}$  for 1h before the addition of freshly prepared  $\text{MgBr}_2 \cdot \text{Et}_2\text{O}$  (1.5 eq) via cannula. After a further 2h at  $-78^\circ\text{C}$ , (-)-Anderson's sulfinate (1.5 eq) in THF (1.0 M) was added slowly (syringe pump, 0.5 mL/min). The reaction mixture was stirred at  $-78^\circ\text{C}$  for 1h then allowed to warm to RT 16h. The reaction was quenched with 2M HCl then washed with 2M HCl. The combined aqueous layers were extracted with  $\text{Et}_2\text{O}$ . The combined organics were washed with sat. aq.  $\text{NaHCO}_3$  and brine, dried over anhydrous  $\text{MgSO}_4$  and concentrated under reduced pressure. Purification was aided by silylation of the menthol by-product: The crude mixture was stirred under vacuum for 2h then dissolved in anhydrous DCM (0.5 M).  $\text{Et}_3\text{N}$  (1.5 eq) was added followed by TMSCl (1.3 eq) dropwise. The resulting mixture was stirred at RT under  $\text{N}_2$  for 2h. The reaction mixture was diluted with  $\text{Et}_2\text{O}$ , washed with water, dried over anhydrous  $\text{MgSO}_4$ , filtered and concentrated under reduced pressure. The residue was purified by flash column chromatography (pentane: $\text{Et}_2\text{O}$  100:0 to 0:100) to remove TMS-menthol and most of excess Anderson's sulfinate, then on the Biotage Isolera using 2x100g ultra columns and 7% EtOAc in hexane to afford compound **2** as white solid.

**2:** Yield: 59%.  $^1\text{H}$  NMR (400 MHz,  $\text{CDCl}_3$ )  $\delta$ (ppm): 7.66 (d,  $J = 8.0$  Hz, 2H), 7.37 (d,  $J = 8.0$  Hz, 2H), 7.04 (s, 2H), 5.75 (dd,  $J_1 = 10.0$  Hz,  $J_2 = 3.1$  Hz, 1H), 5.72-5.61 (m, 1H, C3H), 5.12-5.05 (m, 2H), 2.92 (sept,  $J = 6.8$  Hz, 2H), 2.91 (sept,  $J = 6.9$  Hz, 1H), 2.77-2.67 (m, 1H), 2.44 (s, 3H), 2.44-2.37 (m, 1H), 1.29-1.22 (m, 18H);  $^{13}\text{C}$  NMR (100 MHz,  $\text{CDCl}_3$ )  $\delta$ (ppm): 170.5, 151.0, 145.4, 141.9, 137.5, 131.6, 130.2, 128.9, 124.6, 121.1, 119.4, 91.6, 34.6, 31.7, 28.0, 24.6, 24.3, 24.1, 21.6.

Chiral HPLC: (Daicel Chiralcel-IA column (25cm) with guard, Hex: $^t\text{PrOH} = 95:5$ , 0.5 mL/min, RT, 210 nm): tR = 7.2 minutes (minor), 17.7 minutes (major), er >99:1.



Synthesis of (S)-N-(2,3-bis(4,4,5,5-tetramethyl-1,3,2-dioxaborolan-2-yl)propyl)-N-trityl-formamide **8**. According to the literature procedure,<sup>323</sup> anhydrous THF (1.0 M) was added to a mixture of Pt(dba)<sub>3</sub> (2 mol%), (S,S)-ligand **1'** (2.4 mol%) and B<sub>2</sub>pin<sub>2</sub> (1.2 eq) under N<sub>2</sub> and the mixture was stirred at 80°C for 30min. The reaction mixture was cooled to RT, compound **7** was added and the reaction mixture was stirred at 60°C for 16h. The reaction mixture was cooled to RT and concentrated under reduced pressure. The crude was purified by flash column chromatography (pentane:Et<sub>2</sub>O 70:30) to afford compound **8** as white solid.

**8**: Yield = 77%. <sup>1</sup>H NMR (400 MHz, CDCl<sub>3</sub>) δ(ppm): 8.29 (s, 1H), 7.36-7.27 (m, 15H), 3.51 (d, J = 7.2 Hz, 2H), 1.22-1.16 (m, 24H), 0.83 (dd, J = 15.9 Hz, 8.6 Hz, 1H), 0.68 (m, 1H), 0.50 (dd, J = 15.9 Hz, 4.5 Hz, 1H); <sup>13</sup>C NMR (125 MHz, CDCl<sub>3</sub>) δ(ppm): 167.5, 142.9, 130.6, 128.0, 127.6, 82.9, 82.7, 63.6, 53.2, 47.4, 25.2, 25.1, 24.97, 24.95, 8.3; carbon next to boron not observed due to quadrupolar relaxation.



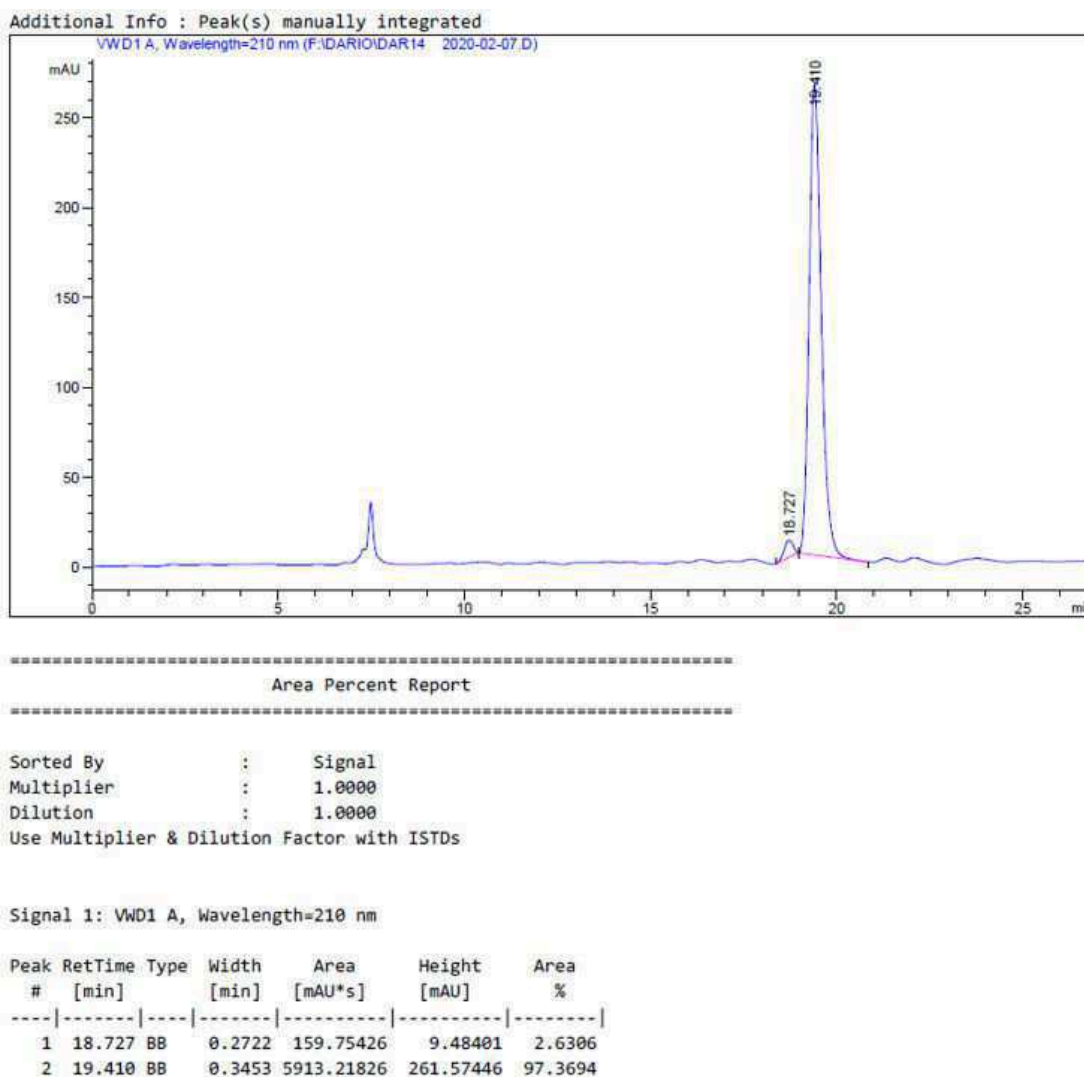
**Synthesis of N-((2S,4S)-2,4-bis(4,4,5,5-tetramethyl-1,3,2-dioxaborolan-2-yl)hept-6-en-1-yl)-N-tritylformamide 9.** PMDTA (2.0 eq) and anhydrous THF (0.2M wrt 2) were added to a mixture of **8** and  $\alpha$ -sulfinyl benzoate **2** (1.5 eq) under N<sub>2</sub>. The mixture was cooled to -78°C before the dropwise addition of <sup>t</sup>BuLi (2.6 M in heptane, 2.0 eq). The reaction mixture was stirred at -78°C for 1h then warmed to RT. THF was removed under reduced pressure and the mixture was redissolved in CHCl<sub>3</sub> (0.2 M) and heated at 60°C for 3h. The reaction mixture was then cooled to RT and diluted with sat. aq. NH<sub>4</sub>Cl and Et<sub>2</sub>O. The layers were separated and the aqueous extracted with Et<sub>2</sub>O. The combined organics were dried over anhydrous MgSO<sub>4</sub>, filtered and concentrated under reduced pressure. The crude residue was purified by flash column chromatography (pentane: Et<sub>2</sub>O 80:20 to 50:50) to afford compound **9** as colourless oil.

**9:** Yield = 39%. <sup>1</sup>H NMR (400 MHz, CDCl<sub>3</sub>)  $\delta$ (ppm): 8.32 (s, 1H), 7.36-7.27 (m, 15H), 5.70 (ddt, J = 17.0 Hz, 10.2 Hz, 6.9 Hz, 1H), 4.92 (dd, J = 17.1 Hz, J = 2.0 Hz, 1H), 4.87 (dd, J = 10.3 Hz, J = 2.0 Hz, 1H), 3.48 (dd, J = 13.4 Hz, J = 8.4 Hz, 1H), 2.87 (dd, J = 13.4 Hz, J = 3.9 Hz, 1H), 1.97 (t, J = 7.3 Hz, 2H), 1.30-1.13 (m, 26H), 0.95-0.80 (m, 2H); <sup>13</sup>C NMR (125 MHz, CDCl<sub>3</sub>)  $\delta$ (ppm): 167.3, 143.0, 138.6, 130.3, 128.1, 127.5, 114.9, 83.0, 82.8, 63.2, 47.8, 36.3, 31.8, 25.7, 25.6, 25.2, 24.8; *carbon next to boron not observed due to quadrupolar relaxation.*

**Synthesis of (R)-3,4-bis(4,4,5,5-tetramethyl-1,3,2-dioxaborolan-2-yl)butyl 2,4,6-triisopropylbenzoate 12.** According to the literature procedure, anhydrous THF (1.0 M) was added to a mixture of Pt(dba)<sub>3</sub> (3.00 mol%), (R,R)-ligand **1** (3.60 mol%) and B<sub>2</sub>pin<sub>2</sub> (1.05 eq) under N<sub>2</sub> and the mixture was stirred at 80°C for 30 min. The reaction mixture was cooled to RT, **6** was added and the reaction mixture was stirred at 60°C for 16h. The reaction mixture was cooled to RT and concentrated under reduced pressure. The crude was purified by flash column chromatography to afford compound **12** as viscous yellow oil.

**12:** Yield = 70%. <sup>1</sup>H NMR (400 MHz, CDCl<sub>3</sub>)  $\delta$ (ppm): 6.98 (s, 2H), 4.36-4.30 (m, 2H), 2.87 (sept, J = 6.9 Hz, 1H), 2.87 (sept, J = 6.8 Hz, 2H), 1.96-1.86 (m, 1H), 1.79-1.69 (m, 1H), 1.33-1.13 (m, 43H), 0.95-0.83 (m, 2H); <sup>13</sup>C NMR (100 MHz, CDCl<sub>3</sub>)  $\delta$ (ppm): 171.1, 150.0, 144.9, 131.1, 120.9, 83.14, 83.07, 64.7, 34.6, 32.2, 31.6, 25.01, 24.96, 24.9, 24.33, 24.31, 24.1; *carbon next to boron not observed due to quadrupolar relaxation.*

An aliquot of bis(boronic ester) **12** was oxidised to the corresponding diol **14** in order to determine the enantiomeric ratio by chiral HPLC. Chiral HPLC: (Daicel Chiralcel-IB column (25cm) with guard, Hex:<sup>i</sup>PrOH = 95:5, 0.5 mL/min, RT, 210):  $t_R$  = 18.7 minutes (minor), 18.4 minutes (major), er = 97:3.



(3R,5S)-3,5-bis(4,4,5,5-tetramethyl-1,3,2-dioxaborolan-2-yl)oct-7-en-1-yl 2,4,6-triisopropylbenzoate **13**. A solution of PMDTA (1.95 eq) in anhydrous THF (0.2M wrt **2**) was added to a mixture of **12** and **2** (1.5 eq) under N<sub>2</sub>. The mixture was cooled to -78°C before the dropwise addition of <sup>t</sup>BuLi (2.56M in heptane, 1.95 eq). The reaction mixture was stirred at -78°C for 1h then 60°C for 3h. The reaction mixture was then cooled to RT and diluted with saturated aqueous NH<sub>4</sub>Cl and Et<sub>2</sub>O. The layers were separated and the aqueous extracted with Et<sub>2</sub>O. The combined organics were dried over anhydrous MgSO<sub>4</sub>, filtered and concentrated under reduced pressure. The crude residue was purified by flash column chromatography on the Biotage Isolera using a 50g Ultra column and 2-20% EtOAc in hexane to afford compound **13** as viscous yellow oil.

**13**: Yield = 63%. <sup>1</sup>H NMR (400 MHz, CDCl<sub>3</sub>) δ(ppm): 6.98 (s, 2H), 5.78 (ddt, J = 17.1, 10.1, 7.2 Hz, 1H), 5.00 (ddt, J = 17.1, 2.2, 1.6 Hz, 1H), 4.93-4.89 (ddt, J = 10.1, 2.2, 1.1 Hz, 1H), 4.37-4.23 (m, 2H), 2.86 (sept, J = 6.8 Hz, 3H), 2.22-2.06 (m, 2H), 1.86-1.73 (m, 2H), 1.68-1.59

(m, 1H), 1.32-1.11 (m, 45H);  $^{13}\text{C}$  NMR (100 MHz,  $\text{CDCl}_3$ )  $\delta$ (ppm): 171.0, 150.0, 144.9, 138.6, 131.1, 120.9, 115.0, 83.2, 83.1, 64.9, 35.2, 34.6, 31.6, 31.3, 29.8, 25.00, 24.97, 24.91, 24.89, 24.3, 24.1; carbon next to boron not observed due to quadrupolar relaxation.

**Synthesis of (3S,4S)-3,4-dibromo-3-methyldihydrofuran-2(3H)-one 14.** According to the literature procedure,<sup>324</sup> bromine (3.0 eq) was added slowly to a solution of furanone (1.0 eq) in DCM (1.0 M) at  $-10^\circ\text{C}$  and the reaction mixture was stirred at RT for 6 days. The reaction mixture was poured into ice/sat. aq.  $\text{Na}_2\text{S}_2\text{O}_3$  (1:1 g:mL), stirring vigorously. DCM was added and the layers separated. The organic phase was washed with brine, dried over anhydrous  $\text{MgSO}_4$ , filtered and concentrated under reduced pressure. The crude material was purified by flash column chromatography to afford compound **14** as pale yellow solid. **14:** Yield = 90%.  $^1\text{H}$  NMR (400 MHz,  $\text{CDCl}_3$ )  $\delta$ (ppm): 5.00 (dd,  $J = 11.1$  Hz, 3.7 Hz, 1H), 4.84 (d,  $J = 3.7$  Hz, 1H), 4.55 (d,  $J = 11.1$  Hz, 1H), 2.10 (s, 3H);  $^{13}\text{C}$  NMR (100 MHz,  $\text{CDCl}_3$ )  $\delta$ (ppm): 171.9, 73.9, 54.4, 52.9, 25.4.

**Synthesis of (E)-3-bromobut-2-en-1-ol 15.** According to the literature procedure,<sup>324</sup>  $\text{Li}\cdot\text{H}_2\text{O}$  (3.0 eq) was added to a solution of **14** in DMF/ $\text{H}_2\text{O}$  (4:1, 0.5 M) at RT. After stirring at RT overnight, the reaction mixture was directly purified by flash column chromatography to afford compound **15** as pale yellow oil.

**15:** Yield = 62%.  $^1\text{H}$  NMR (400 MHz,  $\text{CDCl}_3$ )  $\delta$ (ppm): 6.10 (tq,  $J = 7.2$  Hz, 1.3 Hz, 1H), 4.12 (d,  $J = 7.2$  Hz, 2H), 2.30 (d,  $J = 1.3$  Hz, 3H);  $^{13}\text{C}$  NMR (100 MHz,  $\text{CDCl}_3$ )  $\delta$ (ppm): 131.0, 124.4, 59.8, 23.8.

**Synthesis of (E)-((3-bromobut-2-en-1-yl)oxy)(tert-butyl)dimethylsilane 16.** tert-Butyldimethylsilyl chloride (1.3 eq) was added to a solution of **15** and imidazole (1.5 eq) in DCM (0.2 M) at  $0^\circ\text{C}$  and the reaction mixture was stirred at RT overnight. The reaction mixture was quenched with  $\text{H}_2\text{O}$  and the layers separated. The aqueous phase was extracted with DCM. The combined organics were washed with brine, dried over anhydrous  $\text{MgSO}_4$ , filtered and concentrated under reduced pressure. The crude residue was purified by flash column chromatography to afford compound **16** as colourless oil.

**16:** Yield = 88%.  $^1\text{H}$  NMR (400 MHz,  $\text{CDCl}_3$ )  $\delta$ (ppm): 6.00 (tq,  $J = 6.7$  Hz, 1.3 Hz, 1H), 4.13 (dq,  $J = 6.7, 0.9$  Hz, 2H), 2.26 (dt,  $J = 1.3$  Hz, 0.9 Hz, 3H), 0.90 (s, 9H), 0.07 (s, 6H);  $^{13}\text{C}$  NMR (100 MHz,  $\text{CDCl}_3$ )  $\delta$ (ppm): 131.9, 122.0, 60.5, 26.0, 23.9, 18.5, -5.0.



---

## Appendix

---

The reuse license for this published article cited in this work, which required it, are reported below.

27/12/2020

RightsLink Printable License

SPRINGER NATURE LICENSE  
TERMS AND CONDITIONS

Dec 27, 2020

---

This Agreement between ALMA MATER STUDIORUM - University of Bologna -- Dario Corbisiero ("You") and Springer Nature ("Springer Nature") consists of your license details and the terms and conditions provided by Springer Nature and Copyright Clearance Center.

License Number 4977090244179

License date Dec 27, 2020

Licensed Content  
Publisher Springer Nature

Licensed Content  
Publication Amino Acids

Licensed Content Title Synthesis of  $\alpha/\beta$  dipeptides containing linear or cyclic  $\alpha$ -dehydro- $\beta$ -amino acids as scaffolds for bioactive compounds



---

## Bibliography

---

1. World Health Organization. <https://gco.iarc.fr>.
2. S. Rakoff-Nahoum. Why cancer and inflammation? *Yale Journal of Biology and Medicine*, 79:123–130, 2006.
3. D. Hanahan and R.A. Weinberg. The hallmarks of cancer. *Cell*, 100:57–70, 2000.
4. P Rous and JG Kidd. Conditional neoplasms and subthreshold neoplastic states : A study of the tar tumors of rabbits. *The Journal of experimental medicine*, 73(3):365–390, February 1941.
5. Kenneth W Kinzler and Bert Vogelstein. Lessons from hereditary colorectal cancer. *Cell*, 87(2):159–170, 1996.
6. Judah Folkman. Role of angiogenesis in tumor growth and metastasis. *Seminars in Oncology*, 29(6, Supplement 16):15–18, 2002.
7. H. Kuper, H.-O. Adami, and D. Trichopoulos. Infections as a major preventable cause of human cancer. *Journal of Internal Medicine*, 248(3):171–183, 2000.
8. A. Mantovani, P. Allavena, A. Sica, and F. Balkwill. Cancer-related inflammation. *Nature*, 454:436–444, 2008.
9. S. Chettibi and M.W.J. Ferguson. *Inflammation: Basic Principles and Clinical Correlates*. Lippincott Williams-Wilkins, 1999.
10. Lisa M Coussens and Zena Werb. Inflammation and cancer. *Nature*, 420(6917):860–867, 2002.
11. F. Colotta, P. Allavena, A. Sica, A. Garlanda, and A. Mantovani. Cancer-related inflammation, the seventh hallmark of cancer: Links to genetic instability. *Carcinogenesis*, 30:1073–1081, 2009.

12. S. Schoppmann, P. Birner, J. Stöckl, R. Kalt, R. Ullrich, C. Caucig, E. Kriehuber, K. Nagy, K. Alitalo, and D. Kerjaschki. Tumor-associated macrophages express lymphatic endothelial growth factors and are related to peritumoral lymphangiogenesis. *The American Journal of Pathology*, 161:947–956, 2002.
13. M. Karin. Nuclear factor- $\kappa$ B in cancer development and progression. *Nature*, 441:431–436, 2006.
14. Heehyoung Lee, Andreas Herrmann, Jie-Hui Deng, Maciej Kujawski, Guilian Niu, Zhiwei Li, Steve Forman, Richard Jove, Drew M. Pardoll, and Hua Yu. Persistently activated stat3 maintains constitutive nf- $\kappa$ B activity in tumors. *Cancer Cell*, 15(4):283–293, 2009.
15. S. Grivennikov, E. Karin, J. Terzic, D. Mucida, G.Y. Yu, S. Vallabhapurapu, J. Scheller, S. Rose-John, H. Cheroutre, L. Eckmann, and M. Karin. Il-6 and stat3 are required for survival of intestinal epithelial cells and development of colitis-associated cancer. *Cancer Cell*, 15:103–113, 2009.
16. B.K. Popivanova, K. Kitamura, Y. Wu, T. Kondo, T. Kagaya, S. Kaneko, M. Oshima, C. Fujii, and N. Mukaida. Blocking tnf-alpha in mice reduces colorectal carcinogenesis associated with chronic colitis. *The Journal of Clinical Investigation*, 118:560–570, 2008.
17. J.L. Luo, W. Tan, J.M. Ricono, O. Korchynskji, M. Zhang, S.L. Gonias, D.A. Cheresch, and M. Karin. Nuclear cytokine-activated ikkalpha controls prostate cancer metastasis by repressing maspin. *Nature*, 446:690–694, 2007.
18. L. Soucek, E.R. Lawlor, D. Soto, K. Shchors, L. Brown Swigart, and G.I. Evan. Mast cells are required for angiogenesis and macroscopic expansion of myc-induced pancreatic islet tumors. *Nature Medicine*, 13:1211–1218, 2007.
19. M.J. Smyth, G.P. Dunn, and R.D. Schreiber. Cancer immunosurveillance and immunoediting: the roles of immunity in suppressing tumor development and shaping tumor immunogenicity. *Advances in Immunology*, 90:1–50, 2006.
20. M.E. Hemler. V $\alpha$  proteins in the integrin family: Structures, functions, and their role on leukocytes. *Annual Review of Immunology*, 8:365–400, 1990.
21. H. Hamidi and J. Ivaska. Every step of the way: Integrins in cancer progression and metastasis. *Nature Reviews*, 18:533–548, 2018.
22. O. R. Hynes. Integrins: Bidirectional, allosteric signaling machines. *Cell*, 110:673–687, 2002.



23. J. D. Humphries, A. Byron, and M. J. Humphries. Integrin ligands at a glance. *Journal of Cell Science*, 119:3901–3903, 2006.
24. A. Tolomelli, P. Galletti, M. Baiula, and D. Giacomini. Can integrin agonists have cards to play against cancer? a literature survey of small molecules integrin activators. *Cancers*, 9:78–95, 2017.
25. Klaus Ley, Jesus Rivera-Nieves, William J Sandborn, and Sanford Shattil. Integrin-based therapeutics: biological basis, clinical use and new drugs. *Nature reviews Drug discovery*, 15(3):173, 2016.
26. Nicola De Franceschi, Hellyeh Hamidi, Jonna Alanko, Pranshu Sahgal, and Johanna Ivaska. Integrin traffic—the update. *Journal of cell science*, 128(5):839–852, 2015.
27. Timothy A Springer and Michael L Dustin. Integrin inside-out signaling and the immunological synapse. *Current opinion in cell biology*, 24(1):107–115, 2012.
28. Martina A Müller, Leonora Brunie, Anne-Sophie Bächer, Horst Kessler, Kay-Eberhard Gottschalk, and Ute Reuning. Cytoplasmic salt bridge formation in integrin  $\alpha v\beta 3$  stabilizes its inactive state affecting integrin-mediated cell biological effects. *Cellular signalling*, 26(11):2493–2503, 2014.
29. Sanford J Shattil, Chungho Kim, and Mark H Ginsberg. The final steps of integrin activation: the end game. *Nature reviews Molecular cell biology*, 11(4):288–300, 2010.
30. Sanford J Shattil, Chungho Kim, and Mark H Ginsberg. The final steps of integrin activation: the end game. *Nature reviews Molecular cell biology*, 11(4):288–300, 2010.
31. Gianfranco Bazzoni and Martin E Hemler. Are changes in integrin affinity and conformation overemphasized? *Trends in biochemical sciences*, 23(1):30–34, 1998.
32. Jing Li, Yang Su, Wei Xia, Yan Qin, Martin J Humphries, Dietmar Vestweber, Carlos Cabañas, Chafen Lu, and Timothy A Springer. Conformational equilibria and intrinsic affinities define integrin activation. *The EMBO journal*, 36(5):629–645, 2017.
33. Edward R Horton, Jonathan D Humphries, Jenny James, Matthew C Jones, Janet A Askari, and Martin J Humphries. The integrin adhesome network at a glance. *Journal of cell science*, 129(22):4159–4163, 2016.
34. Sabine Raab-Westphal, John F Marshall, and Simon L Goodman. Integrins as therapeutic targets: successes and cancers. *Cancers*, 9(9):110, 2017.
35. Francesca Roggiani, Delia Mezzanzanica, Katia Rea, and Antonella Tomassetti. Guidance of signaling activations by cadherins and integrins in epithelial ovarian cancer cells. *International journal of molecular sciences*, 17(9):1387, 2016.

36. HG Munshi and MS Stack. Reciprocal interactions between adhesion receptor signaling and mmp regulation. *Cancer and Metastasis Reviews*, 25(1):45–56, 2006.
37. Steven M Frisch, Kristiina Vuori, Erkki Ruoslahti, and Po-Ying Chan-Hui. Control of adhesion-dependent cell survival by focal adhesion kinase. *The Journal of cell biology*, 134(3):793–799, 1996.
38. Boris Strilic and Stefan Offermanns. Intravascular survival and extravasation of tumor cells. *Cancer Cell*, 32(3):282–293, 2017.
39. Arthur W Lambert, Diwakar R Pattabiraman, and Robert A Weinberg. Emerging biological principles of metastasis. *Cell*, 168(4):670–691, 2017.
40. Anna Ludlow, Karen O Yee, Ruth Lipman, R Bronson, P Weinreb, Xiaozhu Huang, D Sheppard, and J Lawler. Characterization of integrin  $\beta 6$  and thrombospondin-1 double-null mice. *Journal of cellular and molecular medicine*, 9(2):421–437, 2005.
41. Hoa H Truong, Jiangling Xiong, Veerander PS Ghotra, Ella Nirmala, Lizette Haazen, Sylvia E Le Devedec, Hayri E Balcioglu, Shuning He, B Ewa Snaar-Jagalska, Erno Vreugdenhil, et al.  $\beta 1$  integrin inhibition elicits a prometastatic switch through the  $\text{tgf}\beta$ -mir-200-zeb network in e-cadherin-positive triple-negative breast cancer. *Science signaling*, 7(312):ra15–ra15, 2014.
42. Bartlomiej Waclaw, Ivana Bozic, Meredith E Pittman, Ralph H Hruban, Bert Vogelstein, and Martin A Nowak. A spatial model predicts that dispersal and cell turnover limit intratumour heterogeneity. *Nature*, 525(7568):261–264, 2015.
43. Paolo P Provenzano, Kevin W Eliceiri, Jay M Campbell, David R Inman, John G White, and Patricia J Keely. Collagen reorganization at the tumor-stromal interface facilitates local invasion. *BMC medicine*, 4(1):1–15, 2006.
44. Patrick T Caswell, Suryakiran Vadrevu, and Jim C Norman. Integrins: masters and slaves of endocytic transport. *Nature reviews Molecular cell biology*, 10(12):843–853, 2009.
45. Jay S Desgrosellier, Leo A Barnes, David J Shields, Miller Huang, Steven K Lau, Nicolas Prévost, David Tarin, Sanford J Shattil, and David A Cheresh. An integrin  $\alpha v \beta 3$ -c-src oncogenic unit promotes anchorage-independence and tumor progression. *Nature medicine*, 15(10):1163–1169, 2009.
46. Ayuko Hoshino, Bruno Costa-Silva, Tang-Long Shen, Goncalo Rodrigues, Ayako Hashimoto, Milica Tesic Mark, Henrik Molina, Shinji Kohsaka, Angela Di Giannatale, Sophia Ceder, et al. Tumour exosome integrins determine organotropic metastasis. *Nature*, 527(7578):329–335, 2015.

47. JMPC Holash, PC Maisonpierre, D Compton, P Boland, CR Alexander, D Zagzag, GD Yancopoulos, and SJ Wiegand. Vessel cooption, regression, and growth in tumors mediated by angiopoietins and vegf. *Science*, 284(5422):1994–1998, 1999.
48. Laura Hakanpaa, Tuomas Sipila, Veli-Matti Leppanen, Prson Gautam, Harri Nurmi, Guillaume Jacquemet, Lauri Eklund, Johanna Ivaska, Kari Alitalo, and Pipsa Saharinen. Endothelial destabilization by angiopoietin-2 via integrin  $\beta 1$  activation. *Nature communications*, 6(1):1–12, 2015.
49. Ying Cao, Luke H Hoepfner, Steven Bach, E Guangqi, Yan Guo, Enfeng Wang, Jianmin Wu, Mark J Cowley, David K Chang, Nicola Waddell, et al. Neuropilin-2 promotes extravasation and metastasis by interacting with endothelial  $\alpha 5$  integrin. *Cancer research*, 73(14):4579–4590, 2013.
50. Hisashi Kato, Zhongji Liao, John V Mitsios, Huan-You Wang, Elena I Deryugina, Judith A Varner, James P Quigley, and Sanford J Shattil. The primacy of  $\beta 1$  integrin activation in the metastatic cascade. *PLoS One*, 7(10):e46576, 2012.
51. Robert Pytela, Michael D Pierschbacher, and Erkki Ruoslahti. Identification and isolation of a 140 kd cell surface glycoprotein with properties expected of a fibronectin receptor. *Cell*, 40(1):191–198, 1985.
52. Jonathan D Humphries, Adam Byron, and Martin J Humphries. Integrin ligands at a glance. *Journal of cell science*, 119(19):3901–3903, 2006.
53. Ronen Zaidel-Bar, Christoph Ballestrem, Zvi Kam, and Benjamin Geiger. Early molecular events in the assembly of matrix adhesions at the leading edge of migrating cells. *Journal of cell science*, 116(22):4605–4613, 2003.
54. Sabri Rahmouni, Aaron Lindner, Florian Rechenmacher, Stefanie Neubauer, Tariq Rashad Ali Sobahi, Horst Kessler, Elisabetta Ada Cavalcanti-Adam, and Joachim Pius Spatz. Hydrogel micropillars with integrin selective peptidomimetic functionalized nanopatterned tops: A new tool for the measurement of cell traction forces transmitted through  $\alpha v\beta 3$ -or  $\alpha 5\beta 1$ -integrins. *Advanced Materials*, 25(41):5869–5874, 2013.
55. Herbert B Schiller, Michaela-Rosemarie Hermann, Julien Polleux, Timothée Vignaud, Sara Zanivan, Caroline C Friedel, Zhiqi Sun, Aurelia Raducanu, Kay-E Gottschalk, Manuel Théry, et al.  $\beta 1$ -and  $\alpha v$ -class integrins cooperate to regulate myosin ii during rigidity sensing of fibronectin-based microenvironments. *Nature cell biology*, 15(6):625–636, 2013.
56. BG Keselowsky, L Wang, Z Schwartz, AJ Garcia, and BD Boyan. Integrin  $\alpha 5$  controls osteoblastic proliferation and differentiation responses to titanium substrates presenting

- different roughness characteristics in a roughness independent manner. *Journal of Biomedical Materials Research Part A*, 80(3):700–710, 2007.
57. Carlos Mas-Moruno, Roberta Fraioli, Florian Rechenmacher, Stefanie Neubauer, Tobias G Kapp, and Horst Kessler.  $\alpha v\beta 3$ -or  $\alpha 5\beta 1$ -integrin-selective peptidomimetics for surface coating. *Angewandte Chemie International Edition*, 55(25):7048–7067, 2016.
58. Olivia Fromigué, Julia Brun, Caroline Marty, Sophie Da Nascimento, Pascal Sonnet, and Pierre J Marie. Peptide-based activation of alpha5 integrin for promoting osteogenesis. *Journal of cellular biochemistry*, 113(9):3029–3038, 2012.
59. Rachit Agarwal, Cristina González-García, Brennan Torstrick, Robert E Guldberg, Manuel Salmerón-Sánchez, and Andrés J García. Simple coating with fibronectin fragment enhances stainless steel screw osseointegration in healthy and osteoporotic rats. *Biomaterials*, 63:137–145, 2015.
60. Timothy A Petrie, Jenny E Raynor, Catherine D Reyes, Kellie L Burns, David M Collard, and Andrés J García. The effect of integrin-specific bioactive coatings on tissue healing and implant osseointegration. *Biomaterials*, 29(19):2849–2857, 2008.
61. Chung-Fang Lai and Su-Li Cheng.  $\alpha v\beta$  integrins play an essential role in bmp-2 induction of osteoblast differentiation. *Journal of bone and mineral research*, 20(2):330–340, 2005.
62. Kristopher A Kilian and Milan Mrksich. Directing stem cell fate by controlling the affinity and density of ligand–receptor interactions at the biomaterials interface. *Angewandte Chemie*, 124(20):4975–4979, 2012.
63. Le T Duong and Gideon A Rodan. Integrin-mediated signaling in the regulation of osteoclast adhesion and activation. *Front Biosci*, 3:d757–d768, 1998.
64. Christie J Avraamides, Barbara Garmy-Susini, and Judith A Varner. Integrins in angiogenesis and lymphangiogenesis. *Nature Reviews Cancer*, 8(8):604–617, 2008.
65. Gabriele Bergers and Laura E Benjamin. Tumorigenesis and the angiogenic switch. *Nature reviews cancer*, 3(6):401–410, 2003.
66. Sara M Weis and David A Cheresh. Tumor angiogenesis: molecular pathways and therapeutic targets. *Nature medicine*, 17(11):1359–1370, 2011.
67. Peter C Brooks, Richard A Clark, and David A Cheresh. Requirement of vascular integrin alpha v beta 3 for angiogenesis. *Science*, 264(5158):569–571, 1994.

68. Louise E Reynolds, Lorenza Wyder, Julie C Lively, Daniela Taverna, Stephen D Robinson, Xiaozhu Huang, Dean Sheppard, Richard O Hynes, and Kairbaan M Hodivala-Dilke. Enhanced pathological angiogenesis in mice lacking  $\beta 3$  integrin or  $\beta 3$  and  $\beta 5$  integrins. *Nature medicine*, 8(1):27–34, 2002.
69. Patricia Parsons-Wingerter, Ian M Kasman, Scott Norberg, Anette Magnussen, Sara Zanivan, Alberto Rissone, Peter Baluk, Cecile J Favre, Ursula Jeffry, Richard Murray, et al. Uniform overexpression and rapid accessibility of  $\alpha 5\beta 1$  integrin on blood vessels in tumors. *The American journal of pathology*, 167(1):193–211, 2005.
70. Arjan van der Flier, Kwabena Badu-Nkansah, Charles A Whittaker, Denise Crowley, Roderick T Bronson, Adam Lacy-Hulbert, and Richard O Hynes. Endothelial  $\alpha 5$  and  $\alpha v$  integrins cooperate in remodeling of the vasculature during development. *Development*, 137(14):2439–2449, 2010.
71. Michael D Pierschbacher and Erkki Ruoslahti. Cell attachment activity of fibronectin can be duplicated by small synthetic fragments of the molecule. *Nature*, 309(5963):30–33, 1984.
72. Ake Oldberg, Ahnders Franzén, and Dick Heinegård. Cloning and sequence analysis of rat bone sialoprotein (osteopontin) cDNA reveals an arg-gly-asp cell-binding sequence. *Proceedings of the National Academy of Sciences*, 83(23):8819–8823, 1986.
73. Derrick S Grant, Ken-Ichiro Tashiro, Bartolome Segui-Real, Yoshihiko Yamada, George R Martin, and Hynda K Kleinman. Two different laminin domains mediate the differentiation of human endothelial cells into capillary-like structures in vitro. *Cell*, 58(5):933–943, 1989.
74. Robert Pytela, Michael D Pierschbacher, and Erkki Ruoslahti. A 125/115-kDa cell surface receptor specific for vitronectin interacts with the arginine-glycine-aspartic acid adhesion sequence derived from fibronectin. *Proceedings of the National Academy of Sciences*, 82(17):5766–5770, 1985.
75. Shin-ichi Aota, Motoyoshi Nomizu, and Kenneth M Yamada. The short amino acid sequence pro-his-ser-arg-asn in human fibronectin enhances cell-adhesive function. *Journal of Biological Chemistry*, 269(40):24756–24761, 1994.
76. Erkki Ruoslahti and Michael D Pierschbacher. New perspectives in cell adhesion: Rgd and integrins. *Science*, 238(4826):491–497, 1987.
77. Horst Kessler. Conformation and biological activity of cyclic peptides. *Angewandte Chemie International Edition in English*, 21(7):512–523, 1982.

78. Michael D Pierschbacher and Erkki Ruoslahti. Influence of stereochemistry of the sequence arg-gly-asp-xaa on binding specificity in cell adhesion. *Journal of Biological Chemistry*, 262(36):17294–17298, 1987.
79. Juan J Calvete, Wolfram Schaefer, Tomasz Soszka, Weiqu Lu, Jacquelynn Cook, Bradford A Jameson, and Stefan Niewiarowski. Identification of the disulfide bond pattern in albolabrin, an rgd-containing peptide from the venom of *trimeresurus albolabris*: Significance for the express of platelet aggregation inhibitory activity. *Biochemistry*, 30(21):5225–5229, 1991.
80. Roland Haubner, Dirk Finsinger, and Horst Kessler. Stereoisomeric peptide libraries and peptidomimetics for designing selective inhibitors of the  $\alpha v\beta 3$  integrin for a new cancer therapy. *Angewandte Chemie International Edition in English*, 36(13-14):1374–1389, 1997.
81. Elisabeth Lohof, Eckart Planker, Christian Mang, Fred Burkhart, Michael A Dechantsreiter, Roland Haubner, Hans-Jürgen Wester, Markus Schwaiger, Günther Hölzemann, Simon L Goodman, et al. Carbohydrate derivatives for use in drug design: cyclic  $\alpha v$ -selective rgd peptides. *Angewandte Chemie International Edition*, 39(15):2761–2764, 2000.
82. Carlos Mas-Moruno, Johannes G Beck, Lucas Doedens, Andreas O Frank, Luciana Marinelli, Sandro Cosconati, Ettore Novellino, and Horst Kessler. Increasing  $\alpha v\beta 3$  selectivity of the anti-angiogenic drug cilengitide by n-methylation. *Angewandte Chemie International Edition*, 50(40):9496–9500, 2011.
83. Sylwia Urman, Katharina Gaus, Yi Yang, Ulf Strijowski, Norbert Sewald, Silvia De Pol, and Oliver Reiser. The constrained amino acid  $\beta$ -acc confers potency and selectivity to integrin ligands. *Angewandte Chemie International Edition*, 46(21):3976–3978, 2007.
84. Jayanta Chatterjee, Florian Rechenmacher, and Horst Kessler. N-methylation of peptides and proteins: an important element for modulating biological functions. *Angewandte Chemie International Edition*, 52(1):254–269, 2013.
85. Warren P Mason. End of the road: confounding results of the core trial terminate the arduous journey of cilengitide for glioblastoma, 2015.
86. Anne-Marie Ray, Florence Schaffner, Hana Janouskova, Fanny Noulet, Didier Rognan, Isabelle Lelong-Rebel, Laurence Choulier, Anne-Florence Blandin, Maxime Lehmann, Sophie Martin, et al. Single cell tracking assay reveals an opposite effect of selective small non-peptidic  $\alpha 5\beta 1$  or  $\alpha v\beta 3/\beta 5$  integrin antagonists in u87mg glioma cells. *Biochimica et Biophysica Acta (BBA)-General Subjects*, 1840(9):2978–2987, 2014.

87. Simon L Goodman and Martin Picard. Integrins as therapeutic targets. *Trends in pharmacological sciences*, 33(7):405–412, 2012.
88. Alexander Bochen, Udaya Kiran Marelli, Elke Otto, Diego Pallarola, Carlos Mas-Moruno, Francesco Saverio Di Leva, Heike Boehm, Joachim P Spatz, Ettore Novellino, Horst Kessler, et al. Biselectivity of isodgr peptides for fibronectin binding integrin subtypes  $\alpha 5\beta 1$  and  $\alpha v\beta 6$ : conformational control through flanking amino acids. *Journal of medicinal chemistry*, 56(4):1509–1519, 2013.
89. Roland Haubner, Rainer Gratias, Beate Diefenbach, Simon L Goodman, Alfred Jonczyk, and Horst Kessler. Structural and functional aspects of rgd-containing cyclic pentapeptides as highly potent and selective integrin  $\alpha v\beta 3$  antagonists. *Journal of the American chemical society*, 118(32):7461–7472, 1996.
90. Andreas O Frank, Elke Otto, Carlos Mas-Moruno, Herbert B Schiller, Luciana Marinelli, Sandro Cosconati, Alexander Bochen, Dörte Vossmeier, Grit Zahn, Roland Stragies, et al. Conformational control of integrin-subtype selectivity in isodgr peptide motifs: a biological switch. *Angewandte Chemie International Edition*, 49(48):9278–9281, 2010.
91. Jian-Ping Xiong, Thilo Stehle, Rongguang Zhang, Andrzej Joachimiak, Matthias Frech, Simon L Goodman, and M Amin Arnaut. Crystal structure of the extracellular segment of integrin  $\alpha v\beta 3$  in complex with an arg-gly-asp ligand. *Science*, 296(5565):151–155, 2002.
92. Luciana Marinelli, Axel Meyer, Dominik Heckmann, Antonio Lavecchia, Ettore Novellino, and Horst Kessler. Ligand binding analysis for human  $\alpha 5\beta 1$  integrin: strategies for designing new  $\alpha 5\beta 1$  integrin antagonists. *Journal of medicinal chemistry*, 48(13):4204–4207, 2005.
93. Dominik Heckmann, Axel Meyer, Luciana Marinelli, Grit Zahn, Roland Stragies, and Horst Kessler. Probing integrin selectivity: rational design of highly active and selective ligands for the  $\alpha 5\beta 1$  and  $\alpha v\beta 3$  integrin receptor. *Angewandte Chemie International Edition*, 46(19):3571–3574, 2007.
94. Joanne M Smallheer, Carolyn A Weigelt, Francis J Woerner, Jennifer S Wells, Wayne F Daneker, Shaker A Mousa, Ruth R Wexler, and Prabhakar K Jadhav. Synthesis and biological evaluation of nonpeptide integrin antagonists containing spirocyclic scaffolds. *Bioorganic & medicinal chemistry letters*, 14(2):383–387, 2004.
95. William H Miller, Doreen P Alberts, Pradip K Bhatnagar, William E Bondinell, James F Callahan, Raul R Calvo, Russell D Cousins, Karl F Erhard, Dirk A Heerding, Richard M

- Keenan, et al. Discovery of orally active nonpeptide vitronectin receptor antagonists based on a 2-benzazepine gly-asp mimetic. *Journal of medicinal chemistry*, 43(1):22–26, 2000.
96. Paola Galletti, Roberto Soldati, Matteo Pori, Margherita Durso, Alessandra Tolomelli, Luca Gentilucci, Samantha Deianira Dattoli, Monica Baiula, Santi Spampinato, and Daria Giacomini. Targeting integrins  $\alpha v \beta 3$  and  $\alpha 5 \beta 1$  with new  $\beta$ -lactam derivatives. *European Journal of Medicinal Chemistry*, 83:284–293, 2014.
97. Alessandra Tolomelli, Luca Gentilucci, Elisa Mosconi, Angelo Viola, Samantha Deianira Dattoli, Monica Baiula, Santi Spampinato, Laura Belvisi, and Monica Civera. Development of isoxazoline-containing peptidomimetics as dual  $\alpha v \beta 3$  and  $\alpha 5 \beta 1$  integrin ligands. *ChemMedChem*, 6:2264–2272, 2011.
98. Alessandra Tolomelli, Luca Gentilucci, Elisa Mosconi, Angelo Viola, Samantha Deianira Dattoli, Monica Baiula, Santi Spampinato, Laura Belvisi, and Monica Civera. Development of isoxazoline-containing peptidomimetics as dual  $\alpha v \beta 3$  and  $\alpha 5 \beta 1$  integrin ligands. *ChemMedChem*, 6:2264–2272, 2011.
99. Stephen Caltabiano, Wah-Tung Hum, Gwilym J Attwell, David N Gralnick, Lori J Budman, AnnaMarie Cannistraci, and Frederick J Bex. The integrin specificity of human recombinant osteopontin. *Biochemical pharmacology*, 58(10):1567–1578, 1999.
100. Jing Huang, Lihong Bu, Jin Xie, Kai Chen, Zhen Cheng, Xingguo Li, and Xiaoyuan Chen. Effects of nanoparticle size on cellular uptake and liver mri with polyvinylpyrrolidone-coated iron oxide nanoparticles. *ACS nano*, 4(12):7151–7160, 2010.
101. Jose Aléman and Silvia Cabrera. Applications of asymmetric organocatalysis in medicinal chemistry. *Chemical Society Reviews*, 42(2):774–793, 2013.
102. Nigel B Perry, John W Blunt, Murray HG Munro, and Lewis K Pannell. Mycalamide a, an antiviral compound from a new zealand sponge of the genus mycale. *Journal of the American Chemical Society*, 110(14):4850–4851, 1988.
103. Preecha Phuwapraisirisan, Shigeki Matsunaga, and Nobuhiro Fusetani. Mycapolyols a- f, new cytotoxic metabolites of mixed biogenesis from the marine sponge mycale i zuensis. *Organic letters*, 7(11):2233–2236, 2005.
104. Daniele Leonori and Varinder K Aggarwal. Lithiation–borylation methodology and its application in synthesis. *Accounts of chemical research*, 47(10):3174–3183, 2014.



105. Jake L Stymiest, Guillaume Dutheil, Adeem Mahmood, and Varinder K Aggarwal. Lithiated carbamates: chiral carbenoids for iterative homologation of boranes and boronic esters. *Angewandte Chemie*, 119(39):7635–7638, 2007.
106. GP Moss, PAS Smith, and D Tavernier. Glossary of class names of organic compounds and reactivity intermediates based on structure (iupac recommendations 1995). *Pure and applied chemistry*, 67(8-9):1307–1375, 1995.
107. T Eicher and S Hauptmann. Edition iind,"the chemistry of heterocycles: Structure. *Reactions, Syntheses, and Applications"*, Wiley-VCH, 2003.
108. George A Patani and Edmond J LaVoie. Bioisosterism: a rational approach in drug design. *Chemical reviews*, 96(8):3147–3176, 1996.
109. Irving Langmuir. Isomorphism, isosterism and covalence. *Journal of the American Chemical Society*, 41(10):1543–1559, 1919.
110. HG Grimm. Structure and size of the non-metallic hydrides. *Z. Electrochem*, 31:474–480, 1925.
111. Hans Erlenmeyer and Martin Leo. Über pseudoatome. *Helvetica Chimica Acta*, 15(1):1171–1186, 1932.
112. Harris L Friedman. Influence of isosteric replacements upon biological activity. *Nasnrns*, 206:295–358, 1951.
113. Alfred Burger. Isosterism and bioisosterism in drug design. In *Progress in Drug Research/Fortschritte der Arzneimittelforschung/Progrès des recherches pharmaceutiques*, pages 287–371. Springer, 1991.
114. Chérif F Matta, Alya A Arabi, and Donald F Weaver. The bioisosteric similarity of the tetrazole and carboxylate anions: clues from the topologies of the electrostatic potential and of the electron density. *European journal of medicinal chemistry*, 45(5):1868–1872, 2010.
115. Pragi Arora, Varun Arora, HS Lamba, and Deepak Wadhwa. Importance of heterocyclic chemistry: A review. *International Journal of Pharmaceutical Sciences and Research*, 3(9):2947, 2012.
116. A Gomtsyan. Heterocycles in drugs and drug discovery. *Chemistry of heterocyclic compounds*, 48(1):7–10, 2012.

117. Shu-chi Hsiung, Mella Adlersberg, Victoria Arango, J John Mann, Hadassah Tamir, and Kuo-peing Liu. Attenuated 5-ht<sub>1a</sub> receptor signaling in brains of suicide victims: involvement of adenylyl cyclase, phosphatidylinositol 3-kinase, akt and mitogen-activated protein kinase. *Journal of neurochemistry*, 87(1):182–194, 2003.
118. VY Dudkin. Bioisosteric equivalence of five-membered heterocycles. *Chemistry of Heterocyclic Compounds*, 48(1):27–32, 2012.
119. Christian Laurence, Ken A Brameld, Jerome Graton, Jean-Yves Le Questel, and Eric Renault. The p k bhx database: toward a better understanding of hydrogen-bond basicity for medicinal chemists. *Journal of medicinal chemistry*, 52(14):4073–4086, 2009.
120. Nicholas A McGrath, Matthew Brichacek, and Jon T Njardarson. A graphical journey of innovative organic architectures that have improved our lives. *Journal of Chemical Education*, 87(12):1348–1349, 2010.
121. Andrew D Abell. Heterocyclic-based peptidomimetics. *Letters in Peptide Science*, 8(3-5):267–272, 2001.
122. Alfred Burger and Manfred E Wolff. *Burger's medicinal chemistry and drug discovery*, volume 1. Wiley, 1994.
123. Josef Vagner, Hongchang Qu, and Victor J Hruby. Peptidomimetics, a synthetic tool of drug discovery. *Current opinion in chemical biology*, 12(3):292–296, 2008.
124. Matthew David Fletcher and Malcolm M Campbell. Partially modified retro-inverso peptides: development, synthesis, and conformational behavior. *Chemical reviews*, 98(2):763–796, 1998.
125. Xuyuan Gu, Jinfa Ying, Byoung Min, James P Cain, Peg Davis, Patrick Willey, Edita Navratilova, Henry I Yamamura, Frank Porreca, and Victor J Hruby. Parallel synthesis and biological evaluation of different sizes of bicyclo [2, 3]-leu-enkephalin analogues. *Peptide Science: Original Research on Biomolecules*, 80(2-3):151–163, 2005.
126. Josef Vagner, Hongchang Qu, and Victor J Hruby. Peptidomimetics, a synthetic tool of drug discovery. *Current opinion in chemical biology*, 12(3):292–296, 2008.
127. Ao Zhang, Guochun Zhou, Suo-Bao Rong, Kenneth M Johnson, Mei Zhang, and Alan P Kozikowski. Thiophene derivatives: A new series of potent norepinephrine and serotonin reuptake inhibitors. *Bioorganic & medicinal chemistry letters*, 12(7):993–995, 2002.

128. Mette B Hermit, Jeremy R Greenwood, Birgitte Nielsen, Lennart Bunch, Charlotte G Jørgensen, Henrik T Vestergaard, Tine B Stensbøl, Connie Sanchez, Povl Krosgaard-Larsen, Ulf Madsen, et al. Ibotenic acid and thioibotenic acid: a remarkable difference in activity at group iii metabotropic glutamate receptors. *European journal of pharmacology*, 486(3):241–250, 2004.
129. Kamalneet Kaur, Vinod Kumar, Anil Kumar Sharma, and Girish Kumar Gupta. Isoxazoline containing natural products as anticancer agents: A review. *European journal of medicinal chemistry*, 77:121–133, 2014.
130. Mathéo Berthet, Thomas Cheviet, Gilles Dujardin, Isabelle Parrot, and Jean Martinez. Isoxazolidine: a privileged scaffold for organic and medicinal chemistry. *Chemical Reviews*, 116(24):15235–15283, 2016.
131. Eduard Buchner. Einwirkung von diazoessigäther auf die aether ungesättigter säuren. *Berichte der deutschen chemischen Gesellschaft*, 21(2):2637–2647, 1888.
132. Rolf Huisgen. Kinetics and mechanism of 1, 3-dipolar cycloadditions. *Angewandte Chemie International Edition in English*, 2(11):633–645, 1963.
133. Ro Bo Woodward and Roald Hoffmann. Stereochemistry of electrocyclic reactions. *Journal of the American Chemical Society*, 87(2):395–397, 1965.
134. KN Houk, Joyner Sims, RE Duke, RW Strozier, and John K George. Frontier molecular orbitals of 1, 3 dipoles and dipolarophiles. *Journal of the American Chemical Society*, 95(22):7287–7301, 1973.
135. Kurt V Gothelf and Karl Anker Jørgensen. Asymmetric 1, 3-dipolar cycloaddition reactions. *Chemical Reviews*, 98(2):863–910, 1998.
136. Kendall N Houk, Javier Gonzalez, and Yi Li. Pericyclic reaction transition states: Passions and punctilios, 1935-1995. *Accounts of Chemical Research*, 28(2):81–90, 1995.
137. Reiner Sustmann. A simple model for substituent effects in cycloaddition reactions. i. 1, 3-dipolar cycloadditions. *Tetrahedron Letters*, 12(29):2717–2720, 1971.
138. P Perlmutter. *Conjugate addition reactions in organic synthesis*. Elsevier, 2013.
139. Ian Fleming et al. *Frontier orbitals and organic chemical reactions*. Wiley, 1977.
140. Teruhiko Ishikawa, Keita Nagai, Takayuki Kudoh, and Seiki Saito. Asymmetric synthesis of substituted isoxazolidinone from  $\alpha$ ,  $\beta$ -unsaturated esters and hydroxylamines by means of double stereodifferentiation. *Synlett*, 1995(11):1171–1173, 1995.

141. Lamiaa A Shaala, Diaa TA Youssef, Mansour Sulaiman, Fathy A Behery, Ahmed I Foudah, and Khalid A El Sayed. Subreamolline a as a potent breast cancer migration, invasion and proliferation inhibitor and bioactive dibrominated alkaloids from the red sea sponge pseudoceratina arabica. *Marine drugs*, 10(11):2492–2508, 2012.
142. J Gal and P Cintas. Biochirality: Origins, evolution and molecular recognition. *Topics Curr. Chem*, 333:1–40, 2012.
143. L Pasteur. On the relations crystalline form, chemical composition and direction of polarization rotatorie. *Ann. Chim. Phys.*, 24:442–459, 1848.
144. Louis Pasteur. *Mémoire sur la fermentation alcoolique*. Mallet-Bachelier, 1860.
145. A Piutti. Ein neues asparagin. *Berichte der deutschen chemischen Gesellschaft*, 19(2):1691–1695, 1886.
146. George C Cotzias, Paul S Papavasiliou, and Rosemary Gellene. Modification of parkinsonism-chronic treatment with l-dopa. *New England Journal of Medicine*, 280(7):337–345, 1969.
147. RR Shah and SK Branch. Regulatory requirements for the development of chirally active drugs. In *Stereochemical Aspects of Drug Action and Disposition*, pages 379–399. Springer, 2003.
148. Kateri A Ahrendt, Christopher J Borths, and David WC MacMillan. New strategies for organic catalysis: the first highly enantioselective organocatalytic diels- alder reaction. *Journal of the American Chemical Society*, 122(17):4243–4244, 2000.
149. Zoltan G Hajos and David R Parrish. Asymmetric synthesis of bicyclic intermediates of natural product chemistry. *The Journal of organic chemistry*, 39(12):1615–1621, 1974.
150. Ulrich Eder, Gerhard Sauer, and Rudolf Wiechert. New type of asymmetric cyclization to optically active steroid cd partial structures. *Angewandte Chemie International Edition in English*, 10(7):496–497, 1971.
151. Teresa D Beeson, Anthony Mastracchio, Jun-Bae Hong, Kate Ashton, and David WC MacMillan. Enantioselective organocatalysis using sono activation. *Science*, 316(5824):582–585, 2007.
152. Santanu Mukherjee, Jung Woon Yang, Sebastian Hoffmann, and Benjamin List. Asymmetric enamine catalysis. *Chemical Reviews*, 107(12):5471–5569, 2007.

153. Anna G Wenzel and Eric N Jacobsen. Asymmetric catalytic mannich reactions catalyzed by urea derivatives: enantioselective synthesis of  $\beta$ -aryl- $\beta$ -amino acids. *Journal of the American Chemical Society*, 124(44):12964–12965, 2002.
154. Sarah E Reisman, Abigail G Doyle, and Eric N Jacobsen. Enantioselective thiourea-catalyzed additions to oxocarbenium ions. *Journal of the American Chemical Society*, 130(23):7198–7199, 2008.
155. Carl A Busacca, Daniel R Fandrick, Jinhua J Song, and Chris H Senanayake. The growing impact of catalysis in the pharmaceutical industry. *Advanced Synthesis & Catalysis*, 353(11-12):1825–1864, 2011.
156. Peter I Dalko and Lionel Moisan. In the golden age of organocatalysis. *Angewandte Chemie International Edition*, 43(39):5138–5175, 2004.
157. Yonggui Chi and Samuel H Gellman. Diphenylprolinol methyl ether: a highly enantioselective catalyst for michael addition of aldehydes to simple enones. *Organic Letters*, 7(19):4253–4256, 2005.
158. Yujiro Hayashi, Hiroaki Gotoh, Takaaki Hayashi, and Mitsuru Shoji. Diphenylprolinol silyl ethers as efficient organocatalysts for the asymmetric michael reaction of aldehydes and nitroalkenes. *Angewandte Chemie International Edition*, 44(27):4212–4215, 2005.
159. Chandraiah Lagiseti, Alan Pourpak, Qin Jiang, Xiaoli Cui, Tinopiwa Goronga, Stephan W Morris, and Thomas R Webb. Antitumor compounds based on a natural product consensus pharmacophore. *Journal of medicinal chemistry*, 51(19):6220–6224, 2008.
160. Chunling Shi, Juxian Wang, Hui Chen, and Daqing Shi. Regioselective synthesis and in vitro anticancer activity of 4-aza-podophyllotoxin derivatives catalyzed by l-proline. *Journal of Combinatorial Chemistry*, 12(4):430–434, 2010.
161. Joel F Austin and David WC MacMillan. Enantioselective organocatalytic indole alkylations. design of a new and highly effective chiral amine for iminium catalysis. *Journal of the American Chemical Society*, 124(7):1172–1173, 2002.
162. Zhenhua Dong, Lijia Wang, Xiaohong Chen, Xiaohua Liu, Lili Lin, and Xiaoming Feng. Organocatalytic enantioselective michael addition of 4-hydroxycoumarin to  $\alpha$ ,  $\beta$ -unsaturated ketones: a simple synthesis of warfarin. *European Journal of Organic Chemistry*, 2009(30):5192–5197, 2009.
163. Ilker Avan, C Dennis Hall, and Alan R Katritzky. Peptidomimetics via modifications of amino acids and peptide bonds. *Chemical Society Reviews*, 43(10):3575–3594, 2014.

164. Chiara Cabrele, Tamás A Martinek, Oliver Reiser, and Łukasz Berlicki. Peptides containing  $\beta$ -amino acid patterns: challenges and successes in medicinal chemistry. *Journal of medicinal chemistry*, 57(23):9718–9739, 2014.
165. Michael North. Incorporation of conformationally constrained  $\beta$ -amino acids into peptides. *Journal of peptide science: an official publication of the European Peptide Society*, 6(7):301–313, 2000.
166. Dieter Seebach and Jennifer L Matthews.  $\beta$ -peptides: a surprise at every turn. *Chemical Communications*, (21):2015–2022, 1997.
167. Richard P Cheng, Samuel H Gellman, and William F DeGrado.  $\beta$ -peptides: from structure to function. *Chemical reviews*, 101(10):3219–3232, 2001.
168. Tamás A Martinek and Ferenc Fülöp. Side-chain control of  $\beta$ -peptide secondary structures. *European Journal of Biochemistry*, 270(18):3657–3666, 2003.
169. James W Checco, Erinna F Lee, Marco Evangelista, Nerida J Sleebbs, Kelly Rogers, Anne Pettikiriarachchi, Nadia J Kershaw, Geoffrey A Eddinger, David G Belair, Julia L Wilson, et al.  $\alpha/\beta$ -peptide foldamers targeting intracellular protein–protein interactions with activity in living cells. *Journal of the American Chemical Society*, 137(35):11365–11375, 2015.
170. Rossella De Marco, Alessandra Tolomelli, Eusebio Juaristi, and Luca Gentilucci. Integrin ligands with  $\alpha/\beta$ -hybrid peptide structure: design, bioactivity, and conformational aspects. *Medicinal Research Reviews*, 36(3):389–424, 2016.
171. S Rajesh, Jyoti Srivastava, Biswadip Banerji, and Javed Iqbal.  $\alpha$ -dehydro  $\beta$ -amino acid derivatives as turn inducer: Synthesis of potential hiv protease inhibitors based on structural mimicry. 2001.
172. Roberta Galeazzi, Gianluca Martelli, Eleonora Marcucci, Mario Orena, Samuele Rinaldi, Roberta Lattanzi, and Lucia Negri. Analogues of both leu-and met-enkephalin containing a constrained dipeptide isostere prepared from a baylis-hillman adduct. *Amino acids*, 38(4):1057–1065, 2010.
173. A Tolomelli, M Baiula, A Viola, L Ferrazzano, L Gentilucci, SD Dattoli, S Spampinato, E Juaristi, and M Escudero. Dehydro- $\beta$ proline containing peptidomimetics as selective  $\alpha_4\beta_1$  integrin antagonists: a stereochemical recognition in ligand-receptor interaction. *ACS Med. Chem. Lett*, 6:701–706, 2015.
174. Fides Benfatti, Giuliana Cardillo, Luca Gentilucci, Elisa Mosconi, and Alessandra Tolomelli. Synthesis of dehydro- $\beta$ -amino esters via highly regioselective amination of allylic carbonates. *Organic letters*, 10(12):2425–2428, 2008.

175. Alessandra Tolomelli, Luca Gentilucci, Elisa Mosconi, Angelo Viola, and Enrico Paradisi. A straightforward route to enantiopure 2-substituted-3, 4-dehydro- $\beta$ -proline via ring closing metathesis. *Amino acids*, 41(3):575–586, 2011.
176. Barry M Trost and Matthew L Crawley. Asymmetric transition-metal-catalyzed allylic alkylations: applications in total synthesis. *Chemical Reviews*, 103(8):2921–2944, 2003.
177. Ryoichi Kuwano. Usage of the carboxylate leaving group in transition-metal-catalyzed cross-coupling and related reactions. *Journal of Synthetic Organic Chemistry, Japan*, 69(11):1263–1270, 2011.
178. Barry M Trost and Daniel R Fandrick. Palladium-catalyzed dynamic kinetic asymmetric allylic alkylation with the dppba ligands. *ChemInform*, 39(51):no–no, 2008.
179. Jianping Qu and Günter Helmchen. Applications of iridium-catalyzed asymmetric allylic substitution reactions in target-oriented synthesis. *Accounts of Chemical Research*, 50(10):2539–2555, 2017.
180. Alessandra Tolomelli, Monica Baiula, Laura Belvisi, Angelo Viola, Luca Gentilucci, Stefano Troisi, Samantha Deianira Dattoli, Santi Spampinato, Monica Civera, Eusebio Juaristi, et al. Modulation of  $\alpha v\beta 3$ - and  $\alpha 5\beta 1$ -integrin-mediated adhesion by dehydro- $\beta$ -amino acids containing peptidomimetics. *European Journal of Medicinal Chemistry*, 66:258–268, 2013.
181. Angelo Viola, Lucia Ferrazzano, Roberto Greco, Lucia Cerisoli, Jonathan Caldi, and Alessandra Tolomelli. One-pot two-step microwave-assisted synthesis of alkylidene acetoacetamido esters, useful intermediates for  $\beta$ -dehydropeptides. *European Journal of Organic Chemistry*, 2016(19):3217–3222, 2016.
182. Jean Louis Luche. Lanthanides in organic chemistry. 1. selective 1, 2 reductions of conjugated ketones. *Journal of the American Chemical Society*, 100(7):2226–2227, 1978.
183. Chutian Shu, Andreas Leitner, and John F Hartwig. Enantioselective allylation of aromatic amines after in situ generation of an activated cyclometalated iridium catalyst. *Angewandte Chemie International Edition*, 43(36):4797–4800, 2004.
184. Fanrong Mu, Debbie J Lee, Donald E Pryor, Ernest Hamel, and Mark Cushman. Synthesis and investigation of conformationally restricted analogues of lavendustin a as cytotoxic inhibitors of tubulin polymerization. *Journal of medicinal chemistry*, 45(21):4774–4785, 2002.

185. Mark H Norman, Greg C Rigdon, William R Hall, and Frank Navas. Structure- activity relationships of a series of substituted benzamides: potent d2/5-ht2 antagonists and 5-ht1a agonists as neuroleptic agents. *Journal of medicinal chemistry*, 39(5):1172–1188, 1996.
186. Guoqiang Dong, Shengzheng Wang, Zhenyuan Miao, Jianzhong Yao, Yongqiang Zhang, Zizhao Guo, Wannian Zhang, and Chunquan Sheng. New tricks for an old natural product: discovery of highly potent evodiamine derivatives as novel antitumor agents by systemic structure–activity relationship analysis and biological evaluations. *Journal of medicinal chemistry*, 55(17):7593–7613, 2012.
187. Ming Chen and John F Hartwig. Iridium-catalyzed regio- and enantioselective allylic substitution of trisubstituted allylic electrophiles. *Angewandte Chemie*, 128(38):11823–11827, 2016.
188. Qiang Cheng, Hang-Fei Tu, Chao Zheng, Jian-Ping Qu, Günter Helmchen, and Shu-Li You. Iridium-catalyzed asymmetric allylic substitution reactions. *Chemical reviews*, 119(3):1855–1969, 2018.
189. Jevgenij A Raskatov, Stephanie Spiess, Christian Gnam, Kerstin Brödner, Frank Rominger, and Günter Helmchen. Ir-catalysed asymmetric allylic substitutions with cyclometalated (phosphoramidite) ir complexes-resting states, catalytically active ( $\pi$ -allyl) ir complexes and computational exploration. *Chemistry–A European Journal*, 16(22):6601–6615, 2010.
190. Sherzod T Madrahimov, Qian Li, Ankit Sharma, and John F Hartwig. Origins of regioselectivity in iridium catalyzed allylic substitution. *Journal of the American Chemical Society*, 137(47):14968–14981, 2015.
191. Nicolas Agenet, Christian Amatore, Sophie Gamez, Hadia Gérardin, Anny Jutand, Gilbert Meyer, and Céline Orthwein. Effect of the leaving group and the allylic structure on the kinetics and thermodynamics of the reaction of allylic carboxylates with palladium (0) complexes. *Arkivoc*, 92:101, 2002.
192. Daniel J Weix, Dean Markovic, Mitsuhiro Ueda, and John F Hartwig. Direct, intermolecular, enantioselective, iridium-catalyzed allylation of carbamates to form carbamate-protected, branched allylic amines. *Organic letters*, 11(13):2944–2947, 2009.
193. Craig P Butts, Emame Filali, Guy C Lloyd-Jones, Per-Ola Norrby, David A Sale, and York Schramm. Structure-based rationale for selectivity in the asymmetric allylic alkylation of cycloalkenyl esters employing the trost 'standard ligand'(tsl): isolation, analysis



- and alkylation of the monomeric form of the cationic  $\eta^3$ -cyclohexenyl complex  $[(\eta^3\text{-c-c6h9})\text{pd}(\text{tsl})]^+$ . *Journal of the American Chemical Society*, 131(29):9945–9957, 2009.
194. Erkki Ruoslahti. Rgd and other recognition sequences for integrins. *Annual review of cell and developmental biology*, 12(1):697–715, 1996.
195. Kai Chen and Xiaoyuan Chen. Integrin targeted delivery of chemotherapeutics. *Theranostics*, 1:189, 2011.
196. Roger Stupp, Monika E Hegi, Thierry Gorlia, Sara C Erridge, James Perry, Yong-Kil Hong, Kenneth D Aldape, Benoit Lhermitte, Torsten Pietsch, Danica Grujicic, et al. Cilengitide combined with standard treatment for patients with newly diagnosed glioblastoma with methylated mgmt promoter (centric eortc 26071-22072 study): a multicentre, randomised, open-label, phase 3 trial. *The lancet oncology*, 15(10):1100–1108, 2014.
197. Fabienne Danhier, Aude Le Breton, and Véronique Préat. Rgd-based strategies to target alpha (v) beta (3) integrin in cancer therapy and diagnosis. *Molecular pharmaceutics*, 9(11):2961–2973, 2012.
198. Paul Cruciani, Robert Stammer, Corinne Aubert, and Max Malacria. New cobalt-catalyzed cycloisomerization of  $\varepsilon$ -acetylenic  $\beta$ -keto esters. application to a powerful cyclization reactions cascade. *The Journal of organic chemistry*, 61(8):2699–2708, 1996.
199. Alessandra Tolomelli, Giuliana Cardillo, Luca Gentilucci, Riccardo Juris, Angelo Viola, and Eusebio Juaristi. *Exploring the reactivity of alkylidene malonamides: synthesis of polyfunctionalized isoxazolidinones, aziridines and oxazolines*. Ann Arbor, MI: Michigan Publishing, University of Michigan Library, 2012.
200. Lucia Ferrazzano, Angelo Viola, Elena Lonati, Alessandra Bulbarelli, Rosario Musumeci, Clementina Cocuzza, Marco Lombardo, and Alessandra Tolomelli. New isoxazolidinone and 3, 4-dehydro- $\beta$ -proline derivatives as antibacterial agents and mao-inhibitors: A complex balance between two activities. *European journal of medicinal chemistry*, 124:906–919, 2016.
201. Giuliana Cardillo, Luca Gentilucci, Massimo Gianotti, Rossana Perciaccante, and Alessandra Tolomelli. Synthesis of aziridine-2, 2-dicarboxylates via 1, 4-addition of n, o-(bistrimethylsilyl) hydroxylamine to  $\alpha$ ,  $\beta$ -unsaturated malonates. *The Journal of organic chemistry*, 66(25):8657–8660, 2001.

202. Cátia Ornelas, Johannes Broichhagen, and Marcus Weck. Strain-promoted alkyne azide cycloaddition for the functionalization of poly (amide)-based dendrons and dendrimers. *Journal of the American Chemical Society*, 132(11):3923–3931, 2010.
203. Xavier Creary, Andrew Anderson, Carl Brophy, Frances Crowell, and Zachary Funk. Method for assigning structure of 1, 2, 3-triazoles. *The Journal of organic chemistry*, 77(19):8756–8761, 2012.
204. John M Ndungu, Yang J Lu, Shijun Zhu, Chao Yang, Xu Wang, Georgia Chen, Dong M Shin, James P Snyder, Mamoru Shoji, and Aiming Sun. Targeted delivery of paclitaxel to tumor cells: synthesis and in vitro evaluation. *Journal of medicinal chemistry*, 53(8):3127–3132, 2010.
205. Yuqin Jiang, Baoqi Ren, Xiaomeng Lv, Weiwei Zhang, Wei Li, and Guiqing Xu. Design, synthesis and antifungal activity of novel paeonol derivatives linked with 1, 2, 3-triazole moiety by the click reaction. *Journal of Chemical Research*, 39(4):243–246, 2015.
206. Ying Tu and Lin Zhu. Enhancing cancer targeting and anticancer activity by a stimulus-sensitive multifunctional polymer-drug conjugate. *Journal of Controlled Release*, 212:94–102, 2015.
207. Stephen Caltabiano, Wah-Tung Hum, Gwilym J Attwell, David N Gralnick, Lori J Budman, AnnaMarie Cannistraci, and Frederick J Bex. The integrin specificity of human recombinant osteopontin. *Biochemical pharmacology*, 58(10):1567–1578, 1999.
208. Monica Baiula, Paola Galletti, Giulia Martelli, Roberto Soldati, Laura Belvisi, Monica Civera, Samantha Deianira Dattoli, Santi Mario Spampinato, and Daria Giacomini. New  $\beta$ -lactam derivatives modulate cell adhesion and signaling mediated by rgd-binding and leukocyte integrins. *Journal of Medicinal Chemistry*, 59(21):9721–9742, 2016.
209. Marina Pisano, Ivan De Paola, Valentina Nieddu, Ilaria Sassu, Sara Cossu, Grazia Galleri, Annarita Del Gatto, Mario Budroni, Antonio Cossu, Michele Saviano, et al. In vitro activity of the  $\alpha v \beta 3$  integrin antagonist rgdechi-hcit on malignant melanoma cells. *Anticancer research*, 33(3):871–879, 2013.
210. Lorenzo Sernissi, Andrea Trabocchi, Dina Scarpi, Francesca Bianchini, and Ernesto G Occhiato. Cyclic rgd peptidomimetics containing 4-and 5-amino-cyclopropane pipercolic acid (cpa) templates as dual  $\alpha v \beta 3$  and  $\alpha 5 \beta 1$  integrin ligands. *Bioorganic & medicinal chemistry*, 24(4):703–711, 2016.
211. Rosemary J Santulli, William A Kinney, Shyamali Ghosh, Bart L DeCorte, Li Liu, Robert WA Tuman, Zhao Zhou, Norman Huebert, Sven E Bursell, Alan C Clermont,

- et al. Studies with an orally bioavailable  $\alpha v$  integrin antagonist in animal models of ocular vasculopathy: retinal neovascularization in mice and retinal vascular permeability in diabetic rats. *Journal of Pharmacology and Experimental Therapeutics*, 324(3):894–901, 2008.
212. Hideki Fujii, Hiroyuki KOMAZAWA, Hideto MORI, Masayoshi KOJIMA, Isamu ITOH, Jun MURATA, Ichiro AZUMA, and Ikuo SAIKI. Antimetastatic activities of synthetic arg-gly-asp-ser (rgds) and arg-leu-asp-ser (rls) peptide analogues and their inhibitory mechanisms. *Biological and Pharmaceutical Bulletin*, 18(12):1681–1688, 1995.
213. Fides Benfatti, Giuliana Cardillo, Serena Fabbroni, Patrizia Galzerano, Luca Gentilucci, Riccardo Juris, Alessandra Tolomelli, Monica Baiula, Antonino Spartà, and Santi Spampinato. Synthesis and biological evaluation of non-peptide  $\alpha v\beta 3/\alpha 5\beta 1$  integrin dual antagonists containing 5, 6-dihydropyridin-2-one scaffolds. *Bioorganic & medicinal chemistry*, 15(23):7380–7390, 2007.
214. Sara M Weis, Dwayne G Stupack, and David A Cheresh. Agonizing integrin antagonists? *Cancer cell*, 15(5):359–361, 2009.
215. Braden D Cox, Meera Natarajan, Michelle R Stettner, and Candace L Gladson. New concepts regarding focal adhesion kinase promotion of cell migration and proliferation. *Journal of cellular biochemistry*, 99(1):35–52, 2006.
216. David D Schlaepfer, Christof R Hauck, and David J Sieg. Signaling through focal adhesion kinase. *Progress in biophysics and molecular biology*, 71(3-4):435–478, 1999.
217. Nicola De Franceschi, Hellyeh Hamidi, Jonna Alanko, Pranshu Sahgal, and Johanna Ivaska. Integrin traffic—the update. *Journal of cell science*, 128(5):839–852, 2015.
218. Patrick T Caswell and Jim C Norman. Integrin trafficking and the control of cell migration. *Traffic*, 7(1):14–21, 2006.
219. Teijo Pellinen and Johanna Ivaska. Integrin traffic. *Journal of cell science*, 119(18):3723–3731, 2006.
220. Marta A Dozynkiewicz, Nigel B Jamieson, Iain MacPherson, Joan Grindlay, Peter VE van den Berghe, Anne von Thun, Jennifer P Morton, Charlie Gourley, Paul Timpson, Colin Nixon, et al. Rab25 and clic3 collaborate to promote integrin recycling from late endosomes/lysosomes and drive cancer progression. *Developmental cell*, 22(1):131–145, 2012.
221. Viola Hélène Lobert and Harald Stenmark. The esct machinery mediates polarization of fibroblasts through regulation of myosin light chain. *Journal of cell science*, 125(1):29–36, 2012.

222. Aliakbar Taherian, Xinlei Li, Yongqing Liu, and Thomas A Haas. Differences in integrin expression and signaling within human breast cancer cells. *BMC cancer*, 11(1):293, 2011.
223. Ahmed R Qasem, Claudio Bucolo, Monica Baiula, Antonino Spartà, Paolo Govoni, Andrea Bedini, Domenico Fasci, and Santi Spampinato. Contribution of  $\alpha 4\beta 1$  integrin to the antiallergic effect of levocabastine. *Biochemical pharmacology*, 76(6):751–762, 2008.
224. Erpan Ahat, Yi Xiang, Xiaoyan Zhang, Michael E Bekier, and Yanzhuang Wang. Grasp depletion–mediated golgi destruction decreases cell adhesion and migration via the reduction of  $\alpha 5\beta 1$  integrin. *Molecular biology of the cell*, 30(6):766–777, 2019.
225. Joseph Gal. *Chiral drugs from a historical point of view*, volume 33. WILEY-VCH: Weinheim, 2006.
226. RR Shah. Improving clinical risk/benefit through stereochemistry. In *Stereochemical aspects of drug action and disposition*, pages 401–432. Springer, 2003.
227. Laure-Elie Carloni, Stefan Mohnani, and Davide Bonifazi. Synthesis of 3, 5-disubstituted isoxazoles through a 1, 3-dipolar cycloaddition reaction between alkynes and nitrile oxides generated from o-silylated hydroxamic acids. *European Journal of Organic Chemistry*, 2019(44):7322–7334, 2019.
228. Wendy S Jen, John JM Wiener, and David WC MacMillan. New strategies for organic catalysis: the first enantioselective organocatalytic 1, 3-dipolar cycloaddition. *Journal of the American Chemical Society*, 122(40):9874–9875, 2000.
229. Jose Aléman, Alberto Fraile, Leyre Marzo, Jose Luis Garcia Ruano, Cristina Izquierdo, and Sergio Diaz-Tendero. Enantioselective synthesis of 4-isoxazolines by 1, 3-dipolar cycloadditions of nitrones to alkynals catalyzed by fluorodiphenylmethylpyrrolidines. *Advanced Synthesis & Catalysis*, 354(9):1665–1671, 2012.
230. Sara Morales, Fernando G Guijarro, Inés Alonso, José Luis García Ruano, and M Belén Cid. Dual role of pyrrolidine and cooperative pyrrolidine/pyrrolidinium effect in nitron formation. *ACS Catalysis*, 6(1):84–91, 2016.
231. Oliver Goerz and Helmut Ritter. N-alkylated dinitrones from isosorbide as cross-linkers for unsaturated bio-based polyesters. *Beilstein journal of organic chemistry*, 10(1):902–909, 2014.
232. Y Sanlaville, S Guittonneau, M Mansour, EA Feicht, P Meallier, and A Kettrup. Photo-sensitized degradation of terbuthylazine in water. *Chemosphere*, 33(2):353–362, 1996.

233. Sankar K Guchhait and Chetna Madaan. Towards molecular diversity: dealkylation of tert-butyl amine in ugi-type multicomponent reaction product establishes tert-butyl isocyanide as a useful convertible isonitrile. *Organic & Biomolecular Chemistry*, 8(16):3631–3634, 2010.
234. Alan E Walts and William R Roush. A stereorational total synthesis of (-)-ptilocaulin. *Tetrahedron*, 41(17):3463–3478, 1985.
235. Can Zhu and Shengming Ma. Coupling and cyclization of o-iodoanilines and propargylic bromides via allenes: an efficient entry to indomethacin. *Organic letters*, 15(11):2782–2785, 2013.
236. L Ferrazzano, G Martelli, T Fantoni, A Daka, D Corbisiero, A Viola, A Ricci, W Cabri, and A Tolomelli. Fast heck–cassar–sonogashira (hcs) reactions in green solvents. *Organic Letters*, 22(10):3969–3973, 2020.
237. L Hunakova, J Sedlak, M Klobusicka, M Sulikova, and B Chorvath. Phorbol ester (tpa)-induced differential modulation of cell surface antigens in human pluripotential leukemia (k-562) cell line: effects of protein kinase inhibitors with broad-and pkc selective inhibitory activity. *Neoplasma*, 42(5):249–253, 1995.
238. Hideto Shibata and Tatsuhiko Yagi. Rate assay of n-acetyl- $\beta$ -d-hexosaminidase with 4-nitrophenyl n-acetyl- $\beta$ -d-glucosaminide as an artificial substrate. *Clinica chimica acta*, 251(1):53–64, 1996.
239. Andrea Bedini, Monica Baiula, and Santi Spampinato. Transcriptional activation of human mu-opioid receptor gene by insulin-like growth factor-i in neuronal cells is modulated by the transcription factor rest. *Journal of neurochemistry*, 105(6):2166–2178, 2008.
240. Sean A McKinney, Christopher S Murphy, Kristin L Hazelwood, Michael W Davidson, and Loren L Looger. A bright and photostable photoconvertible fluorescent protein. *Nature methods*, 6(2):131–133, 2009.
241. Filippo G Giancotti and Erkki Ruoslahti. Elevated levels of the  $\alpha 5 \beta 1$  fibronectin receptor suppress the transformed phenotype of chinese hamster ovary cells. *Cell*, 60(5):849–859, 1990.
242. Ileana Guzzetti, Monica Civera, Francesca Vasile, Daniela Arosio, Cristina Tringali, Umberto Piarulli, Cesare Gennari, Luca Pignataro, Laura Belvisi, and Donatella Potenza. Insights into the binding of cyclic rgd peptidomimetics to  $\alpha 5 \beta 1$  integrin by using live-cell nmr and computational studies. *ChemistryOpen*, 6(1):128, 2017.

243. Ayres G Dias, Carlos EV Santos, Fatima ZGA Cyrino, Eliete Bouskela, and Paulo RR Costa. N-tert-butyl and n-methyl nitrones derived from aromatic aldehydes inhibit macromolecular permeability increase induced by ischemia/reperfusion in hamsters. *Bioorganic & medicinal chemistry*, 17(11):3995–3998, 2009.
244. C. Dubernet L. Bildstein and P. Couvreur. Prodrug-based intracellular delivery of anticancer agents. *Advanced Drug Delivery Reviews*, 63(1):3–23, 2011.
245. Zhiping Zhang, Lin Mei, and Si-Shen Feng. Paclitaxel drug delivery systems. *Expert opinion on drug delivery*, 10(3):325–340, 2013.
246. Kira Nultsch and Oliver Germershaus. Matrix metalloprotease triggered bioresponsive drug delivery systems—design, synthesis and application. *European Journal of Pharmaceutics and Biopharmaceutics*, 131:189–202, 2018.
247. Twan Lammers, Fabian Kiessling, Wim E Hennink, and Gert Storm. Drug targeting to tumors: principles, pitfalls and (pre-) clinical progress. *Journal of controlled release*, 161(2):175–187, 2012.
248. Alain Beck, Liliane Goetsch, Charles Dumontet, and Nathalie Corvaia. Strategies and challenges for the next generation of antibody–drug conjugates. *Nature reviews Drug discovery*, 16(5):315–337, 2017.
249. David Schrama, Ralph A Reisfeld, and Jürgen C Becker. Antibody targeted drugs as cancer therapeutics. *Nature reviews Drug discovery*, 5(2):147–159, 2006.
250. Pamela A Trail. Antibody drug conjugates as cancer therapeutics. *Antibodies*, 2(1):113–129, 2013.
251. Alexander H Staudacher and Michael P Brown. Antibody drug conjugates and bystander killing: is antigen-dependent internalisation required? *British journal of cancer*, 117(12):1736–1742, 2017.
252. Nikolaus Krall, Joerg Scheuermann, and Dario Neri. Small targeted cytotoxics: current state and promises from dna-encoded chemical libraries. *Angewandte Chemie International Edition*, 52(5):1384–1402, 2013.
253. Ann M Thayer. Building antibody-drug conjugates. *Chemical & Engineering News*, 92(3):13–13, 2014.
254. Madduri Srinivasarao, Chris V Galliford, and Philip S Low. Principles in the design of ligand-targeted cancer therapeutics and imaging agents. *Nature reviews Drug discovery*, 14(3):203–219, 2015.

255. Jin-Wook Yoo, Elizabeth Chambers, and Samir Mitragotri. Factors that control the circulation time of nanoparticles in blood: challenges, solutions and future prospects. *Current pharmaceutical design*, 16(21):2298–2307, 2010.
256. Rubi Mahato, Wanyi Tai, and Kun Cheng. Prodrugs for improving tumor targetability and efficiency. *Advanced drug delivery reviews*, 63(8):659–670, 2011.
257. Iontcho R Vlahov and Christopher P Leamon. Engineering folate–drug conjugates to target cancer: from chemistry to clinic. *Bioconjugate chemistry*, 23(7):1357–1369, 2012.
258. Christopher P Leamon, Iontcho R Vlahov, Joseph A Reddy, Marilyn Vetzal, Hari Krishna R Santhapuram, Fei You, Alicia Bloomfield, Ryan Dorton, Melissa Nelson, Paul Kleindl, et al. Folate–vinca alkaloid conjugates for cancer therapy: a structure–activity relationship. *Bioconjugate chemistry*, 25(3):560–568, 2014.
259. Pamela T Wong and Seok Ki Choi. Mechanisms of drug release in nanotherapeutic delivery systems. *Chemical reviews*, 115(9):3388–3432, 2015.
260. Divya Dheer, Julien Nicolas, and Ravi Shankar. Cathepsin-sensitive nanoscale drug delivery systems for cancer therapy and other diseases. *Advanced Drug Delivery Reviews*, 151:130–151, 2019.
261. Yuan Liu, Krishna Mohan Bajjuri, Cheng Liu, and Subhash C Sinha. Targeting cell surface  $\alpha(v)\beta(3)$  integrin increases therapeutic efficacies of a legumain protease-activated auristatin prodrug. *Molecular pharmaceuticals*, 9(1):168–175, 2012.
262. Scott C Jeffrey, Jamie B Andreyka, Starr X Bernhardt, Kim M Kissler, Toni Kline, Joel S Lenox, Ruth F Moser, Minh T Nguyen, Nicole M Okeley, Ivan J Stone, et al. Development and properties of  $\beta$ -glucuronide linkers for monoclonal antibody- drug conjugates. *Bioconjugate chemistry*, 17(3):831–840, 2006.
263. Thibaut Legigan, Jonathan Clarhaut, Isabelle Tranoy-Opalinski, Arnaud Monvoisin, Brigitte Renoux, Mikael Thomas, Alain Le Pape, Stéphanie Lerondel, and Sébastien Papot. The first generation of  $\beta$ -galactosidase-responsive prodrugs designed for the selective treatment of solid tumors in prodrug monotherapy. *Angewandte Chemie*, 124(46):11774–11778, 2012.
264. Ki Young Choi, Magdalena Swierczewska, Seulki Lee, and Xiaoyuan Chen. Protease-activated drug development. *Theranostics*, 2(2):156, 2012.
265. Gene M Dubowchik and Raymond A Firestone. Cathepsin b-sensitive dipeptide prodrugs. 1. a model study of structural requirements for efficient release of doxorubicin. *Bioorganic & medicinal chemistry letters*, 8(23):3341–3346, 1998.

266. Nareshkumar Jain, Sean W Smith, Sanjeevani Ghone, and Bruce Tomczuk. Current adc linker chemistry. *Pharmaceutical research*, 32(11):3526–3540, 2015.
267. Alberto Dal Corso, Luca Pignataro, Laura Belvisi, and Cesare Gennari. Innovative linker strategies for tumor-targeted drug conjugates. *Chemistry—A European Journal*, 25(65):14740–14757, 2019.
268. Heather Donaghy. Effects of antibody, drug and linker on the preclinical and clinical toxicities of antibody-drug conjugates. In *MAbs*, volume 8, pages 659–671. Taylor & Francis, 2016.
269. Magdalena Dorywalska, Russell Dushin, Ludivine Moine, Santiago E Farias, Dahui Zhou, Thayalan Navaratnam, Victor Lui, Adela Hasa-Moreno, Meritxell Galindo Casas, Thomas-Toan Tran, et al. Molecular basis of valine-citrulline-pabc linker instability in site-specific adcs and its mitigation by linker design. *Molecular cancer therapeutics*, 15(5):958–970, 2016.
270. Yasuaki Anami, Chisato M Yamazaki, Wei Xiong, Xun Gui, Ningyan Zhang, Zhiqiang An, and Kyoji Tsuchikama. Glutamic acid–valine–citrulline linkers ensure stability and efficacy of antibody–drug conjugates in mice. *Nature communications*, 9(1):1–9, 2018.
271. Janina Schmitz, Erik Gilberg, Reik Löser, Jürgen Bajorath, Ulrike Bartz, and Michael Gütschow. Cathepsin b: Active site mapping with peptidic substrates and inhibitors. *Bioorganic & medicinal chemistry*, 27(1):1–15, 2019.
272. BinQing Wei, Janet Gunzner-Toste, Hui Yao, Tao Wang, Jing Wang, Zijin Xu, Jinhua Chen, John Wai, Jim Nonomiya, Siao Ping Tsai, et al. Discovery of peptidomimetic antibody–drug conjugate linkers with enhanced protease specificity. *Journal of medicinal chemistry*, 61(3):989–1000, 2018.
273. Morshed A Chowdhury, Ignace A Moya, Shardul Bhilocha, Cody C McMillan, Brady G Vigliarolo, Ingeborg Zehbe, and Christopher P Phenix. Prodrug-inspired probes selective to cathepsin b over other cysteine cathepsins. *Journal of medicinal chemistry*, 57(14):6092–6104, 2014.
274. Alberto Dal Corso, Samuele Cazzamalli, Rémy Gébleux, Martin Mattarella, and Dario Neri. Protease-cleavable linkers modulate the anticancer activity of noninternalizing antibody–drug conjugates. *Bioconjugate chemistry*, 28(7):1826–1833, 2017.
275. Felix Kratz, Ivonne A Müller, Claudia Ryppa, and Andre Warnecke. Prodrug strategies in anticancer chemotherapy. *ChemMedChem*, 3(1):20–53, 2008.



276. Marcelo Calderón, Ralph Graeser, Felix Kratz, and Rainer Haag. Development of enzymatically cleavable prodrugs derived from dendritic polyglycerol. *Bioorganic & medicinal chemistry letters*, 19(14):3725–3728, 2009.
277. Marek Kovář, Jiří Strohalm, Tomáš Etrych, Karel Ulbrich, and Blanka Říhová. Star structure of antibody-targeted hpma copolymer-bound doxorubicin: a novel type of polymeric conjugate for targeted drug delivery with potent antitumor effect. *Bioconjugate chemistry*, 13(2):206–215, 2002.
278. Maureen Redza-Dutordoir and Diana A Averill-Bates. Activation of apoptosis signalling pathways by reactive oxygen species. *Biochimica et Biophysica Acta (BBA)-Molecular Cell Research*, 1863(12):2977–2992, 2016.
279. Rémy Gébleux, Marco Stringhini, Ruben Casanova, Alex Soltermann, and Dario Neri. Non-internalizing antibody–drug conjugates display potent anti-cancer activity upon proteolytic release of monomethyl auristatin e in the subendothelial extracellular matrix. *International journal of cancer*, 140(7):1670–1679, 2017.
280. Samuele Cazzamalli, Alberto Dal Corso, and Dario Neri. Acetazolamide serves as selective delivery vehicle for dipeptide-linked drugs to renal cell carcinoma. *Molecular cancer therapeutics*, 15(12):2926–2935, 2016.
281. André Raposo Moreira Dias, Arianna Pina, Amelia Dean, Hans-Georg Lerchen, Michele Caruso, Fabio Gasparri, Ivan Fraietta, Sonia Troiani, Daniela Arosio, Laura Belvisi, et al. Neutrophil elastase promotes linker cleavage and paclitaxel release from an integrin-targeted conjugate. *Chemistry—A European Journal*, 25(7):1696–1700, 2019.
282. Ahmed Alouane, Raphaël Labruère, Thomas Le Saux, Frederic Schmidt, and Ludovic Jullien. Self-immolative spacers: kinetic aspects, structure–property relationships, and applications. *Angewandte Chemie International Edition*, 54(26):7492–7509, 2015.
283. Philip L Carl, Prasun K Chakravarty, and John A Katzenellenbogen. A novel connector linkage applicable in prodrug design. *Journal of Medicinal Chemistry*, 24(5):479–480, 1981.
284. André Raposo Moreira Dias, Lizeth Boderó, Ana Martins, Daniela Arosio, Silvia Gazzola, Laura Belvisi, Luca Pignataro, Christian Steinkühler, Alberto Dal Corso, Cesare Gennari, et al. Synthesis and biological evaluation of rgd and isodgr–monomethyl auristatin conjugates targeting integrin  $\alpha v \beta 3$ . *ChemMedChem*, 14(9):938–942, 2019.
285. Leanna R Staben, Stefan G Koenig, Sophie M Lehar, Richard Vandlen, Donglu Zhang, Josefa Chuh, Shang-Fan Yu, Carl Ng, Jun Guo, Yanzhou Liu, et al. Targeted drug

- delivery through the traceless release of tertiary and heteroaryl amines from antibody–drug conjugates. *Nature chemistry*, 8(12):1112, 2016.
286. Donglu Zhang, Hoa Le, Josefa dela Cruz-Chuh, Sudheer Bobba, Jun Guo, Leanna Staben, Chenghong Zhang, Yong Ma, Katherine R Kozak, Gail D Lewis Phillips, et al. Immolation of p-aminobenzyl ether linker and payload potency and stability determine the cell-killing activity of antibody–drug conjugates with phenol-containing payloads. *Bioconjugate chemistry*, 29(2):267–274, 2018.
287. Franciscus MH De Groot, Walter J Loos, Ralph Koekkoek, Leon WA van Berkomp, Guuske F Busscher, Antoinette E Seelen, Carsten Albrecht, Peter de Bruijn, and Hans W Scheeren. Elongated multiple electronic cascade and cyclization spacer systems in activatable anticancer prodrugs for enhanced drug release. *The Journal of organic chemistry*, 66(26):8815–8830, 2001.
288. Wim Dokter, Ruud Ubink, Miranda van der Lee, Monique van der Vleuten, Tanja van Achterberg, Danielle Jacobs, Eline Loosveld, Diels van den Dobbelssteen, David Egging, Ellen Mattaar, et al. Preclinical profile of the her2-targeting adc syd983/syd985: introduction of a new duocarmycin-based linker–drug platform. *Molecular Cancer Therapeutics*, 13(11):2618–2629, 2014.
289. Shang-Fan Yu, Bing Zheng, MaryAnn Go, Jeff Lau, Susan Spencer, Helga Raab, Robert Soriano, Suchit Jhunjhunwala, Robert Cohen, Michele Caruso, et al. A novel anti-cd22 anthracycline-based antibody–drug conjugate (adc) that overcomes resistance to auristatin-based adcs. *Clinical Cancer Research*, 21(14):3298–3306, 2015.
290. Neta Pessah, Mika Reznik, Marina Shamis, Ferda Yantiri, Hong Xin, Katherine Bowdish, Noam Shomron, Gil Ast, and Doron Shabat. Bioactivation of carbamate-based 20 (s)-camptothecin prodrugs. *Bioorganic & medicinal chemistry*, 12(8):1859–1866, 2004.
291. Robert V Kolakowski, Karl T Haelsig, Kim K Emmerton, Chris I Leiske, Jamie B Miyamoto, Julia H Cochran, Robert P Lyon, Peter D Senter, and Scott C Jeffrey. The methylene alkoxy carbamate self-immolative unit: utilization for the targeted delivery of alcohol-containing payloads with antibody–drug conjugates. *Angewandte Chemie International Edition*, 55(28):7948–7951, 2016.
292. Daniel V Santi, Eric L Schneider, and Gary W Ashley. Macromolecular prodrug that provides the irinotecan (cpt-11) active-metabolite sn-38 with ultralong half-life, low c<sub>max</sub>, and low glucuronide formation. *Journal of medicinal chemistry*, 57(6):2303–2314, 2014.

293. Uland Y Lau, Lauren T Benoit, Nicole S Stevens, Kim K Emmerton, Margo Zaval, Julia H Cochran, and Peter D Senter. Lactone stabilization is not a necessary feature for antibody conjugates of camptothecins. *Molecular Pharmaceutics*, 15(9):4063–4072, 2018.
294. Yusuke Ogitani, Tetsuo Aida, Katsunobu Hagihara, Junko Yamaguchi, Chiaki Ishii, Naoya Harada, Masako Soma, Hiromi Okamoto, Masataka Oitate, Shingo Arakawa, et al. Ds-8201a, a novel her2-targeting adc with a novel dna topoisomerase i inhibitor, demonstrates a promising antitumor efficacy with differentiation from t-dm1. *Clinical Cancer Research*, 22(20):5097–5108, 2016.
295. Jeffrey C Kern, Deborah Dooney, Rena Zhang, Linda Liang, Philip E Brandish, Mangeng Cheng, Guo Feng, Andrew Beck, Damien Bresson, Juhi Firdos, et al. Novel phosphate modified cathepsin b linkers: improving aqueous solubility and enhancing payload scope of adcs. *Bioconjugate chemistry*, 27(9):2081–2088, 2016.
296. Nils Johnsson and Kai Johnsson. Chemical tools for biomolecular imaging. *ACS chemical biology*, 2(1):31–38, 2007.
297. Graham B Jones, Curtis F Crasto, Jude E Mathews, Longfei Xie, Miguel O Mitchell, Ahmed El-Shafey, Anthony V D’Amico, and Glenn J Bublely. An image contrast agent selectively activated by prostate specific antigen. *Bioorganic & medicinal chemistry*, 14(2):418–425, 2006.
298. Roy Weinstein, Ehud Segal, Ronit Satchi-Fainaro, and Doron Shabat. Real-time monitoring of drug release. *Chemical Communications*, 46(4):553–555, 2010.
299. Krishna Kalyani Behara, Y Rajesh, Yarra Venkatesh, Bhaskar Rao Pinninti, Mahitosh Mandal, and ND Pradeep Singh. Cascade photocaging of diazeniumdiolate: a novel strategy for one and two photon triggered uncaging with real time reporting. *Chemical Communications*, 53(68):9470–9473, 2017.
300. Christopher Sandford and Varinder K Aggarwal. Stereospecific functionalizations and transformations of secondary and tertiary boronic esters. *Chemical Communications*, 53(40):5481–5494, 2017.
301. Beatrice SL Collins, Claire M Wilson, Eddie L Myers, and Varinder K Aggarwal. Asymmetric synthesis of secondary and tertiary boronic esters. *Angewandte Chemie International Edition*, 56(39):11700–11733, 2017.
302. Donald S Matteson. . alpha.-halo boronic esters: intermediates for stereodirected synthesis. *Chemical Reviews*, 89(7):1535–1551, 1989.

303. Donald S Matteson. General reactions of organoboranes. In *Stereodirected Synthesis with Organoboranes*, pages 48–119. Springer, 1995.
304. Donald S Matteson and Hon-Wah Man. Hydrolysis of substituted 1, 3, 2-dioxaborolanes and an asymmetric synthesis of a differentially protected syn, syn-3-methyl-2, 4-hexanediol. *The Journal of Organic Chemistry*, 61(17):6047–6051, 1996.
305. Jake L Stymiest, Guillaume Dutheil, Adeem Mahmood, and Varinder K Aggarwal. Lithiated carbamates: chiral carbenoids for iterative homologation of boranes and boronic esters. *Angewandte Chemie*, 119(39):7635–7638, 2007.
306. Gilbert Besong, Krzysztof Jarowicki, Philip J Kocienski, Eric Sliwinski, and F Thomas Boyle. Synthesis of (s)-(-)-n-acetylcolchicinol using intramolecular biaryl oxidative coupling. *Organic & biomolecular chemistry*, 4(11):2193–2207, 2006.
307. Andrea Bottoni, Marco Lombardo, Andrea Neri, and Claudio Trombini. Migratory aptitudes of simple alkyl groups in the anionotropic rearrangement of quaternary chloromethyl borate species: A combined experimental and theoretical investigation. *The Journal of organic chemistry*, 68(9):3397–3405, 2003.
308. Matthew Burns, Stéphanie Essafi, Jessica R Bame, Stephanie P Bull, Matthew P Webster, Sébastien Balieu, James W Dale, Craig P Butts, Jeremy N Harvey, and Varinder K Aggarwal. Assembly-line synthesis of organic molecules with tailored shapes. *Nature*, 513(7517):183–188, 2014.
309. Alexander Fawcett, Dominik Nitsch, Muhammad Ali, Joseph M Bateman, Eddie L Myers, and Varinder K Aggarwal. Regio- and stereoselective homologation of 1, 2-bis(boronic esters): Stereocontrolled synthesis of 1, 3-diols and sch 725674. *Angewandte Chemie*, 128(47):14883–14887, 2016.
310. Jeremy B Morgan, Steven P Miller, and James P Morken. Rhodium-catalyzed enantioselective diboration of simple alkenes. *Journal of the American Chemical Society*, 125(29):8702–8703, 2003.
311. Kenji Toribatake and Hisao Nishiyama. Asymmetric diboration of terminal alkenes with a rhodium catalyst and subsequent oxidation: Enantioselective synthesis of optically active 1, 2-diols. *Angewandte Chemie*, 125(42):11217–11221, 2013.
312. Thomas P Blaisdell, Thomas C Caya, Liang Zhang, Amparo Sanz-Marco, and James P Morken. Hydroxyl-directed stereoselective diboration of alkenes. *Journal of the American Chemical Society*, 136(26):9264–9267, 2014.

313. Giorgia Casoni, Murat Kucukdisli, James M Fordham, Matthew Burns, Eddie L Myers, and Varinder K Aggarwal.  $\alpha$ -sulfinyl benzoates as precursors to li and mg carbenoids for the stereoselective iterative homologation of boronic esters. *Journal of the American Chemical Society*, 139(34):11877–11886, 2017.
314. Renate D Kimbrough. Toxicity and health effects of selected organotin compounds: a review. *Environmental Health Perspectives*, 14:51–56, 1976.
315. Amanda L Hoyt and Paul R Blakemore. On the nature of the chain-extending species in organolithium initiated stereospecific reagent-controlled homologation reactions using  $\alpha$ -chloroalkyl aryl sulfoxides. *Tetrahedron Letters*, 56(23):2980–2982, 2015.
316. Peter J Rayner, Peter O'Brien, and Richard AJ Horan. Preparation and reactions of enantiomerically pure  $\alpha$ -functionalized grignard reagents. *Journal of the American Chemical Society*, 135(21):8071–8077, 2013.
317. Xun Sun and Paul R Blakemore. Programmed synthesis of a contiguous stereo-triad motif by triple stereospecific reagent-controlled homologation. *Organic letters*, 15(17):4500–4503, 2013.
318. Preecha Phuwapraisirisan, Shigeki Matsunaga, Nobuhiro Fusetani, Nilnaj Chaitanawisuti, Sirusa Kritsanapuntu, and Piamsak Menasveta. Mycaperoxide h, a new cytotoxic norsesterterpene peroxide from a thai marine sponge mycale sp. *Journal of natural products*, 66(2):289–291, 2003.
319. Y Kato, N Fusetani, S Matsunaga, and K Hashimoto. Bioactive marine metabolites ix. mycalisines a and b, novel nucleosides which inhibit cell division of fertilized starfish eggs, from the marine sponge mycale sp. *Tetrahedron letters*, 26(29):3483–3486, 1985.
320. Ingo Koehne, Nico Graw, Thorsten Teuteberg, Regine Herbst-Irmer, and Dietmar Stalke. Introducing nacnac-like bis (4, 6-isopropylbenzoxazol-2-yl) methanide in s-block metal coordination. *Inorganic Chemistry*, 56(24):14968–14978, 2017.
321. Scott N Mlynarski, Christopher H Schuster, and James P Morken. Asymmetric synthesis from terminal alkenes by cascades of diboration and cross-coupling. *Nature*, 505(7483):386–390, 2014.
322. Roly J Armstrong, Cristina García-Ruiz, Eddie L Myers, and Varinder K Aggarwal. Stereodivergent olefination of enantioenriched boronic esters. *Angewandte Chemie International Edition*, 56(3):786–790, 2017.
323. John R Coombs, Fredrik Haeffner, Laura T Kliman, and James P Morken. Scope and mechanism of the pt-catalyzed enantioselective diboration of monosubstituted alkenes. *Journal of the American Chemical Society*, 135(30):11222–11231, 2013.

324. Cheon-Gyu Cho, Won-Suk Kim, and Amos B Smith. A scalable route to trisubstituted (e)-vinyl bromides. *Organic letters*, 7(16):3569–3572, 2005.